

15th INTERNATIONAL CONFERENCE ON ENGINEERING & NATURAL SCIENCES

March 04-06, 2023 Muş, Türkiye



PROCEEDINGS BOOK

EDITORS

Gamze TURUN

Agit Ferhat OZEL

ISBN: 978-625-7720-89-2

15 th INTERNATIONAL CONFERENCE ON
ENGINEERING & NATURAL SCIENCES
March 4-6, 2023, Mus, Türkiye

ISPEC 15. ULUSLARARASI
MÜHENDİSLİK VE FEN BİLİMLERİ KONGRESİ
4-6 Mart, 2023, Muş, Türkiye

PROCEEDINGS BOOK

Editors
Gamze TURUN
Agit Ferhat ÖZEL

By
ISPEC JOURNAL

All rights of this book belong to ISPEC.
Without permission can't be duplicate or
copied. Authors are responsible both
ethically and juridically

ISPEC Publications – 2023 ©
Issued: 19.03.2023

ISBN: 978-625-7720-89-2

CONFERENCE ID

CONFERENCE TITLE

ISPEC

15th INTERNATIONAL CONFERENCE ON ENGINEERING
& NATURAL SCIENCES

DATE and PLACE

March 4-6, 2023, Mus, Türkiye

ORGANISING INSTITUTION

ISPEC PUBLICATIONS

ORGANISING COMMITTEE

Assoc. Prof. Kemal Adem- Sivas Science and Technology University
Assoc. Prof. Ramazan Katırcı- Sivas Science and Technology University
Asisst. Prof. Ali Suat Yıldız- Sivas Science and Technology University
Asisst. Prof. Fuat Erden- Sivas Science and Technology University
Asisst. Prof. Hacı Mehmet Güzey- Sivas Science and Technology University
Asisst. Prof. Salih Özbay- Sivas Science and Technology University
Asisst. Prof. Yaşar Ostovan- Sivas Science and Technology University

COORDINATOR

Gamze TURUN

NUMBER of ACCEPTED PAPERS-70

NUMBER of REJECTED PAPERS-20

TOTAL NUMBER OF PAPERS FROM TURKEY-32

TOTAL NUMBER OF INTERNATIONAL PARTICIPANTS-38

PARTICIPATING COUNTRIES

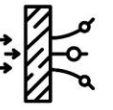
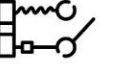
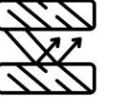
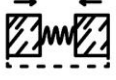
Turkey(32), Pakistan(6), India (5), Nigeria (6), Romania, Morocco(8), Azerbaijan(2), Algeria(9), South
Korea

SCIENTIFIC ADVISORY COMMITTEE

Prof. Dr. Ahmet Yılmaz- Sivas Technology and Science University
Prof. Dr. Ayhan Oral- Çanakkale On Sekiz Mart University
Prof. Dr. H. Emrah Ünal- Middle Eastern Technical University
Prof. Dr. Haydar Livatyalı- Yıldız Technical University
Prof. Dr. Mehmet Şimşir- Sivas Cumhuriyet University
Prof. Dr. Mehmet Yılmaz- Kocaeli University
Prof. Dr. Muhammed Fatih Kılıçaslan- Sivas Technology and Science University
Prof. Dr. Nuran Asmafiliz- Ankara University
Prof. Dr. Özgül Keleş- İstanbul Technical University
Prof. Dr. Servet Turan- Eskişehir Technical University
Prof. Dr. Sıdıka Sungur- İstanbul Health and Technology University
Prof. Dr. Şaban Patat- Erciyes University
Assoc. Prof. Aytuğ Okumuş- Ankara University
Assoc. Prof. Davut Uzun- TÜBİTAK MAM
Assoc. Prof. Emre Biçer- Sivas Technology and Science University
Assoc. Prof. Emre Erdem- Sabancı University
Assoc. Prof. Fehmi Akgün- TÜBİTAK MAM
Assoc. Prof. Gamze Elmas- Ankara University
Assoc. Prof. Kemal Adem- Sivas Technology and Science University
Assoc. Prof. M. Tarık Çakır- Sivas Technology and Science University
Assoc. Prof. Mehmet Kodal- Kocaeli University
Assoc. Prof. Muhsin Mazman- t-Dinamik
Assoc. Prof. Ramazan Katırcı- Sivas Technology and Science University
Assoc. Prof. Sabit Horoz- Sivas Technology and Science University
Assoc. Prof. Savaş Kaya- Sivas Cumhuriyet University
Assoc. Prof. Şölen Kınayyigit- Gebze Technical University
Asisst. Prof. Ali Suat Yıldız- Sivas Technology and Science University
Asisst. Prof. Betül Kafkaslıoğlu Yıldız- Sivas Technology and Science University
Asisst. Prof. Cengiz Coşkun- Sivas Technology and Science University Asisst. Prof. Ebru Yabaş- Sivas Cumhuriyet University
Asisst. Prof. Emre Yurtkuran- Sivas Technology and Science University
Asisst. Prof. Fuat Erden- Sivas Technology and Science University
Asisst. Prof. Hacı Mehmet Güzey- Sivas Technology and Science University
Asisst. Prof. İbrahim Korkut- Sivas Technology and Science University
Asisst. Prof. Kholoud Elmabruk- Sivas Technology and Science University
Asisst. Prof. Mehtap Yakut- Ankara University
Asisst. Prof. Nazım Babacan- Sivas Technology and Science University
Asisst. Prof. Nurbanu Güzey- Sivas Technology and Science University
Asisst. Prof. Oğuzhan Alagöz- Afyon Kocatepe University
Asisst. Prof. Salih Özbay- Sivas Technology and Science University
Asisst. Prof. Selma Yazar- Yeni Yüzyıl University
Asisst. Prof. Şevki Can Cevher- Sivas Technology and Science University
Asisst. Prof. Vildan Burgaz- Eastern Mediterranean University
Asisst. Prof. Yusuf Doğan- Sivas Technology and Science University

Dr. Ahmet Altınay- ASPİLSAN
Dr. Alper Ünlü- TEI
Dr. Aslı Sayar- TÜBİTAK MAM
Dr. Aslıhan Esra Bildirici- Exon Biyotek
Dr. Cem Kaypmaz- AVL Engineering
Dr. Gaye Sağlam- SIEMENS
Dr. Günhan Kaytaz- TÜBİTAK BİLGEM
Dr. Günseli Çubukçuoğlu Deniz- Ankara University
Dr. Serhat Gül- TUSAŞ
Dr. Sinan Yılmaz- IZMIR INSTITUTE OF TECHNOLOGY
Dr. Suat Yıldırım- TÜBİTAK BİLGEM
Dr. Şerif Kaya- Metanikel
Dr. Taner Atalar- TÜBİTAK SAGE
Dr. Ahmet H. ERTAŞ- Bursa Technical University
Dr. Akile ZENGİN- Turgut Özal University
Dr. Almaz AHMEDOV- Bakü State University
Dr. Anatoliy LOGINOV - Ukraine Shevchenko Lugan National University
Dr. Aysel GÜVEN- Başkent University
Dr. Ayslu B. SARSEKENOVA- Orleu National Development Institute
Dr. Ayşe KABATAŞ- Karadeniz Technical University
Dr. Aziz AKSOY- Bitlis Eren University
Dr. BOUKHATEM Mohamed Nadjib- Université Saad Dahlab Blida
Dr. Canan DEMİR- Van Yüzüncü Yıl University
Dr. Cholpon TOKTOSUNOVA- Rasulbekov Kyrgyz Economy University
Dr. Derya OKUYAN- Balıkesir University University
Dr. Elif Ayşe ANLI- Ankara University
Dr. Elif BAŞKAYA- Karadeniz Technical University
Dr. Fatih ÇOLAK- Usak University
Dr. Feda REHIMOV- Bakü State University
Dr. Filiz BORAN- Hitit University
Dr. George RUDIC- Montreal Pedagogy Institute
Dr. Gökhan KÖK- Ege University
Dr. Günay MERHAN MUĞLU- Atatürk University
Dr. Hale UYAR HAZAR- Aydın Adnan Menderes University
Dr. Hilale CAFEROVA- AMEA Institute
Dr. İbrahim GÜNEŞ- Istanbul Cerrahpaşa University
Dr. İsmail ALTINTOP- Kayseri State Hospital
Dr. Jale ÇATAK- Istanbul Sabahattin Zaim University
Dr. Kenes JUSUPOV- M. Tinisbaev Kazakh Vehicle Academy
Dr. Kerem ASMAZ- Yıldız Technical University
Dr. Kevser Sevgi ÜNAL ASLAN- Osmaniye Korkut Ata University
Dr. Khan Nadezhda- E.A. Buketov Karaganda State University
Dr. Leyla ÇİMEN- Gaziantep Islamic Science and Technology University
Dr. Maira ESIMBOLOVA- Kazakhstan Narkhoz University
Dr. Maria LEONTIK- Macedonia Ishtib Gotse Delchev University
Dr. Maha Hamdan ALANAZI- Riyadh King Abdulaziz Technology Institute

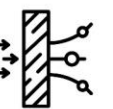
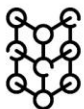
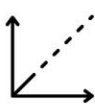
Dr. Mahmut Alkan- Niğde Ömer Halisdemir University
Dr. Mavlyanov ABDIGAPPAR- Kyrgyz Elaralık University
Dr. Meixia HUOU- Capital Normal University
Dr. Merdin DANIŞMAZ-Ahi Evran University
Dr. Merve OKUTAN-Hitit University
Dr. Mevlüt ALBAYRAK- Atatürk University
Dr. Murat EYVAZ- Gebze Technical University
Dr. Murat SÖNMEZ- METU
Dr. Mustafa ŞAHİN- Selçuk University
Dr. Mustafa TALAS- Niğde Ömer Halisdemir University
Dr. Mutlu KESKİN- Altınbaş University
Dr. Nazile Abdullazadeh- Azerbaijan State Pedagogical University
Dr. Nazmiye ÖZLEM ŞANLI- Istanbul University
Dr. Nurhayat ATASOY- Van Yüzüncü Yıl University
Dr. Özlem ÖZDEMİR- Gazi University
Dr. Remzi TUNTAŞ-Van Yüzüncü Yıl University
Dr. Rovshan ALİYEV - Bakü State University
Dr. Sevde AKSU- Balıkesir University
Dr. Seyithan SEYDOŞOĞLU- Siirt University
Dr. Şevket TULUN-Aksaray University
Dr. Şeyma AYDEMİR- Hitit University
Dr. Ümran SEVİL- Ege University
Dr. Yılmaz KOÇAK- Van Yüzüncü Yıl University
Dr. Yüksel KAPLAN - Niğde Ömer Halisdemir University



ISPEC
**15 th INTERNATIONAL CONFERENCE ON
ENGINEERING & NATURAL SCIENCES**
March 04-06, 2023 / Muş, Türkiye

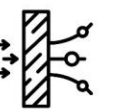
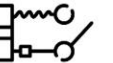
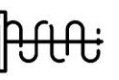
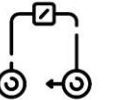
CONFERENCE PROGRAM

Online (with Video Conference) Presentation



Meeting ID: 827 4482 6818
Passcode: 040506

<https://us02web.zoom.us/j/82744826818?pwd=ejd6Q3JlbTl1TlQyQzNVdkpvL0MyUT09>



Önemli, Dikkatle Okuyunuz Lütfen

- ❖ Kongremizde Yazım Kurallarına uygun gönderilmiş ve bilim kurulundan geçen bildiriler için online (video konferans sistemi üzerinden) sunum imkanı sağlanmıştır.
- ❖ Online sunum yapabilmek için <https://zoom.us/join> sitesi üzerinden giriş yaparak “Meeting ID or Personal Link Name” yerine ID numarasını girerek oturuma katılabilirsiniz.
- ❖ Zoom uygulaması ücretsizdir ve hesap oluşturmaya gerek yoktur.
- ❖ Zoom uygulaması kaydolmadan kullanılabilir.
- ❖ Uygulama tablet, telefon ve PC’lerde çalışıyor.
- ❖ Her oturumdaki sunucular, sunum saatinden 5 dk öncesinde oturuma bağlanmış olmaları gerekmektedir.
- ❖ Tüm kongre katılımcıları canlı bağlanarak tüm oturumları dinleyebilir.
- ❖ Moderatör – oturumdaki sunum ve bilimsel tartışma (soru-cevap) kısmından sorumludur.

Dikkat Edilmesi Gerekenler- TEKNİK BİLGİLER

- ◆ Bilgisayarınızda mikrofon olduğuna ve çalıştığına emin olun.
- ◆ Zoom'da ekran paylaşma özelliğine kullanabilmelisiniz.
- ◆ Kabul edilen bildiri sahiplerinin mail adreslerine Zoom uygulamasında oluşturduğumuz oturuma ait ID numarası gönderilecektir.
- ◆ Katılım belgeleri kongre sonunda tarafınıza pdf olarak gönderilecektir
- ◆ Kongre programında yer ve saat değişikliği gibi talepler dikkate alınmayacaktır

IMPORTANT, PLEASE READ CAREFULLY

- ❖ To be able to attend a meeting online, login via <https://zoom.us/join> site, enter ID “Meeting ID or Personal Link Name” and solidify the session.
- ❖ The Zoom application is free and no need to create an account.
- ❖ The Zoom application can be used without registration.
- ❖ The application works on tablets, phones and PCs.
- ❖ The participant must be connected to the session 5 minutes before the presentation time.
- ❖ All congress participants can connect live and listen to all sessions.
- ❖ Moderator is responsible for the presentation and scientific discussion (question-answer) section of the session.

Points to Take into Consideration - TECHNICAL INFORMATION

- ◆ Make sure your computer has a microphone and is working.
- ◆ You should be able to use screen sharing feature in Zoom.
- ◆ Attendance certificates will be sent to you as pdf at the end of the congress.
- ◆ Requests such as change of place and time will not be taken into consideration in the congress program.

**Before you login to Zoom please indicate your name surname and hall number,
exp. H-1, Fatih SAYIN**

Date: 04.03.2023
Ankara Local Time: 16⁰⁰ : 18³⁰
Session - 1, Hall - 2

HEAD OF SESSION: Assoc. Prof. İsmail Kırbaş		
Moses Adeolu Agoi Oluwanifemi Opeyemi Agoi	Lagos State University of Education Obafemi Awolowo University	EVALUATING THE EFFICACY OF ARTIFICIAL INTELLIGENCE IN WIRELESS SENSOR NETWORKS
Özge Özgüner Taner Uçkan Ebubekir Seyyarer	Van Yüzüncü Yıl University Van Yüzüncü Yıl University Van Yüzüncü Yıl University	TEXT CLASSIFICATION USING MACHINE LEARNING ALGORITHMS AND DEEP LEARNING MODELS
Mohamed Al-Hattab Essaadia Oublal Mustapha Sahal L'houcine Moudou Omar Bajjou Khalid Rahmani	Government College University University Sultan Moulay Slimane University Sultan Moulay Slimane University Sultan Moulay Slimane University Sultan Moulay Slimane University Sultan Moulay Slimane University Sultan Moulay Slimane	NUMERICAL SIMULATION OF A NEW HETEROSTRUCTURE CIGS/GaSe SOLAR CELL SYSTEM USING SCAPS- 1D SOFTWARE
Preeti Singh Bahadur Shalini Jaiswal	Amity University Amity University	DIVERSE APPLICATIONS OF OPTICAL FIBER SENSORS
Gölge Ögücü Yetkin Zaid Attrah	Gaziantep University Gaziantep University	WIDEBAND MIMO 5G ANTENNAS IN HANDSETS
Kamil Aykotalp Gündüz Fatih Başçiftçi Züleyha Yılmaz Acar	Selçuk University Selçuk University Selçuk University	PERFORMANCE COMPARISON OF DIFFERENT CABLE LENGTHS IN ESP8266 BASED MICROCONTROLLER CIRCUIT OF ANALOG pH SENSOR
Ayhan Dukkancı İsmail Kırbaş	Burdur Mehmet Akif Ersoy University Burdur Mehmet Akif Ersoy University	ANOMALY DETECTION TECHNIQUES AND APPLICATIONS
Tarık Kabak İsmail Kırbaş	Burdur Mehmet Akif Ersoy University Burdur Mehmet Akif Ersoy University	CHATGPT WITH OPPORTUNITIES AND RISKS
Mourad Derra	Ibn Zohr University	MONITORING MILK ADULTERATION USING ULTRASOUND TECHNIQUE

Date: 04.03.2023
Ankara Local Time: 16⁰⁰ : 18³⁰
Session - 1, Hall - 3

HEAD OF SESSION: Asisst. Prof. Ceren Orak

M. Said Bayraklılar	Siirt University	DETERMINING THE JOHNSON COOK MODEL PARAMETERS
Ceren Orak Gülin Ersöz	Sivas University of Science and Technology Ege University	TREATMENT OF TARTRAZINE VIA SOLAR-FENTON-LIKE OXIDATION
Badis Bendjemil Khaoula Safi Ilyas Kouahla Jacques Guillome Noudem Mohamed Mouyane Jérôme Bernard David Houivet	University 8 May 1945 Guelma University 8 May 1945 Guelma ENSICAEN University of Caen Basse-Normandie University of Caen Basse-Normandie University of Caen Basse-Normandie	PRODUCTION OF β -type Nb _x Ti (x =50 at%) /SWCNTs INTERMETALLIC MATRIX NANOCOMPOSITE BY FAST-SPS FOR BIOMEDICAL AND NANOTECHNOLOGY APPLICATIONS (ITER)
E. Cuce P. M. Cuce H. Sen	Recep Tayyip Erdogan University Recep Tayyip Erdogan University Recep Tayyip Erdogan University	NUMERICAL ANALYSIS OF THE EFFECT OF COLLECTOR HEIGHT IN SOLAR CHIMNEY POWER PLANTS
E. Cuce P. M. Cuce H. Sen	Recep Tayyip Erdogan University Recep Tayyip Erdogan University Recep Tayyip Erdogan University	THE EFFECT OF THE BARRIER DESIGN ON THE HEAT CONDUCTION IN DOUBLE GLASS WINDOWS
Faqeer Muhammad Muhammad Ashan Hafiz Badaruddin Ahmad	Bahauddin Zakarya University Government Graduate College Bahauddin Zakarya University	SYNTHESIS AND CHARACTERIZATION OF HALOGEN SUBSTITUTED ORGANIC/INORGANIC HYBRID HALIDE PEROVSKITES
N. Boughazi F. Gaci A. Haddad	University 8 May 1945 Guelma University of Constantine University 8 May 1945 Guelma	MONITORING OF A PETROLEUM PRODUCT STORED IN A FLOATING ROOF STORAGE TANK
N. Boughazi A. Haddad	University 8 May 1945 Guelma University 8 May 1945 Guelma	DESIGN METHOD OF ASYMMETRIC SUPERSONIC NOZZLES
Safak Aktas Yasemin Budama-Kılınc	Yildiz Technical University Yildiz Technical University	DEVELOPMENT OF NANO DRUG CANDIDATE WITH PLANT EXTRACT FORMULATION FOR THE TREATMENT OF ATHEROSCLEROSIS AND EVALUATING IT'S IN-VITRO SAFETY

Date: 05.03.2023
Ankara Local Time: 10⁰⁰ : 12³⁰
Session - 1, Hall - 2

HEAD OF SESSION: Assist. Prof. Halil Yılmaz

Muhammed Zahid Kasapoglu Esra Avcı Osman Sağdıç	Yildiz Technical University Yildiz Technical University Yildiz Technical University	THE EFFECT OF DIFFERENT DRYING METHODS ON DRYING TIME, BIOACTIVE AND COLOR PROPERTIES OF BLUEBERRY FRUIT
Dursun Ekren	Iskenderun Technical University	TOWARD IMPROVED THERMOELECTRIC PROPERTIES IN SRTIO3
Mustafa Ertürk Söylemez Rasim Behçet Zekeriya Parlak	Muş Alparslan University Inönü University Sakarya University	NUMERICAL MODEL AND VERIFICATION OF EXPERIMENTAL RESULTS OF CENTRIFUGAL COMPRESSOR
Mustafa Ertürk Söylemez Zekeriya Parlak Rasim Behçet	Muş Alparslan University Sakarya University Inönü University	CFD ANALYSIS AND OPTIMIZATION OF TANDEM BLADE RADIAL COMPRESSOR
Muhammed Zahid Kasapoglu Esra Avcı Salih Karasu Osman Sağdıç	Yildiz Technical University Yildiz Technical University Yildiz Technical University Yildiz Technical University	POTENTIAL USE OF COLD PRESSED PUMPKIN SEED OIL BY-PRODUCTS IN THE PRODUCTION OF PLANT-BASED MILK AND LOW-FAT ICE CREAM
Halil Yılmaz Cem Örnek Bilgehan M Sesen Beste Payam	Muş Alparslan University Istanbul Technical University Max Planck Institute for Iron Research Istanbul Technical University	MICROSTRUCTURE CHARACTERIZATION AND TENSILE TESTING OF HIGH STRENGTH HYBRID STEEL TO UNDERSTAND THE EFFECT OF ELECTROCHEMICAL HYDROGEN CHARGING
E. Cuce P. M. Cuce T. Guclu	Recep Tayyip Erdogan University Recep Tayyip Erdogan University Recep Tayyip Erdogan University	RECENT APPLICATIONS OF THERMOELECTRIC COOLING DEVICES: A REVIEW OF PERFORMANCE PARAMETERS
E. Cuce P. M. Cuce T. Guclu	Recep Tayyip Erdogan University Recep Tayyip Erdogan University Recep Tayyip Erdogan University	THE EFFECT OF PELTIER POSITION ON COOLING PERFORMANCE IN THERMOELECTRIC COOLERS
Hayriye Hale Aygün	Kahramanmaraş Sütçü İmam University	OPENNED-UP E-GLASS FIBER REINFORCED EPOXY COMPOSITES: RELATIONSHIP BETWEEN FIBER ASPECT RATIO AND FLAME RESISTANCY

Date: 05.03.2023
Ankara Local Time: 10⁰⁰ : 12³⁰
Session - 1, Hall - 3

HEAD OF SESSION: Res. Asisst. Halil Kuyrukçu

Halil Kuyrukcu	Zonguldak Bülent Ecevit University	TORSION-FREE FIELD EQUATIONS OF THE VACUUM POINCARÉ GAUGE GRAVITY MODEL IN THE NONCOMPACTIFIED KALUZA-KLEIN THEORY
Hasan Kemal Sürmen Tolga Güven	İstanbul University- Cerrahpaşa İstanbul University- Cerrahpaşa	STATIC ANALYSIS OF AN AIRPLANE PASSENGER SEAT ARMREST USING THE FINITE ELEMENT METHOD
Ibrahim Maouhoubi	Sidi Mohammed ben Abdallah University	ELECTRON-IMPURITY CONFINED IN QUANTUM DOST DISK-SHAPED: INVESTIGATION OF ELECTRONIC PROPERTIES
Ibrahim Maouhoubi	Sidi Mohammed ben Abdallah University	THE INFLUENCE OF EXTERNAL/INTERNAL CONTRIBUTION ON THE IONIZATION ENERGY AND DIAMAGNETIC RESPONSE: SIZE AND APPLIED FIELDS
Muhammet Kamal	Pamukkale University	OPTIMUM DESIGN OF RC SHORT CANTILEVER OF PRECAST INDUSTRIAL BUILDINGS USING DIFFERENTIAL EVOLUTION ALGORITHM
Sabira Shahmarova Samid Shahmarov Rasim Bayramlı	Khazar University Khazar University Khazar University	EVALUATION OF AGGREGATES IN THE REGIONS OF AZERBAIJAN IN TERMS OF ALKALI-SILICA REACTION
Aminaga Sadıgov Maharram Şaliyev Samid Şahmarov	ANAS ASOIU Khazar University	APPLICATION OF GRANODIORITE AND CRUSHED RIVER STONE AGGREGATE IN PERVIOUS CONCRETE AND INVESTIGATION OF SOME PROPERTIES
Oualid Rholam	University Ibn Tofail	HERMITE-HADAMARD TYPE INEQUALITIES FOR S-CONVEX AND S-CONCAVE STOCHASTIC PROCESSES VIA FRACTIONAL INTEGRALS

Date: 05.03.2023
Ankara Local Time: 13⁰⁰ : 15³⁰
Session - 2, Hall - 2

HEAD OF SESSION: Preeti Singh Bahadur

Vidya Padmakumar Murugan Shanthakumar	Bangalore University Bangalore University	EFFECT OF METHANE GAS ON JAVELINA POPULATIONS IN THE SOUTHWESTERN US
Syed Makhdoom Hussain	Government College University	USE OF DIFFERENT SUPPLEMENTS IN CONVENTIONAL AND NON- CONVENTIONAL PLANT BY-PRODUCTS BASED AQUA-FEEDS
Yusuf Rabe Yusuf Muhammad Sanyinna Abdulhamid Ahmed	Nigerian Defence Academy Nigerian Army University Umaru Musa Yar'adua University	IDENTITY AND DISTRIBUTION OF LARVAL AND ADULT MOSQUITO SPECIES IN ZANGO LOCAL GOVERNMENT AREA, KATSINA STATE, NORTH-WESTERN NIGERIA
Irum Shaheen Khuram Shahzad Ahmad	Fatima Jinnah Women University Fatima Jinnah Women University	ORGANIC TEMPLATE ASSISTED SUSTAINABLE SYNTHESIS OF FACILE ZnONiOPdO/Pd NANOMATERIAL: ENVIRONMENTALLY BENIGN PHOTOCATALYSTS
Shalini Jaiswal Preeti Singh Bahadur	Amity University Amity University	NOVELTY IN SOCIETY WITH GREEN REVOLUTION
Mohamed Al-Hattab Essaadia Oublal Mustapha Sahal L'houcine Moudou Omar Bajjou Khalid Rahmani	University Sultan Moulay Slimane University Sultan Moulay Slimane University Sultan Moulay Slimane University Sultan Moulay Slimane University Sultan Moulay Slimane University Sultan Moulay Slimane	FIRST-PRINCIPLES CALCULATION OF THE STRUCTURAL, ELECTRONIC AND OPTICAL PROPERTIES OF GaSe _{1-x} S _x (x = 0, 0.25, 0.5 and 1) COMPOUNDS
Ibrahim Maouhoubi Izeddine Zorkani	Sidi Mohamed Ben Abdellah University Sidi Mohamed Ben Abdellah University	EFFECTS OF APPLIED MAGNETIC FIELD AND PRESSURE ON THE DIAMAGNETIC SUSCEPTIBILITY AND BINDING ENERGY OF DONOR IMPURITY IN A CIRCULAR QUANTUM DISK MADE OUT OF GaAs
Saïd Et-Taleb Asma Amjlef Salaheddine Farsad Noureddine El Alem	, Ibnou Zohr University , Ibnou Zohr University , Ibnou Zohr University , Ibnou Zohr University	EFFECT OF SPECIFIC SURFACE FOR REMOVAL OF METHYLENE BLUE DYE USING TWO TYPE OF NATURAL SAND BEFORE AND AFTER GRINDING
Gasmi Boutheyna Yallese Mohamed Athmane Bouchrit sebti Djouambi Nahla	May 8th 1945 University May 8th 1945 University May 8th 1945 University May 8th 1945 University	MODELING AND OPTIMIZATION OF SURFACE ROUGHNESS, CONSUMED POWER AND PRODUCTIVITY DURING DRY TURNING OF GRAY CAST IRON

Date: 05.03.2023
Ankara Local Time: 13⁰⁰ : 15³⁰
Session - 2, Hall - 3

HEAD OF SESSION: Asisst. Prof. Pelin Sertyesilisik

Pelin Sertyesilisik	Afyon Kocatepe University	EFFECT OF IMPERMEABLE SURFACES ON STORM WATER MANAGEMENT
Hüseyin Albayrak	Süleyman Demirel University	ROUGH FILTER CONVERGENCE OF A SEQUENCE OF FUNCTIONS
Hanane Boumaza Salim Belhadi Mohamed Athmane Yallese Abdelkrim Haddad Hadjela Salah	May 8th 1945 University May 8th 1945 University May 8th 1945 University May 8th 1945 University May 8th 1945 University	OPTIMIZATION OF MACHINING PARAMETERS IN TURNING OF INCONEL 718 WITH CERAMIC COMPOSITE TOOLS USING VIKOR METHODOLOGY
Hafiz Ubaid Ur Rehman Maaz Khan Noor Elahi Ahmad Abdullah Shees Ur Rehman	University of Engineering & Technology University of Engineering & Technology University of Engineering & Technology University of Engineering & Technology University of Engineering & Technology	REDUCTION OF LOCAL SCOUR AROUND SQUARE BRIDGE PIER USING DOUBLE HOOKED COLLAR AND BAR AS A COUNTERMEASURE
Maaz Khan Ghufran Ahmed Pasha , Sohail Iqbal Usman Ghani Afzal Ahmad	University of Engineering & Technology University of Engineering & Technology University of Engineering & Technology University of Engineering & Technology University of Engineering & Technology	NUMERICAL STUDY IN A RECIRCULATION ZONE BETWEEN TWO SUCCESSIVE SPUR DIKES WITH LARGE ROUGHNESS ELEMENTS
Merve Yılmaz Arıcı Mert Kılınçel Şenol Şirin	Düzce University Düzce University Düzce University	AN INVESTIGATION ON THE MACHINABILITY OF CARBON FIBER REINFORCED COMPOSITE PIPES IN DIFFERENT WINDING DIRECTIONS BY TURNING METHOD
Hasan Üstün Başaran	Izmir Kâtip Celebi University	COMBINING LATE EXHAUST VALVE OPENING AND CYLINDER DEACTIVATION TO ACHIEVE RAPID AFTER-TREATMENT HEAT UP IN DIESEL VEHICLES
Hadjela Salah Belhadi Salim Ouelaa Nouredine Yallese Mohamed Athmane Safi Khaoula Hanane Boumaza	University 8 may 1945 University 8 may 1946 University 8 may 1947 University 8 may 1948 University 8 may 1949 University 8 may 1950	APPLICATION OF ARAS METHOD FOR THE SELECTION OF OPTIMUM PROCESS PARAMETERS IN TURNING OF AISI 4140 ALLOY STEEL

Date: 05.03.2023
Ankara Local Time: 16⁰⁰ : 18³⁰
Session - 3, Hall - 2

HEAD OF SESSION: Prof. Dr. Suhendan Mol

Yusuf Doğru	Air Training Command	ON SOME PROPERTIES OF RICCI SOLITONS
Araz Mohammed Faraj Furgan Aslanoglu	Van Yuzuncu Yil University Van Yuzuncu Yil University	SYNTHESIS AND ACETOACETYLATION OF DIHYDROPYRIMIDINE-2,4-DIONE DERIVATIVES
Şafak Ulusoy Tamer Akan Sehban Kartal Didem Üçok Alakavuk Şehnaz Yasemin Tosun Hande Doğruyol Serap Coşansu Kamil Bostan Suhendan Mol	İstanbul University Eskişehir Osmangazi University İstanbul University İstanbul University İstanbul University İstanbul University Sakarya University İstanbul Aydın University İstanbul University	RETARDING SPOILAGE AND MAINTAINING THE QUALITY OF SEA BASS USING ATMOSPHERIC COLD PLASMA
Serap Coşansu Tamer Akan Sehban Kartal Suhendan Mol Şehnaz Yasemin Tosun Didem Üçok Alakavuk Şafak Ulusoy Hande Doğruyol Kamil Bostan	Sakarya University Eskişehir Osmangazi University İstanbul University İstanbul University İstanbul University İstanbul University İstanbul University İstanbul University İstanbul Aydın University	REDUCTION OF SALMONELLA ENTERITIDIS ON SEABASS (DICENTRARCHUS LABRAX) BY ATMOSPHERIC PRESSURE AIR AND HELIUM COLD PLASMA
Resul Özdemir Murat Taşyürek Veysel Aslantaş	Erciyes University Kayseri University Erciyes University	A NEW DEEP LEARNING MODEL FOR CHRONIC KIDNEY DISEASE PREDICTION
Tuğba Göcen	Zonguldak Bulent Ecevit University	MOLECULAR STRUCTURE ANALYSIS, ELECTRONIC PROPERTIES (HOMO-LUMO, MEP), HIRSHFELD SURFACE ANALYSIS AND MOLECULAR DOCKING STUDIES OF LUTEOLIN AS POTENT ANTIBACTERIAL AND ANTIFUNGAL AGENT
Muhammad Ikram	GC University Lahore	GO/PAA DOPED SnO ₂ QUANTUM DOTS FOR BACTERICIDAL ACTION AND INDUSTRIAL DYE DEGRADATION
Vladimir Saveljev	Konyang University	MODIFIED METHOD OF DEFERRED MOIRÉ PATTERNS TO MEASURE DISPLACEMENT
Ajiboye, A.E. Jimoh, M.O.	Kwara State University Kwara State University	ISOLATION, IDENTIFICATION AND ANTIBIOGRAM OF BACTERIA FROM SELECTED FOOD CONDIMENTS SOLD IN ILORIN, NIGERIA

Date: 05.03.2023
Ankara Local Time: 16⁰⁰ : 18³⁰
Session - 3, Hall - 3

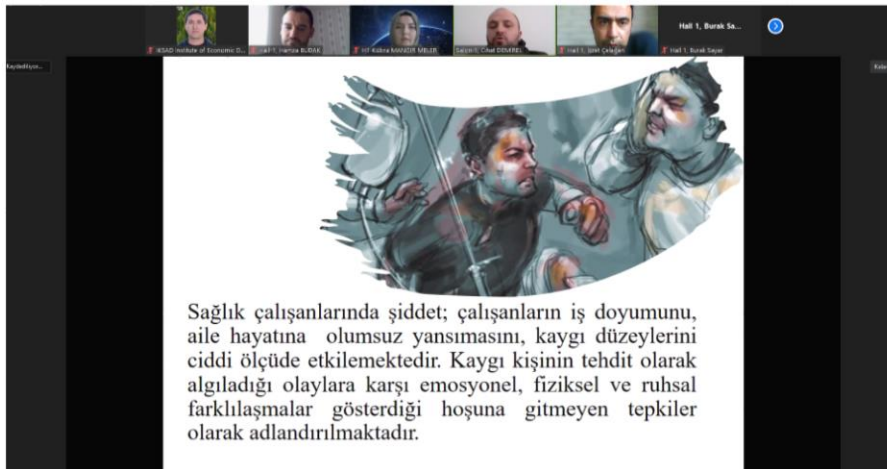
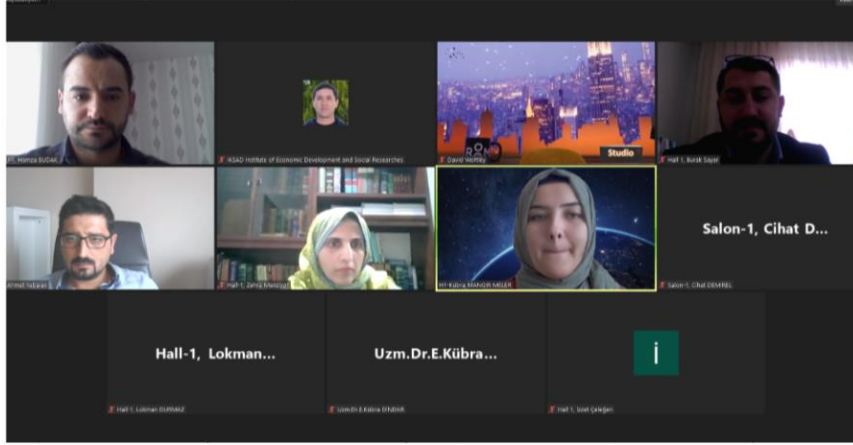
HEAD OF SESSION: Giurgiu Gheorghe

Salah Belaidi Yassmine Chennai	Mohamed Khaidhar University Mohamed Khaidhar University	QSAR MODELING USING GAUSSIAN PROCESS APPLIED FOR A SERIES OF FLAVONOIDS AS POTENTIAL ANTIOXIDANTS
Chennai Yassmine Ouassaf Mebarka	Mohamed Khaidhar University	CONTRIBUTION TO DRUG DISCOVERY THROUGH COMPUTATIONAL ANALYSIS OF SEVERAL SERIES OF HETEROCYCLIC MOLECULES
Aminu Musa Maryam Zakari Ahmed Lawal Mashi	Umaru Musa Yar'adua University Umaru Musa Yar'adua University Umaru Musa Yar'adua University	METRONIDAZOLE ADSORPTION FROM AQUEOUS SOLUTION USING NANO CRYSTALLINE CELLULOSE OBTAINED FROM LUFFA AEGYPTIACA SPONGE
Giurgiu Gheorghe Cojocaru Manole Simona Criste	Deniplant-Aide Sante Medical Center Titu Maiorescu University Central Clinic Military Hospital	DENIPLANT NUTRACEUTICALS MAY HELP FOR ENDOMETRIOSIS PAIN
Jyoti Sinha Vinod Kumar	Sushant University Sushant University	PREDILECTION OF INDIAN PORTFOLIO FRAMEWORK IN COVID-19 INFODEMIC - AN ANALYSIS
Yassmine Chennai Assma Fetteh	Mohamed Khaidhar University Mohamed Khaidhar University	ANTIBACTERIAL AND ANTI- OXIDANT ACTIVITIES OF EXTRACTS FROM MEDICINAL PLANTS
Vignesh K Manikandan K Sathiya Aravindan V Vishnupriya K	Annamalai University Annamalai University Annamalai University Annamalai University	IN VITRO EFFICACY OF TRICHODERMA ASPERELLUM AGAINST COLLAR ROT OF BRINJAL CAUSED BY SCLEROTIUM ROLFSII
Majekodunmi Racheal Adedayo Olupona Risikatun	Kwara State University Kwara State University	ANTIBIOTIC SUSCEPTIBILITY PATTERN OF STAPHYLOCOCCUS AUREUS ISOLATED FROM COMMONLY SOLD YOGHURTS IN ILORIN METROPOLIS
Ibrahim Babangida Abubakar Isah Musa Fakai Maryam Ibrahim Tukur	Kebbi State University of Science and Technology Kebbi State University of Science and Technology Kebbi State University of Science and Technology	JAUNDICE AMELIORATIVE ACTIVITY OF F. ALBIDA METHANOL STEM BARK EXTRACT

PHOTO GALLERY

Tablo 1: Sağlık Otelciliği Hizmet Kriterleri ve Gözlem Ortalamaları (Devam)

(1=Tamamen Yetersiz, 2=Yetersiz, 3=Kısmen Yeterli, 4=Yeterli, 5=Tamamen Yeterli)	
Yeterli	Gör
5.Çamaşırhane ve Terzilik Hizmetleri	
1. Kullanılan kimyasallara ait bilgi ve talimatların bulunması.	
2. Çamaşır yıkama, kurutma ve ütöleme alanlarının iş akışına göre düzenlenmesi.	
3. Gelen tekstillerin yıkama talimatlarına uygun yıkanması.	
4. Enfekte çamaşırların servislere göre ayrılarak temizlenmesi.	
5. Hastaneye ait tekstil ürünlerinin zamanında tadilatlarının yapıp ilgili birimlere teslim edilmesi.	
6. Terzihane işlem görecekt tüm ürünlerin teslim alıp/verme işlemlerinin kayıt altına alınması.	
ORTALAMA	3,8



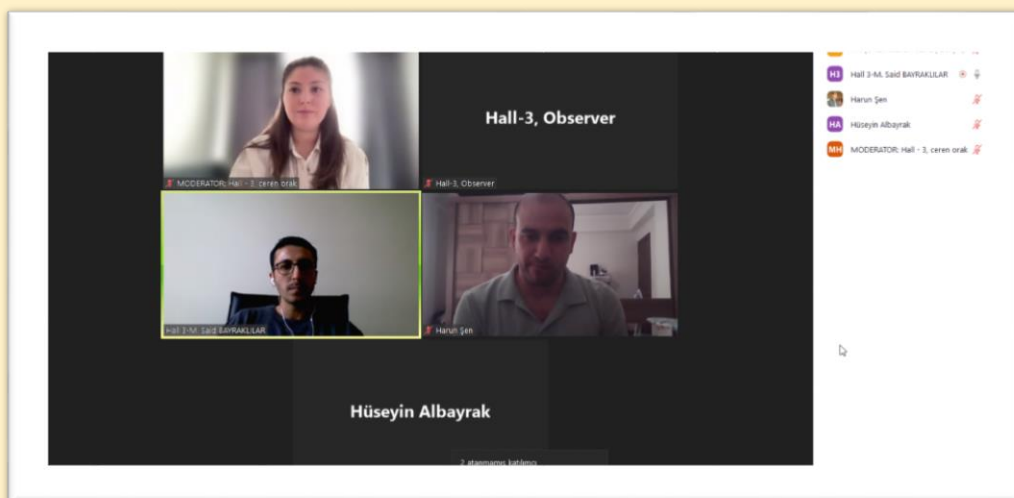


PHOTO GALLERY

ISPEC 15. ULUSLARARASI MÜHENDİSLİK VE FEN BİLİMLERİ KONGRESİ

JOHNSON COOK MODEL PARAMETRELERİNİN BELİRLENMESİ

Dr. Öğr. Üyesi M. Said BAYRAKLILAR-Siirt Üniversitesi

MODERATOR: Hall-3, C...

Hall-3, Observer

Hall-3, Observer

Hall-3 M. Said BAYRAKLILAR

Harun Şen

Hüseyin Albayrak

Hüseyin Albayrak

Nahla

Nahla

H3

Hall-3-M. Said BAYRAKLILAR

H3

Harun Şen

HA

Hüseyin Albayrak

MH

MODERATOR: Hall-3, çeren orak

N

Nahla

About 15% of these dyes are expelled into the environment with no treatment at all.

The presence of dyes in water bodies could cause environmental consequences:

- They become an obstacle for the spreading of oxygen and light
- Dyes have **complex aromatic molecular structure** and are generally **resistant** to light, temperature and oxidizers.
- This characteristic feature makes the dye **non-degradable** and thus causes **bioaccumulation** in living **organisms**, leading to severe diseases and disorders and some of their precursors and sub-product are **cancer agents**.
- They might affect the aquatic life and food web as most of them are **mutagenic and carcinogenic**.



MODERATOR: Hall-3, C...

Hall-3, Observer

Hall-3, Observer

Hall-3 M. Said BAYRAKLILAR

Harun Şen

Hüseyin Albayrak

Hüseyin Albayrak

Nahla

Nahla

H3

Hall-3-M. Said BAYRAKLILAR

H3

Harun Şen

HA

Hüseyin Albayrak

MH

MODERATOR: Hall-3, çeren orak

N

Nahla

SS

S1-H3- SAFAK AKTAS

TG

Tolga Güven

JOHNSON COOK MODEL PARAMETRELERİ

Eşdeğer Sıcaklık

$$\sigma_p = (A + B \cdot \epsilon_p^n) \cdot (1 + C \cdot \ln \dot{\epsilon}^*) \cdot (1 - \hat{T}^m)$$

Burada;

T , T_i , T_m sırasıyla mevcut sıcaklık, camsi geçiş sıcaklığı ve erime sıcaklığıdır.

Eğer $T < T_i$ ve $T > T_m \Rightarrow \hat{T}^m = 0$

Eğer $T_i < T < T_m \Rightarrow \hat{T}^m = \frac{T - T_i}{T_m - T_i}$

CY, Zhang, Z.B., Chang, X.W., Liu, X.P., Zhang, S.Z., He, J.Y., Wang, Q., Liu, J.J., 2022. "The investigation on Johnson-Cook model and dynamic mechanical behaviors of ultra-high strength steel MS4", Materials Science and Engineering-A 555, 113895.

de, B., Ferro-Cancho, F., Antico, R., Ismail, I., 2009. "An experimental and modeling study of the thermomechanical behavior of an ABS polymer structural component during an impact test", International Journal of Impact Engineering, 33(8), 547-561.

MODERATOR: Hall-3, C...

Hall-3, Observer

Hall-3, Observer

Hall-3 M. Said BAYRAKLILAR

Harun Şen

Hüseyin Albayrak

Hüseyin Albayrak

Nahla

Nahla

H3

Hall-3-M. Said BAYRAKLILAR

H3

Harun Şen

HA

Hüseyin Albayrak

MH

MODERATOR: Hall-3, çeren orak

N

Nahla

SS

S1-H3- SAFAK AKTAS

TG

Tolga Güven

PHOTO GALLERY

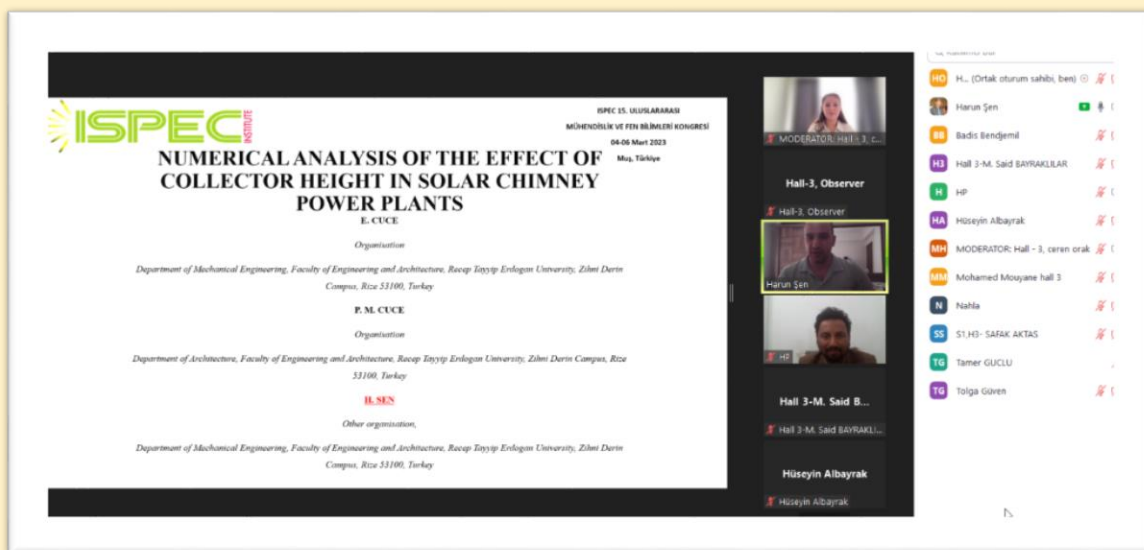
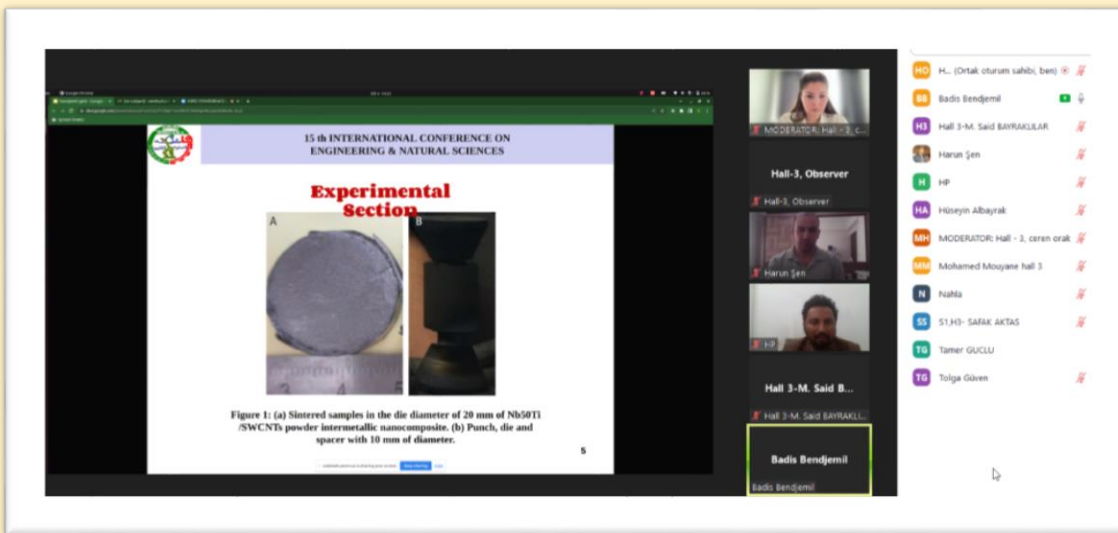
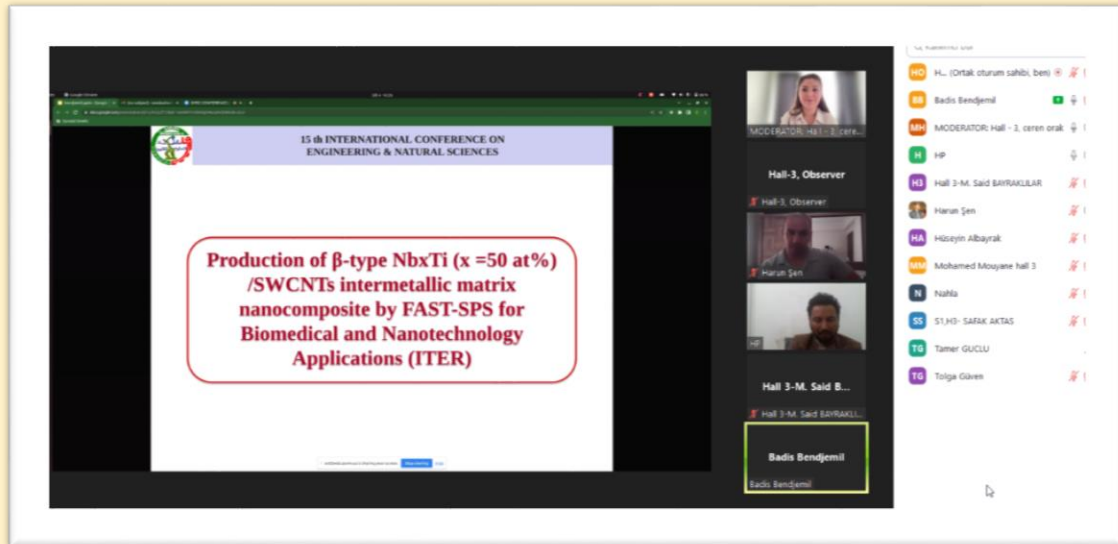
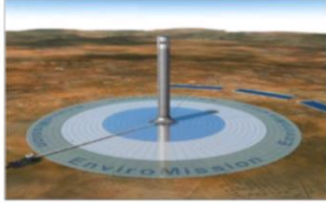




PHOTO GALLERY

SOLAR CHIMNEY POWER PLANTS



MODERATOR: Hall 3, C...

Hall-3, Observer

Hall-3, Observer

Harun Şen

HP

Hall 3-M, Said B...

Hall 3-M, Said BAYRAKL...

Hüseyin Albayrak

Hüseyin Albayrak

H., (Ortak oturum sahibi, ben)

Harun Şen

Badis Bendjemil

H3 Hall 3-M, Said BAYRAKLAR

HP

HA Hüseyin Albayrak

MH MODERATOR: Hall - 3, ceren orak

MH Mohamed Mouyane hall 3


N Nahla

SS S1.H3- SAFAK AKTAS

TG Tamer GUCLU

TG Tolga Güven

Experimental Studies



MODERATOR: Hall 3, C...

Hall-3, Observer

Hall-3, Observer

Harun Şen

HP

Hall 3-M, Said B...

Hall 3-M, Said BAYRAKL...

Nahla

Nahla

H., (Ortak oturum sahibi, ben)

Harun Şen

Badis Bendjemil

H3 Hall 3-M, Said BAYRAKLAR

HP

MH MODERATOR: Hall - 3, ceren orak


MH Mohamed Mouyane hall 3

N Nahla


SS S1.H3- SAFAK AKTAS

TG Tamer GUCLU

TG Tolga Güven



ISPEC 15. ULUSLARARASI
MÜHENDİSLİK VE FEN BİLİMLERİ KONGRESİ



ATEROSKLEROZ TEDAVİSİNDE KULLANILMAK ÜZERE BİTKİ EKSTRAKTI İÇEREN
NANO İLAÇ ADAYI GELİŞTİRİLMESİ VE *İN VİTRO* GÜVENLİĞİNİN
DEĞERLENDİRİLMESİ

...

Şafak AKTAŞ¹, Yasemin BUDAMA-KILIÇ^{2,3}

¹ Yıldız Technical University, Graduate School of Science and Engineering, Department of Biotechnology, Davutpaşa Campus, Esenler, İstanbul, Turkey
² Yıldız Technical University, Faculty of Chemical and Metallurgical Engineering, Bioengineering Department, Davutpaşa Campus, Esenler, İstanbul, Turkey
³ Health Biotechnology Joint Research and Application Center of Excellence, İstanbul, Turkey

4-6 Mart 2023 / Muş, Türkiye

MODERATOR: Hall 3, C...

Hall-3, Observer

Hall-3, Observer

HP

H3 SAFAK AKTAS

HP

Badis Bendjemil

H3 Hall 3-M, Said BAYRAKLAR

Harun Şen

MH MODERATOR: Hall - 3, ceren orak

MH Mohamed Mouyane hall 3

N Nahla

TG Tolga Güven

H., (Ortak oturum sahibi, ben)

H3.SAFAK AKTAS

MH MODERATOR: Hall - 3, ceren orak

HP

Badis Bendjemil

H3 Hall 3-M, Said BAYRAKLAR

Harun Şen

MH Mohamed Mouyane hall 3

N Nahla

TG Tolga Güven

PHOTO GALLERY

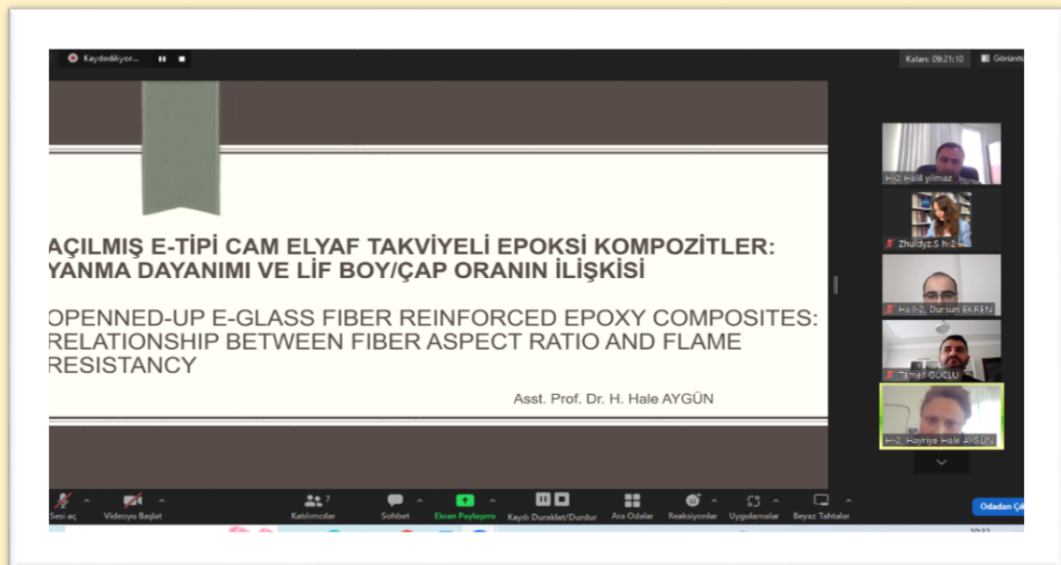
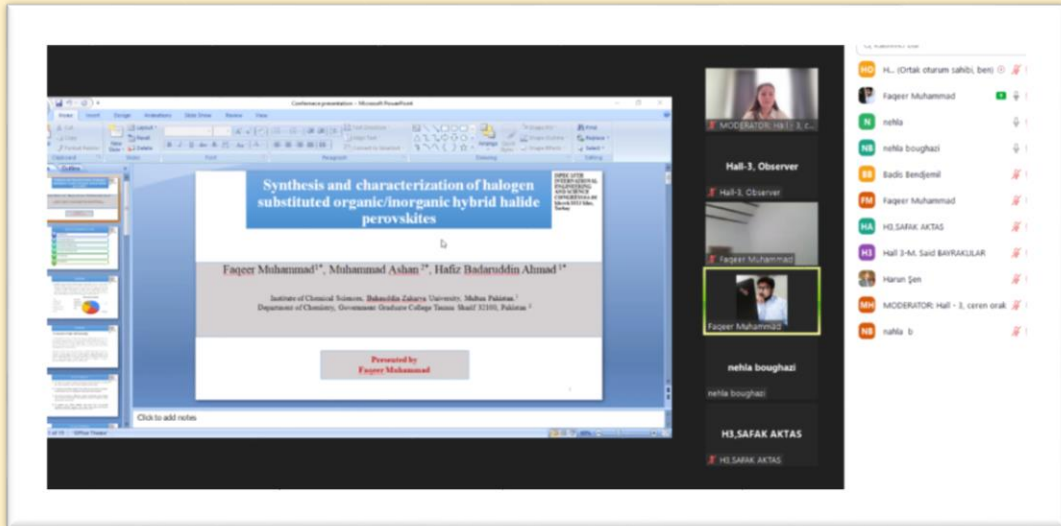


PHOTO GALLERY

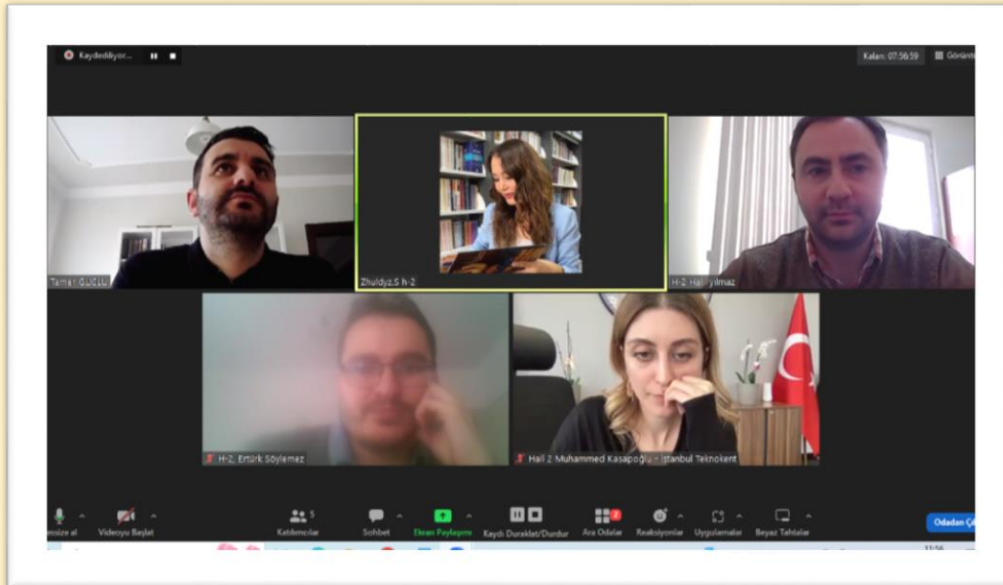
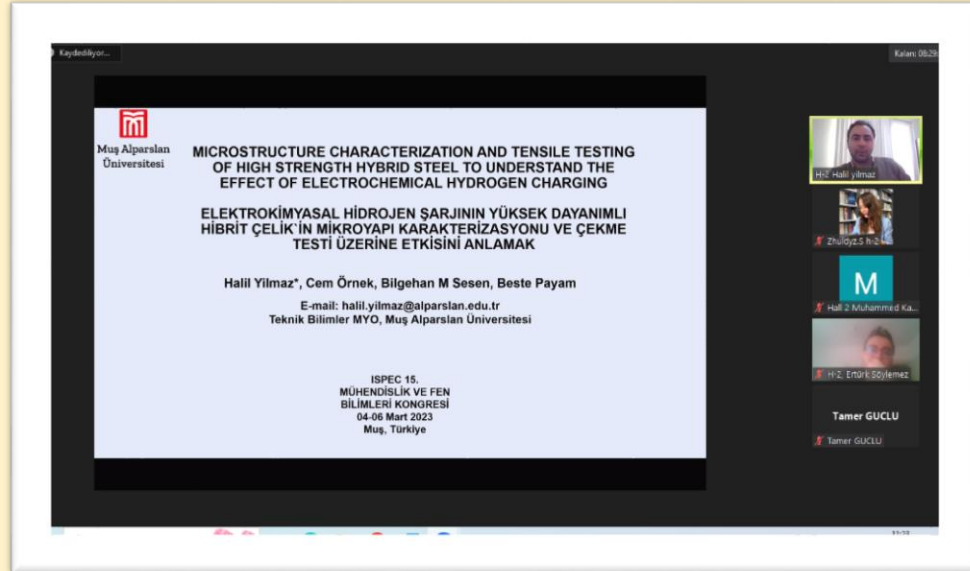
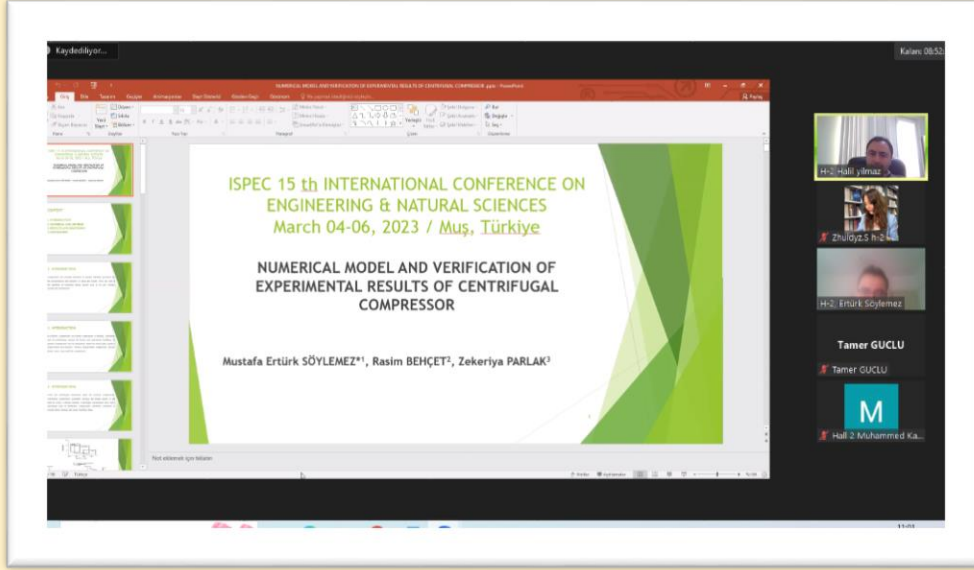


PHOTO GALLERY

GİRİŞ

- En iyi kurutma yöntemi olarak kabul edilen **dondurarak kurutma yöntemi**, duyuşali besleyici kalitesi ve rehidrasyon kapasitesi yüksek kurutulmuş ürünler elde edilmesi açısından avantajlıdır.
- Diğer yöntem ise kurutma sıcaklığını veya kurutma süresini düşürerek kurutulan ürünlerin kalitesini artırmak için sıcak hava ile kurutma yerine yaygın olarak tercih edilen **vakumlu kurutma yöntemi**dir. Vakumlu kurutma yönteminde, atmosfer basıncından daha düşük sıcaklıktaki suyun buharlaşması sonucu meyveler yüksek sıcaklıklara maruz bırakılmadan kurutulur. Ayrıca dehidrasyon sırasında oksijensiz ortamda gerçekleştiği için oksidasyon reaksiyonlarını azaltır. Bu avantajlardan dolayı kurutulmuş ürünlerin renk, tat ve aroma gibi fiziksel kaliteleri iyileştirilir.



2 atlanmış katılımcı

Thermoelectrics

- Generating electricity from waste heat through Seebeck effect.
- Performance is evaluated using dimensionless figure of merit, zT .

Power factor

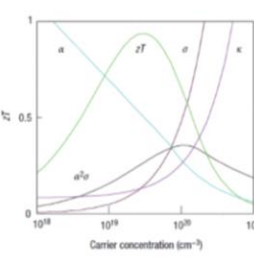
Electrical conductivity

Seebeck coefficient

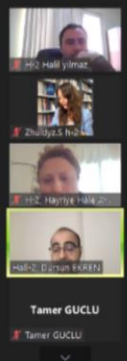
$zT = \frac{\sigma \alpha^2}{\kappa} T$

Thermal conductivity

Absolute temperature



Snyder et al., Nature Materials, 7, 185, (2008)



Tamer GÜÇLÜ

Tamer GÜÇLÜ

Thermoelectrics

- Generating electricity from waste heat through Seebeck effect.
- Performance is evaluated using dimensionless figure of merit, zT .

Power factor

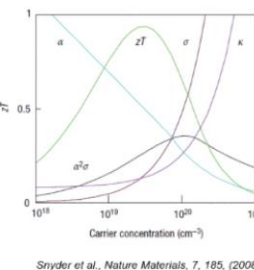
Electrical conductivity

Seebeck coefficient


$zT = \frac{\sigma \alpha^2}{\kappa} T$

Thermal conductivity

Absolute temperature



Snyder et al., Nature Materials, 7, 185, (2008)



Tamer GÜÇLÜ

Tamer GÜÇLÜ

PHOTO GALLERY

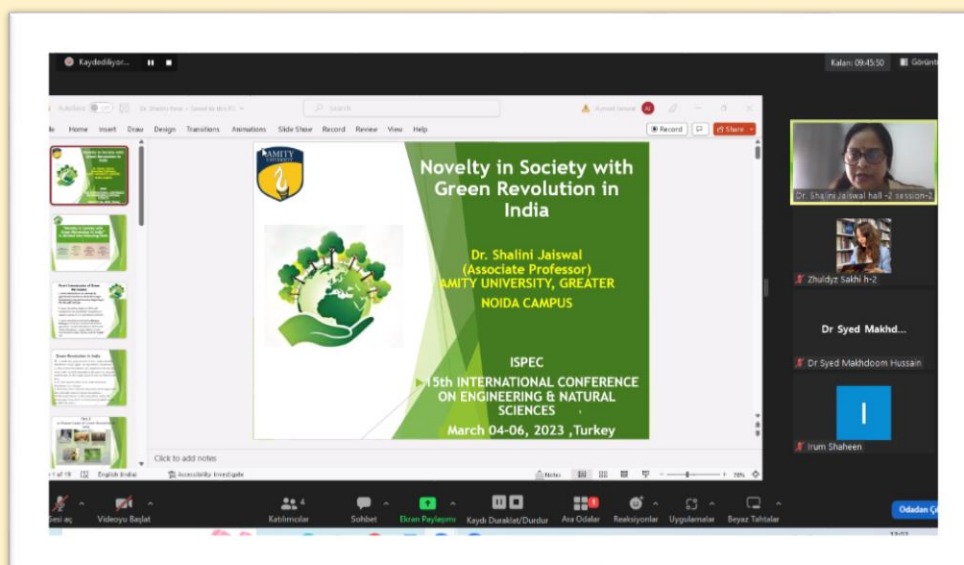
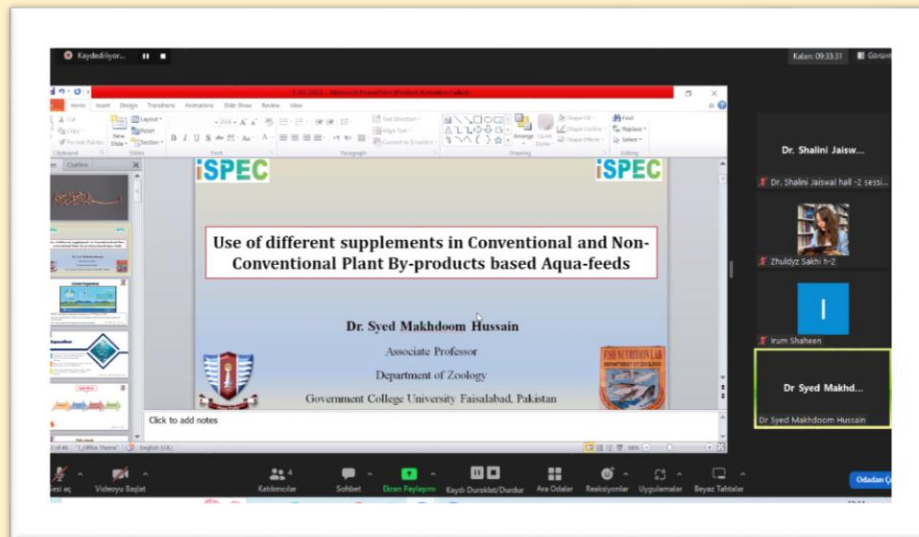


PHOTO GALLERY

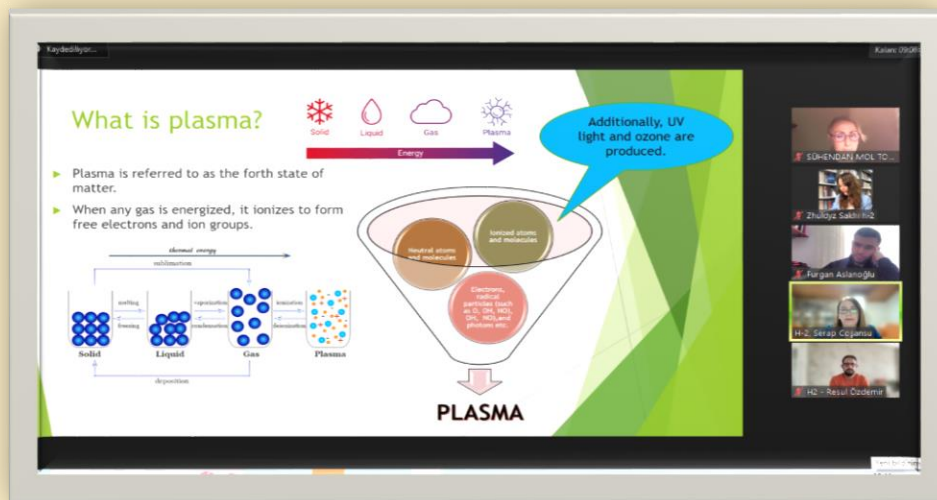
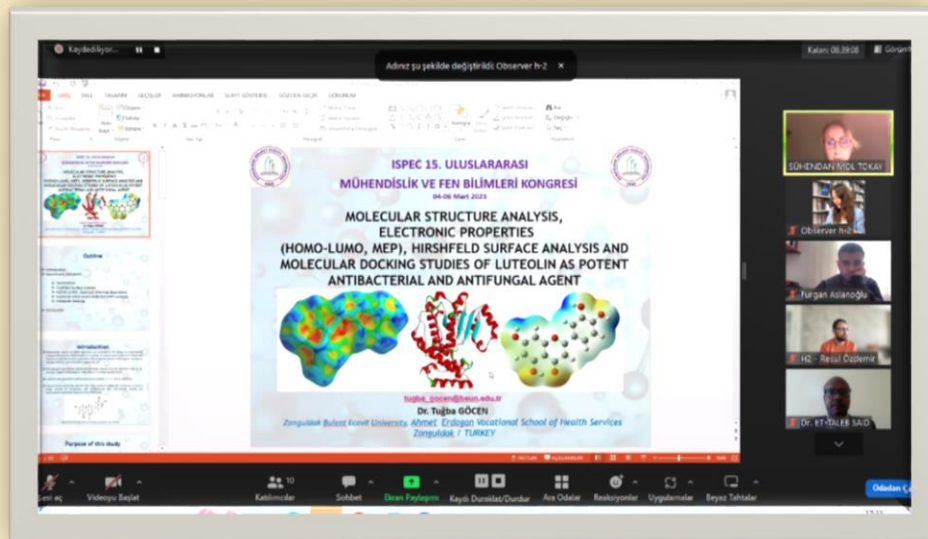
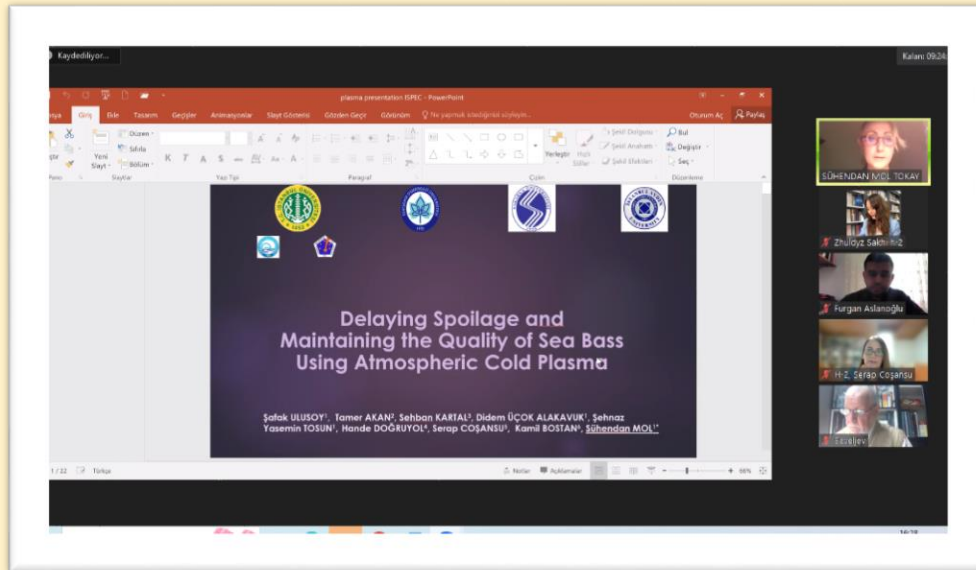
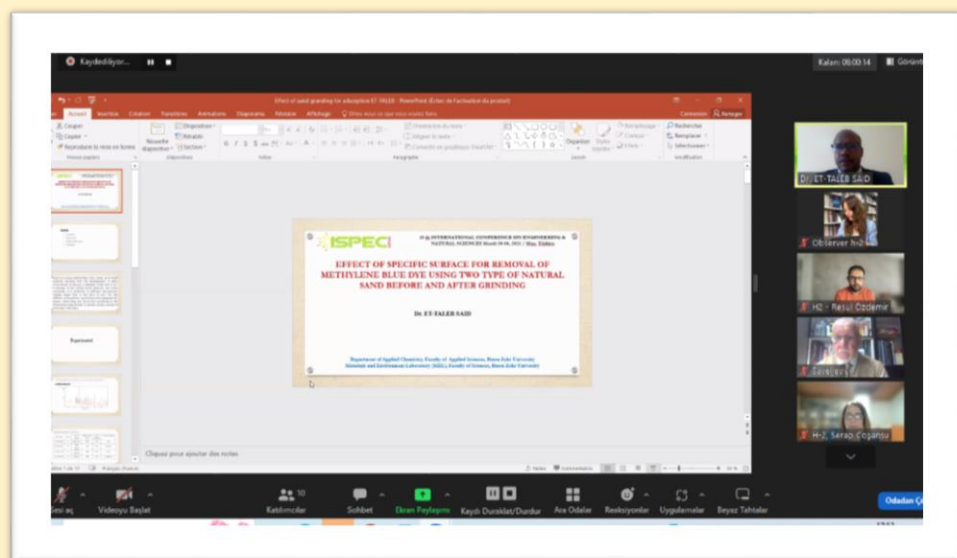
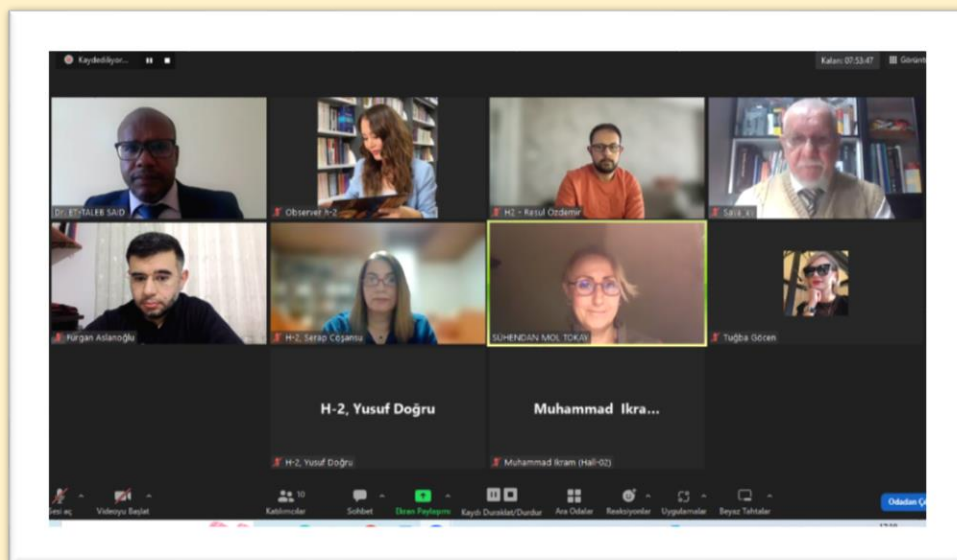
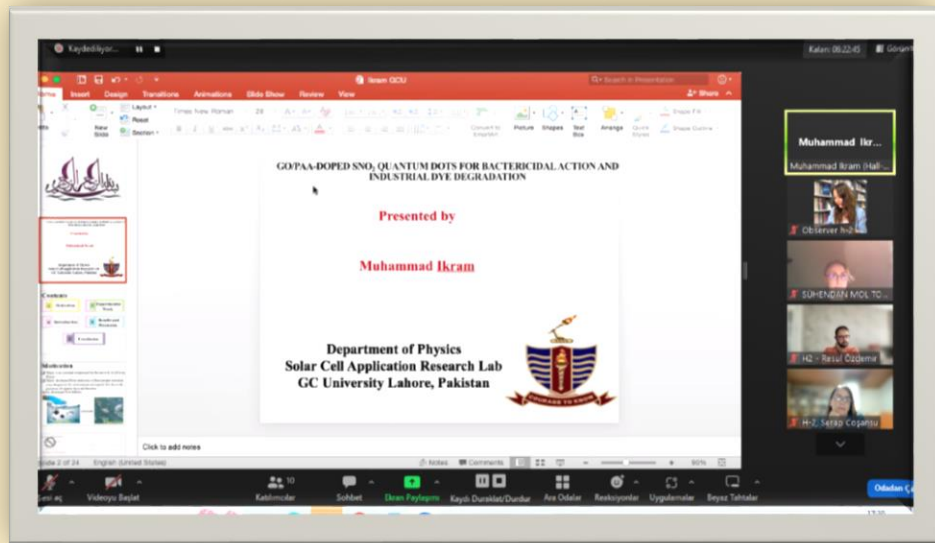


PHOTO GALLERY



CONTENT

CONFERENCE ID	I
PROGRAM	II
PHOTO GALLERY	III
CONTENT	IV

Author	Title	No
Ibrahim Maouhoubi Izeddine Zorkani	EFFECTS OF APPLIED MAGNETIC FIELD AND PRESSURE ON THE DIAMAGNETIC SUSCEPTIBILITY AND BINDING ENERGY OF DONOR IMPURITY IN A CIRCULAR QUANTUM DISK MADE OUT OF GAAS	1
Muhammad Ikram	GO/PAA DOPED SNO ₂ QUANTUM DOTS FOR BACTERICIDAL ACTION AND INDUSTRIAL DYE DEGRADATION	2
Oualid Rholam	HERMITE-HADAMARD TYPE INEQUALITIES FOR S-CONVEX AND S-CONCAVE STOCHASTIC PROCESSES VIA FRACTIONAL INTEGRALS	3
Dursun Ekren	IMPROVED THERMOELECTRIC PROPERTIES IN SRTIO ₃	4
Halil Kuyrukçu	TORSION-FREE FIELD EQUATIONS OF THE VACUUM POINCARÉ GAUGE GRAVITY MODEL IN THE NONCOMPACTIFIED KALUZA-KLEIN THEORY	5
Tuğba Göcen	MOLECULAR STRUCTURE ANALYSIS, ELECTRONIC PROPERTIES (HOMO-LUMO, MEP), HIRSHFELD SURFACE ANALYSIS AND MOLECULAR DOCKING STUDIES OF LUTEOLIN AS POTENT ANTIBACTERIAL AND ANTIFUNGAL AGENT	6
Vidya Padmakumar Murugan Shanthakumar	EFFECT OF METHANE GAS ON JAVELINA POPULATIONS IN THE SOUTHWESTERN US	7
Muhammed Zahid Kasapoglu Esra Avcı Salih Karasu Osman Sağdıç	POTENTIAL USE OF COLD PRESSED PUMPKIN SEED OIL BY-PRODUCTS IN THE PRODUCTION OF PLANT-BASED MILK AND LOW-FAT ICE CREAM	8
Muhammed Zahid Kasapoglu Esra Avcı Osman Sağdıç	THE EFFECT OF DIFFERENT DRYING METHODS ON DRYING TIME, BIOACTIVE AND COLOR PROPERTIES OF BLUEBERRY FRUIT	9
M. Said Bayraklılar	DETERMINING THE JOHNSON COOK MODEL PARAMETERS	10
Hüseyin Albayrak	ROUGH FILTER CONVERGENCE OF A SEQUENCE OF FUNCTIONS	11
Syed Makhdoom Hussain	USE OF DIFFERENT SUPPLEMENTS IN CONVENTIONAL AND NON-	12

CONVENTIONAL PLANT BY-PRODUCTS
BASED AQUA-FEEDS

Mohamed Al-Hattab L'houcine Moudou Khalid Rahmani Omar Bajjou Younes Chrafi	NUMERICAL SIMULATION OF A NEW HETEROSTRUCTURE CIGS/GASE SOLAR CELL SYSTEM USING SCAPS-1D SOFTWARE	13
Mohamed Al-Hattab Essaadia Oublal Mustapha Sahal L'houcine Moudou Omar Bajjou Khalid Rahmani	FIRST-PRINCIPLES CALCULATION OF THE STRUCTURAL, ELECTRONIC AND OPTICAL PROPERTIES OF GASE1-XX (X = 0, 0.25, 0.5 AND 1) COMPOUNDS	14
Yusuf Rabe Yusuf Muhammad Sanyinna Abdulhamid Ahmed	IDENTITY AND DISTRIBUTION OF LARVAL AND ADULT MOSQUITO SPECIES IN ZANGO LOCAL GOVERNMENT AREA, KATSINA STATE, NORTH-WESTERN NIGERIA	15
Ibrahim Maouhoubi	ELECTRON-IMPURITY CONFINED IN QUANTUM DOST DISK-SHAPED: INVESTIGATION OF ELECTRONIC PROPERTIES	16
Ibrahim Maouhoubi	THE INFLUENCE OF EXTERNAL/INTERNAL CONTRIBUTION ON THE IONIZATION ENERGY AND DIAMAGNETIC RESPONSE: SIZE AND APPLIED FIELDS	17
Badis Bendjemil Khaoula Safi Ilyas Kouahla Jacques Guillome Noudem Mohamed Mouyane Jérôme Bernard David Houivet	PRODUCTION OF B-TYPE NBXTI (X =50 AT%) /SWCNTS INTERMETALLIC MATRIX NANOCOMPOSITE BY FAST-SPS FOR BIOMEDICAL AND NANOTECHNOLOGY APPLICATIONS (ITER)	18
Salah Belaidi Yassmine Chennai	QSAR MODELING USING GAUSSIAN PROCESS APPLIED FOR A SERIES OF FLAVONOIDS AS POTENTIAL ANTIOXIDANTS	19
Chennai Yassmine Ouassaf Mebarka	CONTRIBUTION TO DRUG DISCOVERY THROUGH COMPUTATIONAL ANALYSIS OF SEVERAL SERIES OF HETEROCYCLIC MOLECULES	20
Muhammet Kamal	OPTIMUM DESIGN OF RC SHORT CANTILEVER OF PRECAST INDUSTRIAL BUILDINGS USING DIFFERENTIAL EVOLUTION ALGORITHM	21
Irum Shaheen Khuram Shahzad Ahmad	ORGANIC TEMPLATE ASSISTED SUSTAINABLE SYNTHESIS OF FACILE ZNONIOPDO/PD NANOMATERIAL: ENVIRONMENTALLY BENIGN PHOTOCATALYSTS	23
Shalini Jaiswal Preeti Singh Bahadur	NOVELTY IN SOCIETY WITH GREEN REVOLUTION	24

Serap Coşansu Tamer Akan Sehban Kartal Suhendan Mol Şehnaz Yasemin Tosun Didem Üçok Alakavuk Şafak Ulusoy Hande Doğruyol Kamil Bostan	REDUCTION OF SALMONELLA ENTERITIDIS ON SEABASS (DICENTRARCHUS LABRAX) BY ATMOSPHERIC PRESSURE AIR AND HELIUM COLD PLASMA	25
Şafak Ulusoy Tamer Akan Sehban Kartal Didem Üçok Alakavuk Şehnaz Yasemin Tosun Hande Doğruyol Serap Coşansu Kamil Bostan Suhendan Mol	RETARDING SPOILAGE AND MAINTAINING THE QUALITY OF SEA BASS USING ATMOSPHERIC COLD PLASMA	26
Hanane Boumaza Salim Belhadi Mohamed Athmane Yallese Abdelkrim Haddad Hadjela Salah	OPTIMIZATION OF MACHINING PARAMETERS IN TURNING OF INCONEL 718 WITH CERAMIC COMPOSITE TOOLS USING VIKOR METHODOLOGY	27
Aminu Musa Maryam Zakari Ahmed Lawal Mashi	METRONIDAZOLE ADSORPTION FROM AQUEOUS SOLUTION USING NANO CRYSTALLINE CELLULOSE OBTAINED FROM LUFFA AEGYPTIACA SPONGE	28
Araz Mohammed Faraj Furgan Aslanoglu	SYNTHESIS AND ACETOACETYLATION OF DIHYDROPYRIMIDINE-2,4-DIONE DERIVATIVES	29
Yusuf Doğru	ON SOME PROPERTIES OF RICCI SOLITONS	30
Halil Yılmaz Cem Örnek Bilgehan M Sesen Beste Payam	MICROSTRUCTURE CHARACTERIZATION AND TENSILE TESTING OF HIGH STRENGTH HYBRID STEEL TO UNDERSTAND THE EFFECT OF ELECTROCHEMICAL HYDROGEN CHARGING	31
Mourad Derra	MONITORING MILK ADULTERATION USING ULTRASOUND TECHNIQUE	32
Preeti Singh Bahadur Shalini Jaiswal	DIVERSE APPLICATIONS OF OPTICAL FIBER SENSORS	33
Hasan Üstün Başaran	COMBINING LATE EXHAUST VALVE OPENING AND CYLINDER DEACTIVATION TO ACHIEVE RAPID AFTER-TREATMENT HEAT UP IN DIESEL VEHICLES	34
Safak Aktas Yasemin Budama-Kılınc	DEVELOPMENT OF NANO DRUG CANDIDATE WITH PLANT EXTRACT FORMULATION FOR THE TREATMENT OF ATHEROSCLEROSIS AND EVALUATING IT'S IN-VITRO SAFETY	35
Hadjela Salah Belhadi Salim Ouelaa Nouredine Yallese Mohamed Athmane	APPLICATION OF ARAS METHOD FOR THE SELECTION OF OPTIMUM PROCESS PARAMETERS IN TURNING OF AISI 4140 ALLOY STEEL	37

Safi Khaoula Hanane Boumaza		
Saïd Et-Taleb Asma Amjlef Salaheddine Farsad Noureddine El Alem	EFFECT OF SPECIFIC SURFACE FOR REMOVAL OF METHYLENE BLUE DYE USING TWO TYPE OF NATURAL SAND BEFORE AND AFTER GRINDING	38
Gölge Ögücü Yetkin Zaid Attrah	WIDEBAND MIMO 5G ANTENNAS IN HANDSETS	39
Faqeer Muhammad Muhammad Ashan Hafiz Badaruddin Ahmad	SYNTHESIS AND CHARACTERIZATION OF HALOGEN SUBSTITUTED ORGANIC/INORGANIC HYBRID HALIDEPEROVSKITES	40
N. Boughazi F. Gaci A. Haddad	MONITORING OF A PETROLEUM PRODUCT STORED IN A FLOATING ROOF STORAGE TANK	41
N. Boughazi A. Haddad	DESIGN METHOD OF ASYMMETRIC SUPERSONIC NOZZLES	42
Giurgiu Gheorghe Cojocaru Manole Simona Criste	DENIPLANT NUTRACEUTICALS MAY HELP FOR ENDOMETRIOSIS PAIN	43
Jyoti Sinha Vinod Kumar	PREDILECTION OF INDIAN PORTFOLIO FRAMEWORK IN COVID-19 INFODEMIC - AN ANALYSIS	44
Yassmine Chennai Assma Fetteh	ANTIBACTERIAL AND ANTI- OXIDANT ACTIVITIES OF EXTRACTS FROM MEDICINAL PLANTS	45
Vignesh K Manikandan K Sathiya Aravindan V Vishnupriya K	IN VITRO EFFICACY OF TRICHODERMA ASPERELLUM AGAINST COLLAR ROT OF BRINJAL CAUSED BY SCLEROTIUM ROLFSSII	46
Majekodunmi Racheal Adedayo Olupona Risikatun	ANTIBIOTIC SUSCEPTIBILITY PATTERN OF STAPHYLOCOCCUS AUREUS ISOLATED FROM COMMONLY SOLD YOGHURTS IN ILORIN METROPOLIS	47
Ibrahim Babangida Abubakar Isah Musa Fakai Maryam Ibrahim Tukur	JAUNDICE AMELIORATIVE ACTIVITY OF F. ALBIDA METHANOL STEM BARK EXTRACT	48
Ajiboye, A.E. Jimoh, M.O.	ISOLATION, IDENTIFICATION AND ANTIBIOGRAM OF BACTERIA FROM SELECTED FOOD CONDIMENTS SOLD IN ILORIN, NIGERIA	49
Gasmi Boutheyne Yallese Mohamed Athmane Bouchrit Sebti Djouambi Nahla	MODELING AND OPTIMIZATION OF SURFACE ROUGHNESS, CONSUMED POWER AND PRODUCTIVITY DURING DRY TURNING OF GRAY CAST IRON	50
Hafiz Ubaid Ur Rehman Maaz Khan Noor Elahi Ahmad Abdullah Shees Ur Rehman	REDUCTION OF LOCAL SCOUR AROUND SQUARE BRIDGE PIER USING DOUBLE HOOKED COLLAR AND BAR AS A COUNTERMEASURE	51
FULL TEXTS		
Moses Adeolu Agoi	EVALUATING THE EFFICACY OF	52

Oluwanifemi Opeyemi Agoi	ARTIFICIAL INTELLIGENCE IN WIRELESS SENSOR NETWORKS	
Mustafa Ertürk Söylemez Rasim Behçet Zekeriya Parlak	NUMERICAL MODEL AND VERIFICATION OF EXPERIMENTAL RESULTS OF CENTRIFUGAL COMPRESSOR	57
Mustafa Ertürk Söylemez Rasim Behçet Zekeriya Parlak	CFD ANALYSIS AND OPTIMIZATION OF TANDEM BLADE RADIAL COMPRESSOR	67
Hasan Kemal Sürmen Tolga Güven	STATIC ANALYSIS OF AN AIRPLANE PASSENGER SEAT ARMREST USING THE FINITE ELEMENT METHOD	76
Özge Özgüner Taner Uçkan Ebubekir Seyyarer	TEXT CLASSIFICATION USING MACHINE LEARNING ALGORITHMS AND DEEP LEARNING MODELS	82
Ceren Orak Gülin Ersöz	TREATMENT OF TARTRAZINE VIA SOLAR- FENTON-LIKE OXIDATION	89
Resul Özdemir Murat Taşyürek Veysel Aslantaş	A NEW DEEP LEARNING MODEL FOR CHRONIC KIDNEY DISEASE PREDICTION	95
Sabira Shahmarova Samid Shahmarov Rasim Bayramlı	EVALUATION OF AGGREGATES IN THE REGIONS OF AZERBAIJAN IN TERMS OF ALKALI-SILICA REACTION	106
Aminaga Sadıgov Maharram Şaliyev Samid Şahmarov	APPLICATION OF GRANODIORITE AND CRUSHED RIVER STONE AGGREGATE IN PERVIOUS CONCRETE AND INVESTIGATION OF SOME PROPERTIES	115
Maaz Khan Ghufran Ahmed Pasha Sohail Iqbal Usman Ghani Afzal Ahmad	NUMERICAL STUDY IN A RECIRCULATION ZONE BETWEEN TWO SUCCESSIVE SPUR DIKES WITH LARGE ROUGHNESS ELEMENTS	122
Merve Yılmaz Arıcı Mert Kilingel Şenol Şirin	AN INVESTIGATION ON THE MACHINABILITY OF CARBON FIBER REINFORCED COMPOSITE PIPES IN DIFFERENT WINDING DIRECTIONS BY TURNING METHOD	130
Vladimir Saveljev	MODIFIED METHOD OF DEFERRED MOIRÉ PATTERNS TO MEASURE DISPLACEMENT	141
Pelin Sertyesilisik	EFFECT OF IMPERMEABLE SURFACES ON STORM WATER MANAGEMENT	145
Kamil Aykutanp Gündüz Fatih Başçiftçi Züleyha Yılmaz Acar	PERFORMANCE COMPARISON OF DIFFERENT CABLE LENGTHS IN ESP8266 BASED MICROCONTROLLER CIRCUIT OF ANALOG pH SENSOR	152
E. Cuce P. M. Cuce T. Guclu	RECENT APPLICATIONS OF THERMOELECTRIC COOLING DEVICES: A REVIEW OF PERFORMANCE PARAMETERS	159
E. Cuce P. M. Cuce T. Guclu	THE EFFECT OF PELTIER POSITION ON COOLING PERFORMANCE IN THERMOELECTRIC COOLERS	163
Ayhan Dükkancı Ismail Kırbaş	ANOMALY DETECTION TECHNIQUES AND APPLICATIONS	169

Tarık Kabak İsmail Kırbaş	CHATGPT WITH OPPORTUNITIES AND RISKS	178
Hayriye Hale Aygün	OPENNED-UP E-GLASS FIBER REINFORCED EPOXY COMPOSITES: RELATIONSHIP BETWEEN FIBER ASPECT RATIO AND FLAME RESISTANCY	188
E. Cuce P. M. Cuce H. Sen	NUMERICAL ANALYSIS OF THE EFFECT OF COLLECTOR HEIGHT IN SOLAR CHIMNEY POWER PLANTS	197
E. Cuce P. M. Cuce H. Sen	THE EFFECT OF THE BARRIER DESIGN ON THE HEAT CONDUCTION IN DOUBLE GLASS WINDOWS	204

EFFECTS OF APPLIED MAGNETIC FIELD AND PRESSURE ON THE DIAMAGNETIC SUSCEPTIBILITY AND BINDING ENERGY OF DONOR IMPURITY IN A CIRCULAR QUANTUM DISK MADE OUT OF GAAS

Ibrahim Maouhoubi
Izeddine Zorkani

ABSTRACT

In this work, we investigate the influence of the hydrostatic pressure, magnetic field, and conduction band non-parabolicity on both the diamagnetic susceptibility and the binding energy of shallow donor impurity in a quantum disk made out of GaAs. The Hamiltonian of the investigated problem has been solved within the framework of the effective-mass approximation. The energy minimization has been performed using variational approach. Our results reveal that both the diamagnetic susceptibility and binding energy have been reduced with increasing the disk size. Moreover, the diamagnetic susceptibility increases as the impurity moves from the extremity to the center of the disk. However, both the diamagnetic susceptibility and binding energy have been improved under applied magnetic field, hydrostatic pressure, and by considering the conduction band non-parabolicity model as well. We hope that the reported results will be a modest contribution to further theoretical research in the field of nanostructures.

Keywords: Quantum disk; Hydrostatic pressure; Magnetic field; Non-parabolicity; Diamagnetic susceptibility; Binding energy.

GO/PAA DOPED SnO_2 QUANTUM DOTS FOR BACTERICIDAL ACTION AND INDUSTRIAL DYE DEGRADATION

Muhammad Ikram

ABSTRACT

The present work demonstrates the systematic incorporation of different concentrations of graphene oxide (GO) into a fixed amount of polyacrylic acid (PAA) doped SnO_2 quantum dots (QDs) through a co-precipitation approach. The research aimed to evaluate the catalytic and antibacterial action of GO/PAA- SnO_2 QDs. Moreover, optical properties, surface morphology, crystal structure, elemental composition and d-spacing of prepared QDs were examined. XRD patterns revealed the tetragonal configuration of SnO_2 , and the crystallinity of QDs was suppressed upon dopants verified by the SAED patterns. Electronic spectra identified the blue shift by incorporating GO, and PAA led to a reduction in band gap energy. FTIR spectra showed the existence of rotational and vibrational modes associated with the functional groups during the synthesis process. A drastic increase in the catalytic efficacy of QDs was observed in the neutral medium by including dopants, indicating that GO/PAA- SnO_2 is the promising catalyst. GO/PAA- SnO_2 showed strong bactericidal efficacy against *Escherichia coli* (*E.coli*) at higher GO concentrations. Molecular docking studies predicted given nanocomposites, i.e. SnO_2 , PAA- SnO_2 and GO/PAA- SnO_2 , as potential inhibitors of beta-lactamase_{*E.coli*} and DNA gyrase_{*E.coli*}. (submitted in ACS Omega)

Keywords: SnO_2 ; PAA; graphene oxide; antimicrobial activity; catalysis

HERMITE-HADAMARD TYPE INEQUALITIES FOR S-CONVEX AND S-CONCAVE STOCHASTIC PROCESSES VIA FRACTIONAL INTEGRALS

Oualid Rholam

ABSTRACT

Abstract in this paper, we establish several inequalities for some differentiable mappings that are connected with the Riemann-Liouville fractional integrals. The analysis used allow us to obtain, some new Hermite-Hadamard type inequalities for RiemannLiouville fractional integral for stochastic processes that are s-convex and s-concave.

Keywords: Hermite-Hadamard's inequality; s-convex stochastic processe; s-concave stochastic processes; Riemann-Liouville fractional integration

TOWARD IMPROVED THERMOELECTRIC PROPERTIES IN SrTiO_3

Dursun Ekren

ORCID: 0000-0002-9080-9094

ABSTRACT

Increasing global demand for energy pushes the investigation into limiting/using the wasted energy during many industrial processes forward. The energy is mainly lost as wasted heat, and thermoelectrics (TEs) offers to generate electricity from this wasted energy to electricity. Among the materials studied for thermoelectric applications oxides are studied for high temperature applications due to their thermal and chemical stability, low toxicity, and abundance of raw materials. SrTiO_3 offers high thermoelectric power, but its thermoelectric dimensionless figure of merit is low due to its high thermal conductivity. One of the latest approaches to improving TE performance is the addition of graphene. However, the interplay between processing parameters and graphene addition complicates understanding this enhancement. Herein, we examine the effects of processing parameters and graphene addition on the thermoelectric performance of La-doped SrTiO_3 (LSTO). The thermoelectric properties of LSTO can be controlled through processing and graphene addition. By adjusting the sintering environment, the level of oxygen vacancy concentration at grain boundaries can be controlled. This is supported by the experimental work with addition of theoretical modelling. Moreover, the addition of graphene regardless of the synthesis method is beneficial for thermoelectric performance. However, the method by which the graphene is prepared is also important for maximising the improvement in the performance.

Keywords: thermoelectric, SrTiO_3 , graphene, grain boundary

TORSION-FREE FIELD EQUATIONS OF THE VACUUM POINCARÉ GAUGE GRAVITY MODEL IN THE NONCOMPACTIFIED KALUZA–KLEIN THEORY

Halil Kuyrukçu
ORCID: 0000-0002-5585-9838

ABSTRACT

By considering the five-dimensional noncompactified Kaluza–Klein metric ansatz, we investigate the vacuum field equations of the quadratic Poincaré gauge theory of gravity in the torsion-free limit. Owing to torsion, the energy–momentum tensor and spin tensor vanish, and the five-dimensional Einstein-like field equation reduces to $\hat{R}_{ANCD}\hat{R}_B{}^{NCD}-(1/4)\hat{g}_{AB}\hat{R}_{MNCD}\hat{R}^{MNCD}=0$, whereas the five-dimensional Cartan-like field equation becomes $\hat{D}_A\hat{R}^A{}_{BCD}=0$. Dimensionally reduced forms of those equations are presented in the context of Wesson’s induced matter theory, implying that a five-dimensional metric consists of a four-dimensional metric and scalar field that depend on the fifth coordinate, y , without considering the electromagnetic vector potential. Accordingly, we have six field equations that can be reduced to equations obtained by considering the limit in which the five-dimensional cylinder condition, $\partial_y\hat{g}_{AB}=0$, is applied. We examine these equations in detail. Particularly, the stress–energy tensor and spin tensor naturally emerge from the field equations as source terms in this modified gravity model. This situation is also known as the Kaluza miracle in the ordinary Kaluza–Klein theory.

Keywords: Poincaré gauge theory, Kaluza–Klein, Noncompactified, Reduced equations

MOLECULAR STRUCTURE ANALYSIS, ELECTRONIC PROPERTIES (HOMO-LUMO, MEP), HIRSHFELD SURFACE ANALYSIS AND MOLECULAR DOCKING STUDIES OF LUTEOLIN AS POTENT ANTIBACTERIAL AND ANTIFUNGAL AGENT

Tuğba Göcen

ORCID: 0000-0003-0078-8531

ABSTRACT

Luteolin is a tetrahydroxyflavone which corresponds to a flavone substituted by hydroxyl groups at the 5, 7, 3' and 4' positions. In this work, the optimized structure geometry and vibrational frequencies of the compound were obtained by DFT theory at B3LYP functional and 6-311 + +G(d,p) basis set. The optimized structural parameters (bond lengths, bond angles, torsion angles) were found to be in agreement with the X-ray crystallographic data in the literature. The 3D Hirshfeld surface and 2D fingerprint plot analyses were performed to investigate the intermolecular interactions in the crystal structure of Luteolin. The highest molecular orbital (HOMO), the lowest unoccupied molecular orbital (LUMO), and the molecular electrostatic potential (MEP) were calculated to research the nucleophilic and electrophilic attack sites. In addition, the reactivity of the molecule has been discussed by calculating some quantum chemical descriptors such as chemical potential, hardness, softness, electronegativity, electrophilicity and dipol moment. Besides, the molecular docking studies with different receptors (1LRY and 6F0E) have been performed to demonstrate that Luteolin has good antibacterial and antifungal activity.

Keywords: Luteolin, DFT calculations, HOMO, LUMO, Molecular Docking

EFFECT OF METHANE GAS ON JAVELINA POPULATIONS IN THE SOUTHWESTERN US

Vidya Padmakumar

ORCID: 0000-0002-3830-4232

Murugan Shanthakumar

ORCID: 0000-0002-6132-6288

ABSTRACT

The collared peccary, also known as the javelina (*Tayassu tajacu*), is a moderate mammal that resembles a wild boar. They are found throughout Texas, New Mexico, Arizona, and as far south as Argentina. They are characterized by their mostly short, coarse hair, short legs, and pig-like snout. Although javelinas are given a moderate conservation status, the population is in threat of extinction in a variety of its habitats. Although there are inexplicable large drop deaths that are indicative of illnesses, the territories of javelinas are also impacted by poaching and habitat degradation. An additional significant factor in the decline of javelinas is the rise in surface temperatures, which impacts the semen quality and slows down spermatogenesis. The main reasons for the rise in temperatures in the southwest US are methane emissions from oil and natural gas exploration. The ever-increasing abundance of methane in the environment is harming many wildlife species by expediting climate crisis. Reducing methane emissions from the oil and gas sector is the easiest and most cost-efficient way to slow down the rate of climate change that is now occurring and protect the wellbeing of human populations and wildlife. Controlling methane emissions is vital for javelinas, which continue to be affected from oil and gas production that destroys their habitat and increases stress on other vulnerable species by accelerating global warming.

Keywords: Javelina; *Tayassu tajacu*; methane; global warming; climate change; spermatogenesis

SOĞUK PRES KABAK ÇEKİRDEĞİ YAĞI YAN ÜRÜNLERİNİN BİTKİ BAZLI SÜT VE DÜŞÜK
YAĞLI DONDURMA ÜRETİMİNDE POTANSİYEL KULLANIMI
POTENTIAL USE OF COLD PRESSED PUMPKIN SEED OIL BY-PRODUCTS IN THE
PRODUCTION OF PLANT-BASED MILK AND LOW-FAT ICE CREAM

Muhammed Zahid Kasapoglu

ORCID: 0000-0002-2397-6984

Esra Avcı

ORCID: 0000-0003-0317-2118

Salih Karasu

ORCID: 0000-0002-2324-1865

Osman Sağdıç

ORCID: 0000-0002-2063-1462

ÖZET

Bu çalışmada, bitki bazlı süt ve dondurma üretimi için ucuz bir alternatif kaynak olarak soğuk pres kabak çekirdeği yağı yan ürününün (POB) potansiyel kullanımını araştırılmıştır. Bu amaçla dondurma karışımlarının reolojik özellikleri ile dondurma örneklerinin erime özellikleri, renk, taşma ve duyuşal özellikleri incelenmiştir. Az yağlı vegan dondurma karışımları, %0.4 ksantan sakızı (XG), %2.5 yağ, %1-3 POB ve POB sütü ve %2.5-12.5 yağ içeren kontrol vegan dondurma numuneleri kullanılarak formüle edildi. Reolojik analizi sonucu tüm dondurma numunelerinin kayma incelmeleri, katı benzeri ve geri kazanılabilir karakterler sergileyerek tam yağlı ve az yağlı bitki bazlı dondurma üretiminde ucuz bir hammadde kaynağı olarak başarıyla kullanılabileceğini göstermiştir. Emülsiyon örneklerinin kıvam katsayısı (K) değerleri arasında anlamlı fark vardı ($p<0,05$). Dondurma numunelerinin termal özellikleri, bir diferansiyel tarama kalorimetresi (DSC) ile analiz edildi. %3 POB ile stabilize edilmiş düşük yağlı POB dondurması ve tam yağlı POB dondurma örneklerinden daha düşük ΔH_f değerleri gösterdi, bu da POB dondurmasının istenen termal özellikleri gösterdiğini gösterir. Dondurma üretiminde POB kullanılan dondurma örneklerinin erime profili ve duyuşal özellikleri üzerinde olumsuz bir etki gözlemlenmemiştir.

Anahtar Kelimeler: Soğuk sıkım kabak çekirdeği yağı yan ürünü süt, vegan dondurma, DSC, duyuşal

ABSTRACT

In this study, the potential use of cold pressed pumpkin seed oil by-product (POB) as an inexpensive alternative source for plant-based milk and ice cream production was investigated. For this purpose, rheological properties of ice cream mixtures and melting properties, color, overflow and sensory properties of ice cream samples were investigated. Low-fat vegan ice cream mixes were formulated using control vegan ice cream samples containing 0.4% xanthan gum (XG), 2.5% fat, 1-3% POB and POB milk, and 2.5-12.5% fat. As a result of the rheological analysis, all ice cream samples exhibited shear thinning, solid-like and recoverable characters, showing that they can be successfully used as an inexpensive raw material source in the production of full-fat and low-fat plant-based ice cream. There was a significant difference between the consistency coefficient (K) values of the emulsion samples ($p<0.05$). The thermal properties of the ice cream samples were analyzed with a differential scanning calorimeter (DSC). Low-fat POB ice cream stabilized with 3% POB and full-fat POB ice cream showed lower ΔH_f values than samples, indicating that POB ice cream exhibited the desired thermal properties. No adverse effects were observed on the melting profile and sensory properties of ice cream samples using POB in ice cream production.

Keywords: Cold-pressed pumpkin seed oil by-product milk, vegan ice cream, DSC, sensory

FARKLI KURUTMA YÖNTEMLERİNİN YABAN MERSİNİ MEYVESİNİN KURUMA SÜRESİ, BİYOAKTİF VE RENK ÖZELLİKLERİNE ETKİSİ THE EFFECT OF DIFFERENT DRYING METHODS ON DRYING TIME, BIOACTIVE AND COLOR PROPERTIES OF BLUEBERRY FRUIT

Muhammed Zahid Kasapoglu

ORCID: 0000-0002-2397-6984

Esra Avcı

ORCID: 0000-0003-0317-2118

Osman Sağdıç

ORCID: 0000-0002-2063-1462

ÖZET

Bu çalışmada, dondurarak kurutma (FD), 50°C'de ultrason destekli vakumlu kurutma (UAVD), vakumlu kurutma (VD) ve sıcak hava (HAD) kurutma kullanılarak yaban mersini örneklerinin kurutma hızı ve bazı kalite özellikleri üzerindeki etkilerinin araştırılması amaçlanmıştır. Farklı kurutma yöntemlerinin yaban mersini meyve örneklerinin antioksidan aktiviteleri ve renk özellikleri üzerine etkileri değerlendirilmiştir. Farklı kurutma yöntemleri, yaban mersini örneklerinin tüm parametrelerini önemli ölçüde etkilemiştir ($P<0.05$). 50°C'de yaban mersini örneklerinin kuruma süresi UAVD, VD ve HAD için sırasıyla 990 dakika, 1050 dakika ve 1170 dakika olmuştur. Toplam fenolik içerik (TPC) ve antioksidan aktivite (DPPH ve ABTS yöntemi) analizine göre, FD ve VD diğer yöntemlere göre daha yüksek TPC'ye sahiptir. Diğer kurutulmuş örneklerle karşılaştırıldığında FD en yüksek renk kalitesine sahipken, VD HAD'a göre daha kısa kuruma süresi göstermiştir. Yaban mersinin kurutulmasında daha yüksek biyoaktif bileşen, daha iyi renk ve yüzey kalitesi nedeniyle HAD tekniğine bir alternatif olan UAVD, VD tekniği ile yaban mersini meyvesinin kurutulmasında farklı kurutma tekniklerinin kullanılabileceği öne sürülmüştür. Bu nedenle, yaban mersini meyvesini kurutmak için UAVD ve VD başarıyla kullanılabilir ve daha yüksek kurutma hızı ve biyoaktif bileşikler korunabilir.

Anahtar Kelimeler: Kurutma, Fenolik, Vakum Kurutma, Ultrason

ABSTRACT

In this study, it was aimed to investigate the effects of freeze drying (FD), ultrasound assisted vacuum drying at 50°C (UAVD), vacuum drying (VD) and hot air (HAD) drying on the drying rate and some quality properties of blueberry samples. The effects of different drying methods on the antioxidant activities and color properties of blueberry fruit samples were evaluated. Different drying methods significantly affected all parameters of blueberry samples ($P<0.05$). The drying time of blueberry samples at 50°C was 990 minutes, 1050 minutes and 1170 minutes for UAVD, VD and HAD, respectively. According to total phenolic content (TPC) and antioxidant activity (DPPH and ABTS method) analysis, FD retained more bioactive compounds than other methods, followed by VD. Compared to other dried samples, FD had the highest color quality, while VD showed shorter drying time compared to HAD. It has been suggested that different drying techniques can be used in the drying of blueberry fruit with the UAVD, VD technique, which is an alternative to the HAD technique due to its higher bioactive component, better color and surface quality in the drying of blueberry. Therefore, UAVD and VD can be successfully used to dry blueberry fruit, and higher drying rate and bioactive compounds can be preserved.

Keywords: Drying, Phenolic, Vacuum Drying, Ultrasound

JOHNSON COOK MODEL PARAMETRELERİNİN BELİRLENMESİ DETERMINING THE JOHNSON COOK MODEL PARAMETERS

M. Said Bayraklılar
ORCID: 0000-0002-5365-4441

ÖZET

Sonlu elemanlar yöntemi, farklı yükler altındaki dinamik tepkiyi anlamaya yardımcı olacak etkili ve düşük maliyetli bir yol olarak geniş çapta kabul görmektedir. Bu yöntem, pahalı deneyler yapmak yerine az sayıdaki deneyle doğrulanmış bir model üzerinden sonsuz sayıda deney yapma imkânı sunmaktadır. Ancak öncelikle malzemenin davranışının tanımlanması gerekmektedir. Mekanik yüklere maruz kalan malzemeler önce elastik sonra plastik şekil değiştirir ve nihayetinde kopar. Malzemenin elastik davranışı lineer olduğundan Hooke kanunuyla modellemek mümkündür. Ancak akma noktasından sonra plastik bölgeye geçilir ve lineerlik bozulur. Hooke kanunu plastik bölgedeki davranışı modelleyemeyeceğinden yeni modellere ihtiyaç duyulur. Bu modellerden birisi de Johnson Cook modelidir. Johnson Cook modeli, çeşitli yükleme koşulları altında malzemelerin davranışını tahmin etmek için genellikle sonlu elemanlar analizlerinde kullanılmaktadır. Johnson Cook model parametreleri, tasarım mühendislerinin hem deneylerde hem de simülasyonlarda farklı çalışma koşullarında malzemenin plastik davranışı üzerindeki deformasyon miktarının, genleme hızının ve sıcaklığın birleşik etkisini analiz etmesi için çok önemlidir. Johnson Cook modelinde A, B, C, n ve m olmak üzere toplam 5 parametre bulunmaktadır. Bu parametreler veya başka model parametreleri olmadan Ansys gibi simülasyon programlarında dinamik analiz yapmak mümkün değildir. Bu parametreleri bulmak için farklı genleme hızlarında ve farklı sıcaklıklarda mekanik testler yapmak gerekmektedir. Referans genleme hızında yapılan mekanik test sonucundan akma gerilmesi ve nihai gerilme sırasıyla A ve B parametrelerini oluşturacaktır. Referans genleme hızında yapılan mekanik test sonuçlarından n parametresi, farklı genleme hızlarında yapılan mekanik test sonuçlarından C parametresi ve farklı sıcaklıklarda yapılan mekanik test sonuçlarından m parametresi doğrusal olmayan GRG yöntemiyle bulunur. Bu çalışmada, ANSYS'de kullanılan Johnson Cook model parametrelerinin nasıl elde edileceği açıklanacaktır.

Anahtar Kelimeler: Johnson Cook model, Dinamik deformasyon davranışları, Genleme hızı, Sonlu Elemanlar Analizi

ABSTRACT

The finite element method is widely accepted as an effective and cost-effective way to help understand the dynamic response under different loads. This method offers the opportunity to perform an infinite number of experiments on a model that has been validated by a small number of experiments, instead of expensive experiments. However, first of all, the behavior of the material needs to be defined. Materials subjected to mechanical loads deform first elastically, then plastically, and eventually failure. Since the elastic behavior of the material is linear, it is possible to model it with Hooke's law. However, after the yield point, the plastic region is passed and the linearity is deteriorated. Since Hooke's law cannot model the behavior in the plastic region, new models are needed. One of these models is the Johnson Cook model. The Johnson Cook model is often used in finite element analysis to predict the behavior of materials under various loading conditions. Johnson Cook model parameters are crucial for design engineers to analyze the combined effect of the amount of deformation, strain rate, and temperature on the plastic behavior of the material under different operating conditions, both in experiments and simulations. The Johnson Cook model has a total of 5 parameters, A, B, C, n and m. Without these parameters or other model parameters, dynamic analysis is not possible in simulation programs such as Ansys. To find these parameters, it is necessary to perform mechanical tests at different strain rates and different temperatures. The yield stress and ultimate stress will form the parameters A and B, respectively, from the mechanical test result at the reference strain rate. The n parameter from the mechanical test results at the reference strain rate, the C parameter from the mechanical test results at different strain rates, and the m parameter from the mechanical test results at different temperatures are found by nonlinear GRG method. In this study, it will be explained how to obtain Johnson Cook model parameters used in ANSYS.

Keywords: Johnson Cook Model, Dynamic deformation behaviors, Strain rate, Finite Element Analysis.

ROUGH FILTER CONVERGENCE OF A SEQUENCE OF FUNCTIONS

Hüseyin Albayrak
ORCID: 0000-0001-8275-089X

ABSTRACT

A family F is called a filter on the set \mathbb{N} of positive integers if it satisfies the following properties:

- (1) $\emptyset \notin F$,
- (2) If $A, B \in F$ then $A \cap B \in F$,
- (3) If $A \in F$ and $A \subseteq B$ then $B \in F$.

Let (X, ρ_X) be a metric space and let $(x_n)_{n \in \mathbb{N}}$ be a sequence in this space. The sequence (x_n) is said to be filter convergent (briefly, F -convergence) to the number $x \in X$ if for every $\varepsilon > 0$ we have

$$\{n \in \mathbb{N} : \rho_X(x_n, x) < \varepsilon\} \in F.$$

In this case we write $F\text{-}\lim_{n \rightarrow \infty} x_n = x$.

Let $r \geq 0$. The sequence (x_n) is called rough filter convergent (briefly, r - F -convergence) to $x \in X$ by r roughness degree, if

$$\{n \in \mathbb{N} : \rho_X(x_n, x) < r + \varepsilon\} \in F$$

for every $\varepsilon > 0$. Then we write $r\text{-}F\text{-}\lim_{n \rightarrow \infty} x_n = x$.

In this work, we introduce the concepts of rough filter pointwise convergence (briefly, r - F -pointwise convergence), rough filter uniform convergence (briefly, r - F -uniform convergence) and rough filter α -convergence (briefly, r - F - α -convergence) for the sequences of functions defined on metric spaces. In addition, we define the concepts of rough exhaustiveness (briefly, r -exhaustiveness) and rough filter exhaustiveness (briefly, r - F -exhaustiveness) by generalizing the concept of exhaustiveness. Then the relationships between these types of convergence and their classical versions are given. Similarly, we give the relationships among exhaustiveness, r -exhaustiveness and r - F -exhaustiveness. Moreover using the concept of exhaustiveness, we examine the relationships among r - F -pointwise convergence, r - F -uniform convergence and r - F - α -convergence. Finally, we give some results related to rough continuity of the limit function using these types of convergences

Keywords: Rough filter pointwise convergence, rough filter uniform convergence, rough filter α -convergence, rough exhaustive, rough filter exhaustive

15th INTERNATIONAL CONFERENCE ON ENGINEERING & NATURAL SCIENCES

March 04-06, 2023 Muş, TÜRKİYE

USE OF DIFFERENT SUPPLEMENTS IN CONVENTIONAL AND NON-CONVENTIONAL PLANT BY-PRODUCTS BASED AQUA-FEEDS

Syed Makhdoom Hussain

ABSTRACT

In the current talk will discuss about the use of conventional and non-conventional plant by-products in aqua-feeds to promote the sustainable production of multiple fish species in aquaculture. The development of sustainable protein sources to substitute fish meal in aqua-feeds is critical to the continued growth and intensification of aquaculture productivity. Fish feed plays an important role in the growth of the aquaculture industry. Fishmeal (FM) has been employed as the principal protein element in aquaculture because of its beneficial essential amino acids, high digestibility, and palatability. Fishmeal prices are expected to rise by 20% between now and 2030 because of rising demand and increased output. This requires the search for better FM alternatives for long term aqua-feed production. In this light, much efforts have been conducted to seek the sustainable supplies of protein sources to substitute FM. Good nutrition in production systems is essential to economically produce a healthy, high product the first consideration for formulation of feed is the quality of the feed ingredients. Use of plant protein source in the feed industry has been in practice for various advantages such as sustainability, availability, cost effectiveness etc. Because of their high protein content, excellent amino acid profile, low cost, and year-round availability, they are commonly utilized as a cost-effective alternative to high-quality fish meal in diets for many aquaculture fish species. *Moringa oleifera* leaf meal, *Moringa oleifera* seed meal, Canola meal, Sunflower meal, and Cottonseed meal have all been studied extensively. Different supplements, such as enzymes, probiotics, organic acids, and Nano-particles, are also given to fish meals in addition to plant by-products. All of these factors help fish species enhance their growth, nutrient digestibility, and body composition.

Keywords: plant by-products, replacement, feed formulation, cost effective, environment friendly

NUMERICAL SIMULATION OF A NEW HETEROSTRUCTURE CIGS/GASE SOLAR CELL SYSTEM USING SCAPS-1D SOFTWARE

Mohamed Al-Hattab
L'houcine Moudou
Khalid Rahmani
Omar Bajjou
Younes Chrafi

ABSTRACT

This paper presents numerical studies of the novel heterostructure (Mo/CIGS/GaSe/ITO and ITO/GaSe/CIGS/CIGS-HTL/Mo) of the GaSe-based solar cell using the SCAPS-1D simulator. The objective of this research is to explore the influence of different parameter on the performance of the proposed cell. Based on the proposed device architecture, the effects of thickness, carrier concentration, working temperature and resistors R_s and R_{sh} are investigated for improving cell performance. The performance of the cell was found to depend on the concentration of carriers and the thickness of the GaSe-ETL (Electron transport layer) electron transport layer, CIGS absorber layer and CIGS-HTL (Hole transport layer), respectively. The open circuit voltage of the proposed cell was increased to 309 mV after using CIGS-HTL, indicating a significant reduction in the rate of surface recombination at the CIGS/electrode interface. An efficiency improvement of about 10.06 % was observed after using CIGS-HTL in the GaSe-based heterojunction solar cell.

Keywords: SCAPS-1D; CIGS; CIGS-HTL; GaSe-ETL; heterojunction solar cell;

FIRST-PRINCIPLES CALCULATION OF THE STRUCTURAL, ELECTRONIC AND OPTICAL PROPERTIES OF $\text{GaSe}_{1-x}\text{S}_x$ ($x = 0, 0.25, 0.5$ AND 1) COMPOUNDS

Mohamed Al-Hattab
Essaadia Oublal
Mustapha Sahal
L'houcine Moudou
Omar Bajjou
Khalid Rahmani

ABSTRACT

The industry has long sought ever more efficient materials, allowing it to meet market demand. For this purpose, doping remains a good choice for improving the properties of a material. The structural, electronic, optical properties of the $\text{GaSe}_{1-x}\text{S}_x$ ($x = 0, 0.25, 0.5$ and 1) compounds are studied using the pseudopotential method of first principles in the Density Functional Theory using CASTEP code. The calculated results show that the lattice constants of $\epsilon\text{-GaSe}$ decrease as function of the impurity concentration increases. Also, the increase of doping by the *sulphur* leads to a decrease of $D_{\text{Ga-X}}$ and an increase of $D_{\text{Ga-Ga}}$. The values of the gap energy are increased with the increase in *sulphur* content. For optical calculations the results show the appearance of an absorption peak in all $\text{GaSe}_{1-x}\text{S}_x$ ($x = 0, 0.25, 0.5$ and 1) structures, with different intensities and a shift of the band to lower wavelengths when the doping content by the *sulphur* is increased. The insertion of the *sulphur* atom reduces the refractive index of $\epsilon\text{-GaSe}$, and increases its birefringence which is important for non-linear optics applications. Raman lines move to higher frequencies with increasing *sulphur* content indicating a change in the crystal structure of $\epsilon\text{-GaSe}$.

Keywords: $\text{GaSe}_{1-x}\text{S}_x$; structural property; electronic property; optical property; DFT

IDENTITY AND DISTRIBUTION OF LARVAL AND ADULT MOSQUITO SPECIES IN ZANGO LOCAL GOVERNMENT AREA, KATSINA STATE, NORTH-WESTERN NIGERIA

Yusuf Rabe
Yusuf Muhammad Sanyinna
Abdulhamid Ahmed

ABSTRACT

Mosquitoes (Diptera: Culicidae) transmit several most important life-threatening infectious diseases worldwide, including Malaria, Encephalitis, Lymphatic Filariasis, West Nile Virus, Chikungunya, Yellow Fever, as well as Zika and Dengue Virus. This study examined the identity and distribution of larval and adult mosquito species in Zango Local Government Area, Katsina State, North-Western Nigeria. This is a descriptive cross sectional research that employed survey and laboratory practical to generate data. Four communities (Rogogo, Yardaje, Rindi and Zango) in the study area were randomly selected for the study. Eight houses were randomly selected from each community for entomological studies of indoor-biting and resting mosquitoes. Ladles/pipetting were used for collection of larvae in small ground pools, earthen pots and discarded tyres whereas dipping method was used to collect larvae in large breeding sites such as pond and dams. MS-Excel and Graph Pad Instat software were used for data analysis. Five hundred and thirty-one (531) mosquito larvae and 785 adult mosquitoes were collected from 35 breeding sites and 32 households respectively. Majority of the larvae collected belong to the genus *Anopheles* with *A. gambiae* species accounting for 56.3%. The adult mosquito species collected were identified as: *Anopheles gambiae* (69.2%), *Anopheles arabiensis* (5.7%) and *Anopheles funestus* (4.5%), while non-malaria vectors were: *Culex quinquefasciatus* (14.4%) and *Aedes aegypti* (6.2%) respectively. This study provides a baseline data on the mosquito vector species (especially *Anopheles*) in the area. Proper environmental sanitation, proper sewage system, clearing bushes around the houses and any possible mosquito breeding sites are therefore, recommended.

Keywords: Identity, Distribution, Mosquito; Malaria; Zango Local Government Area.

ELECTRON-IMPURITY CONFINED IN QUANTUM DOST DISK-SHAPED: INVESTIGATION OF ELECTRONIC PROPERTIES

Ibrahim Maouhoubi
ORCID: 0000-0002-7331-329X

ABSTRACT

In this work, we investigate the influence of the hydrostatic pressure, magnetic field, and conduction band non-parabolicity on both the diamagnetic susceptibility and the binding energy of shallow donor impurity in a quantum disk made out of GaAs. The Hamiltonian of the investigated problem has been solved within the framework of the effective-mass approximation. The energy minimization has been performed using variational approach. Our results reveal that both the diamagnetic susceptibility and binding energy have been reduced with increasing the disk size. Moreover, the diamagnetic susceptibility increases as the impurity moves from the extremity to the center of the disk. However, both the diamagnetic susceptibility and binding energy have been improved under applied magnetic field, hydrostatic pressure, and by considering the conduction band non-parabolicity model as well. We hope that the reported results will be a modest contribution to further theoretical research in the field of nanostructures.

Keywords: Quantum disk; Hydrostatic pressure; Magnetic field; Non-parabolicity; Diamagnetic susceptibility; Binding energy.

THE INFLUENCE OF EXTERNAL/INTERNAL CONTRIBUTION ON THE IONIZATION ENERGY AND DIAMAGNETIC RESPONSE: SIZE AND APPLIED FIELDS

Ibrahim Maouhoubi
ORCID: 0000-0002-7331-329X

ABSTRACT

In this study, the electron-impurity distance and the binding energy of a semiconductor quantum disk made out of GaAs are theoretically investigated by solving the Schrödinger equation in presence of an external lateral electric field by considering the position-dependent effective masse and dimension effects. The calculations have been performed by adopting the variational approach within the effective mass theory considering an infinite confining potential. Our findings indicate that the size and electric field strength decrease the binding energy while improving the electron-impurity distance. Furthermore, the incorporation of the position-dependent effective masse enhances the binding energy but reduces the electron-impurity distance. Hence, the direction of the lateral electric field plays a significant role in the behavior change of the quantum disk's binding energy and electron-impurity distance

Keywords: Binding energy; Quantum disk; lateral electric field; donor impurity; position dependent effective masse.

PRODUCTION OF B-TYPE Nb_xTi (X =50 AT%) /SWCNTs INTERMETALLIC MATRIX NANOCOMPOSITE BY FAST-SPS FOR BIOMEDICAL AND NANOTECHNOLOGY APPLICATIONS (ITER)

Badis Bendjemil
Khaoula Safi
Ilyas Kouahla
Jacques Guillome Noudem
Mohamed Mouyane
Jérôme Bernard
David Houivet

ABSTRACT

The synthesis of β -type Nb_xTi (x =50 at%) /SWCNTs intermetallic matrix nanocomposite by mechanical alloying (MA) to ensure the effective distribution of single walled carbon nanotubes (SWCNTs) within the matrix. It has been stated by several researchers that during ball-milling of Nb_xTi (x =50 at%) powder mixtures, Nb-Ti intermetallic compound formation occurs either gradually along milling time, or suddenly through a mechanically self-propagating reaction (MSPR), which occurs after a ignition time of MA. For this purpose, 0.4 and 0.8 wt% of SWCNTs were added to the powder mixture after the completion of reaction between Nb and Ti. The resultant powders Nb₅₀Ti intermetallic compound and with an addition of powder of SWCNTs and then also ball-milled.

Bulk samples were compacted and then sintered by field activated sintering technique spark plasma sintering method (FAST-SPS) at lower temperature in the range (1273 to 1473 K) with short time that retained the integrity of SWCNTs in the intermetallic matrix. Structural and characteristics evolutions of the nanocomposites were investigated by X-ray diffractometry (XRD). field emission scanning electron microscopy (FESEM) micrographs showed that the offered MA approach caused the SWCNTs to uniformly embed in the in situ synthesized NbTi intermetallic matrix. Meanwhile better distribution of SWCNTs resulted in higher density of FAST-SPS-FCT bulk nanocomposite as well as higher hardness up to 2.75 GPa compared to 2.4 of Nb₅₀Ti intermetallic alloy obtained from the after MA time. The total porosity, compressive strength, and compressive elastic modulus of the FAST-SPS-FCT manufactured material were determined as 7%, (600 and 120) MPa, respectively. The alloy's and its intermetallic nanocomposite have Young's elastic modulus is comparable to that of healthy cancellous bone which makes it applicable in the biomedical field.

The in vitro biocompatibility will be performed in the near future. The comparable results for the FAST-SPS-FCT nanocomposites were 3%, (650 and 130) MPa. The alloy's elastic modulus is comparable to that of healthy cancellous bone. This difference in mechanical properties results from different porosity and phase composition of the β -phase Nb_xTi (x =50 at%) and Nb_xTi (x =50 at%) /SWCNTs intermetallic matrix nanocomposite.

More other nanotechnologies applications of the nanocomposite will be focused in the study of the superconducting type I for the ITER Poloidal Field Coils by measuring of J_c (T, B) characteristics.

Keywords: β - Nb_xTi (x =50 at%), SWCNTs, FAST-SPS-FCT, compressive strength, compressive elastic modulus, Porosity architecture, Cancellous bone, ITER Poloidal Field Coils

QSAR MODELING USING GAUSSIAN PROCESS APPLIED FOR A SERIES OF FLAVONOIDS AS POTENTIAL ANTIOXIDANTS

Salah Belaidi
Yassmine Chennai

ABSTRACT

For decades, flavonoids have been the core of diverse research, especially for their significant antioxidant activity. They have several biological activities, and they are used as anticancer, antileishmanial, anti-inflammatory, and antiaging compounds. However, current researchers are very much interested in the antioxidant activity of flavonoids since oxidative stress is strongly related to several diseases. In this study, we have chosen to elaborate on a quantitative structure-antioxidant activity relationship (QSAR) using a statistical method called Gaussian process (GP). The main advantage of this method compared to other techniques currently used in QSAR studies is that it does not increase the complexity of learning tests. Typical QSAR studies use common techniques such as the artificial neural method, multiple linear regression, and partial least squares regression. The aim of this work was to use a statistical technique little known in pharmaceutical chemistry, the Gaussian process regression which is rarely used to build a QSAR model. Finally, we have also demonstrated that GP is reliable and capable of predicting the antioxidant activity with a respectable record (R^2_{pred}) which is equal to 0.86, so it is much higher than the reference value of 0.6. Therefore, we estimate that this reliable model can be used to predict the antioxidant activity of a series of new molecules. Also, based on the HC results, our set was divided into four separate clusters according to the presence of glycosides and the molar weight of the flavonoids.

Keywords: Flavonoids, Antioxidant, QSAR, Gaussian process, PCA, HCA.

CONTRIBUTION TO DRUG DISCOVERY THROUGH COMPUTATIONAL ANALYSIS OF SEVERAL SERIES OF HETEROCYCLIC MOLECULES

Chennai Yassmine
Ouassaf Mebarka

ABSTRACT

Breast cancer is the most common type of female cancer. One class of hormonal therapy for breast cancer drugs -non steroidal aromatase inhibitors- are triazole analogues. In this work a fundamental and original research was made on the molecule of triazole heterocyclic, whose aim is to predict the reactivity and biological activity studied of the compound. It is based on different computational and approaches used in computer aided -drug-design. (SPR, QSAR, molecular docking, ADMET). A study of structure – property relationships (SPR) for 1,2,3 triazole derivatives has been carried. A linear quantitative structure activity relationship model is obtained using Multiple Linear Regression (MLR) analysis as applied to a series of triazole derivatives with inhibitory activity of the aromatase. The accuracy of the proposed MLR model is illustrated using the following evaluation techniques: cross validation, and external test. Docking process, the interaction and binding of ligands – protein was done and visualized using software Molegro Virtual Docking. Molinspiration and ADMETSAR web servers used to calculate ADMET and physicochemical properties of the target compounds respectively. The results are reported and discussed in the present investigation. A close agreement with experimental results was found which improves the affinity of the present work.

Keywords: 1,2,3-triazole, aromatase inhibitory, density functional theory, QSAR, MLR, ADMET, docking molecular

ÖNÜRETİMLİ BETONARME BİNALARDAKİ KISA KONSOL ELEMANLARIN DİFERANSİYEL EVRİM ALGORİTMASI KULLANILARAK OPTİMUM TASARIMI OPTIMUM DESIGN OF RC SHORT CANTILEVER OF PRECAST INDUSTRIAL BUILDINGS USING DIFFERENTIAL EVOLUTION ALGORITHM

Muhammet Kamal
ORCID: 0000-0001-6648-2346

ÖZET

Önüretimli (prefabrik) betonarme yapı tipi, büyük açıklıkların geçilebilmesi, hızlı yapım süresi ve kontrollü koşullarda beton dökülebilmesi gibi avantajları nedeniyle endüstriyel yapılarda sıklıkla tercih edilmektedir. Önüretimli betonarme elemanlar şantiye (saha) ortamında birleştirileceği için bu yapılarda genellikle pimli (moment aktarmayan) birleşimler tercih edilmektedir. Parça parça üretilen kolon ve kiriş elemanlarının birleşim noktalarında kısa bir konsola ihtiyaç duyulmaktadır. Bu elemanlar, kirişlerden (mertek veya vinç kirişi vb.) gelen düşey ve yatay yükleri kolonlara güvenli bir şekilde aktarma konusunda başarılıdır. Bu nedenle, "kısa konsol" olarak adlandırılan bu elemanlar, endüstriyel prefabrik betonarme yapılarda yaygın olarak kullanılmaktadır. Bu betonarme kısa konsolun tasarımı, yüklerin güvenli bir şekilde iletilmesinin yanı sıra sınırlı kaynakların etkin kullanımı adına minimum malzeme ile tasarlanması önemlidir. Minimum malzeme kullanımının hedeflenebilmesi için optimizasyon tekniklerinin tasarım süreçlerine dahil edilmesi gerekmektedir. Birçok karmaşık mühendislik probleminin çözümünde, kolay programlanabilir ve optimum çözüme yakın sonuçlar üretebilmesinden dolayı sezgisel optimizasyon algoritmaları kullanılmıştır. Bu çalışmada, betonarme kısa konsolların optimum tasarımı probleminin çözümü için Diferansiyel Evrim (DE) algoritması kullanılmıştır. Tasarım sürecinde, konsolun kesit boyutları, U-biçimli firketelerin çapı, çekme ve etriye donatılarının sayıları ve çapları karar değişkenleri olarak dikkate alınmıştır. Toplamda altı farklı karar değişkeni belirlenmiştir. Saha ekipleri tarafından uygulamanın kolay olabilmesi adına, konsolun boyutları kesikli değişken olarak seçilmiştir. Beton ve çelik malzemelerin minimum maliyette olması, tasarım probleminin amaç fonksiyonu olarak belirlenmiştir. Tasarım probleminin kısıtlarını ise TS500' de yer alan kesme dayanımı ve minimum donatı gereksinimleri belirlemiştir. Bu çalışmada, betonarme bir kısa konsolun tasarımı, DE algoritması kullanılarak minimum maliyet ile başarılı bir şekilde gerçekleştirilmiştir.

Anahtar Kelimeler: Önüretimli binalar, betonarme kısa konsol, optimum tasarım, diferansiyel evrim algoritması

ABSTRACT

Precast concrete buildings are frequently preferred for industrial buildings due to advantages such as allowing large spacing to be passed, fast construction time and being cast under controlled conditions. Since the plant-cast concrete elements will be joined at the construction site, pinned connections (moment-free) are generally preferred in these structures. A short cantilever is required at the junction points for the connection of the column and beam elements, which are produced piece by piece. It is successful in safely transmitting the vertical and horizontal loads from the beams (rafter or crane beam etc.) to the columns. Thus, short cantilever, called "concrete bracket" or "corbel", is widely used in industrial precast concrete structures. It is important that the design of this reinforced concrete (RC) short cantilever is designed with minimum materials for the efficient use of limited resources as well as the safely transmission of the loads. Optimization techniques need to be incorporated into the design processes in order to target minimum material usage. In the solution of many complex engineering problems, heuristic optimization algorithms have been frequently used because they can be easily programmed and can produce results close to the global optimum solution. In this study, Differential Evolution (DE) algorithm is used to solve the optimum design problem of RC short cantilevers. During the design process, the cross-sectional dimensions of the cantilever, the diameter of the U-shaped hairpins, the numbers and diameters of the tension and stirrup reinforcements were taken into account as decision variables. In total, six different decision variables were determined. The dimensions of the cantilever have been chosen as a discrete variable for easily implemented by the field teams. The minimum cost of concrete and steel materials was determined as the objective function of the design problem. The constraints of the design

problem were determined by the shear strength and minimum reinforcement requirements in TS500. In this study, the design of a RC short cantilever was successfully carried out using the DE algorithm with minimum cost.

Keywords: Precast buildings, RC short cantilever, optimum design, differential evolution (DE) algorithm

ORGANIC TEMPLATE ASSISTED SUSTAINABLE SYNTHESIS OF FACILE ZNONIOPDO/PD NANOMATERIAL: ENVIRONMENTALLY BENIGN PHOTOCATALYSTS

Irum Shaheen
Khuram Shahzad Ahmad

ABSTRACT

To contribute to water remediation by degradation of organic pollutants, sustainable and efficient nano-catalysts are highly desirable. In this regard, mixed metal oxide nano-catalyst of ZnONiOPdO/Pd nanomaterial was synthesized via organic template for degrade methyl orange (MO) in an aqueous environment. The organic compounds of *A.Pindrow* were reacted with the precursor's solution following the sol-gel synthesis methodology. We furthered modified the chemistry and morphology of mixed metal oxides with organic spices. The synthesized nanomaterial of ZnONiOPdO/Pd was characterized by X-ray diffraction, energy dispersive spectroscopy, Raman spectroscopy, and field emission scanning electron microscopy. We have not only synthesized nanostructures of ZnONiOPdO/Pd but have successfully functionalized the chemistry of ZnONiOPdO/Pd via organic compounds. The effect of organic functional groups of incorporated bio compounds was studied for degradation of MO in the presence of sunlight as well as under dark conditions. Therefore, bio organic compounds enhanced the active sites of the catalyst for efficient degradation of methyl orange with the catalytic efficiency of 92% and 82% under light and dark conditions respectively and in aqueous environment. This degradation efficiency was achieved within 15 minutes for dark conditions and 10 minutes for dark conditions. Such catalytic excellent behavior was ascribed to the synergetic effects of nanostructures and increased active sites by C and O related functional groups. Consequently, the current work is envisioned to present the cost effective and sustainable fabrication porous nanoscopic mixed metal oxides with organic-inorganic framework and projected its practical application nanostructure as photocatalyst for dye degradation.

Keywords: Inorganic-Organic template; Mixed Metal Oxide; Nanostructures; Dye degradation; dark conditions

NOVELTY IN SOCIETY WITH GREEN REVOLUTION

Shalini Jaiswal
Preeti Singh Bahadur

ABSTRACT

Green revolution is used to manage the surrounding environment and to reduce human inclusion. Green innovation is thought to be frame stock that can be saved or reused completely. The primary goals of green advancements are to reduce waste and pollution. It primarily includes regular clean-up stock, waste, innovations, vitality sources, wear, and a slew of others. Green procedures and advancements make use of renewable and consistent resources that never deplete. Advancement towards sustainable development necessitates changes at each residence, as well as on a global scale. The overarching hope is that this field will inspire curiosity and development changes in the same diurnal lifetime as information innovation. Furthermore, natural cultivating, unpractised vitality, green building development, eco-materials, and the creation of applicable stock and materials to help green business are among the possible regions where these manifestations and development are required to return from. In this paper, we are proposing the revolutions by counting green part so they will maintain a strategic distance from surroundings debasement and help to supply a perfect domain for who and what is to come. The paper conjointly talks about the opportunities and difficulties for un-practiced innovation in a few areas.

Keywords: Green innovation, Environmental issues, green approach, multi-disciplinary applications

REDUCTION OF SALMONELLA ENTERITIDIS ON SEABASS (DICENTRARCHUS LABRAX) BY ATMOSPHERIC PRESSURE AIR AND HELIUM COLD PLASMA

Serap Coşansu
ORCID:0000-0003-2875-1335
Tamer Akan
ORCID:0000-0003-0907-2724
Sehban Kartal
ORCID:0000-0002-0491-4219
Suhendan Mol
ORCID:0000-0003-3831-5107
Şehnaz Yasemin Tosun
ORCID: 0000-0003-3764-0020
Didem Üçok Alakavuk
ORCID:0000-0003-0162-4731
Şafak Ulusoy
ORCID:0000-0003-1725-3269
Hande Doğruyol
ORCID: 0000-0002-0856-3823
Kamil Bostan
ORCID:0000-0001-7583-0066

ABSTRACT

Plasma is an ionized gas composed of reactive oxygen species, ozone, reactive nitrogen species, UV radiation, free radicals, and charged particles. The UV light and reactive chemical products are responsible for decontamination effect of cold plasma. Atmospheric pressure air and helium cold plasma applications were evaluated as non-thermal decontamination techniques to ensure the safety of fish for *Salmonella*. The stationary phase cells of *Salmonella* Enteritidis (ATCC 13076) were surface inoculated on 10-gram seabass fillets at a level of 10^7 CFU/g. Air or helium cold plasma were applied for 1, 2, 3 and 4 min on inoculated site of fish fillets. The control samples were inoculated with *S. Enteritidis* but not treated with cold plasma. Then cold plasma treated samples were homogenized and serially diluted with maximum recovery diluent. From the appropriate dilutions, 0.1 ml portions were spread on XLT4 agar and incubated at 37°C for 24 h. The helium plasma yielded a higher reduction in *S. Enteritidis* count. The reduction rate was gradually increased with the treatment time. After 5 min air plasma and helium plasma treatments, the total reduction rates were 0.88 and 0.98 log CFU/g, respectively. For higher reductions, treatment times may be extended, or cold plasma may be combined with other hurdles.

Keywords: Cold plasma, fish, helium, *Salmonella*

RETARDING SPOILAGE AND MAINTAINING THE QUALITY OF SEA BASS USING ATMOSPHERIC COLD PLASMA

Şafak Ulusoy

ORCID:0000-0003-1725-3269

Tamer Akan

ORCID:0000-0003-0907-2724

Sehban Kartal

ORCID:0000-0002-0491-4219

Didem Üçok Alakavuk

ORCID:0000-0003-0162-4731

Şehnaz Yasemin Tosun

ORCID: 0000-0003-3764-0020

Hande Doğruyol

ORCID: 0000-0002-0856-3823

Serap Coşansu

ORCID:0000-0003-2875-1335

Kamil Bostan

ORCID:0000-0001-7583-0066

Suhendan Mol

ORCID:0000-0003-3831-5107

ABSTRACT

An atmospheric cold plasma-generating device was designed, and the effect of cold plasma on the quality of seabass was studied. The whole seabass were treated with cold plasma and stored at $2\pm1^{\circ}\text{C}$. The samples were kept in styrofoam boxes to imitate marketing conditions. The cold plasma was applied to the samples for either 1 min or 7 min, in order to determine the effect of treatment time. The sensory characteristics of fish did not get negatively affected by the treatment and even scored higher ($P \leq 0.05$) than control samples during storage. Sensory scores of the samples treated for 7 min were higher ($P \leq 0.05$) than the others during storage. Higher total color change (ΔE) was determined in plasma-treated groups. The longer treatment time resulted in higher total color change, but panelists did not declare an apparent color change during the study. The Thiobarbituric acid reactive substances (TBARS) values were below the acceptable limits, showing no adverse effect of cold plasma treatment on lipid oxidation. The Trimethylamine Nitrogen (TMA-N) values of the control group were higher than the treated groups. According to the Texture Profile Analysis (TPA), the texture characteristics of sea bass samples did not change due to the plasma treatment. It was also determined that the groups treated with cold plasma contained significantly lower ($P < 0.05$) mesophilic and psychrophilic aerobic bacteria counts during cold storage compared to the untreated control samples. It was seen that atmospheric cold plasma delayed microbial growth during cold storage, without changing the sensory characteristics of the whole sea bass. This finding showed that cold plasma could be a promising technology for the fresh fish industry.

Keywords: atmospheric cold plasma, fish, spoilage, shelf life, food safety

OPTIMIZATION OF MACHINING PARAMETERS IN TURNING OF INCONEL 718 WITH CERAMIC COMPOSITE TOOLS USING VIKOR METHODOLOGY

Hanane Boumaza
Salim Belhadi
Mohamed Athmane Yallese
Abdelkrim Haddad
Hadjela Salah

ABSTRACT

Inconel 718 is a nickel based super alloy that can withstand significant mechanical stress and strain while resisting corrosion and creep. Due of their desirable properties represented mainly by high mechanical strengths, corrosion resistance, heat and fatigue resistance and low thermal conductivity, such nickel based alloys are widely used in the manufacture of aircraft, rocket and submarine engine components. These much sought characteristics are unfortunately responsible for its poor machinability. This is mainly why numerous investigations have been and are being carried out on the machining of Inconel 718 under different cutting and lubrication conditions and by using different type of cutting tools. The present study focuses on an experimental investigation as well as an efficient approach in order to optimize the turning characteristics of Inconel 718 through multiple output responses represented by tool wear (V_b), surface roughness (R_a), cutting power (P_c), cutting temperature (T°) and material removal rate (MRR). A statistical study was made using the multi-objective optimization method VIKOR in order to study the best combination obtained by this method. The machining was carried out with a composite ceramic cutting tool (CC670) and the tests are carried out according to a Taguchi plan (L_{18}), the objective being the identification of the best combination of cutting parameters, namely the speed (V_c), feed (f), depth of cut (a_p) and insert radius (r) for the simultaneous minimization of (V_b), (T), (P_c) and (R_a) and the maximization of (MRR).

Keywords: Machining, Inconel 718, Optimization, VIKOR.

METRONIDAZOLE ADSORPTION FROM AQUEOUS SOLUTION USING NANO CRYSTALLINE CELLULOSE OBTAINED FROM *LUFFA AEGYPTIACA* SPONGE

Aminu Musa
Maryam Zakari
Ahmed Lawal Mashi

ABSTRACT

Water bodies may contain residues of antibiotics which causes chemical contamination. The design of several waste water treatment plants may not be able to degrade and eliminate these contaminants completely. Hence in this study, the removal of metronidazole from aqueous solution using the adsorption method was investigated. *Luffa aegyptiaca* sponge was utilized to extract cellulose which was then used to prepare Nanocrystalline cellulose (NCC) for the removal of the metronidazole. The formed NCC was characterized by FTIR, BET, TGA & XRD. The BET result showed that NCC of surface area 114 m²/g was formed. On the other hand, XRD result showed a typical cellulose I crystalline structure. Batch adsorption studies were conducted to investigate the effects of pH, adsorbent dosage, initial concentration, time & temperature. The metronidazole adsorption isotherm and kinetic data on the NCC were also analyzed. The results showed that maximum removal efficiency of 70.2 % was obtained at an initial metronidazole concentration of 50 mg/L, pH of 7, 0.08 g adsorbent mass and 60 mins contact time. The adsorption process was in agreement with the pseudo-second order kinetic model and the Langmuir adsorption isotherm. The thermodynamic study revealed that the metronidazole removal by the NCC was thermodynamically feasible and endothermic in nature.

Keywords: *Luffa aegyptiaca*, Metronidazole, Adsorption.

SYNTHESIS AND ACETOACETYLATION OF DIHYDROPYRIMIDINE-2,4-DIONE DERIVATIVES

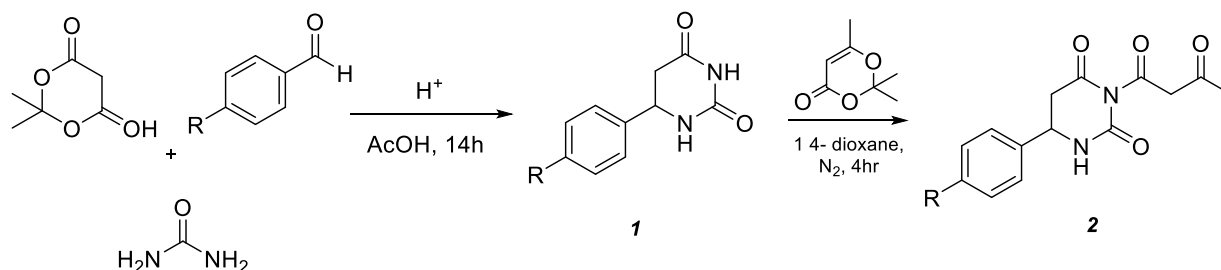
Araz Mohammed Faraj
ORCID: 0000-0002-4715-351X
Furgan Aslanoglu
ORCID: 0000-0002-5740-1716

ABSTRACT

Pyrimidine is often called 1,3-diazine due to its six-membered ring and two nitrogen atoms at positions 1,3. It is a heterocyclic compound with a biologically fascinating skeletal structure. Chemical similarities exist between the pyrimidine ring and benzene. Pyrimidine, similar to benzene, has an irregular hexagonal shape and is aromatic in nature, but unlike benzene, pyrimidine is an electron-deficient species similar to pyridine. In nucleic acid, the nitrogenous bases cytosine, thymine and uracil are examples of naturally occurring pyrimidine analogs.

A wide range of compounds of biological importance is represented by pyrimidine heterocycles. Numerous pyrimidine compounds are widely used in pharmaceuticals.¹ Minoxidil is a widely used hypertension vasodilator and hair loss treatment. Vitamin B1 treatment for thiamine deficiency. Rosuvastatin is used to stop heart disease. Fluacrypyrim. fluoxastrobin is used as an estrogen antagonist and is treated as a fungicide.

In this study, different dihydropyrimidine-2,4-dione derivatives (**1**) were synthesised and their acetyl acetylation reaction was carried out. In the first step of the study, different dihydro pyrimidine derivatives were synthesized by the Biginelli method.² Then, these synthesized dihydropyridine derivatives were reacted with a 2,2,6-trimethyl-4*H*-1,3-dioxine-4-one compound and acetyl acetylation of dihydropyridines was achieved.³



Keywords: Dihydropyrimidine-2,4-dione, Acetoacetylation, 2,2,6-trimethyl-4*H*-1,3-dioxine-4-one

ON SOME PROPERTIES OF RICCI SOLITONS

Yusuf Doğru

ORCID:0000-0002-1875-0243

ABSTRACT

Let (M, g) be a Riemannian manifold. R. S. Hamilton introduced the Ricci flow $\frac{\partial g(t)}{\partial t} = -2Ric(g(t))$. The Ricci flow is an evolution equation for Riemannian metrics. Ricci solitons correspond to self-similar solutions of Ricci flow. A smooth vector field v on a Riemannian manifold (M, g) is considered to define a Ricci soliton should a real constant exist λ such that $\frac{1}{2} \mathcal{L}_v g + Ric = \lambda g$, where v is vector field, $\mathcal{L}_v g$ denotes the Lie derivative of g in the direction of v , Ric is the Ricci curvature. A vector field v on a Riemannian manifold (M, g) is called recurrent if $\nabla_{x_1} v = \varphi(x_1)v$, where φ is a 1-form and ∇ is the Levi-Civita connection of g . we consider some properties of Ricci solitons on Riemannian manifolds and their submanifolds when the potential vector field is a recurrent vector field. Under some certain conditions, we show that the manifold (or submanifold) is a generalization of an Einstein manifold. Let (M, g) be a Riemannian manifold admitting an affine connection, U a parallel unit vector field with respect to the Levi-Civita connection ∇ and v a recurrent vector field with respect non-metric affine connection on M . Assume that a 1-form φ is the g -dual of v . Then (M, g) is a Ricci soliton (v, λ) if and only if M is a quasi-Einstein manifold.

Keywords: Ricci soliton, Riemannian manifolds, potential vector field, recurrent vector field.

MICROSTRUCTURE CHARACTERIZATION AND TENSILE TESTING OF HIGH STRENGTH HYBRID STEEL TO UNDERSTAND THE EFFECT OF ELECTROCHEMICAL HYDROGEN CHARGING

Halil Yılmaz

ORCID: 0000-0003-3585-0665

Cem Örnek

ORCID: 0000-0002-3029-6493

Bilgehan M Sesen

ORCID: 0000-0002-3029-6493

Beste Payam

ORCID: 0000-0001-8469-7893

ABSTRACT

Nowadays materials are increasingly used under harsh conditions in which the liberation of hydrogen by electrochemical processes can lead to material degradation due to hydrogen embrittlement (HE). Hydrogen in metals alters the microstructure; voids, dislocations, cracks, hydrides can be formed, the surface can be structurally altered, and the strain/stress states within the microstructure can be affected, often resulting in embrittlement and enhanced susceptibility to localized corrosion. High-strength stainless steels (single/duplex phase) and high-strength steels (transformation/twinning-induced, low alloy, maraging) are widely used in our society and are most susceptible to HE, a phenomenon which remained less understood. The amount of hydrogen in microstructures, that causes HE, can be minor (down to ppb level), sufficient causing catastrophic failure. The main problem of hydrogen is that it can be easily generated during material fabrication (e.g., pickling) and during service (e.g., cathodic protection, corrosion), and that it can be ultra-fast absorbed by steels and further rapidly diffuse through it.

The aim of the proposed work is to understand hydrogen embrittlement and plastic deformation behaviour of a 6Cr-5Ni-2Al-1MoV novel high-strength steel (Hybrid) through tensile experiments. Hybrid steel offers high-strength by a double-precipitation hardening mechanism of aluminides and carbides, all embedded in a tempered martensitic matrix. Miniature type tensile specimens in gauge length of 10 mm and 25 mm were subjected to electrochemical hydrogen charging at -10 mA/cm^2 for 48 hours followed by tensile testing to understand the deformation characteristics induced by the presence of hydrogen in the microstructure. The microstructure with and without absorbed hydrogen was characterized for a comprehensive crystallographic assessment using the optical, scanning electron microscope and electron backscattered diffraction (EBSD). The EBSD results showed that the martensite structure formed after solution treatment in Hybrid steel is predominantly lath type. The deformation behaviour of samples with and without absorbed hydrogen was tested and found that hydrogen caused HE in the samples with absorbed hydrogen.

Keywords: Hydrogen Embrittlement; Local Plasticity; High-Strength Hybrid Steel, Mechanical Testing

MONITORING MILK ADULTERATION USING ULTRASOUND TECHNIQUE

Mourad Derra

ORCID: 0000-0003-2395-2859

ABSTRACT

Adulteration in food products means the addition of prohibited substance either partly or wholly for the state of financial gain or lack of hygienic conditions of processing and storing which leads to the consumer being cheated. Ignorance of this fact is not fair since this may endanger consumer health.

In the dairy industry, milk quality is measured by criteria such as fat, lactose, protein, and water content. This later is a property of major importance in milk powders and food products in general. It influences storing conditions and shelf life as well as textural and technological qualities. On the other hand, when pure milk is cheated, its physical properties change, such as electrical conductivity, electrical admittance, boiling point, freezing point, viscosity, etc. During the experiments, milk adulteration was performed by blending variable amounts, ranging from 87.36% to 93.98% (by dose of 5mL) in volume of water into 91mL of the original milk sample. Each sample was conducted under different levels of temperatures ranging from 20°C to 40°C, with a step of 5° C.

In order to evaluate the water content in powdered milk, an ultrasound technique in backscattering pulse echo mode has been tested and proved to be a simple, fast, inexpensive and non-destructive alternative tool for evaluating the quality of powdered milk. In addition, our technique involves only one transducer and it is non-invasive, which is very important in the food industry for hygiene reasons.

Keywords: Milk Adulteration, Pulse-Echo, CND, Ultrasound Parameters

DIVERSE APPLICATIONS OF OPTICAL FIBER SENSORS

Preeti Singh Bahadur
Shalini Jaiswal

ABSTRACT

The paper focuses on the introduction of fiber optics, a mix of science and fabricating and portrays the materials generally used for its improvement close by the procedure used to design the strands. It gives an idea of the materials used for the advancement close by sides and drawbacks related with them and distinctive components speaking to the spread of brilliant, infrared or clear radiations. An optical fiber made up of a center conveys the light heartbeats which are utilized for detecting as well as for the brightening reason. Fiber optic tests experience add up to inward reflection and help in conceivable future biomedical applications to complete the concurrent gathering and investigation of tests for medicate security assessment. It additionally helps in the detecting of biomolecules, distinguishing proof of medication atoms, profluent checking and general pharmaceutical quality control of the item. Tests help in the advancement of energy profile and are related with short specimen times, permitting the distinguishing proof and estimation more exact and dependable. The central base turns on the usages of optical strands in the remedial and biomedical field and expanding the use of the same in pharmaceutical industry as tests in quality control and estimations shape examination.

Keywords: Fiber optics, Dosage analysis, Glucose sensor, Protein analysis, Pesticide identification, DNA oligomers

COMBINING LATE EXHAUST VALVE OPENING AND CYLINDER DEACTIVATION TO ACHIEVE RAPID AFTER-TREATMENT HEAT UP IN DIESEL VEHICLES

Hasan Üstün Başaran
ORCID: 0000-0002-1491-0465

ABSTRACT

Exhaust after-treatment (EAT) thermal management is a significant concern for diesel vehicles to meet the stringent emission norms. Many on-engine measures such as delayed main fuel injection timing, close or late post-fuel injection and exhaust throttling necessitate undesirable high thermal inefficiency to raise EAT system temperature above 250°C in automotive vehicles. This work considers to combine late exhaust valve opening (LEVO) and cylinder deactivation (CDA) to obtain EAT thermal management with a relatively mild fuel consumption penalty.

At first, LEVO is individually examined at a low-loaded operation condition (1200 RPM speed and 2.5 bar BMEP) on the 6-cylinder diesel engine model and found to be highly effective to maintain high exhaust temperature (~ 250°C) and improve EAT get-warm period. However, LEVO-alone mode leads to a dramatic thermal inefficiency (up to % 5) which may result in elevated NO_x rates until EAT unit temperature reaches 250°C. Therefore, secondly, instead of applying LEVO in all 6-cylinders, two cylinders are deactivated (all valves & fuel injection are switched off) and only the rest of the four cylinders are actively operated in LEVO mode on the model (LEVO + CDA combined mode). CDA is found to enhance thermal efficiency (close to % 7) via decreasing the engine pumping loss. That improvement allows LEVO + CDA combined mode to boost the exhaust temperature above 250°C with much lower fuel injection need compared to LEVO-alone mode. The fast temperature improvement is attributed to decreased air-to-fuel ratio corresponding to lower active cylinder (thus, lower airflow) use of the engine. Those passive cylinders cause a serious decline in exhaust flow rate (close to % 30) which degrades the EAT get-warm period particularly at low EAT bed temperatures. However, LEVO + CDA combined mode can achieve up to 295°C exhaust temperature with a limited fuel penalty (up to % 8) which is not possible in LEVO-alone mode with even a significant fuel penalty rise (% 20). This excessive temperature rise overcompensates the exhaust flow rate reduction due to CDA and causes elevated heat transfer rates (up to % 143) to the EAT unit. Under the same fuel consumption penalty (% 8), LEVO + CDA combined mode is advantageous to use as it improves EAT get-hot & stay-hot periods more than LEVO-alone mode.

Keywords: Late exhaust valve opening, cylinder deactivation, diesel engines, after-treatment systems, thermal management.

ATEROSKLEROZ TEDAVİSİNDE KULLANILMAK ÜZERE BİTKİ EKSTRAKTI İÇEREN NANO İLAÇ ADAYI GELİŞTİRİLMESİ VE *İN VİTRO* GÜVENLİĞİNİN DEĞERLENDİRİLMESİ DEVELOPMENT OF NANO DRUG CANDIDATE WITH PLANT EXTRACT FORMULATION FOR THE TREATMENT OF ATHEROSCLEROSIS AND EVALUATING IT'S *IN-VITRO* SAFETY

Safak Aktas

ORCID: 0000-0002-1900-0196

Yasemin Budama-Kılınc

ORCID: 0000-0003-0601-3091

ÖZET

Ateroskleroz, kardiyovasküler damar hastalıkları arasında dünya çapında yüksek morbidite ve mortalite oranlarına sahip olması nedeniyle, görüntüleme, teşhis ve tedavi yöntemleri üzerinde araştırmaların yapılmasını gerektiren bir hastalıktır. Mevcut tedavi yöntemlerinin yanı sıra, son yıllarda klinik çalışmaları devam eden olan nano boyutlu ilaç formülasyonları sayesinde gelecekteki tedavi yöntemleri umut vadetmektedir.

Hedera Helix (duvar sarmaşığı) anti inflamatuvar, anti trombotik, anti mikrobiyal ve anti kanser özellikleri olan, günümüzde diyabet, astım, bronşit hastalıklarının tedavisinde balgam sökücü ve öksürük kesici olarak kullanılan, çeşitli hastalıklar üzerinde etkinliği hala araştırılmakta olan, geniş farmakolojik aktivite çeşitliliğine sahip olan bir bitkidir.

Bu çalışmanın amacı, *Hedera Helix* (duvar sarmaşığı) ekstraktı içeren nano-boyutlu, kontrollü salım özelliği olan formülasyon geliştirilmesi ve *in vitro* güvenliğinin değerlendirilmesidir. Bu doğrultuda, ikili emülsiyon yöntemi kullanılarak *Hedera Helix* ekstraktı (HHE) yüklü Poly(ϵ -caprolactone) (PCL) nanopartikül formülasyonu üretilmiştir. Nanopartikül formülasyonunun karakterizasyonu UV-Vis spektroskopisi ve DLS yöntemleri ile yapılmıştır. Ortalama partikül boyutu, polidispersite indeksi, zeta potansiyel parametreleri belirlenmiştir. Ayrıca nanopartikül formülasyonunun enkapsülasyon verimi ve yükleme kapasitesi hesaplanmıştır. Ek olarak, kontrollü salım özelliği olan HHE-PCL nanopartikül formülasyonunun *in vitro* salım profili belirlenmiştir. Üretilen HHE yüklü PCL nanopartikül formülasyonunun *in vitro* güvenliğinin değerlendirilmesi ve güvenli dozunun belirlenmesi amacıyla hücre kültüründe sitotoksitesite çalışması yapılmıştır.

Sonuçlara göre, HHE-PCL nanopartikül formülasyonunun Zeta-Sizer cihazı ile yapılan analizinde, 202,9 nm'lik ortalama partikül boyutuna, 0,129 polidispersite indeksine ve -13,8 mV'luk zeta potansiyel değerine sahip olduğu bulunmuştur. Enkapsülasyon verimi ve yükleme kapasitesinin sırasıyla, %90 ve %39 olduğu hesaplanmıştır. *In vitro* salım profili çalışmasına göre ilk 5 saat içerisinde HHE'nin %25'nin nanopartikül formülasyonundan salındığı, %100'ün ise 72 saat içerisinde salındığı belirlenmiştir. HHE-PCL nanopartikül formülasyonunun sitotoksitesitesi MTT testi L929 hücre hattı üzerinde değerlendirilmiş ve 0.5 mg/mL'nin güvenli doz olduğu tespit edilmiştir.

Anahtar kelimeler: Ateroskleroz, Nanopartikül, *Hedera Helix*, Kontrollü Salım Sistemi, İlaç Tasarımı, *İn Vitro* Hücre Kültürü, Sitotoksitesite.

ABSTRACT

Atherosclerosis has significant morbidity and mortality rate among the cardiovascular arteries diseases that's the why needs searching on the methods of imaging, diagnostic and treatment. Besides current treatment methods, thanks to nano scale drug formulations which are keep going clinical studies in last years, show promise future treatment methods.

Hedera helix (Ivy) is a plant which has anti-inflammatory, anti-thrombotic, antimicrobial and anti-cancer properties, is used as an expectorant and cough suppressant in the treatment of diabetes, asthma, bronchitis, its effectiveness on various diseases is still being researched, and has a large range of pharmacological activities.

The aim of this study, developing nano-scale formulation with *Hedera Helix* (Ivy) extract which has controlled release property and evaluating it's *in vitro* safety. In this respect, loaded Poly (ϵ -caprolactone (PCL)

nanoparticles with *Hedera Helix* extract (HHE-PCL) formulation were produced with double emission method. Characterization of nanoparticles formulation were done by UV-Vis spectroscopy and DLS method. The parameters which are average particles size, polydispersity index and zeta potential were determined. Also, the encapsulation efficiency and loading capacity of nanoparticles formulation were calculated. In addition, the *in vitro* release profile of the controlled release HHE-PCL nanoparticle formulation was determined. On the purpose of evaluate the *in vitro* safety of the loaded HHE-PCL nanoparticle formulation and to determine the safe dose, cytotoxicity study was performed in cell culture.

According to results, the analysis result of HHE-PCL nanoparticle formulation was found to have an average particle size of 202.9 nm, a polydispersity index of 0.129, and a zeta potential value of -13.8 mV by Zeta-Sizer device. Encapsulation efficiency and loading capacity were determined as 90% and 39% respectively. According to the *in vitro* release profile study, it was determined that 25% of the HHE was released from the nanoparticle formulation within the first 5 hours, and 100% was released within 72 hours. The cytotoxicity of the HHE-PCL nanoparticle formulation was evaluated by MTT on the test L929 cell line and 0.5 mg/mL was found to be a safe dose.

Keywords: Atherosclerosis, nanoparticles, *Hedera Helix*, controlled release system, drug design, *in vitro* cell culture, cytotoxicity.

APPLICATION OF ARAS METHOD FOR THE SELECTION OF OPTIMUM PROCESS PARAMETERS IN TURNING OF AISI 4140 ALLOY STEEL

Hadjela Salah
Belhadi Salim
Ouelaa Nouredine
Yallese Mohamed Athmane
Safi Khaoula
Hanane Boumaza

ABSTRACT

Turning process is one of the fundamental machining operations and its parameters optimization leads to better machining performance. This study applies Additive Ratio Assessment (ARAS) method to determine the optimum process parameters in turning operation of AISI 4140 Alloy Steel, with a coated carbide GC-2025 and the tests carried out according to the Taguchi design (L16). The process parameters considered are cutting speed (V_c), feed rate (a_p), and depth of cut (f). The objective is to minimize the cutting Force (F_z) and maximize the Material Removal Rate (MRR) simultaneously. The result revealed that this proposed method is appropriate for solving multi criteria optimization of process parameters. The highest value of this latter corresponds to the optimal levels combination of machining parameters. Therefore, the optimal levels combination for a simultaneous improvement of F_z and MRR was obtained at $V_c=250$ m/min, $f=0.22$ mm/rev, and $a_p=1.4$ mm. The optimized responses found by the use of optimal levels selected by ARAS method grey were $F_z=278.45$ N and $MRR= 77$ cm³/min.

Keywords: AISI 4140 alloy, Optimization, Taguchi, Cutting Force, ARAS.

EFFECT OF SPECIFIC SURFACE FOR REMOVAL OF METHYLENE BLUE DYE USING TWO TYPE OF NATURAL SAND BEFORE AND AFTER GRINDING

Saïd Et-Taleb
Asma Amjlef
Salaheddine Farsad
Nouredine El Alem

ABSTRACT

The Sand is one of most abundant mineralogical material; it is the matrix of building materials. The sand used in this study is taken from the Assa region south of Morocco (fine sand) and second one in Zagora region (wide sand), both of them are using before and after grinding for removal the methylene blue dye. The analysis of fine sand and wide sand by X-ray diffraction, the fine sand is made of Quartz (SiO_2), Muscovite ($\text{K Al}_2\text{Si}_3\text{AlO}_{10}(\text{OH})_2$) and Albite, calcian ($(\text{Na}, \text{Ca}) \text{Al} (\text{Si}, \text{Al})_3\text{O}_8$). The wide sand is composed of quartz, calcite ($\text{Ca Mg} (\text{CO}_3)_2$), albite ($\text{NaAlSi}_3\text{O}_8$) and dolomite ($\text{Ca Mg} (\text{CO}_3)_2$). The grinding is carried out using a ring mill, installed at the Laboratory of hydrogeology at the Faculty of Sciences of Agadir. The size of the particles obtained after grinding and less than $10 \mu\text{m}$. The grinding of the sand increases the specific surface the adsorbed quantities of methylene blue. For wide sand and fine sand, the quantities of methylene blue adsorbed are respectively 2.13 mg/g and 4.27 mg/g , after the grinding of these sands the quantities adsorbed increase. For wide sand powder, the value is equal to 4.267 mg/g and for fine sand powder, the value is 6.4 mg/g . We notice that the quantity adsorbed after the grinding of wide sand powder is twice as large and for fine sand powder, the quantity adsorbed is 1.5 times greater.

Keywords: sand, X-ray diffraction, specific surface, methylene Blue.

WIDEBAND MIMO 5G ANTENNAS IN HANDSETS

Gölge Ögücü Yetkin
ORCID: 0000-0002-4260-1432
Zaid Attrah

ABSTRACT

This study aimed to improve the performance of MIMO (Multiple Inputs, Multiple Outputs) antenna arrays for 5G terminals by converting the elements from an L-shape to an H-shape. The proposed antenna array consisted of four triple-band antennas capable of supporting 5G New Radio (NR), including n77 (3.3-4.2GHz), n78 (3.3-3.8GHz), and n79 (4.4-5GHz), with a high bandwidth (>1.6 GHz) and high realized gain (>10 dBi). The study also simulates the return loss coefficients for each element and the isolation factor between elements to describe their behavior when installed close together in a single device and on a single PCB. The study evaluates the radiation patterns at several frequencies in the aforementioned fields and compares the results using HFSS simulation software and CST software.

The results showed that the proposed H-shaped MIMO antenna improved the performance of the 5G terminal's MIMO antenna significantly. The S11 parameter dropped to -25dB at 3.75GHz, and it decreased to -26.5 dB at a frequency of 4.85 GHz, while remaining less than -10dB over the entire range of (3.3 to 5GHz) approximately. These results indicate that the designed antenna is wideband and can be used in 5G terminals. Overall, the study suggests that by changing the shape of the antenna elements, MIMO antenna arrays' performance can be significantly improved, leading to better 5G terminal performance.

Keywords: MIMO, 5G, HFSS simulation software and CST software

SYNTHESIS AND CHARACTERIZATION OF HALOGEN SUBSTITUTED ORGANIC/INORGANIC HYBRID HALIDE PEROVSKITES

Faqeer Muhammad
Muhammad Ashan
Hafiz Badaruddin Ahmad

ABSTRACT

Organic and inorganic hybrid perovskites with advantages of facile processing have emerged as a new class of revolutionary optoelectronic semiconductors promising for various applications. Perovskite solar cells constructed with a variety of configurations have demonstrated unprecedented progress in efficiency, reaching about 20% from multiple groups after only several years of active research. A key to this success is the development of various solution-synthesis and film-deposition techniques for controlling the morphology and composition of hybrid perovskites. The rapid progress in material synthesis and device fabrication has also promoted the development of other optoelectronic applications including light-emitting diodes, photodetectors, and transistors. Both experimental and theoretical investigations on organic–inorganic hybrid perovskites have enabled some critical fundamental understandings of this material system. Recent studies have also demonstrated progress in addressing the potential stability issue, which has been identified as a main challenge for future research on halide perovskites. Here, we review recent progress on hybrid perovskites including basic chemical and crystal structures, and chemical synthesis of bulk/nanocrystals. We also discuss the importance of further understanding of the fundamental properties of hybrid perovskites, especially those related to chemical and structural stabilities.

Keywords: Perovskite solar cell, film-deposition techniques, crystal structures, light-emitting diodes

MONITORING OF A PETROLEUM PRODUCT STORED IN A FLOATING ROOF STORAGE TANK

N. Boughazi

F. Gaci

A. Haddad

ABSTRACT

Today's world is undergoing great changes in technology in all areas. As a result, the need for energy is increasing for the daily needs of households and industry. The petroleum industry is the strong witness of this progress, and particularly in Algeria which is one of the first countries exporting hydrocarbons.

In the storage industry it is often necessary to store products that should not be in contact with the air, hence the idea of making a tank with a floating roof to isolate the stored product from the air.

The control of petroleum products is a necessity in order to get to the national and international standards and specifications, thus, quality checks have been appealed. These checks can be performed at different points in the production cycle or transport of the product, including storage locations. The Transportation region complex controls its stored products (crude oil and condensate) in storage tanks with floating roofs, by taking samples before and after each movement (receiving, shipping and delivery to ships) in order to make check quality by laboratory analysis. The objective of this study has been to see the influence of climate on the specific parameters of crude oil and stored condensate as well as the influence of the storage time on the latter.

Keywords: Control, Analysis and Quality

DESIGN METHOD OF ASYMMETRIC SUPERSONIC NOZZLES

N. Boughazi

A. Haddad

ABSTRACT

A variety of aerospace applications require the integration of three-dimensional supersonic propulsion nozzles as the design of their contour contributes greatly to enhance the performances of the propulsive engine. These include three-dimensional nozzles for propulsion engines having nonsymmetrical area constraints and for aircraft where airframe/propulsion integration plays an increasingly important role. Several nozzle concepts that promise a gain in performance over existing conventional ones need to be investigated.

A simple method based on the relatively simple computations of axisymmetric flowfields using a home developed design computer program based on the method of characteristics is presented, and applied to obtain wall contours of supersonic nozzles of arbitrary exit cross sections from determined axisymmetric flow-fields having the required overall nozzle length and exit Mach number from which the desired 3-D shape is later generated. Choosing the desired cross-section shape at the exit, its geometrical parameters are traced back to the throat to constitute the walls of the desired supersonic nozzle contour. Using this approach, an elliptical geometry has been designed and is presented. The preliminary results gathered indicate a smooth transition of the shapes generated from the throat to the exit of the supersonic section of the nozzles.

Numerical analyses were performed through applying two-dimensional simulation of the axisymmetric nozzle from which the elliptic nozzle was generated; a detailed analysis of the flowfields within the asymmetric elliptic nozzle configuration designed will constitute the next step to be carried out.

Keywords: Supersonic flow, design, contour, propulsion, De-Laval nozzle.

DENIPLANT NUTRACEUTICALS MAY HELP FOR ENDOMETRIOSIS PAIN

Giurgiu Gheorghe

ORCID: 0000-0002-5449-2712

Cojocaru Manole

ORCID: 0000-0002-6871-577X

Simona Criste

ORCID: 0000-0003-2949-3032

ABSTRACT

Background Inflammation has a main role in the progression of endometriosis. The mechanisms by which endometriosis induces a chronic pain state remain poorly understood. Unfortunately, there is no known cure for endometriosis. But you can manage it with medication and at - home treatments. Some findings have highlighted the main role of inflammation in endometriosis by acting on proliferation, apoptosis and angiogenesis. The introduction of new agents can be effective in improving the condition of patients; for example, plants are promising sources of bioactive natural components

Objectives These natural compounds could be interesting strategies in therapy. While there is no absolute cure for this condition, some home remedies can relieve pain and discomfort it bring. The purpose of this presentation is to summarize the potential action of Deniplant nutraceuticals in endometriosis by acting on inflammation.

Materials and methods The primary symptoms of endometriosis are pelvic pain and infertility. The use of Deniplant nutraceuticals could be interesting in disease management for women.

Results Treating pain-related aspects of endometriosis would contribute to the improvement of mental health and daytime function. Because the microbiome can influence inflammation, new therapies can develop through its natural modulation. There are other options, including natural remedies, herbs like cinnamon twig or licorice root, or supplements, such as thiamine, magnesium, or omega-3 fatty acids.

Conclusion Deniplant nutraceuticals can downregulate inflammation in endometriosis. Nevertheless, the limited number of studies focusing on the different interactions of Deniplant nutraceuticals in endometriosis restricts its clear and immediate use in a therapeutic strategy.

Keywords: endometriosis, diet, Deniplant nutraceuticals

PREDILECTION OF INDIAN PORTFOLIO FRAMEWORK IN COVID-19 INFODEMIC - AN ANALYSIS

Jyoti Sinha
Vinod Kumar

ABSTRACT

Investors are confronted with plethora of investment alternatives, to make their money work for them, based upon desired risk and return availability. An investment portfolio is a manifest of individual's investment behaviour towards various investment avenues. At this junction of Coronavirus pandemic, the financial portfolio has been acclimatized to maintain balance and profitability. Therefore, the study proposes to assess the influence of socio-economic profile during these turbulent times on the investor's awareness, motivation, risk bearing capacity and attitude towards risk and non-risk mapped financial instruments. A structured questionnaire was administered to a sample of 168 Indian investors using convenience sampling technique and parametric & non-parametric statistics was used for delineating the influence of infodemic on behavioural finance. With worries about a potential stagflation growing, the investors focussed on liquidity instead of growth and invested more in debt or income schemes.

Keywords: Covid-19, Economic impact, Investment avenues, Behavioural portfolio theory, Risk management

ANTIBACTERIAL AND ANTI- OXIDANT ACTIVITIES OF EXTRACTS FROM MEDICINAL PLANTS

Yassmine Chennai
Assma Fetteh

ABSTRACT

The algerian flora provides a diverse range of aromatic plants with a high therapeutic interest due to their secondary biologically active metabolites, which have sparked scientific interest.

In this study, we are interested in the plants *Ocimum basilicum* L. of the Lamiaceae family and *Artemisia campestris* A. of the Asteriaceae family, which are well known locally and have a variety of curative properties in traditional medicine. The first part of this study is devoted to the quality control of the plant powder and the investigation of the metabolites. The phytochemical screening revealed the presence of flavonoids, tannins, coumarine, essential oil, and other metabolic compounds. The HE were obtained using hydrodistillation with a yield of 2.4% for *O.basilicum* L. and 1.8% for *A.campestris* A. The phenolic compounds were obtained by a series of extractions with four solvents of increasing polarity. The concentration of these extracts in total polyphénols, flavonoids, and tanins was determined by using the reactif Folin Ciocalteu, aluminum trichlorure, and vanilline with the addition of chlorhydric acid. In the second section, we investigated the antioxidative capacity of extracts (HE and phenolic compounds) in vitro using the DPPH method.

The results show that our extraits have interesting antioxidant properties, with ethyl acetate being the most effective. Furthermore, the essential oil has a very low antioxidative activity when compared to the benchmark for the two plants.

Finally, we assessed the antibacterial activity of our extracts against ten pathogenic bacteria using the MH diffusion method.

The results show that phenolic extracts of *O.basilicum* L. have higher activity for HE. Unlike *A.campestris* A., the acétate of éthyle extract is the most active on the majority of Gram+ souches.

Keywords: *O.basilicum* L., *Artemisia campestris* A, Antibacterial, oxidant activities

**IN VITRO EFFICACY OF *TRICHODERMA ASPERELLUM* AGAINST COLLAR ROT OF
BRINJAL CAUSED BY *SCLEROTIUM ROLFSII***

Vignesh K

ORCID: 0000-0003-4484-3862

Manikandan K

ORCID: 0000-0002-0677-0159

Sathiya Aravindan V

ORCID: 0000-0002-8556-7801

Vishnupriya K

ORCID: 0000-0001-7805-8294

ABSTRACT

Brinjal (*Solanum melongena* L.) is a small, short lived perennial herb belongs to the family Solanaceae. It is an important summer vegetable crop grown throughout the world. Brinjal crops are susceptible to various diseases caused by biotic and abiotic factors. Among these Collar rot caused by the fungus *Sclerotium rolfsii* causes 30-40% yield loss. In the present investigation an attempt has been made to study the *in vitro* efficacy of *Trichoderma asperellum* against *Sclerotium rolfsii*. The antagonistic effect of *Trichoderma asperellum* were observed by the Dual culture technique and Poison food technique under the *in vitro* conditions. In Dual culture technique the effective antagonists were selected based on the inhibition to the growth of the pathogen. In Poison food technique to determine the antagonistic activities of antibacterial metabolites present in *Trichoderma asperellum* culture filtrate in different concentration level like as 10%, 20%, 30%.

Keywords: Brinjal, Collar rot, *Sclerotium rolfsii*, *Trichoderma asperellum*, Dual Culture technique, Poison food technique

ANTIBIOTIC SUSCEPTIBILITY PATTERN OF *STAPHYLOCOCCUS AUREUS* ISOLATED FROM COMMONLY SOLD YOGHURTS IN ILORIN METROPOLIS

Majekodunmi Racheal Adedayo
Olupona Risikatun

ABSTRACT

Food safety is the proper food handling procedures applied during food preparation, processing, storage, and distribution. Microbiological quality and safety of different yoghurts (designated as samples: A, B, C, D and E sold by street vendors in Ilorin, Kwara State) was assessed. Standard microbiological procedures and techniques were used to enumerate, isolate, identify and characterize *Staphylococcus aureus* from the samples. The bacterial isolates were screened for their sensitivity to common antibiotics using the disc diffusion method on Mueller-Hinton Agar. The isolates were *Staphylococcus aureus*. Sample E had the highest bacteria count of 16×10^1 cfu/ml while sample C had the lowest bacterial count of 3×10^1 cfu/ml. The study recorded all the isolates to be resistant to more than two antibiotics. The result showed that 50 % of the isolates were resistant to Ampiclox (APX), Zinnacef (Z), Amoxicillin (AM), Ciprofloxacin (CPX), Rocephin (R) while 60 % were resistant to Septrin (SXT), Pefloxacin (PEF), Gentamycin (CN) and Streptomycin (S). All the isolates were however, moderately sensitive to Erythromycin. In conclusion, isolation of multi drug resistant *Staphylococcus aureus* from these yoghurt samples may constitute potential health hazard to consumers, therefore there is need for routine quality control checks during production, processing and distribution of these products in order to protect students, pupils and the general public from food borne infection.

Keywords: *Staphylococcus aureus*, Microbiological safety, Yoghurt, Antibiotics, Resistant, Sensitive

JAUNDICE AMELIORATIVE ACTIVITY OF *F. ALBIDA* METHANOL STEM BARK EXTRACT

Ibrahim Babangida Abubakar

Isah Musa Fakai

Maryam Ibrahim Tukur

ABSTRACT

Jaundice is disease caused by accumulation of bilirubin in the blood, treating this type of ailment with medicinal plants have formed basis in folklore system which has a rapid growing economic importance. This study aimed to evaluate *in vivo* jaundice ameliorative activity of *Faidherbia albida* methanol stem bark extract. Hepatoprotective and hematological effect were assessed using standard laboratory procedures. Hepatoprotective effect of *Faidherbia Albida* methanol stem bark extract revealed a significant ($P<0.05$) reduction in serum aspartate amino transferase (AST), alanine amino transferase (ALT) and alkaline phosphatase (ALP) activities. Moreover, serum total protein (TP) and serum bilirubin concentrations also significantly ($P<0.05$) decreased compared to untreated control, but a significant ($P<0.05$) increases in AST, ALT, ALP, TB, DB and TP was observed in untreated control compared to normal control. However, a significant ($P<0.05$) increased in serum albumin (ALB) was observed in all extract treated groups compared to untreated control group, while ALB of untreated control significant ($P<0.05$) decreased compared to normal control. Similarly, red blood cells and hemoglobin concentrations significantly ($P<0.05$) increased, whereas mean cell volume and mean corpuscular hemoglobin significantly ($P<0.05$) decreased in all the treated groups compared to untreated control group. In conclusion, the present study, indicated that *Faidherbia albida* methanol stem bark extract has jaundice ameliorative potential, hence support the traditional use of this plant in treating jaundice.

Keywords: Jaundice, *Faidherbia albida*, *in vivo*, stem bark

ISOLATION, IDENTIFICATION AND ANTIBIOGRAM OF BACTERIA FROM SELECTED FOOD CONDIMENTS SOLD IN ILORIN, NIGERIA

Ajiboye, A.E.
Jimoh, M.O.

ABSTRACT

Condiments are added to food to enhance the aroma and flavour. This improves the taste of food but the purpose can become defeated when food condiment is contaminated with pathogenic bacteria that result in foodborne illnesses. The study was aimed at isolating and identifying bacteria from selected food condiments sold within Ilorin, Kwara State, Nigeria and also to evaluate their sensitivity to standard antibiotics. Four (4) different condiments (ginger, garlic, turmeric and dried pepper) were purchased from Oja-Oba, Ganmo and Yoruba road markets. Isolation and identification were done using standard microbiological methods. Total bacterial counts were obtained using pour plate method. The antibacterial sensitivity testing of the isolates against some antibiotics was carried out using standard procedures.

The total heterotrophic and coliform counts ranged from 1.38 ± 0.38 to $21.52 \pm 5.31 \times 10^5$ cfu/ml and 1.33 ± 0.52 to $6.67 \pm 4.93 \times 10^5$ cfu/ml respectively with garlic sample having the highest counts and turmeric sample having the least counts. Six bacteria were isolated, namely *Staphylococcus aureus*, *Salmonella typhi*, *Bacillus* sp, *Pseudomonas aeruginosa* *Escherichia coli* and *Enterobacter* sp. *Staphylococcus* count ranged from 1.00 ± 1.00 to $4.00 \pm 1.00 \times 10^5$ cfu/ml. *Salmonella Shigella* count ranged from 1.33 ± 0.58 to $4.67 \pm 3.06 \times 10^5$ cfu/ml. *Bacillus* sp demonstrated highest level of susceptibility to Ciproflaxacin, Amoxacillin and Ampiclox (14.00 mm) while *Enterobacter* sp has the lowest sensitivity to Streptomycin (2 .00 mm). All the bacterial isolates were resistant to Zinnacef, Rifampin, trimethoprim-sulfamethoxazole and erythromycin. It can be concluded that these food condiments which are commonly used during cooking can be easily contaminated by pathogenic bacteria which are multidrug resistant, this can cause a public health hazard.

Keywords: Condiments, foodborne illness, pathogenic bacteria, contamination antibiotics.

MODELING AND OPTIMIZATION OF SURFACE ROUGHNESS, CONSUMED POWER AND PRODUCTIVITY DURING DRY TURNING OF GRAY CAST IRON

Gasmi Boutheyna
Yallese Mohamed Athmane
Bouchrit Sebti
Djouambi Nahla

ABSTRACT

Cast irons are mainly used thanks to their low production cost and their mechanical and physical characteristics equivalent to other metal alloys such as wear resistance, compressive strength, moldability, etc. Cast irons are used in various important parts of industry, particularly in the automotive industry. In fact, the machining of gray cast iron with conventional cutting tools such as carbide is severely constrained by the use of low cutting speeds, which impacts productivity and, therefore, the cost of the machining process. In this work, an experimental study was carried out in order to assess the performance of cutting materials (CBN 7050, mixed ceramic 6050, white ceramic 620 and silicon nitride 1690) during dry turning of EN-GJL350 gray cast iron. The experiments are conducted according to the Taguchi design L_{32} and based on ANOVA approach to quantify the impact of input factors on the output parameters, namely, the surface roughness (R_a), the cutting force (F_z) and productivity (MRR). The desirability function method (DF) was used to achieve a multi-objective optimization, the aim is to obtain optimal cutting regime.

Keywords: Turning, Cutting Material, Cast iron, Modeling, Optimization,

REDUCTION OF LOCAL SCOUR AROUND SQUARE BRIDGE PIER USING DOUBLE HOOKED COLLAR AND BAR AS A COUNTERMEASURE

Hafiz Ubaid Ur Rehman

Maaz Khan

Noor Elahi

Ahmad Abdullah

Shees Ur Rehman

ABSTRACT

The scouring around bridge piers has been studied using a variety of methods and approaches. For bridge erosion, the most serious threat comes from local scour near a bridge's anchorage. One of the most difficult aspects of pier building is reducing scouring via the use of a variety of countermeasures. Various methods are used to reduce scouring because of the formation of a vortex and an increase in flow. A square bridge pier is encircled by single and double hooked collars, which are used to test whether scouring may be reduced experimentally. Hooked collars are placed at various depths below and above the streambed level to determine the appropriate depth for reducing scouring to the greatest extent possible. Installing two hooked collars, one at the streambed and the other 0.5B below the streambed, yielded the best results. Even after 48 hours of testing, the bottom collar remained intact, suggesting a scouring reduction of up to 58% when compared to a pier without any protection. Scouring was reduced by 21% and 34% when using a single hooked collar at 0.5B above the streambed and bed levels. By installing a double-hooked collar at 0.5B above the bed, however, it is reduced by half.

Keywords: Square bridge pier, bars, scouring, hook-collar, and countermeasure

EVALUATING THE EFFICACY OF ARTIFICIAL INTELLIGENCE IN WIRELESS SENSOR NETWORKS

Moses Adeolu Agoi
ORCID: 0000-0002-8910-2876
Oluwanifemi Opeyemi Agoi

ABSTRACT

The ultimate goal for the advent of technology is to better the quality of human life. Artificial Intelligence (AI) is the computer replication of human acumen procedures to efficaciously resolve issues in engineering. Appropriate application of AI techniques can be utilized to improve the performance and reliability of any system including Sensor Network (SN). A Sensor Network consists of thousands of very small stations called sensor nodes whose function is to monitor record and notify a network system of specific condition that can make them error free, fast and efficient in almost all aspects. CRULLER et al. (2004) denote that these stations or devices have very little capability on their own but when they are working as aggregate, they have substantial processing capabilities. The applications of Wireless Sensor Networks (WSN) vary but are typically used for monitoring, tracking or controlling of network systems. This paper is a context review of the efficacy of Artificial Intelligence in Wireless Sensor Networks. The paper discussed some of the applications of Wireless Sensor Networks, challenges and properties in WSN network deployment. In order to collect relevant information for the paper discussion, questionnaires were drafted and administered to respondents using online Google form questionnaire instrument. Responses were collated and subjected to reliability analysis. Conclusively, the paper inferred that Artificial Intelligence (AI) has the potentials that can be used to prevent some unknown WSN security problems, find the hidden dangers in the WSN and overall improve network security to a very great extent.

Keywords: Artificial Intelligence (AI), Wireless Sensor Network (WSN), Technology.

INTRODUCTION

The development and incorporation of computational intelligence (CI) into the spheres of human endeavor is channeled towards its betterment. CI denotes the ability of computing objects to learn specific tasks from a set of data or experimental observation. CI is characterized with flexibility, self-reliance and robustness against topology changes, scenario changes and communication failures in sensor networks. A Sensor Network (SN) is a system consisting of small enumerable stations called sensor nodes. Sensor nodes are responsible for monitoring, recording and notifying specific condition at the different locations of other stations. The entire network is under the administration of a base station which is a powerful data processor and storage center and acts as gateway to another network. Advances in wireless communications have made WSNs capable of carrying out a host of large-scale decision and information processing tasks. The applications WSNs varies from tracking, monitoring or controlling to specific applications including object tracking, traffic monitoring, habitat monitoring, nuclear reactor control and fire detection. Wireless sensor networks are developed for the maintenance of condition-based machines because they enable new functionalities and offer significant cost savings.

RELATED LITERATURE

A Sensor Network consists of thousands of very small stations called sensor nodes. According to CRULLER et al. (2004), these stations or devices have very little capability on their own but when they are working as aggregate but have substantial processing capabilities. Russell & Norving (2003) state that A multi-agent system is formed from a number of interacting intelligent systems which can be implemented as a software program, dedicated computer or robot. O'Hare et al., (2006) opine that the fore going is developed to emulate the interaction abilities and intellect of a human as Distributed Artificial Intelligence whose objective is focused on human societies. According to Wang (2016), the manufacturing of robot is necessary as the use modeling could help to realize human intelligence. Ji (2020) Emphasized that smart devices are produced as there is need to simulate human consciousness and thinking processes. Turing (1950), explain further that these equipments can perform language recognition processing and image recognition its thinking ability can

correlate with that of humans. According to Yoo & Yoo (2011), wireless sensor network is based on facility and an organizational network. Wu, et al. (2011), state that these different network sensor nodes are divided into specific monitoring areas base on their functions. According to Zhang, et al. (2010), the practicability and performance of the wireless sensor network nodes determines the efficiency and operating costs of the entire network. In conclusion, Chen, et al. (2010) inferred that low cost nodes and high performance are the key to designing wireless sensor networks.

Applications of Wireless Sensor Networks

Buratti et al. (2009), state that there is limitless range of the applications of WSNs. The application domains of WSNs include: -

1. **Area Monitoring:** In area monitoring, the sensor nodes are deployed over the region where some phenomenon is to be observed. When the sensors detect the occurrence to be monitored (such as heat, pressure etc.), the event is reported to the base stations where appropriate actions are taken.
2. **Military:** WSN is an integral part of military communications, intelligence, control, investigation, battlefield, surveillance and targeting systems.
3. **Transportation:** Real time traffic information are composed by WSNs to later communicate transportation models and keep the drivers alerted of likely congestion and traffic issues.
4. **Environmental Applications:** Environmental Sensor Networks (ESNs) are fundamentally developed to cover numerous WSNs application including the sensing of seas, glaciers, oceans, forest, atmosphere, volcanoes, etc.
5. **Medical Applications:** Medical benefits of WSNs include investigative, diagnostics and drug administration in hospital, integrated patient monitoring, tracking and monitoring of patients or medical practitioners inside the medical facility.
6. **Agricultural Applications:** The deployment of WSNs into the agricultural sector has been reported to be significantly useful in areas including irrigation mechanization, resource maintenance, etc.

Challenges in Wireless Sensor Network Deployment

According to Matin & Islam (2012) and Pan, et al. (2003), there are several challenges placed by the disposition of sensor networks in WSN systems. Viz: -

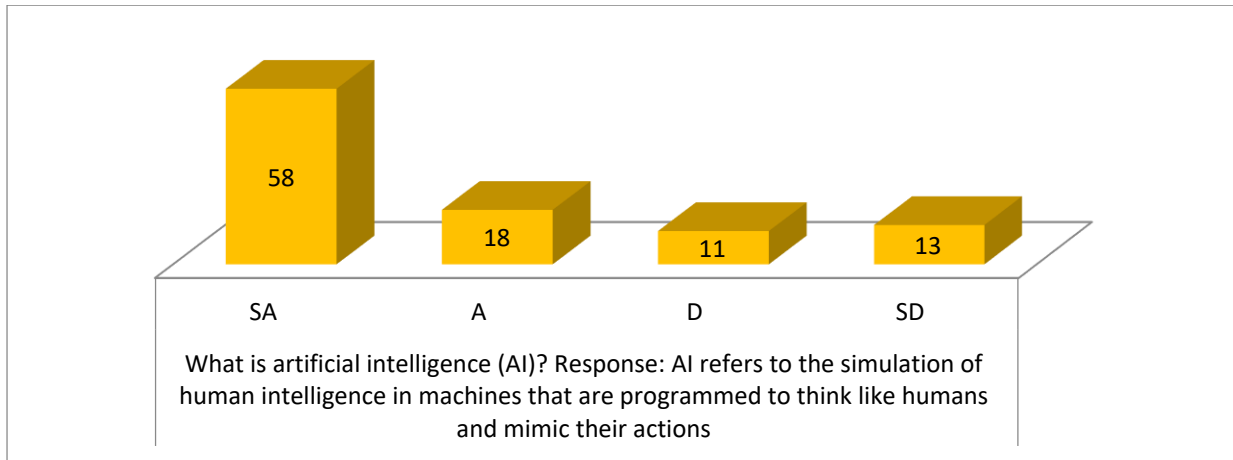
1. **Cost of Production:** The cost of the deployment models in the SNs is considerably high. The intended target price for a NS should preferably be reduced.
2. **Scalability:** There are different scales of SNs ranging from some nodes to possibly several others. The protocols positioned in SNs should be unified to maintain and preserve performance effectively.
3. **Hardware Limitations:** Every NS is expected to have a detecting component, a transmission component, a processing component and a power source component. In some instant, every extra nodes emanates with extra cost and amplifies the power consumption rate of the node.
4. **The Consumption of Power:** The major challenges of WNSs are centered on inadequate power resources. There is an utmost need to cautiously contemplate on the availability of resourceful energy.

MATERIALS AND METHODS

This paper is a context review of the efficacy of Artificial Intelligence in Wireless Sensor Networks. Some of the applications of Wireless Sensor Networks, the challenges and useful properties in WNS network deployment were discussed in the paper. In order to collect important data for the paper discussion, questions were drafted and administered to respondents using online Google form questionnaire instrument. Responses were collated and subjected to reliability analysis. The responses gathered were subjected to Cronbach's alpha reliability analysis. The result of 0.77 gave a good reliability index of the instrument. The entire exercise took place within 48 days before completion.

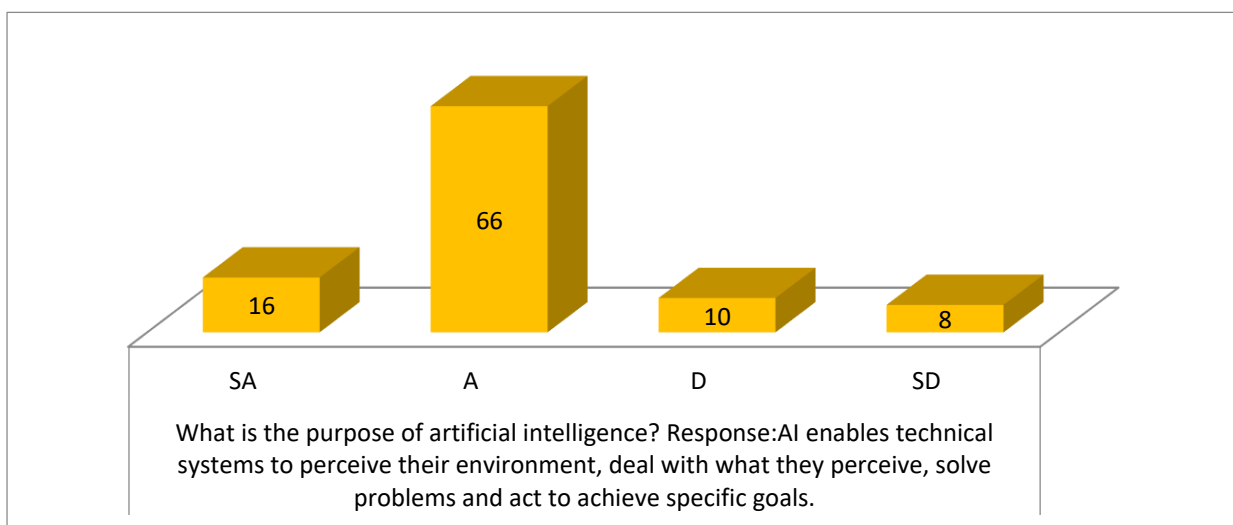
RESULT AND DISCUSSION

Analysis chart 1



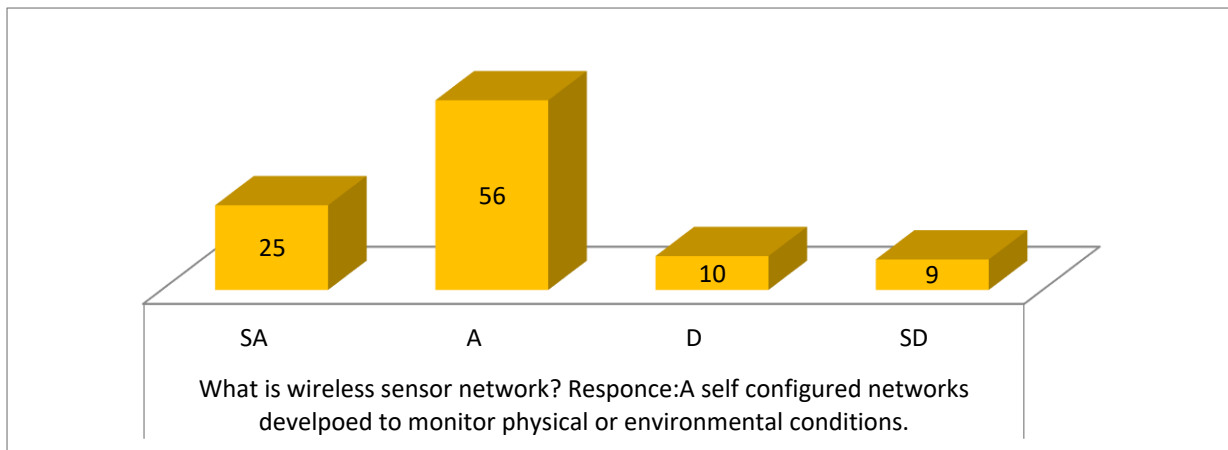
The graph plotted in fig.1 clearly show that a huge number of correspondents sees AI as the simulation of human intelligence by machines. These machines, according to the respondents are programmed to think like humans and mimic their actions. The respondents also explain that the term could applicable to any machine that exhibits traits associated with problem solving.

Fig.2: Chat Analysis



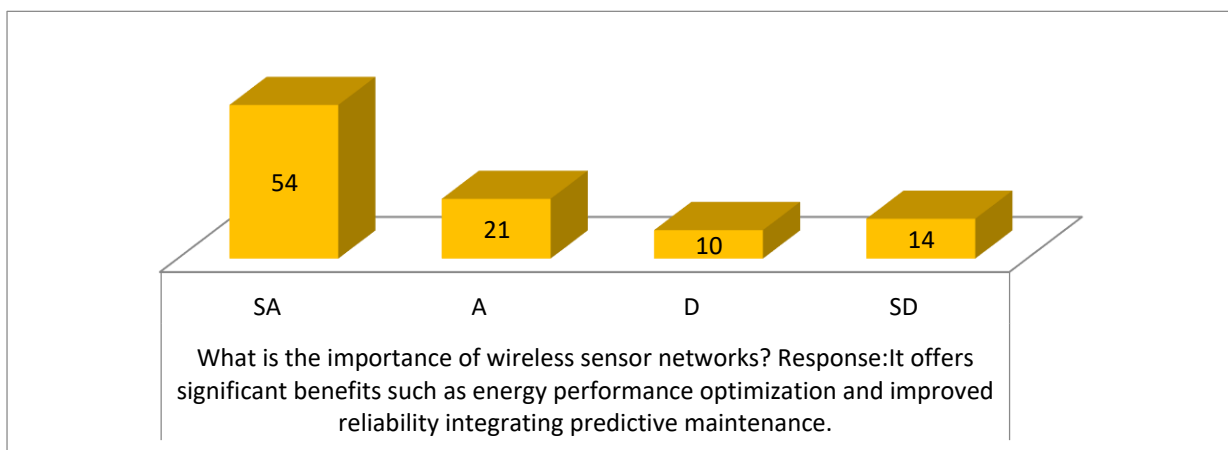
The graph plotted in fig. 2 depicts a significantly high number of the respondents agree that AI enables technical systems to perceive their environment, deal with what they perceive, solve problems and act to achieve a specific goal. The respondents further state that AI functionality display human-like capabilities including learning, planning, reasoning and creativity.

Fig.3: Chat Analysis



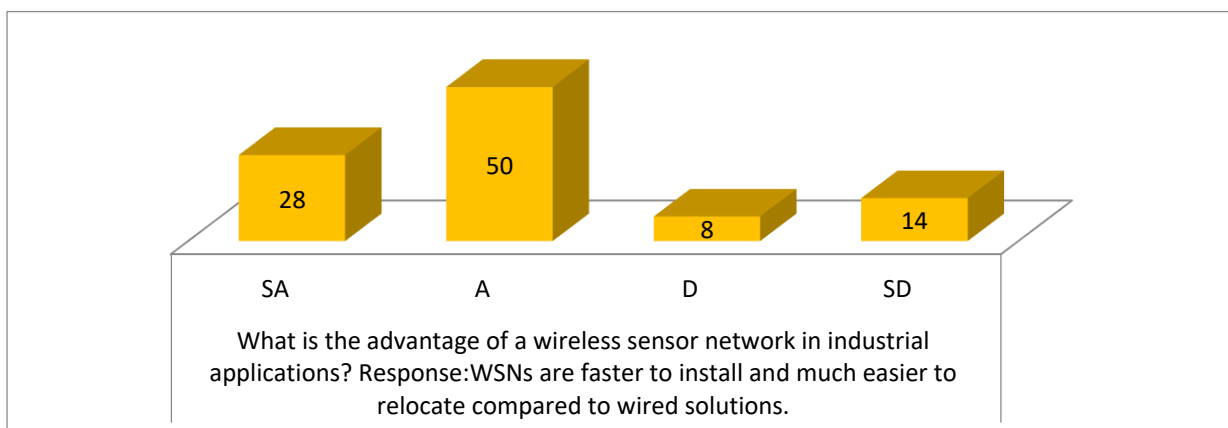
The chat analysis shown in fig.3 depicts that a greater number of the respondents concur with the statement that a wireless sensor network (WSN) is a self-configured network developed to monitor physical or environmental conditions. The respondents denoted that a WSN consists of an evenly distributed sensors including one or more sink nodes.

Fig.4: Chat Analysis



The graph plotted in fig.4, shows that a higher number of respondents agree that WSNs are faster to install and much easier to relocate compared to wired solutions. The respondents explain that WSNs are significantly scalable and offer energy independence and real-time capability when deployed with energy embedded device.

Fig.5: Chat Analysis



A larger number of the respondents in fig.5 agree with the statement that WSN offers significant benefits such as energy performance optimization and improve reliability integrating predictive maintenance. The

respondents explain further that the potential applications of WSN include industrial, building, transportation and many more.

CONCLUSION

The discussion in this paper is focused based on Artificial Intelligence in Wireless Sensor Networks. The paper carefully discussed some of the applications of Wireless Sensor Networks, challenges and properties in WNS network deployment. The paper affirmed that Artificial Intelligence (AI) has the potentials that can be used to prevent some unknown WSN security problems, find the hidden dangers in the WSN and overall improve network security to a very great extent. It is important to note that remarkable advantages are provided with the applications of WSNs in various domains.

REFERENCES

1. Buratti C, Conti A, Dardari D & Verdone R. (2009). An Overview on Wireless Sensor Networks Technology and Evolution. *Sensors*. Vol. 9. Pp. 6869-6896.
2. Chen H., Lou W. & Wang Z. (2010). A Novel Secure Localization Approach in Wireless Sensor Networks. *EURASIP Journal on Wireless Communications and Networking*. Pp. 1-12.
3. Cruller, D., Estrin, D. & Srivastava, M. (2004). Overview of Sensor Networks, *Computer*. Vol. 37(8). Pp. 41-49.
4. Ji S. H. (2020). Research on the Tool Nature of Artificial Intelligence: A Reflection Inspired by the World's First AI Inventor. *China Invention and Patent*. Vol. 17(6). Pp. 54-61.
5. O'Hare, G., O'Grady, M. & Marsh, D. (2006). *Autonomic Wireless Sensor Networks: Intelligent Ubiquitous Sensing*, Proceeding of ANIPLA 2006, International Congress on Methodologies for Emerging Technology in Automation, Publisher, University La Sapienza, Rome, Italy.
6. Russell, S. & Norving, P. (2003). *Artificial Intelligence: A Modern Approach*, Prentice-Hall, Englewood Cliffs,
7. Wang L. R. (2016). Relationship between Artificial Intelligence and Human Intelligence. *Technology Innovation and Application*. Vol. 31. Pp. 76.
8. Yoon E. J. & Yoo K. Y. (2011) Cryptanalysis of Robust Mutual Authentication Protocol for
9. Wireless Sensor Networks. *Proceedings of 10th IEEE International Conference on Cognitive Informatics & Cognitive Computing (ICCI&CC)*. Banff, Canada. Pp. 392-396.
10. Zhang Y., Bao L., Yang S.H., Welling M. & Wu D. (2010). Localization Algorithms for
11. Wireless Sensor Retrieval. *The Computer Journal*. Vol. 53(10). Pp.1594-1605.

NUMERICAL MODEL AND VERIFICATION OF EXPERIMENTAL RESULTS OF CENTRIFUGAL COMPRESSOR

Mustafa Ertürk Söylemez
ORCID: 0000-0002-9953-3362
Rasim Behçet
ORCID: 0000-0002-6897-3066
Zekeriya Parlak
ORCID: 0000-0002-2487-0065

ÖZET

Yüksek basınç sıkıştırma oranı ve kolay imal edilebilmesi sebebiyle tercih edilmekte olan santrifüj kompresörler, küçük gaz türbinlerinin kullanıldığı havacılık uygulamalarında, turbo şarjla sistemlerinde, gaz ve petrol endüstrilerinde oldukça sık kullanılmaktadırlar. Günümüzde çok popüler olan insansız hava araçlarında da yaygın olarak kullanılmaktadır. Virginia Üniversitesi Döner Makine ve Kontrol Laboratuvarında (ROMAC) test düzeneği tasarlanan ve inşa edilen bir endüstriyel boyutlu kompresör bu çalışmada sayısal çalışmaların doğrulanması için seçilmiştir. Bu test düzeneği; kompresör, giriş ve çıkış borulama sistemi, basınç ve sıcaklık ölçerler, debi ölçer ve kısma vanasından meydana gelmektedir ve maksimum çalışma hızının 23000 dev/dak ve 55 kW'lık güç gereksinimi olduğunu belirtmişlerdir. Testleri bu düzenek ile gerçekleştirilmiş olan santrifüj kompresör bu çalışmada 3B olarak tasarlanmış, tasarıma uygun çözüm ağı oluşturulmuş ve gerekli sınır şartları ANSYS CFX programı ile tanımlanarak hesaplamalı akışkanlar dinamiği (HAD) analizleri gerçekleştirilmiştir. Farklı debiler için test ve HAD sonuçları sıkıştırma oranı göz önüne alınarak karşılaştırılmıştır. %0.35 ile %1.98 aralığındaki hata oranları ile HAD sonuçları ve test verileri arasında büyük bir uyum elde edilmiştir.

Anahtar Kelimeler: Santrifüj Kompresör, HAD, Akış Gözlemi, Modelleme, Aerodinamik

ABSTRACT

Centrifugal compressors, which are preferred due to their high-pressure compression ratio and easy manufacturing, are frequently used in aerospace applications where small gas turbines are used, turbocharger systems, gas, chemical, and oil industries. It is also widely used in unmanned aerial vehicles, which are very popular today. An industrial-sized compressor, designed, built, and commissioned in the University of Virginia Rotary Machinery and Control Laboratory (ROMAC) test setup, was chosen in this study to validate the numerical studies. This test setup; consists of a compressor, inlet, exhaust piping system, pressure transducers and thermocouples, orifice flow meter, and throttling valve, and they stated that the maximum operating speed is 23000 rpm and power requirement of 55 kW. The centrifugal compressor, whose tests were carried out with this device, was designed in 3D in this study, a grid structure suitable for the design was created, and the necessary boundary conditions were defined with the ANSYS CFX program and computational fluid dynamics (CFD) analyzes were carried out. The test and CFD results for different mass flow rates were compared considering the compression ratio. A good agreement between CFD results and test data was obtained, with error rates ranging from 0.35% to 1.98%.

Keywords: Centrifugal Compressor, CFD, Flow Observer, Modeling, Aerodynamics

INTRODUCTION

Compressors are virtual machines in modern industrial processes for pressurizing and transporting gases and liquids. They are vital to the operation of essential energy sectors such as oil, gas, mining, nuclear, and hydropower. In addition, compressors are central components of heating, ventilation, and air conditioning systems for homes and commercial buildings [1]. In general, compressors can be categorized under two basic types, positive displacement and dynamic. Positive displacement compressors include piston, screw, vane, and lobe compressors. Axial and centrifugal compressor types are dynamic compressors [2]. Centrifugal compressors essentially increase the kinetic energy of the fluid by using a rotating impeller [3]. Centrifugal

compressors have many advantages, such as robustness, compactness, reliability, resistance to foreign object damage, and wider operating range.

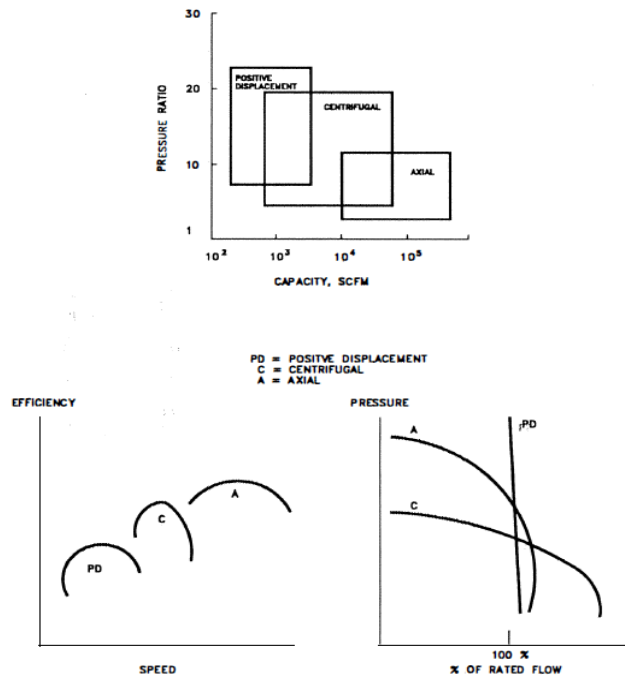


Figure 1. Performance Characteristics of Various Compressor Types [2].

Swain D. et al. used computational fluid dynamics to numerically model four impellers with varying geometries, speeds, and performance characteristics to examine the performance implications and limitations of changing the impeller geometry with the flow or axial correction. They demonstrate that axial correction is an effective method to change the design of a centrifugal compressor [4]. Hadavandi R. et al. aimed to support future numerical simulations by providing as experimentally complete boundary conditions and validation data as possible [5]. Li J. et al. studied the mathematical model of the flow field in the centrifugal compressor of the turbocharger. Based on computational fluid dynamics theory, the performance curves and parameter distributions of the compressor were obtained from 3D numerical simulation using CFX. Meanwhile, the effects of mesh number and distribution on compressor performance were investigated, analyzed, and verified by combining numerical calculation methods with test data. They showed that the increase in mesh number had little effect on compressor performance [6]. Optimization between aerodynamic performance and structural reliability is critical to achieving the maximum potential of compressor performance. Xu C. et al. used an aerodynamic and structural integration process to design a single-stage centrifugal compressor. They built and tested their design and stated that it showed very reasonable agreement with the analyses [7]. The inertia of the compressor significantly affects the airflow and, thus, the dynamic system behavior after a certain load stage [8]. In order to increase its efficiency, the Eckardt O rotor was optimized by changing the blade angle distribution. Elzahaby A. M. et al. performed the optimization process using an automated procedure performed within the ANSYS workbench. They compared the performance of the optimized and original designs, both qualitatively and quantitatively, and reported that the optimized design efficiency increased successfully from 87,994% to 88,481%, according to the CFD results [9]. Aghaei Tog et al. tried to explain how to design and model a good compressor with a CFD model and to explain inconsistencies between testing and 3D analysis. Only one impeller vane model was used to compare the 1D design data obtained from the developed centrifugal compressor design code. The numerical results of the performance data indicated that the experimental data were in good agreement with the experimental data at and near the highest efficiency operating point [10]. Özer A. C. et al. performed performance tests of radial compressors used in turbojet engines capable of producing 0.15 KN thrust. They said the performance map was obtained by measuring the compressor efficiency, pressure increase rate, mass flow rate, and revolution number simultaneously under different operating conditions [11]. Rossbach T. et al. presented the first experimental performance data for a midstage centrifugal compressor test rig built at RWTH Aachen University and designed the measurements based on numerical calculations. Analyzed performance based on a compressor map for design speed

supported by detailed measurements within the diffusion system. They stated the negative effect of the return channel on stage efficiency and pressure recovery at high flow rates [12]. Mostefa B. et al. developed a general analysis and optimization approach in the design and performance analysis of centrifugal turbomachines. Based on different methods, from a one-dimensional approach to the three-dimensional study of internal flow. They have developed a procedure for predicting performance as well as for predicting and understanding events related to the operation of turbomachines. They said they managed to control the aerodynamic profile of the centrifugal compressor impeller blades by changing the number of blades [13].

MATERIAL AND METHOD

An industrial-sized compressor, whose test setup was designed and built by the University of Virginia Rotary Machinery and Control Laboratory (ROMAC), was chosen in this study to validate the numerical studies. The test setup is shown in Figure 1 and consists of a centrifugal compressor, diffuser, exhaust piping system that forms the plenum volume, and a throttle valve for flow control.



Figure. 2. Experimental compressor setup.

Table 1 shows the design and performance parameters of the selected centrifugal compressor.

Table 1. Compressor Design Parameters

Parameter	Value
Maximum speed (RPM)	23000
Design mass flow rate (kg/sec)	0.833
Design pressure ratio	1.68
Inducer hub diameter (mm)	56.3
Inducer tip diameter (mm)	116.72
Impeller tip diameter (mm)	250
Piping diameter (m)	0.203
Inlet piping length (m)	5.2
Exhaust piping length (m)	21.3

They used a total of 12 pressure transducers in the compressor and throughout the piping and obtained the measurements from these. They also used an orifice flow meter to measure the flow.

Computational Fluid Dynamics

Since the model to be designed is a compressor, Vista CCD (Vista Centrifugal Compressor Design) in Ansys workbench was used. In this module, the desired design inputs, such as total pressure ratio, mass flow, shaft speed, isentropic efficiency, inlet temperature, and inlet pressure values, are entered, as shown in Figure 3. In the second step, gas properties, ideal air is selected.

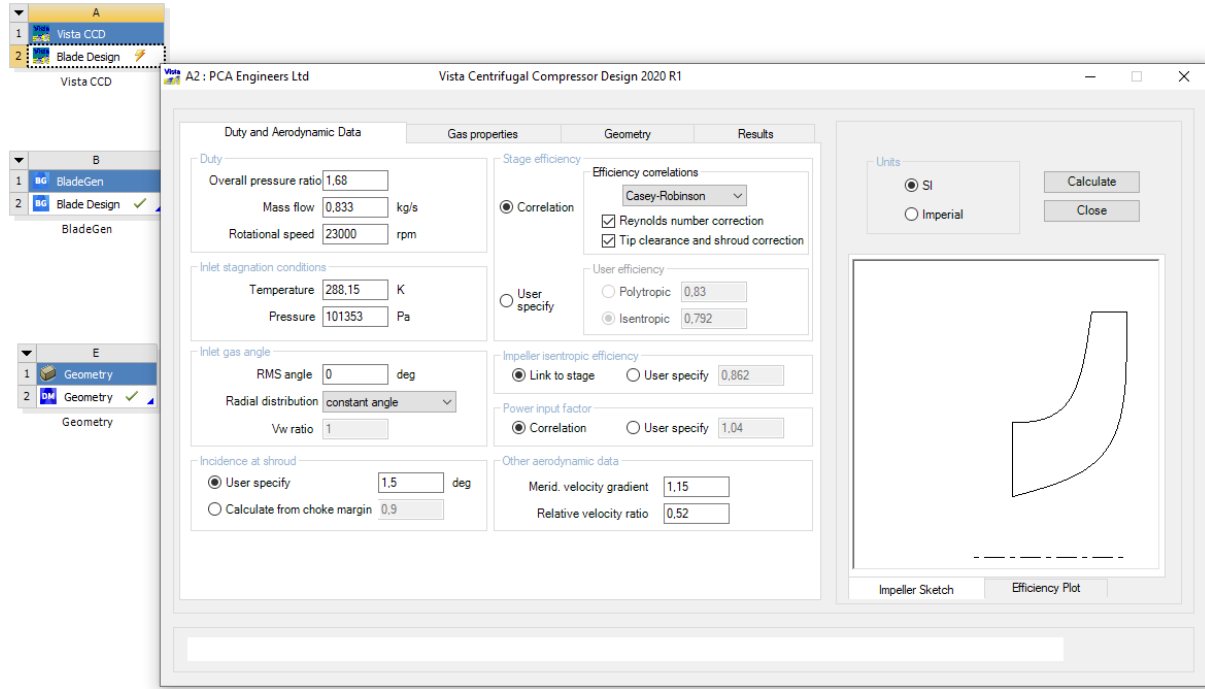


Figure 3. Vista CCD module and entered values

In the next step, in the geometry part, the design dimensions of the hub diameter, shroud diameter, tip clearance, number of blades, and number of splitter blades are entered. Figure 4 shows the Geometry part and the entered values. After the design inputs were defined, the calculation in the SI unit was tried, and the analysis of the meridional flow and the blade design was carried out.

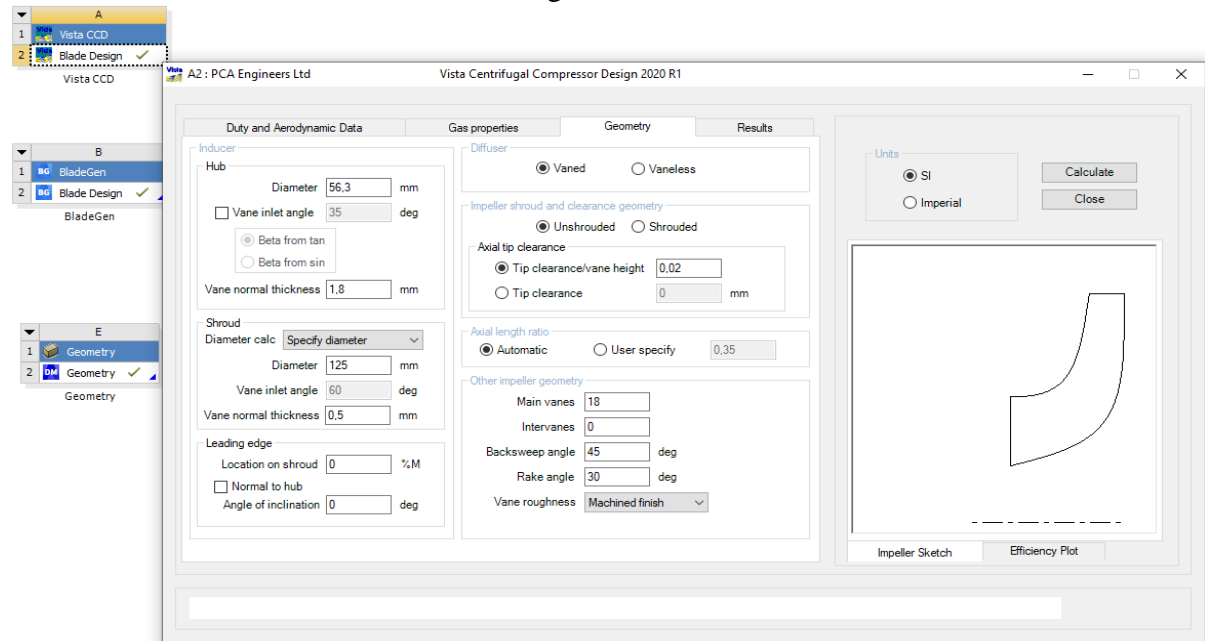


Figure 4. The geometry part of the Vista CCD module and the entered values

Since the structure to be designed is the blade, the BladeGen module that serves this purpose is used, and thus the blade design can be done much more precisely and quickly. If the expected values are not obtained after

the computational fluid dynamics analysis (CFD), the design can be easily changed from here. Blade characteristics, the number of the blade, and the meridional flow profile are defined. The blade structure was adjusted using the M-prime (leading edge to trailing edge) angles in degrees. While adjusting the blade structure, beta and theta curves were used, and bezier control points were selected from the spline curve and bezier control points as control points. In addition, a more understandable design was obtained by making the number of points five instead of four.

TurboGrid

Turbogrid module was used to create the mesh structure for the centrifugal compressor. The first element offset method is used for boundary layer improvement control, and the y+ method is used for element size close to the wall. The program solves conservation equations for each element created. Creating the correct number of mesh ensures that the analysis is solved faster and without problems. Due to the high speed in turbomachines, there is a need for a large number of high-quality mesh. The mesh created for the compressor is shown in Figure 5. It is observed that there is a more frequent and dense mesh structure around the blade. The mesh consists of tetrahedral elements, and therefore the analyzes take longer. Thus, it is expected that the analysis will yield more accurate results.

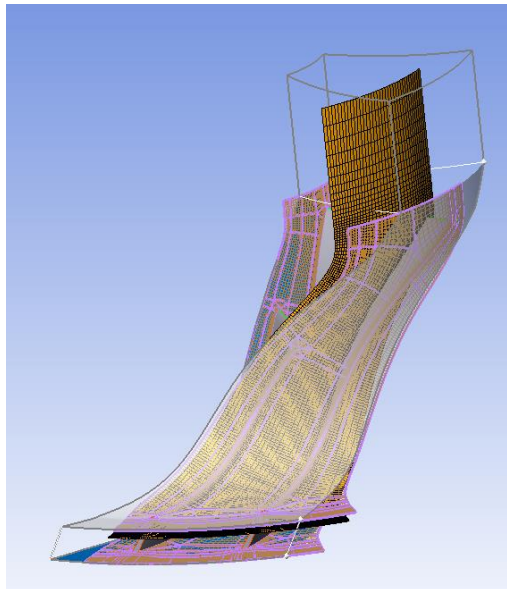


Figure 5. Mesh structure in turbogrid

CFD Analysis

Computational fluid dynamics analyses of the mesh structured design were performed using CFX-Pre. The machine type and coordinate system were entered into the compressor in the ANSYS CFX module. Rotation speed and direction are entered, and necessary physical definitions are made. CFX uses various equations to do solutions. These equations are continuity equation, momentum conservation, and energy conservation. For the flow analysis, 0 atm was chosen as the reference pressure to the basic settings, rotating as the working area, and the turbulent flow model was chosen for the flow model. Since there are many turbulence models in the program, a literature search has been carried out, and the most common k- ϵ and k-w models, have come to the fore. Since the turbulence model directly affects the results, the use of the correct turbulence model is very important. Various analyzes were carried out by choosing the k-w SST model, which is preferred in aviation applications. The k-w SST model is a mixture of k-w and k- ϵ models as a model. While the k-w model makes sensitive solutions for areas close to the wall, the k- ϵ model makes more sensitive solutions in areas away from the wall. In flow analysis, the fluid input boundary type for input and output zones were selected as input and output boundary types. According to these changes, the CFX setup is shown in Figure 6.

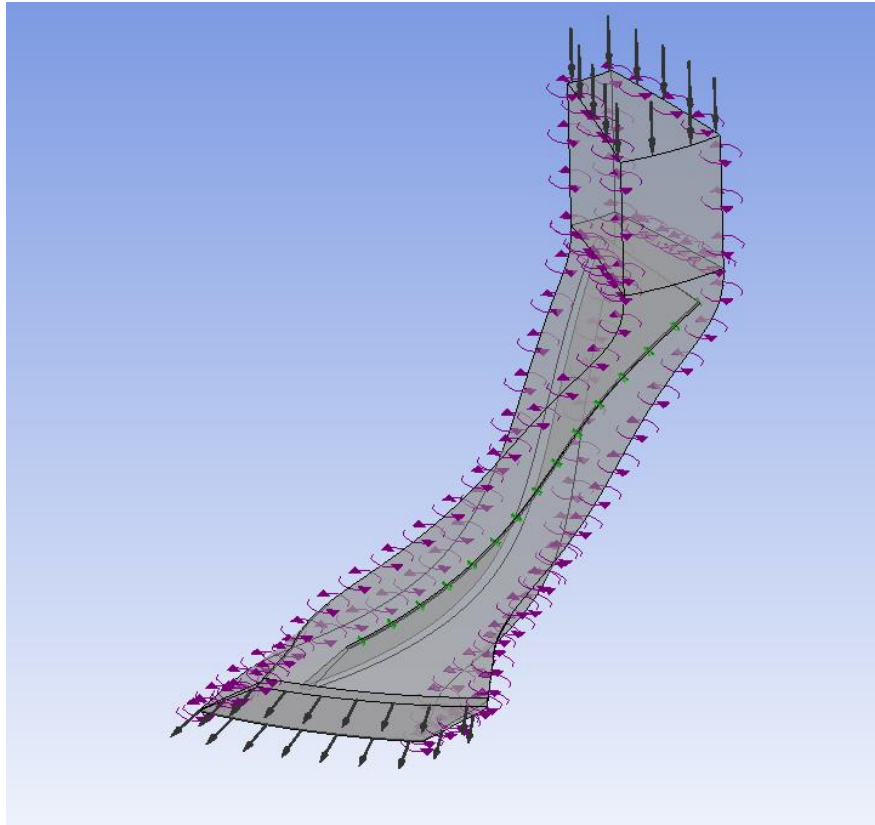


Figure 6. CFX Setup Image

RESULTS AND DISCUSSION

As a result of the analysis, the performance result table of the compressor is shown in Table 2.

Table 2. Compressor Performance Results

Parameter	Value
Rotation speed [radian s ⁻¹]	1829.77
Mass flow rate [kg s ⁻¹]	0.8056
Inlet volume flow rate [m ³ s ⁻¹]	0.6578
Input Power [W]	19438.8
Work Input Coefficient	0.5721
Total pressure ratio	1.2999
Total temperature ratio	1.0834
Total isentropic efficient	93.3362

After the analysis, the isometric three-dimensional view of the compressor is seen.

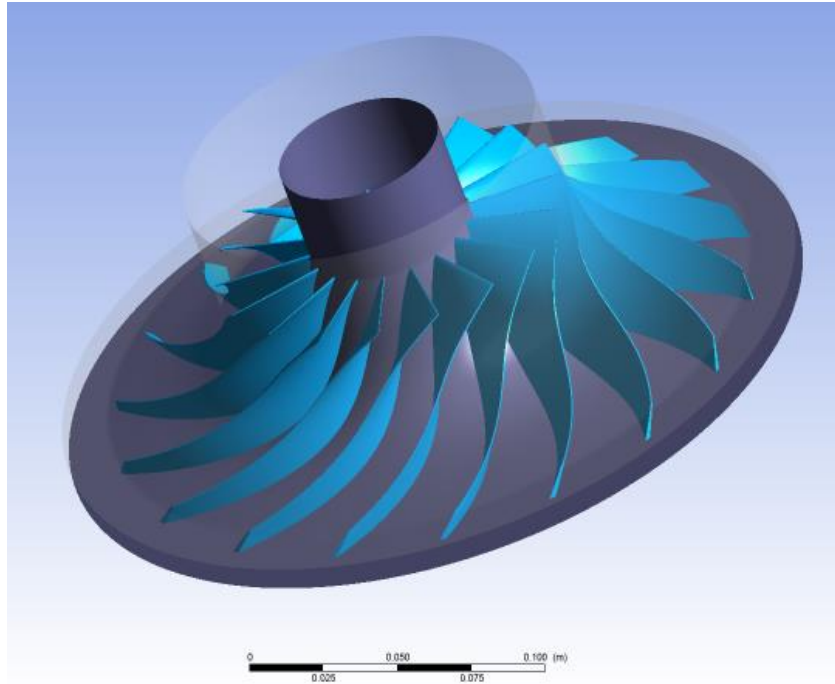


Figure 7. Three dimensional isometric image of the blade

The mesh structure used in the analysis is shown in Figure 8. As can be seen, there is a frequent grid structure near the blade.

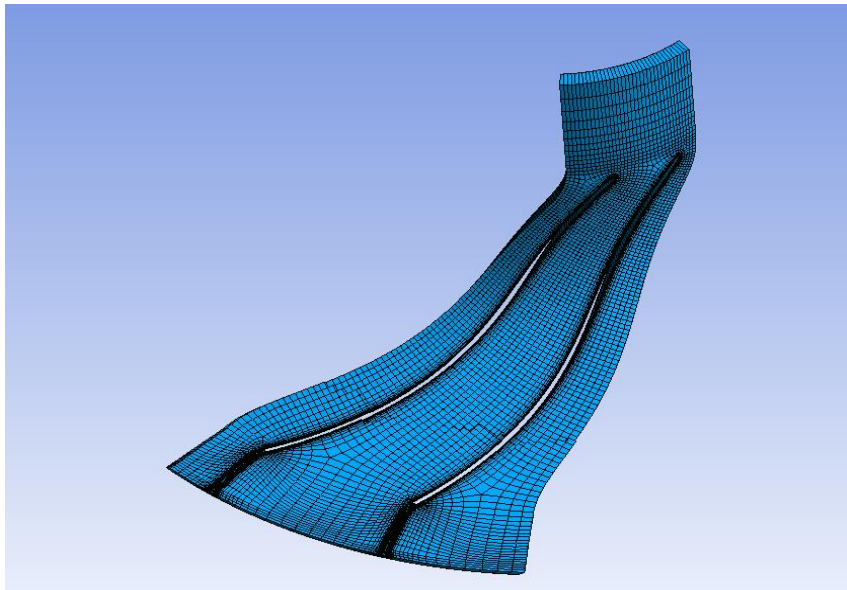


Figure 8. Mesh structure

Figure 9 shows speed vectors 50%. We can say that it shows a similar structure in parallel with the Mach number contour. It is seen that there is a regular flow area.

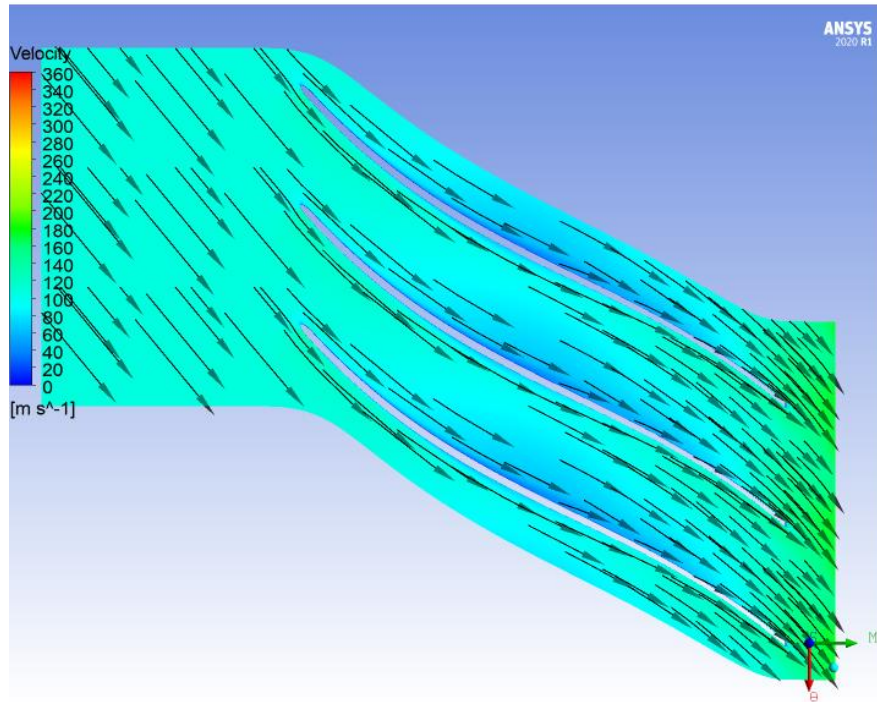


Figure 9. Speed vectors 50%

The results of the compressor, which we made a numerical analysis, and the results of the experimental compressor are seen in Table 3.

Table 3. Pressure Rates percentage comparison

Analysis Mass flow	Analysis Pressure ratio	Experimental Pressure ratio	Experimental Mass flow	Error %
0,341	1,414	1,386	0,341	1,98
0,377	1,4011	1,385	0,377	1,15
0,428	1,3878	1,383	0,428	0,35
0,509	1,3691	1,38	0,509	0,80
0,622	1,3383	1,355	0,622	1,25
0,789	1,2999	1,306	0,789	0,47
0,969	1,2397	1,223	0,969	1,35

As can be seen from Table 3, the highest 1.98 % and the lowest 0.35 % error are between experimental results and numerical analysis results. The graphical demonstration between analysis results and experimental results in different mass flow rates at 17473 RPM speed is shown in Figure 10. Likewise, the mass flow rate and pressure ratios at 16290 RPM and 12184 RPM rates are shown in Figure 11.

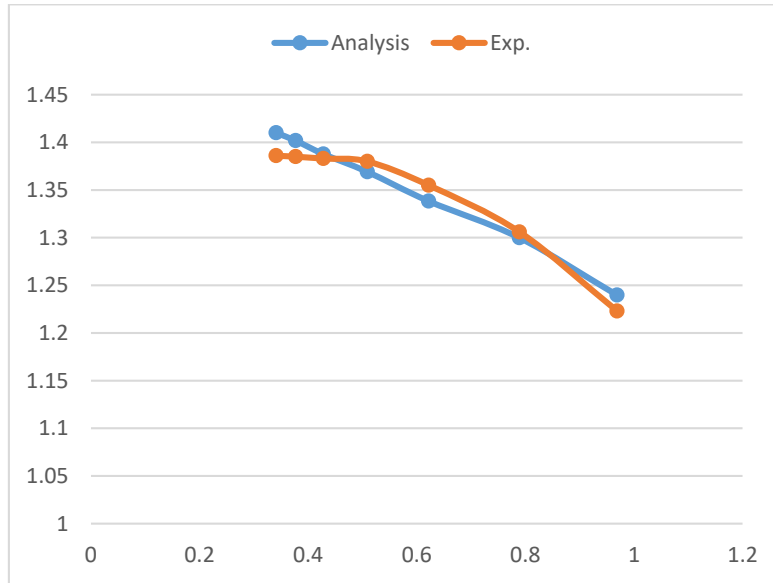


Figure 10. Experimental Results and Analysis Results

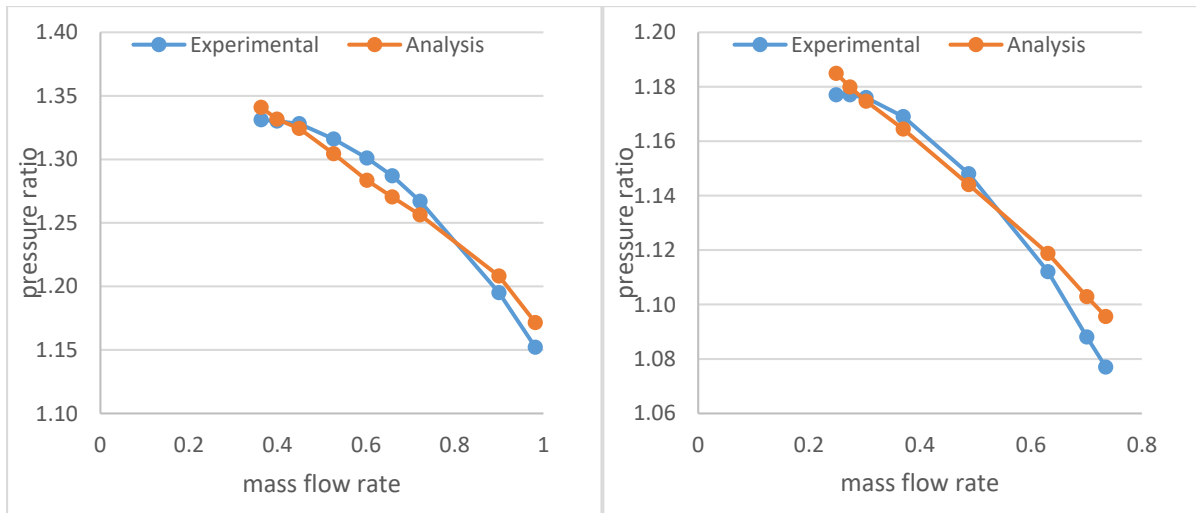


Figure 11. Comparisons in 16290 RPM and 12184 RPM speeds respectively

CONCLUSION

Experimental studies have been modeled using a package program of a centrifugal compressor which was performed by Virginia University Doner Machinery and Control Laboratory (ROMAC). After the design was obtained, numerical analyzes of this model were performed. The results of the analysis were found to be quite close with the experimental results. The analysis of different speeds continued to be compared, and it has been shown graphically that the results of the analysis at different speeds are consistent with experimental results. The highest 1.98 % and the lowest 0.35 % error are obtained between the experimental results at the design point and the numerical analysis results.

REFERENCES

1. Yoon, S. Y., Lin, Z., & Allaire, P. E. (2013). Experimental evaluation of a surge controller for an AMB supported compressor in the presence of piping acoustics. *IEEE Transactions on Control Systems Technology*, 22(3), 1215-1223.
2. Boyce, M. P. (1993). Principles Of Operation And Performance Estimation Of Centrifugal Compressors. In *Proceedings of the 22nd Turbomachinery Symposium*. Texas A&M University. Turbomachinery Laboratories.
3. Kulkarni, V. V., Anil, T. R., & Rajan, N. K. S. (2016). An Impeller Blade Analysis of Centrifugal Gas Compressor Using CFD. *International Journal of Innovations in Engineering and Technology*, 7(4).

4. Swain, D., & Engeda, A. (2014). Performance impact of impeller blade trimming on centrifugal compressors. *Proceedings of the Institution of Mechanical Engineers, Part A: Journal of Power and Energy*, 228(8), 878-888.
5. Hadavandi, R., Fontaneto, F., & Desset, J. (2018). Complete characterization of a highly loaded low pressure compressor at different reynolds numbers for computational fluid dynamics simulations. *Journal of Turbomachinery*, 140(6), 061008.
6. Li, J., Yin, Y., Li, S., & Zhang, J. (2013). Numerical simulation investigation on centrifugal compressor performance of turbocharger. *Journal of Mechanical Science and Technology*, 27, 1597-1601.
7. Xu, C., & Amano, R. S. (2012, June). Aerodynamic and structure considerations in centrifugal compressor design: Blade lean effects. In *Turbo Expo: Power for Land, Sea, and Air* (Vol. 44748, pp. 557-568). American Society of Mechanical Engineers.
8. Pischinger, S., Schönfelder, C., Bornscheuer, W., Kindl, H., & Wiartalla, A. (2001). Integrated air supply and humidification concepts for fuel cell systems. *SAE Transactions*, 86-92.
9. Elzahaby, A. M., Khalil, M. K., & AlMoghazy, M. E. (2018). Automated optimization of centrifugal compressors “Eckardt rotor O”. *Journal of Engineering Research*, 2(August), 48-62.
10. Aghaei tog, R., Mesgharpoor Tousi, A., & Soltani, M. (2007). Design and CFD analysis of centrifugal compressor for a microgasturbine. *Aircraft Engineering and Aerospace Technology*, 79(2), 137-143.
11. Özer A.C., Çoban K., & Akmandor I.S. (2013) “Radyal kompresör performans test sistemi kurulumu” VII. National Aeronautics and Aerospace Engineering Convention
12. Rossbach, T., Rube, C., Wedeking, M., Franz, H., & Jeschke, P. (2015). Performance measurements of a full-stage centrifugal process gas compressor test rig. In *11th European Conference on Turbomachinery Fluid Dynamics & Thermodynamics (ETC11)*, Madrid, Spain, Mar (pp. 23-27).
13. Mostefa, B., Kaddour, R., Embarek, D., & Amar, K. (2021). Analysis and Optimization of the Performances of the Centrifugal Compressor Using the CFD. *Journal homepage: <http://iijeta.org/journals/ijht>*, 39(1), 107-120.

CFD ANALYSIS AND OPTIMIZATION OF TANDEM BLADE RADIAL COMPRESSOR

Mustafa Ertürk Söylemez
ORCID: 0000-0002-9953-3362
Zekeriya Parlak
ORCID: 0000-0002-2487-0065
Rasim Behçet
ORCID: 0000-0002-6897-3066

ÖZET

Radyal kompresörler hem ticari hem de askeri uygulamalarda kullanılmaktadır, ancak, kompresör performansı kararlı çalışma aralığını etkileyen akış kararsızlığı ile sınırlıdır. Yüksek basınç sıkıştırma oranı sebebiyle tercih edilmektedir ancak düşük verimleri ve kötü çalışma aralığı sebebiyle geliştirilmeye açık bir alan olduğu görülmektedir. Radyal kompresörlerin performanslarını artırmak için birçok yenilikçi fikir ortaya konmuş ve çalışmalar gerçekleştirilmiştir. Bunlardan akışkan kontrolünü ekstra hava yapılandırılmasına ihtiyaç duyulmadan gerçekleştirebilen ardışık (tandem) kanatlı radyal kompresör en çok ilgi göreni olmuştur. Bu çalışmada ardışık kanatlı radyal kompresörün performansını etkileyen dört farklı tasarım parametresine göre analiz sonuçları incelenmiştir. İzantropik kompresör verimini ve basınç sıkıştırma oranını etkileyen parametreler literatür araştırması yapılarak belirlenmiştir. Bu parametreler ardışık kanatların dönme eksininde birbirlerine göre konumunu belirleyen saatleme pozisyonu, teta, ardışık kanatlar arasındaki boşluk ve indükleyici kanatların uzunluğudur. Bu parametrelerin her birinin belirlenen alt ve üst değerler arasındaki değişiminin analiz sonuçlarına etkisi cevap yüzeyi metodu ile incelenmiştir. Ayrıca, basınç sıkıştırma oranı ve izantropik verimin maksimum yapan parametre değerleri de MOGA optimizasyon yöntemi ile belirlenmiştir.

Anahtar Kelimeler: Radyal Kompresör, Ardışık kanat, Optimizasyon, HAD

ABSTRACT

Radial compressors are used in both commercial and military applications; however, compressor performance is limited by flow instability, which affects the stable operating range. It is preferred because of its high-pressure compression ratio, but it is an area open to improvement due to its low efficiency and poor working range. Many innovative ideas have been put forward, and studies have been carried out to increase the performance of radial compressors. Among these methods, the tandem-bladed radial compressor, which can perform fluid control without the need for extra air configuration, has attracted the most attention. In this study, the analysis results were examined according to four different design parameters that affect the performance of the tandem blade radial compressor. The parameters affecting the isentropic compressor efficiency and pressure compression ratio were determined by literature research. These parameters are Clocking position, which determines the position of tandem blades relative to each other on the axis of rotation, theta, space between inducer and exducer blades, and the length of the inducer blade. The effect of the variation of each of these parameters between the determined lower and upper values on the analysis results was examined by the response surface method. In addition, the parameter values that maximize the pressure compression ratio and isentropic efficiency were determined by the MOGA optimization method.

Keywords: Radial Compressor, Tandem Blade, Optimization, CFD

INTRODUCTION

Radial compressors are widely used in industry, turbochargers, some gas turbines for aerospace applications, and many other civil and military fields. Flow separation in the radial section is far from satisfactory for reasons such as the efficiency levels of radial compressors due to complex secondary flows, trailing flow irregularity, and intense impeller/diffuser interaction. Tandem blade compressors have become increasingly attractive lately as they achieve flow control without additional complex structures or control costs. The term tandem blade means the radial impeller is divided into two parts: inducer and exducer. A tandem radial

compressor is a mechanism that comes together with various values of many parameters. Some of these parameters are mass flow rate, speed of the impeller, number of blades, blade angle, thickness distribution, and flow meridional profile. The first references to the tandem blade compressor were published in 1977 by the NASA Lewis research center. In this study, a 13.65 cm tandem blade radial compressor was experimentally investigated in order to improve the conventional compressor at the same pressure ratio and mass flow rate. They designed a compressor with a pressure ratio of 6.19, a mass flow rate of 0.907 kg/s, and 80000 rpm. While the mass flow rate at the design speed was 0.911 kg/s, it was found to be 0.44% greater than the choke flow rate (0.907 kg/s). They state that with a vaneless diffuser, peak impeller efficiency at design speed increased from 0.767 to 0.813 [1]. Roberts Douglas A. et al. a numerical study was carried out to examine the aerodynamic properties of a tandem blade impeller design for the backstage of the compressor of a gas turbine. They said that all impellers with tandem blades are less efficient than conventional compressors. They said that the tandem blade has a very large effect on the pressure ratio, temperature ratio, efficiency, and slip factor [2]. Ju Y. P. et al. manufactured and tested a tandem blade radial compressor in 2014. They stated that the impeller with tandem blades has a better discharge flow than the splitter blade impeller, but has lower efficiency. They said that the distance between the inducer and the exducer had a high effect on the efficiency of the tandem impeller, and they also stated that the numerical results were in agreement with the test results [3]. Erdmenger R. R. et al. studied the different aspects of the design of the tandem blade radial compressor and their effects on the performance of the radial compressor with a high flow coefficient and high-pressure ratio. They stated that the axial clearance between the inducer and the exducer has little effect on the compressor performance, clockwise has a significant effect, and the best performance will be obtained when the inducer and exducer are aligned [4]. David H. et al. summarized the evolutionary steps of the modern centrifugal compressor for aerospace applications and made recommendations for such future work. They stated that a properly designed tandem blade radial compressor could achieve higher values than conventional compressors of the same size, which will reduce engine fuel consumption, dimensions, and weight in aviation [5]. Li Ziliang et al. numerically investigated the high-pressure ratio centrifugal compressor at non-design speeds (higher than operating speed). As a result of the study, they said that the tandem blade impeller would increase performance in working conditions. They stated that approximately 1.8 percent improvement in isentropic efficiency and 5 percent improvement in the operating range were achieved. They also stated that there is a decrease in the performance of the tandem blade impeller due to inductive shocks at high speeds [6]. Tao Y. et al. studied the flow characteristics of a supersonic sequential impeller with an input Mach number of 1.2 using a computational fluid dynamics (CFD) solver to expand the application areas of tandem impellers. They stated that tandem blade loss is difficult to control due to complex flow structures with supersonic input, and forward blade loss is equivalent to overall loss under all operating conditions [7]. Li Ziliang et al. conducted computational and experimental tandem investigations within various impeller meridional flow path profiles to explore the tandem application range and underlying flow mechanisms. The performance variation of the compressor, impeller components and diffuser components were investigated in relation to various flow path profiles. They stated that the inner and outer diameter ratios of the impeller are critical and that this ratio increases the compressor efficiency by 1.5 percent in the range of 0.65 to 0.75 ratios. They said that the impeller discharge would not be uniform outside this range and the efficiency would decrease [8]. To explore the flow mechanism and improve the performance of the impellers of the supersonic rotor, pan et al. took the supersonic rotor Rotor37 and redesigned it to obtain the original tandem supersonic rotor. They developed and applied the physical programming method and multi-objective optimization method based on the Kriging model. They stated that the mass flow rate and surge margin are higher when compared to Rotor37, but they stated that the efficiency is very low compared to Rotor37 [9]. Li Ziliang et al. numerically investigated a radial compressor's performance and flow fields with various tandem impeller arrangements to explore the underlying physics of the coupling characteristics of the tandem impeller and the flow fields of the tandem impeller. The main reason for the performance difference in the inducer and exducer lies in the inductive pressure variation at the blade trailing edge determined by the kutta condition [10]. Li Ziliang et al. stated that the tandem impeller is a successful passive flow control method that can locally affect the internal flow field, which can exhibit improved compressor operating ranges without any loss of impeller efficiency or pressure ratio. Results indicated that the tandem impeller method could achieve a maximum operating range

gain of 16.7%. They noted that basic compressor instability is triggered by end zone flow distortion caused by end leak flow [11].

MATERIALS AND METHOD

The tandem compressor design of the radial compressor, which has been verified by numerical analysis, has been carried out. In the geometry design modeler module of the numerical analysis program, the drawings of the tandem compressor were made. The inducer and exducer parts of the radial compressor were designed using the revolve feature of the package program, and their geometry was drawn. This geometry was sent to the turbo grid, a meshing module, using the exportpoints feature. The visual of the designed tandem radial compressor is shown in Figure 1.

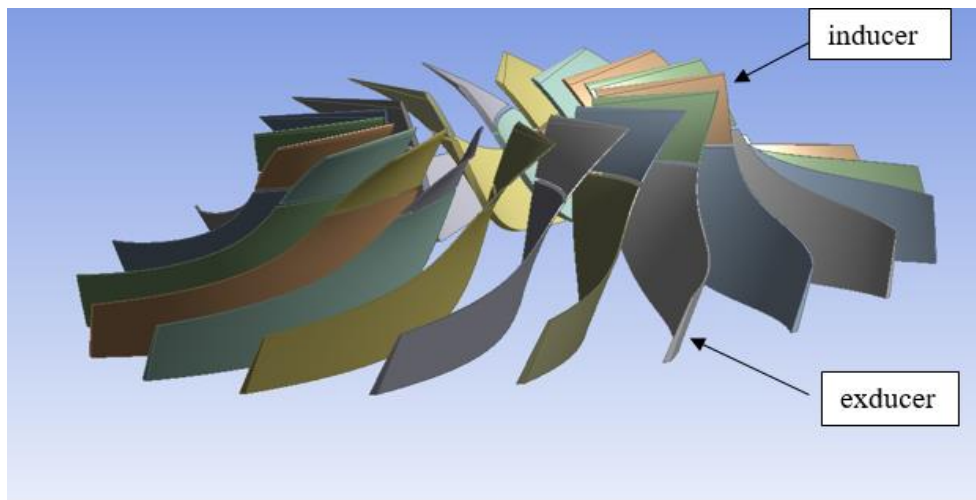


Figure 1. Tandem blade radial compressor design

The design is sent to the meshing module of the package program, and the appropriate mesh structure is selected and divided into a sufficient number of finite elements. The global size factor is selected as the mesh size method, and proportional to mesh size is selected as boundary layer improvement control. The meshing process was completed by deciding on the topology method suitable for the design. The mesh is applied not only to the design but also to the fluid within the design. The mesh of the tandem radial compressor is shown in Figure 2.

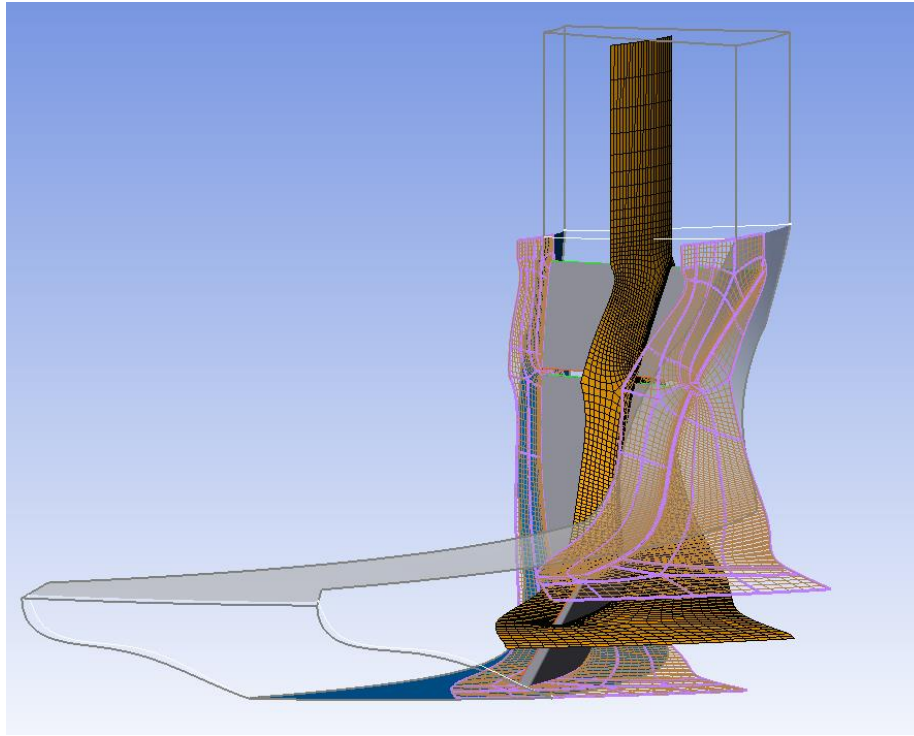


Figure 2. The mesh structure on the radial compressor with tandem blades

The mesh of the single-blade structure is shown to save time and energy, but the analysis results are performed for all blades. Before performing the analysis of the design, some input values are given. 0 atm and ideal gas were chosen as the reference pressure. The total energy is selected as the heat transfer option for the fluid model. Shear Stress Transport was determined as the turbulence model. In the solver controls, the high resolution was selected in the advection chart, and 300 was entered as the number of iterations and continued until convergence. 656502 total nodes and 616476 total elements were generated at the mesh structure.

RESULTS AND DISCUSSION

Numerical analysis of the model was carried out with the above inputs. Analysis results are given in Table 1.

Table 1. Performance results of tandem blade radial compressor

Parameter	Value
Rotation speed [radian s ⁻¹]	1829.77
Mass flow rate[kg s ⁻¹]	0.7736
Inlet volume flow rate [m ³ s ⁻¹]	0.6317
Input Power[W]	23757.7
Work Input Coefficient	0.7109
Total pressure ratio	1.3952
Total temperature ratio	1.1061
Total isentropic efficient	94.3

The visuals of the mesh elements with 50% clearance from the analysis result images are shown in Figure 3. As can be seen in the figure, a very regular mesh structure has been created.

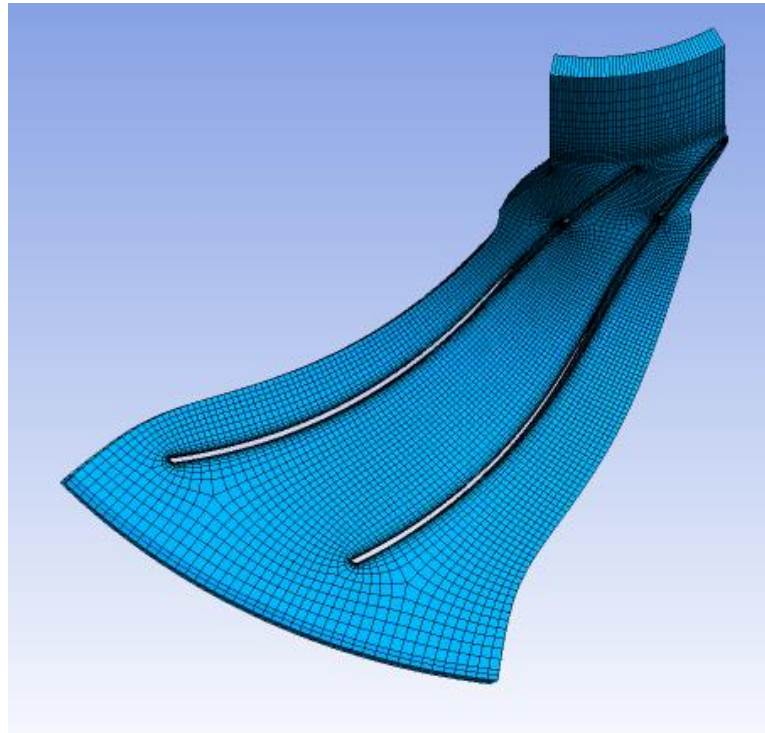


Figure 3. Mesh elements at 50%

The representation of velocity vectors and M_{rel} at 50% is shown in Figure 4. As can be seen in the figure, there is a regular flow area.

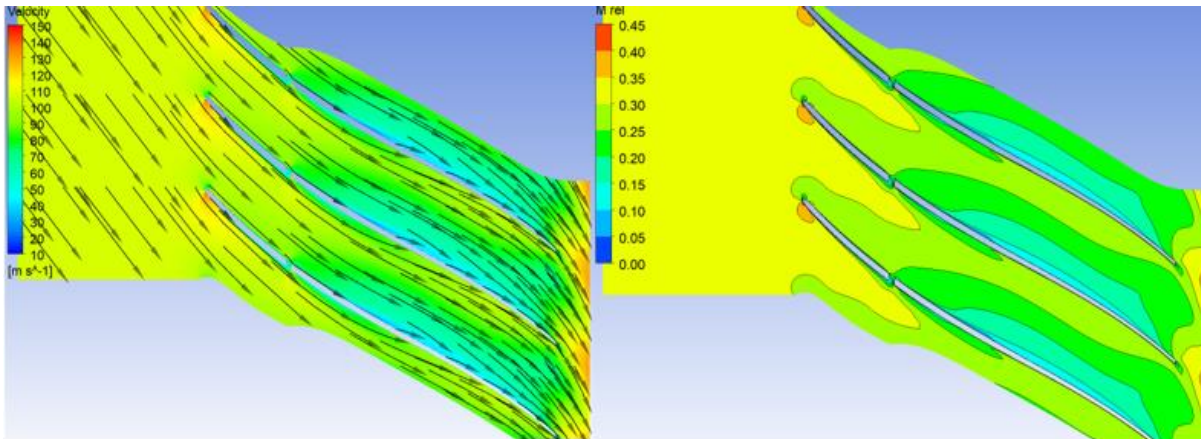


Figure 4. Velocity vectors and M_{rel} at 50%

Parameter Optimization

Parameters that are thought to affect the results of the tandem blade radial compressor were selected, and optimization processes were performed on them. Among these parameters, the input parameters were chosen as the cutting angle, which we call theta (θ), the vertical distance between the inducer and the exducer (X), the angle between the inducer and the exducer, which we call clocking (C), and the vertical length of the inducer, which we call length (L). The pressure ratio and compressor isentropic efficiency were selected as the output parameters. The first step is the determination of the upper and lower bounds of the input parameters. The upper and lower bounds are specified in Table 2.

Table 2. Input and output parameters boundarys

Parameter Name	Lower Bound	Upper Bound
θ (°)	60	105
X (mm)	1	3
C (°)	0	10
L (mm)	15	25

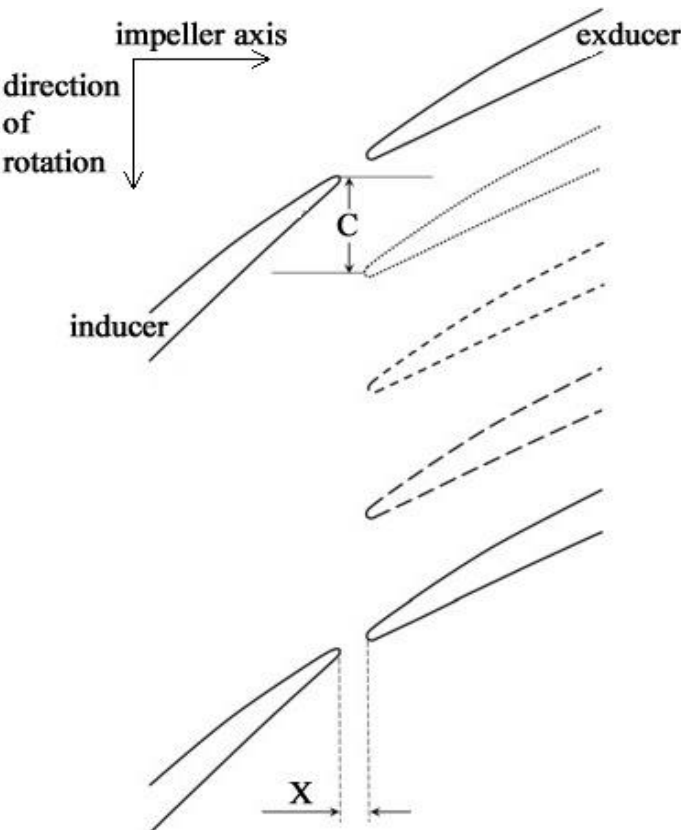


Figure 5. Representation of the X and C parameters

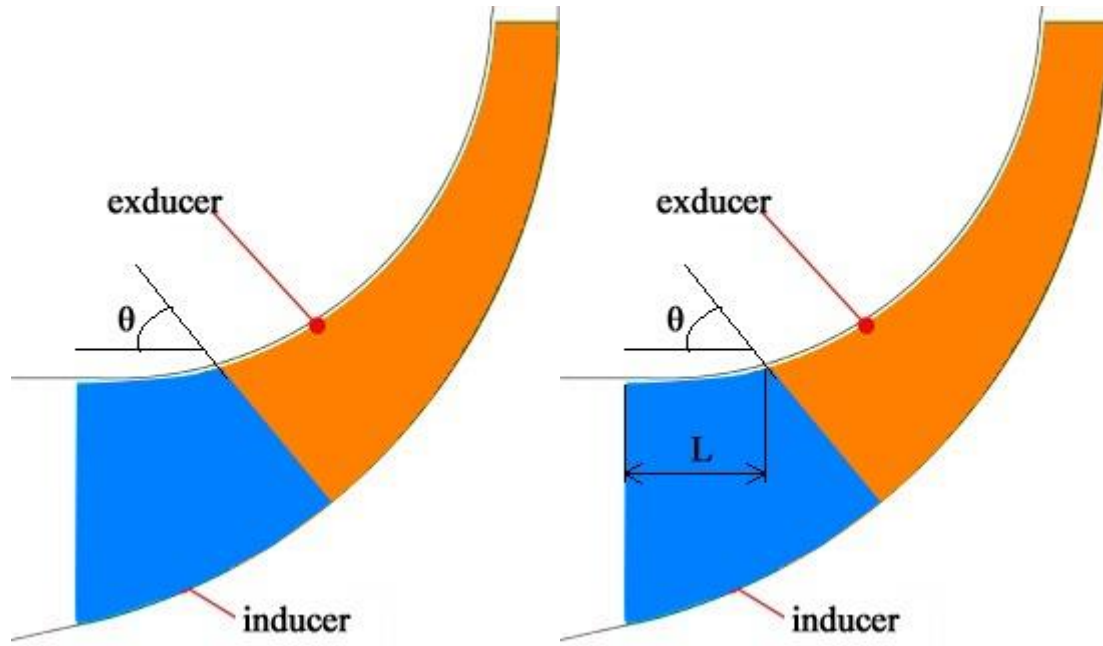


Figure 6. Representation of the θ and L parameters

These parameters are transferred to the module of the package program called response surface optimization. The response surface method module has an interface with input parameters and output parameters. Lower and upper limits were determined for the parameters selected from the literature review and considering our design geometry. This module gives us design points within specified limits. A total of 25 design points have been determined for our four input parameters. Numerical analyzes were made for these determined designs. Table 3 shows the parameter values of the design points in the response surface method.

Table 3. Response surface design points

Name	θ (degree)	X (mm)	C(degree)	L(mm)	Effs out	Total Pressure Ratio
1	82,5	2	5	20	93,4533	1,3935
2	60	2	5	20	92,3513	1,3853
3	105	2	5	20	93,3103	1,3930
4	82,5	1	5	20	94,2262	1,3965
5	82,5	3	5	20	91,9566	1,3858
6	82,5	2	0	20	93,4533	1,3935
7	82,5	2	10	20	93,4533	1,3935
8	82,5	2	5	15	94,4567	1,3968
9	82,5	2	5	25	92,2062	1,3861
10	66,6554	1,2958	1,4790	16,4790	94,2802	1,3969
11	98,3446	1,2958	1,4790	16,4790	93,7074	1,3931
12	66,6554	2,7042	1,4790	16,4790	92,3381	1,3878
13	98,3446	2,7042	1,4790	16,4790	93,4607	1,3928
14	66,6554	1,2958	8,5210	16,4790	94,2802	1,3969
15	98,3446	1,2958	8,5210	16,4790	93,7074	1,3931
16	66,6554	2,7042	8,5210	16,4790	92,3381	1,3878
17	98,3446	2,7042	8,5210	16,4790	93,4607	1,3928
18	66,6554	1,2958	1,4790	23,5210	93,0911	1,3906
19	98,3446	1,2958	1,4790	23,5210	93,2337	1,3927
20	66,6554	2,7042	1,4790	23,5210	92,5612	1,3858

21	98,3446	2,7042	1,4790	23,5210	92,2948	1,3866
22	66,6554	1,2958	8,5210	23,5210	93,0911	1,3906
23	98,3446	1,2958	8,5210	23,5210	93,2337	1,3927
24	66,6554	2,7042	8,5210	23,5210	92,5612	1,3858
25	98,3446	2,7042	8,5210	23,5210	92,2948	1,3866

As can be seen in Figure 8, the values determined at 25 design points and the efficiency and pressure ratio change depending on these values are seen. It is seen that the best result in terms of efficiency is obtained from the 8th design point and the best result in terms of total pressure ratio is obtained from the 10th design point. Apart from these 25 design points, there is also a min-max research section in the module. From here, the design points where the highest and lowest values are given for our output parameters are also examined.

Name	P1 - Teta (degree)	P3 - X (mm)	P8 - docking (degree)	P9 - Length (mm)	P4 - Effs out	P5 - Total Pressure Ratio
Output Parameter Minimums						
P4 - Effs out	83,16	3	4,9919	25	91,721	1,3832
P5 - Total Pressure Ratio	60	3	5,2236	25	91,757	1,3821
Output Parameter Maximums						
P4 - Effs out	76,993	1	4,9993	15	94,611	1,3985
P5 - Total Pressure Ratio	75,709	1	4,9896	15	94,61	1,3986

Figure 7. Min-Max research result

From this section, we can see the values of the design points where the output parameters take the highest and lowest values. For example, for the design with the highest efficiency, we see that the θ value is 76.993, the X value is 1 mm, the clocking angle is 4.9993, and the L is 15 mm. Then, the optimization process was carried out using the MOGA method. After this optimization process, the design point giving the best pressure ratio and efficiency was obtained after iterations. For the optimum design point, θ is 76.166, x 1.001, clocking 5.0217, and L 15.005.

CONCLUSION

The analysis results of four different parameters affecting the performance of the tandem blade radial compressor were examined. These parameters were transferred to the response surface method. Design points were created by the program between the highest and lowest values of these parameters. By using the MOGA optimization method, the optimum design point with the highest pressure ratio and efficiency was obtained as a result of iterations.

REFERENCES

1. Klassen, Hugh A., Jerry R. Wood, and Lawrence F. Schumann. "Experimental performance of a 13.65-centimeter-tip-diameter tandem-bladed sweptback centrifugal compressor designed for a pressure ratio of 6." (1977).
2. Roberts, Douglas A., and Suresh C. Kacker. "Numerical investigation of tandem-impeller designs for a gas turbine compressor." *J. Turbomach.* 124.1 (2002): 36-44.
3. Ju, Y. P., and C. H. Zhang. "Design optimization and experimental study of tandem impeller for centrifugal compressor." *Journal of Propulsion and Power* 30.6 (2014): 1490-1501.
4. Erdmenger, Rodrigo R., and Vittorio Michelassi. "Influence of tandem inducers on the performance of high pressure ratio centrifugal compressors." *Turbo Expo: Power for Land, Sea, and Air*. Vol. 56659. American Society of Mechanical Engineers, 2015.
5. Hlaváček, David, and Daniel Hanus. "Results of the development of a tandem-bladed centrifugal compressor stage." *Studentská tvůrčí činnost 2016* (2016).
6. Li, Ziliang, et al. "The performance of a centrifugal compressor with a tandem impeller in off-design conditions." *Proceedings of the Institution of Mechanical Engineers, Part A: Journal of Power and Energy* 234.2 (2020): 156-172.

15th INTERNATIONAL CONFERENCE ON ENGINEERING & NATURAL SCIENCES

March 04-06, 2023 Muş, TÜRKİYE

7. Tao, Yuan, et al. "Analysis of Flow Characteristic of Transonic Tandem Rotor Airfoil and Its Optimization." *Applied Sciences* 10.16 (2020): 5569.
8. Li, Ziliang, et al. "Numerical and experimental investigation of flow mechanism and application of tandem-impeller for centrifugal compressor." *Aerospace Science and Technology* 100 (2020): 105819.
9. Pan, Ruochi, Zhaoyun Song, and Bo Liu. "Optimization Design and Analysis of Supersonic Tandem Rotor Blades." *Energies* 13.12 (2020): 3228.
10. Li, Ziliang, et al. "Inducer/Exducer Matching Characteristics inside Tandem Impellers of a Highly Loaded Centrifugal Compressor." *Journal of Thermal Science* 29.4 (2020): 928-944.
11. Li, Ziliang, et al. "Improving the operating range using a centrifugal compressor with a tandem impeller." *Aerospace Science and Technology* 96 (2020): 105548.

SONLU ELEMENLAR METODU KULLANILARAK BİR YOLCU UÇAĞI KOLTUK KOLÇAĞININ STATİK ANALİZİ STATIC ANALYSIS OF AN AIRPLANE PASSENGER SEAT ARMREST USING THE FINITE ELEMENT METHOD

Hasan Kemal Sürmen
ORCID: 0000-0001-8045-9193
Tolga Güven
ORCID: 0000-0002-1395-7907

ÖZET

Yolcu uçaklarında kullanılan koltuklar belirli standartlara uygun olacak şekilde tasarlanır ve üretilirler. Uçak koltuğu ve parçalarının çeşitli statik yükleri karşılayacak şekilde hafif ve dayanıklı olması istenir. Bu çalışmanın amacı sonlu elemanlar metodunu (SEM) kullanarak bir yolcu uçağı koltuk kolçağının statik analizinin gerçekleştirilmesidir. Çalışmaya konu olan kolçak, dış kısmı polikarbonat (PC), iç destek kısımları ise AL 6061-T6 malzemesinden üretilmiş üç ana parçadan oluşmaktadır. Yolcular koltuğa oturma ve kalkma sırasında kolçaktan destek alırlar ve bu esnada kolçak üzerine kuvvet uygularlar. Dinamometre kullanılarak yapılan ölçümler sonucunda 80-100 kg ağırlığındaki yolcuların kolçak üzerine yaklaşık 200 N'luk bir yük uyguladıkları görülmüştür. Bu çalışmada ekonomi sınıfı bir koltuk kolçağının üç boyutlu montaj modeli tersine mühendislik yapılarak Solidworks yazılımı ile elde edilmiştir. Model üzerinde malzeme ataması yapıldıktan sonra kolçağın kullanım durumuna göre sınır şartları belirlenmiş ve 200 N'luk yük uygulanmıştır. Mesh işlemi yapıldıktan sonra statik analiz başarılı bir şekilde gerçekleştirilmiştir. Metal ve plastik parçalar üzerinde elde edilen von-Mises gerilmeleri ve montaj modeli üzerindeki toplam deformasyon sonuçları paylaşılmıştır. Yapılan analizler sonucunda PC malzemesinden imal edilmiş olan plastik konstrüksiyon üzerinde oluşan von-Mises gerilmesi 24.7 MPa olarak hesaplanmıştır. Modelde kullanılan malzemenin gerilme dayanımının 62.7 MPa olduğu göz önünde bulundurulduğunda parçanın güvenli olduğu anlaşılmaktadır. Kolçağın iç destek kısımlarını oluşturan Al 6061-T6 alaşımından imal edilmiş olan parçalarda meydana gelen maksimum von-Mises gerilmesi 163,20 MPa olarak hesaplanmıştır. Al 6061-T6 alaşımının akma dayanımı 275 MPa olduğu dikkate alındığında kullanılan destek parçalarının güvenli olduğu görülmüştür.

Anahtar Kelimeler: Yolcu Uçağı Koltuk Kolçağı, Statik Analiz, Gerilme Dayanımı, Sonlu Elemanlar Metodu

ABSTRACT

The seats used in passenger airplane are designed and manufactured to comply with certain standards. It is desirable that the airplane seat and parts are light and durable to provide various static loads. The aim of this study is to perform static analysis of an airplane passenger seat armrest using the finite element method (FEM). The outer part of the armrest is made of polycarbonate (PC), and the inner support parts are made of AL 6061-T6 material. Passengers get support from the armrest during sitting and standing up and apply force on the armrest. As a result of the measurements using a dynamometer, it was seen that passengers between 80-100 kg applied a load of approximately 200 N on the armrest. In this study, a three-dimensional assembly model of an armrest of economy class passenger seat was obtained by reverse engineering with Solidworks software. After the material was assigned on the model, the boundary conditions were determined according to the use of the armrest and a load of 200 N was applied. Static analysis was performed successfully after the mesh process. The results of von-Mises stresses on the metal and plastic parts and the total deformation on the assembly model were shared. According to the results of the analysis, the von-Mises stress on the plastic construction made of PC material was calculated as 24.7 MPa. It is understood that the part is safe considering the 62.7 MPa tensile strength of the material used in the model. The maximum von-Mises stress on the parts made of Al 6061-T6 alloy, which forms the inner support parts of the armrest, was calculated as 163.20 MPa. It is seen that the support parts used are also safe considering the 275 MPa yield strength of Al 6061-T6 alloy.

Keywords: Airplane Passenger Seat Armrest, Static Analysis, Tensile Strength, Finite Element Method

GİRİŞ

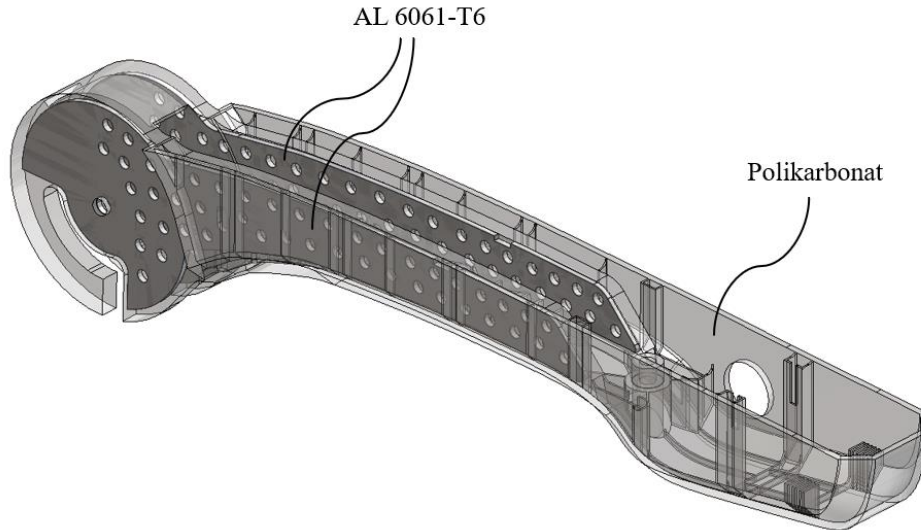
Havacılıkta uçak koltukları insan güvenliğini ve konforunu sağlamada önemli bir yere sahiptirler [1, 2]. Bu yüzden uçak koltukları güvenlik, konfor, ergonomi dikkate alınarak belli standartlara göre tasarlanırlar [3]. Koltuklar farklı görevleri olan birçok bileşenden meydana gelir. Uçak koltuklarında yolcuların konforu için tasarlanan koltuk bileşenlerinden biri de yolcuların kollarını dayadıkları koltuk kolçağıdır. Konforun yanı sıra hafiflik ve dayanım da kolçak tasarımında önemli parametreler arasında yer alır. Bu parametrelere dikkat edilmediğinde koltuk kolçaklarının sıklıkla hasara uğradığı gözlemlenmektedir. Bunun sonucunda hasarlı kolçakların yenisiyle değiştirilmesi zaman ve maddi açıdan kayıplara neden olmaktadır. Hafiflik ve dayanım dikkate alındığında uygun bir tasarımın yapılabilmesi için yapısal analizlerin gerçekleştirilmesi ve elde edilen sonuçların değerlendirilmesi gerekir. Bu bağlamda sonlu elemanlar metodu (SEM) [4] kullanılarak koltuk kolçağının yapısal analizleri az bir maliyetle ve deneysel çalışmalara göre daha kısa sürede yapılabilir. Böylece kullanım esnasındaki oluşabilecek hasarlar önceden tahmin edilebilir ve ona göre tasarım geliştirilebilir.

Bu çalışmada bir yolcu uçağının ekonomi sınıfında kullanılan koltuk kolçağının yolcunun oturması ve kalkması esnasında kolçağa uyguladığı kuvvetler ve sınır şartları dikkate alınarak bir sonlu elemanlar modeli oluşturulmuş ve bu model üzerinde statik analiz gerçekleştirilmiştir. Çalışmada kolçak modeli tersine mühendislik [5] ile üç boyutlu (3B) olarak modellenmiştir. Sonlu elemanlar analizleri (SEA) Solidworks Simulation yazılımı kullanılarak gerçekleştirilmiştir. Bulgular bölümünde kolçağın metal ve plastik parçalarında oluşan gerilme ve montaj modelde meydana gelen toplam deformasyon sonuçları sunulmuştur.

MALZEME VE METOT

Uçaklarda hafiflik ve dayanım son derece önemli olduğu için kompozit malzemelerin oldukça yaygın kullanıldığı görülmektedir [6,7]. Koltuk kolçağı da alüminyum alaşımı ve plastik malzemeden oluşan iki farklı konstrüksiyondan meydana gelmektedir.

Çalışmada sonlu elemanlar analizi için kullanılan koltuk kolçağının 3B modeli aslına uygun bir şekilde Solidworks yazılımı kullanılarak iki farklı konstrüksiyon olarak modellenmiş ve montajı yapılmıştır (Şekil 1). SEA için parçaların kontak kısımları tanımlanmıştır. Bileşen etkileşim tipi birleşmiş olarak seçilmiştir.



Şekil 1. Kolçak parçasının 3B modelinin şeffaf görünümü

Uçak koltuk kolçağı modeli 2 farklı malzemeden oluşmaktadır. Modelin plastik kısımları Polikarbonat (PC), metal kısmı ise AL 6061-T6 malzemelerinden üretilmiştir. SEA'da bu malzemeler modelde ilgili konstrüksiyonlara atanmıştır. Atanan malzeme özellikleri Tablo 1 ve Tablo 2'de verilmiştir.

Tablo 1. PC malzemesinin mekanik özellikleri

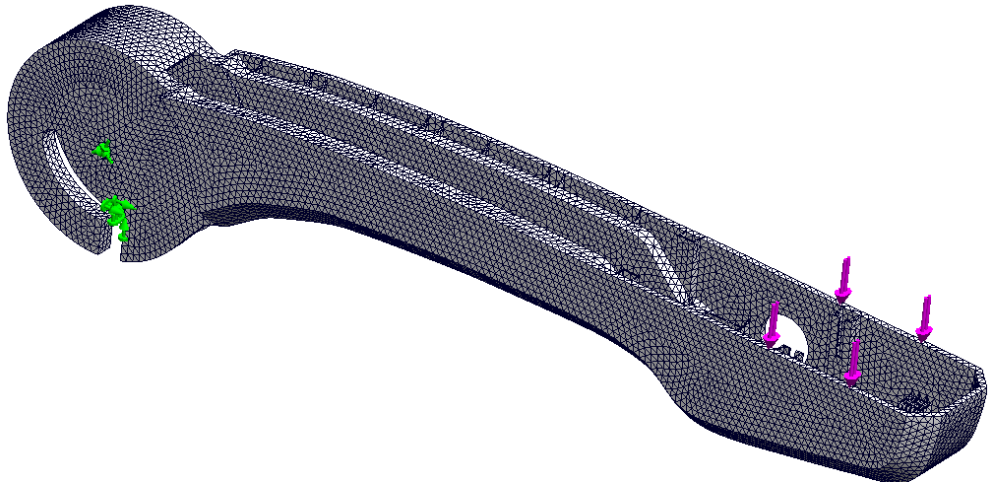
Özellik	Değer	Birimler
Elastikiyet Modülü	2320	MPa
Poisson Oranı	0.3912	-
Yırtılma Modülü	829.1	MPa
Kütle Yoğunluğu	1190	kg/m ³
Gerilme Mukavemeti	62.7	MPa

Tablo 2. AL 6061-T6 malzemesinin mekanik özellikleri

Özellik	Değer	Birimler
Elastikiyet Modülü	69000	MPa
Poisson Oranı	0.33	-
Yırtılma Modülü	26000	MPa
Kütle Yoğunluğu	2700	kg/m ³
Gerilme Mukavemeti	310	MPa
Akma Mukavemeti	275	MPa

Yolcular uçuş esnasında koltuk kolçağına çeşitli yükler uygularlar. Bu yükler yolcunun ağırlığına bağlı olarak değişmektedir. Kolçağın SE modeli Şekil 2’de gösterildiği gibi bağlantı yerlerinden sabitlenmiştir. Dinamometre ile yapılan ölçümler sonucunda en fazla yükün koltuğa otururken ve kalkarken kolçaktan destek alınmasıyla meydana geldiği görülmüştür.

Kuvvetin uygulanma yeri Şekil 2’de gösterildiği gibi belirlenmiştir. Uygulanan yük miktarı 80-100 kg’lık bireyler için yaklaşık 200 N olarak tespit edilmiştir ve SEA için bu değer yüklenme durumu olarak girilmiştir. Sabitleme ve yükleme işleminden sonra üçgensel mesh tipi kullanılarak mesh işlemi yapılmıştır (Şekil 2). Mesh boyutu eğrisel ve karmaşık geometrili kısımlarda küçültülmüştür. Modelde toplam düğüm 257330, toplam eleman 137953 olarak elde edilmiştir.



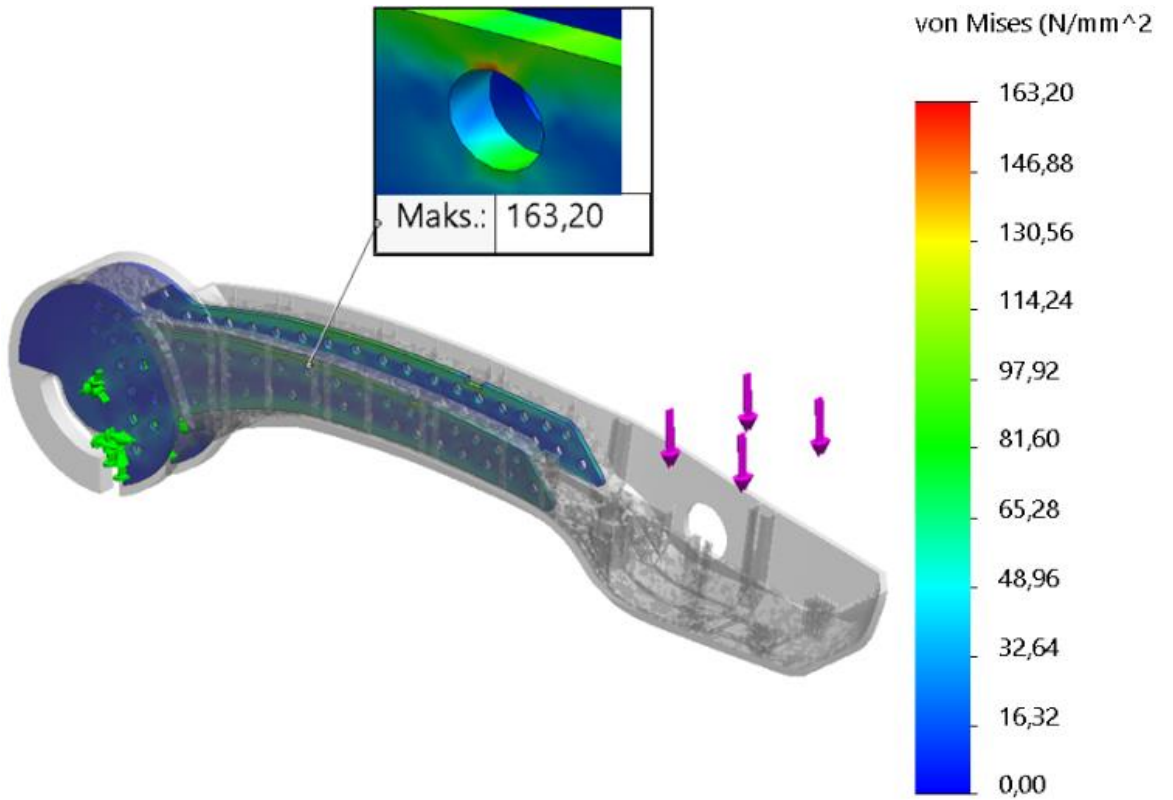
Şekil 2. Kolçak parçasının sonlu elemanlar modeli

BULGULAR

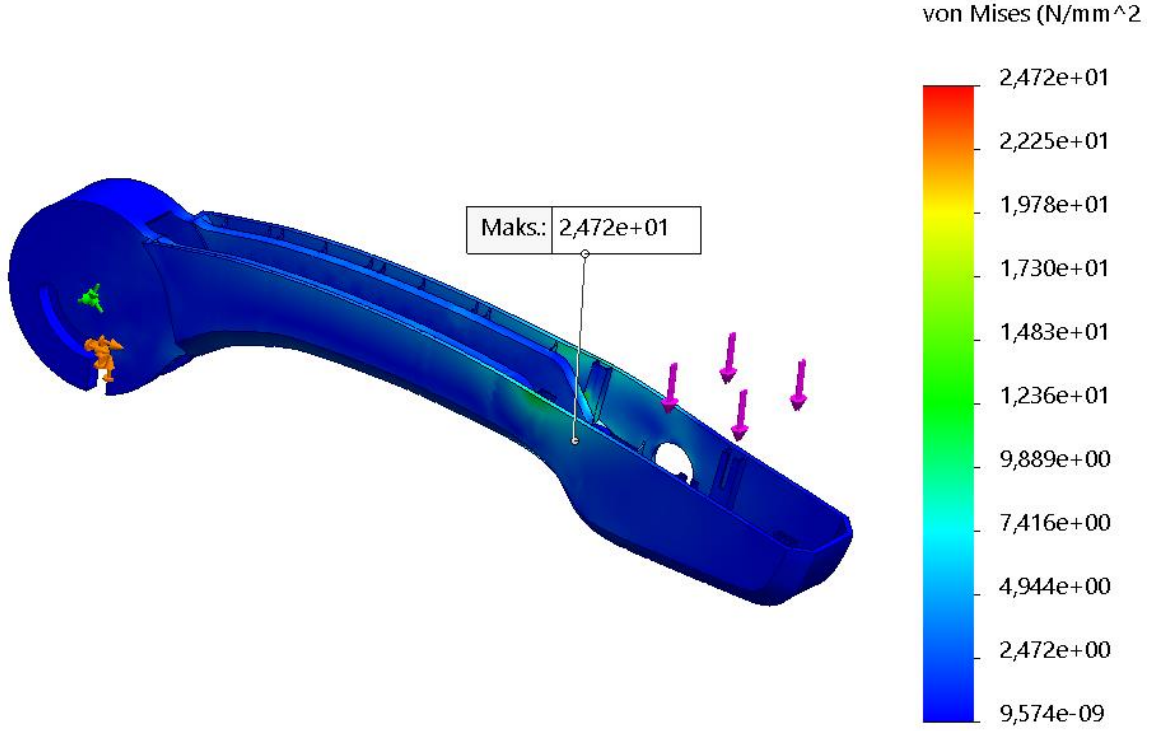
Yapılan yapısal analiz sonucunda Al 6061-T6 alaşımından oluşan, kolçağın iç kısmında her iki tarafta bulunan destek yapılarında meydana gelen maksimum von-Mises gerilmesi Şekil 3'te görüldüğü gibi 163,20 MPa olarak hesaplanmıştır. Al 6061-T6 alaşımının akma dayanımı Tablo 2'de gösterildiği gibi 275 MPa'dır. Belirli bir yük ve gerilme altında bütün malzemeler elastik şekil değişimine uğrarlar. Malzemede kalıcı deformasyon oluşmaması için meydana gelen gerilmenin akma dayanımı sınırını geçmemesi gerekmektedir. Analiz sonucunda elde edilen gerilme değeri malzemenin akma dayanımından oldukça düşüktür.

Uçak koltuk kolçağının PC malzemesinden imal edilen plastik konstrüksiyonu üzerinde oluşan von-Mises gerilme değeri Şekil 4'te görüldüğü gibi 24.72 MPa olarak hesaplanmıştır. PC malzemesinin gerilme dayanımı Tablo 1'de gösterildiği gibi 62.7 MPa'dır. Yapılan analiz sonucuna parçanın güvenilir olduğu anlaşılmaktadır.

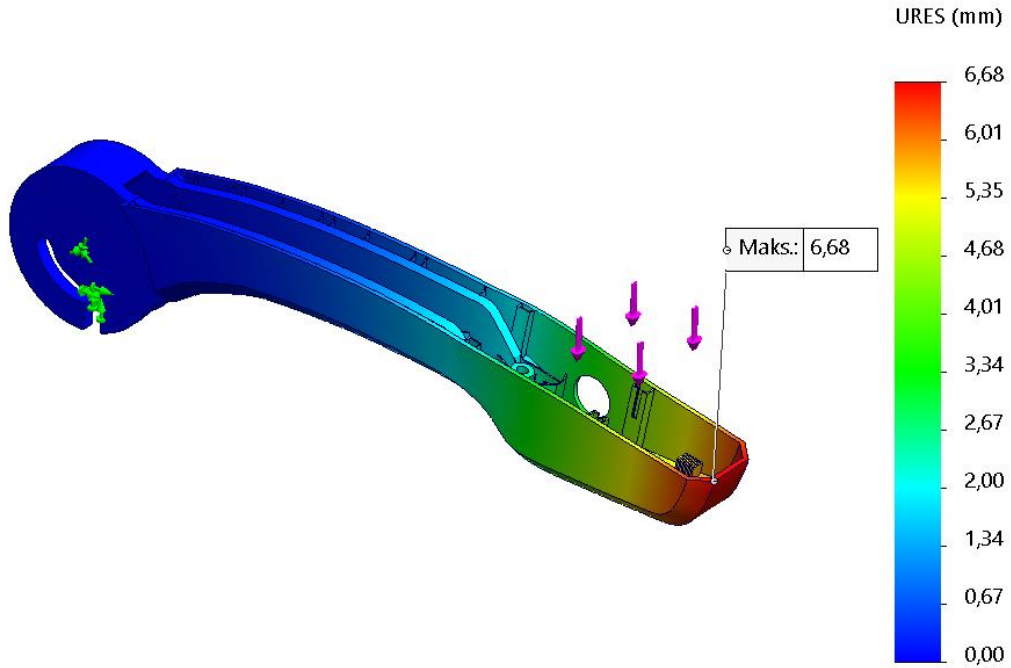
Montaj model üzerinde meydana gelen toplam deformasyonu incelediğimizde en büyük deformasyonun plastik parçanın uç kısmında olduğu görülmektedir (Şekil 5). Maksimum deformasyon 6,68 mm olarak elde edilmiştir.



Şekil 3: Metal parça üzerindeki von-Mises gerilmesi sonuçları



Şekil 4: Plastik parça üzerindeki von-Mises gerilmesi sonuçları



Şekil 5: Montaj üzerindeki toplam deformasyon sonuçları

SONUÇ

Bu çalışmada bir yolcu uçağının ekonomi sınıfında kullanılan koltuk kolçağı tersine mühendislik yöntemleri ile modellenmiş ve yolcuların oturması ve kalkması esnasında belirlenen kuvvetler dikkate alınarak SEM ile statik analizi yapılmıştır. Sınır şartları ve yüklenme koşullarına göre sonlu elemanlar analizleri başarılı bir şekilde gerçekleştirilmiştir. Elde edilen sonuçlar dikkate alındığında koltuk kolçağının yapılan statik analizlere göre güvenli olduğu anlaşılmıştır. Bununla beraber uygulanan yüklerin tekrarlı olması dikkate alındığında, ileriki çalışmalar için yorulma analizlerinin yapıp sonuçlar fiziki modellerle karşılaştırılabilir.

KAYNAKLAR

1. Porta, J., Saco-Ledo, G., & Cabañas, M. D. (2019). The ergonomics of airplane seats: The problem with economy class. *International Journal of Industrial Ergonomics*, 69, 90-95.
2. Bhonge, P. S. (2008). *A methodology for aircraft seat certification by dynamic finite element analysis* (Doctoral dissertation, Wichita State University).
3. Vink, P. (2016). *Aircraft interior comfort and design*. CRC press.
4. Szabó, B., & Babuška, I. (2021). Finite Element Analysis: Method, Verification and Validation.
5. Türkücü, T., & BÖRKLÜ, H. R. (2018). Tersine Mühendislik Yaklaşımına Dayalı Yeni Bir İmalat İçin Tasarım İşlem Modeli. *Gazi University Journal of Science Part C: Design and Technology*, 6(1), 91-104.
6. Baker, A. A. (2004). *Composite materials for aircraft structures*. AIAA.
7. Kalanchiam, M., & Chinnasamy, M. (2012). Advantages of composite materials in aircraft structures. *International Journal of Aerospace and Mechanical Engineering*, 6(11), 2428-2432.

MAKİNE ÖĞRENMESİ ALGORİTMALARI VE DERİN ÖĞRENME MODELLERİ KULLANILARAK METİN SINIFLANDIRMA TEXT CLASSIFICATION USING MACHINE LEARNING ALGORITHMS AND DEEP LEARNING MODELS

Özge Özgüner

ORCID: 0000-0002-4162-9038

Taner Uçkan

ORCID: 0000-0001-5385-6775

Ebubekir Seyyarer

ORCID: 0000-0002-8981-0266

ÖZET

Teknolojinin hızlı gelişmesiyle günlük hayatın vazgeçilmezi olan internet; 2022 yılı istatistiklerine göre 4,95 milyar insanın yani dünya nüfusunun %65,5'i kullanmaktadır. İnternet üzerinden yapılan paylaşımlar büyük veri setlerinin ortaya çıkmasına sebep olmaktadır ve bu veri setleri metinler, videolar, fotoğraflar vb. yapısal olmayan formda verileri içermektedir. Makine öğrenim yöntemleri geliştirilerek yapısal olmayan veriler işlenmektedir. Veri Madenciliğinin bir alt bölümü olan Metin Madenciliği, ilgili bilgileri elde etmek için metni analiz etmek ve ondan bilgi çıkarmak için teknikler ve yöntemler kullanmaktadır. Veri madenciliği yöntemlerini kullanarak metin madenciliği ile elde edilen verileri sınıflandırıp, gruplandırıp ya da eldeki veriler arasındaki ilişkileri istatistiksel sonuçlar oluşturularak modeller oluşturulabilmektedir. Bu modeller ile veri kümesinde olmayan yeni bir veri geldiğinde onun hakkında tahmin yapabilmektedir. Bu çalışmada Stanford Üniversitesi araştırmacıları tarafından 2011 yılında, toplam 50.000 film yorumu ile oluşturulan veri setini etiketlerine göre sınıflandırmak için doğru sonuçlar verebilecek en etkili modelin belirlenmesi amaçlanmıştır. Yapılan çalışmada sırasıyla ön işleme, detaylı veri analizi ve son olarak sınıflandırma işlemi yapılmıştır. Veri setinin %20'si test %80'i eğitim için kullanılmıştır. Yapılan çalışmada değerlendirme metriği olarak doğruluk ve hata oranı metrikleri kullanılmıştır. Bu verilerin üzerinde Karar Ağaçları, Lojistik Regresyon, kNN (k-En Yakın Komşu), Random Forest gibi makine öğrenmesi algoritmaları kullanılmıştır. Derin öğrenme mimarisinden RNN (Özyinelemeli Sinir Ağı / Recurrent Neural Network), CNN (Evrişimli Sinir Ağı / Convolutional Neural Network) ve LSTM (Uzun Kısa Süreli Bellek / Long Short-Term Memory) algoritmaları kullanılarak elde edilen sonuçlar karşılaştırılmıştır. Bu farklı modellerin sonuçları detaylı bir şekilde analiz edilerek sonuçları kısaca verilmiştir. En iyi doğruluk oranı veren algoritmanın %89 ile Lojistik regresyon olduğu bulunmuştur.

Anahtar Kelimeler: Metin madenciliği, Metin sınıflandırma, Karar ağaçları, Lojistik regresyon, k-En yakın komşu, Rastgele orman, Özyinelemeli sinir ağı, Evrişimli sinir ağları, Uzun-kısa vadeli bellek

ABSTRACT

With the rapid development of technology, the internet, is indispensable for daily life; According to 2022 statistics, it is used by 4.95 billion people, that is, 65.5% of the world's population. Sharing over the Internet leads to the emergence of large data sets, and these data sets contain data in unstructured forms such as texts, videos, photographs. Unstructured data is processed by developing machine learning methods. Text mining, a subsection of data mining, uses techniques and procedures to analyze the text and extract information from it to obtain pertinent information. By using data mining methods, models can be created by classifying and grouping the data obtained by text mining or by creating statistical results between the data at hand. By using data mining methods, models can be created by classifying and grouping the data obtained by text mining or by creating statistical results between the data at hand. With these models, new data that is not in the data set can make predictions about it when it comes. In this study, it is aimed to determine the most effective model that can give correct results to classify the data set, which was created with a total of 50,000 movie reviews in 2011 by Stanford University researchers, by their labels. In the study, pre-processing, detailed data analysis, and finally, classification was carried out respectively. 20% of the data set was used for testing and 80% for training. The study's evaluation metrics were used metrics accuracy and mistake rate. Above these data, machine learning algorithms such as Decision Trees, Logistic Regression, kNN (k-Nearest Neighbor), and

Random Forest were used. The results obtained using RNN (Recursive Neural Network), CNN (Convolutional Neural Network), and LSTM (Long Short Term Memory) algorithms from deep learning architecture are compared. These different models' results are thoroughly examined, and the result is briefly presented. It was found that, with an accuracy rate of 89%, the best algorithm was logistic regression. It was found that the algorithm giving the best accuracy rate was Logistic regression with 89%.

Keywords: Text mining, Text classification, Decision tree, Logistik regression, k-Nearest neighbors, Random forest, Reccurent neural network, Convolutional neural network, Long short-term memory

GİRİŞ

Teknolojinin hızlı gelişimiyle insan hayatının vazgeçilmezi olan interneti; 2022 yılı istatistiklerine bakıldığında dünya çapında 4,95 milyar insanın yani dünya nüfusunun %65,5'inin kullandığı görülmektedir [1]. İnternet üzerinden yapılan paylaşımlar büyük veri setlerinin ortaya çıkmasına sebep olmaktadır ve bu veri setleri metinler, videolar, fotoğraflar vb. yapısal olmayan formda verileri içermektedir [2]. Makine öğrenim yöntemleri geliştirilerek yapısal olmayan veriler işlenmektedir. Metinden bazı bilgiler çıkarımında anlamlı bilgiler elde etmek adına, metnin analiz edilmesinde Veri Madenciliğinin alt alanı olarak kabul edilen Metin Madenciliğinin teknik ve yöntemler kullanılmaktadır [3-4]. Veri madenciliği yöntemlerini kullanarak metin madenciliği ile elde edilen verileri sınıflandırıp, gruplandırıp ya da eldeki veriler arasındaki ilişkileri istatistiksel sonuçlar oluşturularak modeller oluşturulabilmektedir. Bu modeller ile veri kümesinde yer almayan yeni bir veri geldiğinde onunla ilgili tahmin yapabilmektedir [5].

Metin sınıflandırma ise metin madenciliğinin alt alanı olup, verileri önceden belirlenen sınıflardan yaralanarak, mevcut kategorilerden biriyle metinlere kategori ataması işlemi yapar [6]. Metnin içeriğine bağlı olarak metne etiketler veya kategoriler atama işlemidir. Metin sınıflandırma işlemi, Denklem 1'deki gibi ifade edilebilir.

$$Y = f(X, \theta) + \varepsilon$$

(1)

Denklem 1'de,

f: eğitim verilerini kullanarak tahminleme yapan sınıflandırma modeli veya sınıflandırıcı

Y: incelenmekte olan metnin önceden tanımlanmış olan bir metin sınıfına üyeliğini belirten değer

X: kelime veya kelime gruplarından oluşan bir metin vektörü

θ : f fonksiyonuyla ilişkilendirilmiş olan bilinmeyen parametrelerin kümesi

ε : sınıflandırma hatasıdır [7-8].

Alan yazın incelendiğinde metin sınıflandırmaya dair birçok çalışma olduğu görülmüştür. Yessenalina ve arkadaşlarının [9], Movie Review isimli veri setindeki film yorumlarını sınıflandırmak için kelimelerin görüş sınıflandırmaya ilişkin etki değerlerini belirlemek amacıyla veri setine destek vektör makineleri sınıflandırma yöntemini kullanmışlardır. Yaptıkları çalışma sonucunda %93.22'lik doğruluk başarı oranı elde etmişlerdir.

Sakkis ve arkadaşlarının [10] yaptığı çalışmalarında Navie Bayes ve k-En Yakın Komşu (kNN) algoritmalarının performanslarını değerlendirmişlerdir. Çalışmaya göre kNN ile %98,8, NB sınıflandırıcılarının %99,5 başarı oranı elde ettiğini göstermiştir.

Sasaki ve Shinnou'nun [11] çalışmalarında Destek Vektör Makineleri (SVM), Navie Bayes ve birçok makine öğrenmesi yaklaşımları kullanmışlardır. Spam algılama için yaptıkları çalışmalarının sonucunda, %97 oranında Destek Vektör Makineleri ile spam e-postalarını doğru tespit etmişlerdir.

Gali, Mariescu-Istodor ve Fränti [12] yaptıkları çalışmalarında, web sayfalarının sınıflandırılmasında HTML yapılarından elde edilen yazı ve metinlere dayalı bir sınıflandırma işlemi yapıldığından, sayfada yer alan herhangi bir reklamdaki dolayı sonucun yanıltıcı olabileceğini ileri sürmüşlerdir. Bu nedenle dil bilgisi, metin bölümler ve istatistiksel teknikler kullanmışlardır. k-En Yakın Komşu (KNN), Naive Bayes ve Destek Vektör Makineleri (SVM) sınıflandırıcıları ile değerlendirilen bu yaklaşımları, metin analizi ve gruplandırılması yönüyle önemli olduğu vurgulanmıştır.

W. Tan, X. Wang ve X. Xu [13] Amazon ürün yorumları üzerinde duygu analizi için Naive Bayes, k-En Yakın Komşu (kNN), Destek Vektör Makineleri (SVM) ve yenilenen sinir ağları sınıflandırıcıları ile başarımlarını değerlendirmişlerdir Uzun Kısa Süreli Bellek (LTSM) yöntemiyle %71.5 ile doğru sınıflandırma elde etmişlerdir.

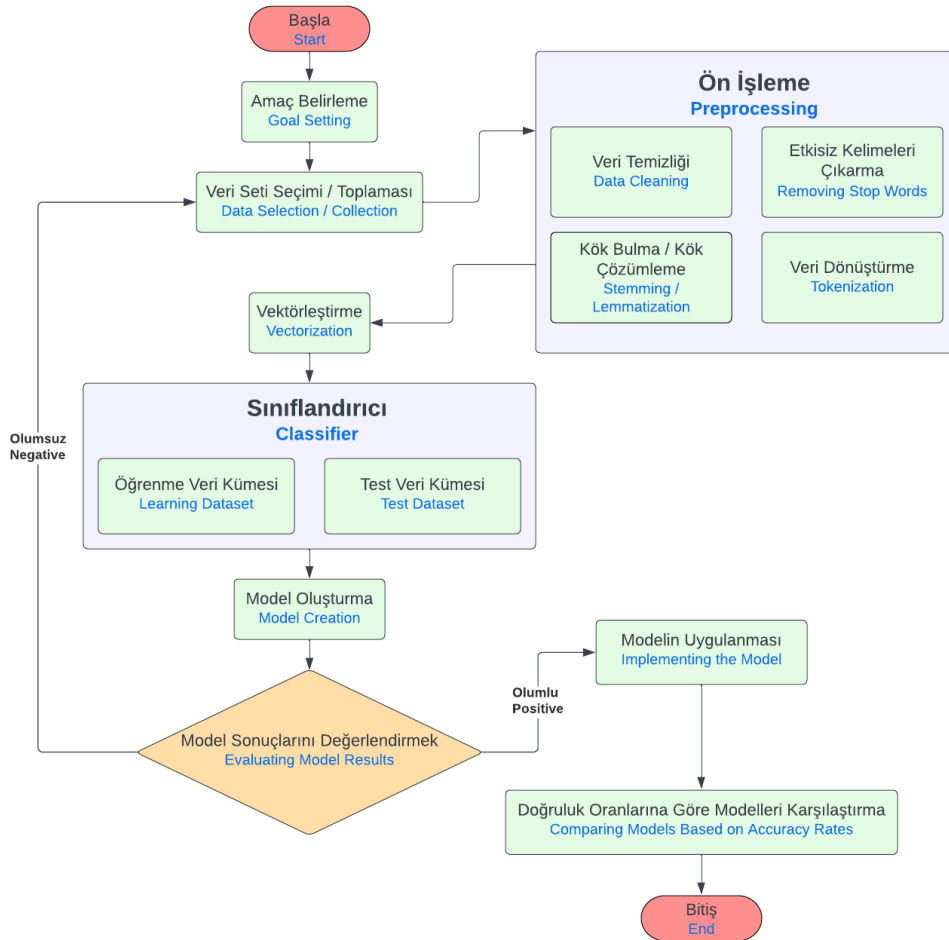
Haggag ve arkadaşları [14] model eğitiminde Uzun Kısa Süreli Bellek (LSTM), Özyinelemeli Sinir Ağı (RNN) ve Çok Katmanlı Algılayıcı (MLP) yöntemleri ayrı ayrı uygulanıp, değerlendirilmiştir. LSTM yöntemiyle KDDTest+ verisinde %85,44, KDDTest-21 verisinde ise %70,59 başarı oranı elde etmişlerdir.

Sastrawan ve arkadaşları [15] çalışmalarında yalan haber tespiti için kullandıkları Çift Yönlü LSTM + fastText modeli ile %99,24 doğruluk performansı ile en iyi performansı sergilemiştir. Ayrıca ResNet + GloVe'nin %98,99 doğruluk, CNN + GloVe %98,24 doğruluk skoru elde etmişlerdir.

Abid Ishaq ve arkadaşları [16] Avrupa'daki 1453 otelin müşteri puanlamasını ve yorumlarını incelemişlerdir. Geliştirdikleri LSTM modeli ile %97 doğruluk sağlamışlardır.

Bu makalede metin sınıflandırma yaklaşımına model (f) olarak; makine öğrenmesi ve derin öğrenme alan yazınında sıklıkla kullanılan ve başarılı sonuçlar vermiş birkaç yaygın yaklaşım kullanılmıştır. Etkinlikler ve başarımları uygun değerlendirme teknikleri ile ölçülmektedir. Sınıflandırılması istenen metin film yorumları içeriği olup, makine öğrenmesi ve derin öğrenme başarımları incelenmektedir. Deneysel analizlerde, Karar Ağaçları (Decision Tree), Lojistik Regresyon (Logistic Regression), k-En Yakın Komşu (K-Nearest Neighbors (KNN)), Rastgele Orman (Random Forest) algoritmaları değerlendirilmiştir. Derin öğrenme mimarisinden Özyinelemeli Sinir Ağı (Recurrent Neural Network(RNN)), Evrişimli Sinir Ağı (Convolutional Neural Network (CNN)) ve Uzun Kısa Süreli Bellek (Long Short-Term Memory (LSTM)) değerlendirilmiştir. Daha sonra bu algoritmalarından elde edilen bulgulara değinilmiştir. Denetimli öğrenmede, elde edilen verilerin belirli bir kısmının eğitilmesiyle sonuçlar elde edilmektedir. Metin sınıflandırma iki kademededen oluşur:

1. Eğitim süreci (öğrenme kümesi – training)
 2. Sınıflandırma süreci (deneme kümesi – test) [17].
- Metin sınıflandırma süreci Şekil 1'de gösterilmiştir.



Şekil 1. Sınıflandırma aşamaları (Classification phases)

MATERYAL VE YÖNTEM

Çalışma kapsamında izlenen adımlar Şekil 1’de verilmiştir. Uygulama kapsamında, öncelikle veri seti seçilmiş ve metin verileri yapısal formata dönüştürülmek için çeşitli ön işleme aşamalarından geçirilmiştir. Son aşamada sınıflandırma algoritmaları kullanılarak başarı oranları karşılaştırılmıştır. Bu bölümde, veri özellikleri, deneysel analizlerde kullanılan kelime gömme yöntemi, makine ve derin öğrenme algoritmaları yaklaşımları sunulmaktadır.

Materyal

Veri Özellikleri

Veri seti Stanford Üniversitesi araştırmacıları tarafından 2011 yılında oluşturulmuştur. Veri setinde toplam 50.000 film yorumu bulunmaktadır. Yorumların 25.000 tanesi olumlu ve 25.000 tanesi ise olumsuzdur. Veri setinde olumlu (1), olumsuz (0) olarak etiketlenmiştir. Bu metinlerin yüzde 80’i eğitim, yüzde 20’si ise test verisi olarak kullanılmıştır. Ham veriler Python programlama dilinin Pandas kütüphanesi aracılığıyla csv dosyasına yazılmıştır. Bu csv dosyasında yer alan verilere bazı metin madenciliği yöntemleri uygulanmıştır.

Yöntem

Yapılan bu çalışmadaki verinin ön işleme, analizi, metin sınıflandırması ve görselleştirmesi yer almaktadır. Çalışmada doğruluk ve hata oranı metrikleri kullanılmıştır. Python programlama dili tercih edilerek uygulamalar gerçekleştirilmiştir ve Google Colab kodlama ortamı kullanılmıştır.

Metin Ön İşleme

Bu makalede kullanılan 50.000 film yorumu makine ve derin öğrenme teknikleri kullanılmadan önce bu yorumların eğitim ve sınıflandırma basamaklarına hazırlanması gerekmektedir. Şekil 2’de metin ön işleme aşamaları yer almaktadır.



Şekil 2. Metin ön işleme aşamaları

Sınıflandırma algoritmalarını kullanabilmek için bazı veri ön işleme ve temizleme işlemleri uygulanmıştır. Bunlar;

- Veri Temizliği: Yanlış karakterlerin kaldırılması (boşluklar noktalama işaretleri vb.), veri setindeki tekrar eden verilerin kaldırılması, eksik verilerin doldurulması, veri standardizasyonu (büyük harfleri küçük harflere dönüştürme vb.),
- Etkisiz Kelimeleri Çıkarma (Removing Stop Words): Veri setinde sık rastlanan ancak analizde önemli olmaya kelimelerin (ve, ama, ile vb.) çıkarılması işlemidir.
- Kök Bulma / Kök Çözümleme (Stemming / Lemmatization): Kök bulma işlemi kelimenin son eklerini veya önemsiz kısımlarını (yürüme - yürü) kesme işlemidir. Kök çözümleme ise kelimenin anlamını korurken dilbilgisi kurallarına uygun bir şekilde köklerine dönüştürülmesi işlemidir.
- Kelimelere Ayırma (Tokenization): Veri setindeki sözcükleri veya metinsel verileri belirli kriterlere göre bölümlere ayırmaya olanak tanımaktadır
- Vektörize Etme (Vectorization): Veri setinde yer alan kelimelerin veya cümlelerin sayısal değerlere dönüştürülmesidir.

Bu işlemler için Python’un scikit-learn, SciPy7, NLTK, Keras8, Pandas ve NumPy kütüphaneleri kullanılmıştır.

Kelime Gömme Yöntemi

GloVe modeli

GloVe modeli (Global Vectors for Word Representation), word2vec tabanlı ve yerel bağlama dayalı öğrenimi, küresel matris çarpanlarına ayırma ile birleştiren bir modeldir. Metin belgesinden kelime gömmelerini (word embeddings) etkili bir şekilde öğrenilmesi için geliştirilen bu modelde, hata fonksiyonunda kelimelerin olasılık oranları dikkate alınmaktadır. Metin belgesi içerisinde birbirlerine yakın gözlemlenen ve birlikte görülme olasılıkları yüksek olan kelimeler, öğrenme sürecinde diğer kelimelere kıyasla daha önemlidir [18-19].

Kullanılan Sınıflandırma Yöntemleri

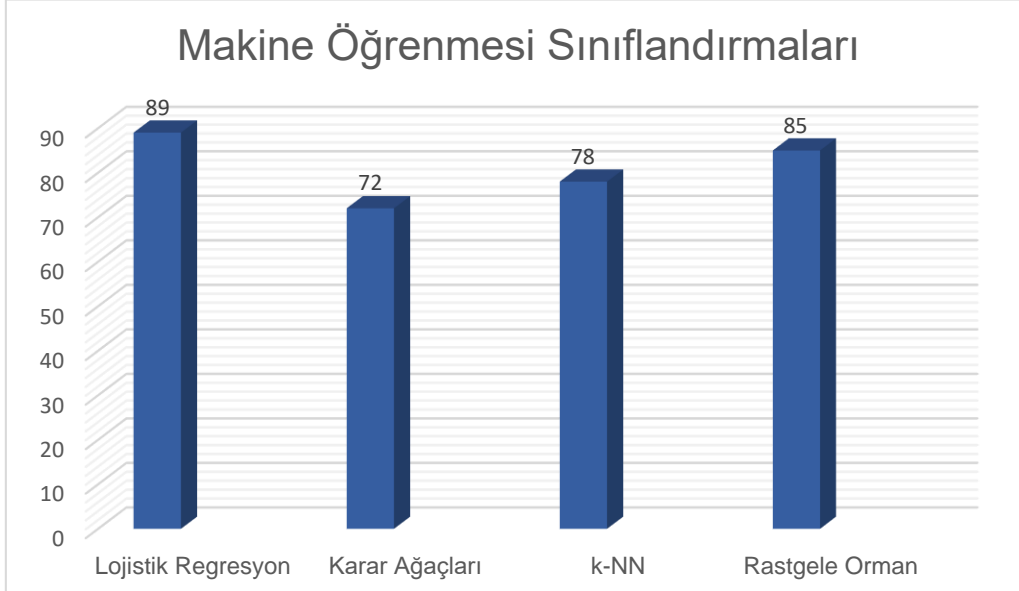
Veri seti metin ön işleme basamaklarından geçirildikten sonra analiz edilebilir hale getirilmiştir. Metin sınıflandırma problemlerine uygunluğu başka çalışmalarca kanıtlanmış olan çeşitli makine öğrenmesi ve derin öğrenme algoritmaları seçilerek uygulama yapılmıştır.

Metin sınıflandırması belirli bir metni önceden tanımlanmış olan sınıflardan hangisine ait olduğunu belirleme işlemidir. $T=\{t_1, t_2, \dots, t_n\}$ kümesindeki her bir metin veya belgenin önceden tanımlı olan $C=\{c_1, c_2, \dots, c_m\}$ kümesindeki sınıflardan herhangi birine ait olup olmadığına bağlı olarak her t_i belgesi veya metin için bir değer üretilmektedir [20].

Bu çalışmada makine öğrenmesi algoritmalarından Karar Ağaçları (Decision Tree), Lojistik Regresyon (Logistic Regression), k-En Yakın Komşu (K-Nearest Neighbors(KNN)), Rastgele Orman (Random Forest) algoritmaları kullanılmıştır. Derin öğrenme mimarisinden Özyinelemeli Sinir Ağı (Recurrent Neural Network(RNN)), Evrişimli Sinir Ağı (Convolutional Neural Network(CNN)) ve Uzun Kısa Süreli Bellek (Long Short-Term Memory(LSTM)) kullanılmıştır.

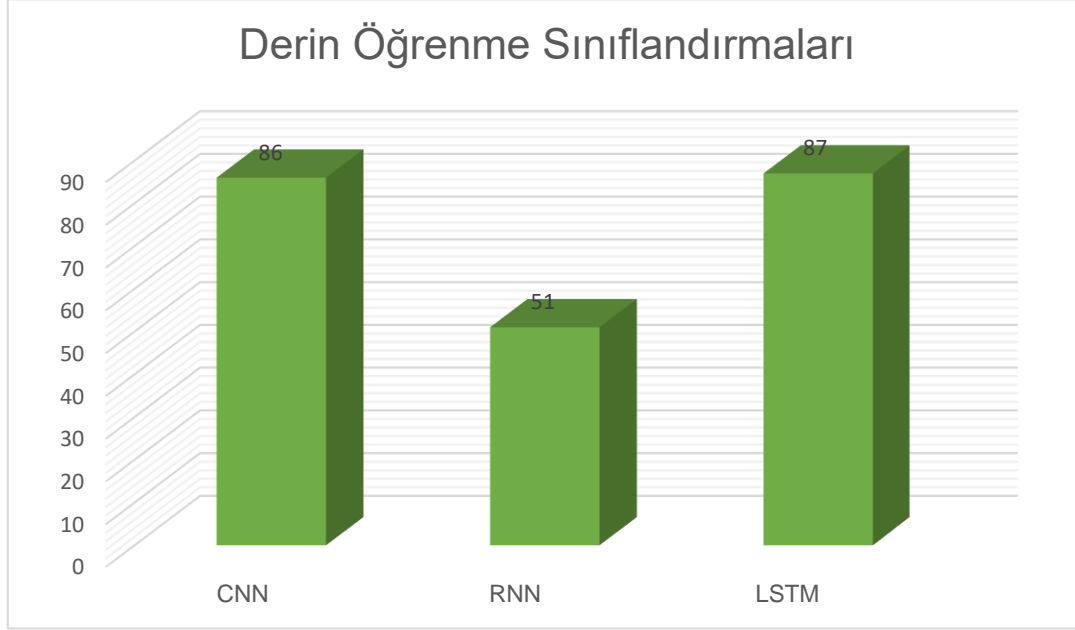
BULGULAR

Bu makalede kullanılan sınıflandırma modellerinin doğruluk oranları aşağıdaki tablolarda belirtilmiştir. Veri setinin %20'si test %80'i eğitim için kullanılmıştır. Şekil 3'te görüldüğü gibi kullanılan makine öğrenmesi sınıflandırmalarında en yüksek doğruluk oranına %89 ile Lojistik Regresyon'un sahip olduğu görülmektedir. Rastgele Orman'ın %85, k-NN'in %78 ve Karar Ağaçları ise %72 doğruluk oranı bulunmuştur.



Şekil 3. Makine öğrenmesi sınıflandırmalarının doğruluk oranları

Şekil 4'te görüldüğü gibi derin öğrenme sınıflandırma sonuçları incelendiğinde ise %87 ile LSTM Sinir Ağı en iyi sonucu veren model olduğu görülmektedir. CNN %86, RNN ise en düşük doğruluk oranı ile %51 bulunmuştur.



Şekil 4. Derin öğrenme sınıflandırmalarının doğruluk oranları

SONUÇ

Bu makalede IMDB internet sitesinde yer alan etiketli kullanıcı yorumları veri seti olarak kullanılmıştır. Toplam 50.000 kullanıcı yorumu bulunmaktadır. Kullanılan veri setinde metin madenciliği yöntemleri kullanılmıştır. Veri setinin değerlendirilmesi için Karar Ağaçları, Lojistik Regresyon, k-En Yakın Komşu, Rastgele Orman, Özyinelemeli Sinir Ağı, Evrişimli Sinir Ağı ve Uzun Kısa Süreli Bellek algoritmaları kullanılmıştır. Veri setindeki sınıflandırma bilgisi gizlenerek yapılan doğruluk performans oranları Python programlama dili ve Google Colab aracı ile yapılmıştır.

Metin sınıflandırma kapsamında en iyi doğruluk oranı %89 ile Lojistik Regresyon algoritması kullanılarak yorumların hangi sınıfa ait oldukları tespit edilmiştir. Çalışmanın sonuçlarının makine öğrenmesi ve derin öğrenmenin farklı algoritmaları ile kıyaslanarak değerlendirilmesi sonraki çalışmalar için kaynak teşkil edecektir.

KAYNAKÇA

1. <https://wearesocial.com/uk/blog/2022/01/digital-2022-another-year-of-bumper-growth-2/>
2. Dolgun, M. Ö., Özdemir, T. G., & Oğuz, D. (2009). Veri madenciliğinde yapısal olmayan verinin analizi: Metin ve web madenciliği. *İstatistikçiler Dergisi: İstatistik ve Aktüerya*, 2(2), 48-58.
3. Visa, A. (2001, July). Technology of text mining. In *International Workshop on Machine Learning and Data Mining in Pattern Recognition* (pp. 1-11). Springer, Berlin, Heidelberg.
4. Korhonen, A., Ó Séaghdha, D., Silins, I., Sun, L., Högberg, J., & Stenius, U. (2012). Text mining for literature review and knowledge discovery in cancer risk assessment and research. *PloS one*, 7(4), e33427.
5. Coşkun, C., & Baykal, A. (2011). Veri madenciliğinde sınıflandırma algoritmalarının bir örnek üzerinde karşılaştırılması. *Akademik Bilişim*, 11, 51-58.
6. Dalal, M. K., & Zaveri, M. A. (2011). Automatic text classification: a technical review. *International Journal of Computer Applications*, 28(2), 37-40.
7. Sebastiani, F. (2002). Machine learning in automated text categorization. *ACM computing surveys (CSUR)*, 34(1), 1-47.
8. Kowsari, K., Jafari Meimandi, K., Heidarysafa, M., Mendu, S., Barnes, L., & Brown, D. (2019). Text classification algorithms: A survey. *Information*, 10(4), 150.
9. Yessenalina, A., Yue, Y., & Cardie, C. (2010, October). Multi-level structured models for document-level sentiment classification. In *Proceedings of the 2010 conference on empirical methods in natural language processing* (pp. 1046-1056).

10. Sakkis, G., Androustopoulos, I., Paliouras, G., Karkaletsis, V., Spyropoulos, C. D., & Stamatopoulos, P. (2001). Stacking classifiers for anti-spam filtering of e-mail. *arXiv preprint cs/0106040*.
11. Sasaki, M., & Shinnou, H. (2005, November). Spam detection using text clustering. In *2005 International Conference on Cyberworlds (CW'05)* (pp. 4-pp). IEEE.
12. Gali, N., Marinescu-Istodor, R., & Fränti, P. (2017). Using linguistic features to automatically extract web page title. *Expert Systems with Applications*, 79, 296-312.
13. Tan, W., Wang, X., & Xu, X. (2018). Sentiment analysis for Amazon reviews. In *International Conference* (pp. 1-5).
14. Haggag, M., Tantawy, M. M., & El-Soudani, M. M. (2020). Implementing a deep learning model for intrusion detection on apache spark platform. *IEEE Access*, 8, 163660-163672.
15. Sastrawan, I. K., Bayupati, I. P. A., & Arsa, D. M. S. (2022). Detection of fake news using deep learning CNN–RNN based methods. *ICT Express*, 8(3), 396-408.
16. Ishaq, A., Umer, M., Mushtaq, M. F., Medaglia, C., Siddiqui, H. U. R., Mehmood, A., & Choi, G. S. (2021). Extensive hotel reviews classification using long short term memory. *Journal of Ambient Intelligence and Humanized Computing*, 12(10), 9375-9385.
17. Deng, Z., & Zhang, M. (2005, December). Improving text categorization using the importance of words in different categories. In *International Conference on Computational and Information Science* (pp. 458-463). Springer, Berlin, Heidelberg.
18. Pennington, J., Socher, R., & Manning, C. D. (2014, October). Glove: Global vectors for word representation. In *Proceedings of the 2014 conference on empirical methods in natural language processing (EMNLP)* (pp. 1532-1543).
19. Mikolov, T., Chen, K., Corrado, G., & Dean, J. (2013). Efficient estimation of word representations in vector space. *arXiv preprint arXiv:1301.3781*.
20. Tantığ, A. C. (2016). Metin Sınıflandırma. Türkiye Bilişim Vakfı Bilgisayar Bilimleri ve Mühendisliği Dergisi, 5 (2), Retrieved from <https://dergipark.org.tr/tr/pub/tbbmd/issue/22245/238796>

TREATMENT OF TARTRAZINE VIA SOLAR-FENTON-LIKE OXIDATION

Ceren Orak

ORCID: 0000-0001-8864-5943

Gülin Ersöz

ORCID: 0000-0002-5875-5946

ABSTRACT

Tartrazine, an acidic azo dye, is commonly used as a food additive and also, it is used in paper and pulp manufacturing. Due to its high usage, it can be detected in various wastewater streams and hence, it can affect aquatic life. In addition, several studies showed it has allergic, carcinogenic, and mutagenic effects over humans; thus, it should be treated. In this study, Fe-doped g-C₃N₄ was used as a photocatalyst to treat tartrazine-containing model solution under solar light irradiation. The effective reaction parameters that are the catalyst loading (0-0.4 g/L), pH (3-9), and initial hydrogen peroxide concentration (0-20 mM) over the degradation of Tartrazine were investigated. The optimum reaction conditions for Tartrazine removal were found as 0.2 g/L of Fe doped g-C₃N₄, pH of 3, and 10 mM of initial hydrogen peroxide concentration and almost 60 % of tartrazine degradation and 90 % decolorization were achieved at the optimum reaction conditions for one hour of reaction duration under solar light. Additionally, a kinetic study was carried out at the three different reaction temperatures (25, 35, and 45 °C) and the highest tartrazine degradation was found as 85.2 % at 45 °C. In addition, complete decolorization was achieved at this reaction temperature. Based on the kinetic study, the degradation of tartrazine followed the second-order reaction kinetic model, and reaction kinetic rate constants were determined as 0.0003, 0.0024, and 0.0034 ppm⁻¹min⁻¹ for the reaction temperatures of 25, 35, and 45 °C, respectively. The activation energy for the observed reaction was calculated as 8.04 kJ/mol.

Keywords: Tartrazine, Solar-Fenton-like Oxidation, Fe/g-C₃N₄

INTRODUCTION

The most common group of synthetic colorants is azo dyes, consisting of half of the produced synthetic dyes. They have a wide usage area; however, they are toxic and could cause mutagenic and carcinogenic effects on living organisms. Because of their malign effects, environmental and human health concerns have been raised. Tartrazine (Acid Yellow 23) is a member of azo dyes used in several industries such as food, textile, and cosmetics. It has resistance to biodegradation and it may cause several health problems (i.e., cancer, asthma, eczema, etc.) in humans (Banerjee et al., 2017; Monser et al., 2009). Various wastewater treatment methods have been employed to remove dyes, and among them, Solar-Fenton-like oxidation has some advantages: i. low-cost ii. easy operation iii. high removal rate, iv. ability to induce complete mineralization (Lin et al., 2022; Jiang et al., 2022). Due to these remarkable features, Solar-Fenton-like oxidation has recently gained interest and it can be employed to degrade tartrazine. In this study, Fe-doped g-C₃N₄ (FeCN) was selected as a solar-driven photocatalyst since it has some excellent functions such as band gap reduction, enhanced visible light absorption, and catalytic performance. For instance; in the literature, FeCN was used to remove methylene blue and almost 80 % of MB was degraded at 3 h of reaction duration under solar light irradiation (Gao et al., 2017; Liu et al., 2021). Due to its excellent properties, in this study, FeCN was used for the degradation and decolorization of tartrazine solution. In this context, the effective reaction parameters (pH, catalyst loading, and initial hydrogen peroxide concentration) were investigated to determine the optimum reaction conditions. In addition, a kinetic study was performed.

MATERIALS AND METHOD

The chemicals -tartrazine, urea, FeCl₃, HCl, NaOH, and H₂O₂ (HP)- used in the experimental study were purchased from Sigma Aldrich.

Fe-doped graphitic carbon nitride (Fe/g-C₃N₄, abbreviated as FeCN in this study) was prepared based on the following procedure. In the catalyst synthesis procedure, 20 g of urea and the required amount of FeCl₃ to obtain Fe (20 wt.%) -containing FeCN were placed in a crucible and put into a muffle oven with an inert atmosphere. Then, it was heated to 550 °C at 30-minute intervals and then, the temperature was kept constant

for 3 hours. After that, it was cooled to room temperature, and the obtained solid product was washed with ultrapure water. The final residue was collected by filtration and dried at room temperature (Li et al., 2016). In addition, to obtain pristine g-C₃N₄ (CN), 20 g of urea was placed in a crucible and put into a muffle oven with an inert atmosphere. Then, it was heated to 550 °C at 30-minute intervals and then, the temperature was kept constant for 3 hours. SEM and BET analyses were carried out for the characterization of FeCN.

The experimental study was carried out using 20 ppm tartrazine solution (100 mL) for 1 h under simulated solar light irradiation. In this context, the effect of reaction parameters that are pH (3-9), catalyst amount (0-0.4 g/L), and initial hydrogen peroxide concentration (0-20 mM) was investigated. During the reaction, liquid samples were taken and analyzed every ten minutes via a spectrophotometer (Spectroquant® NOVA 400 spectrophotometer).

The degradation indicated the breakage of the aromatic rings in tartrazine molecules and the decolorization of tartrazine corresponded to the breakage of the chromophore containing the azo bonds were evaluated at 258 nm and 426 nm, respectively. Degradation and decolorization of tartrazine were calculated based on the following equations:

$$\% \text{ Degradation of tartrazine} = \frac{A_{0 \text{ at } 258 \text{ nm}} - A_{t \text{ at } 258 \text{ nm}}}{A_{t \text{ at } 390 \text{ nm}}} \times 100$$

$$\% \text{ Decolorization of tartrazine} = \frac{A_{0 \text{ at } 426 \text{ nm}} - A_{t \text{ at } 426 \text{ nm}}}{A_{t \text{ at } 426 \text{ nm}}} \times 100$$

The kinetic study was performed at the optimum reaction conditions for 25, 35, and 45 °C and the data was analyzed with first and second-order reaction power law kinetic models.

RESULTS AND DISCUSSION

Characterization Study

SEM analysis was carried out for pristine g-C₃N₄ (CN) and Fe-doped g-C₃N₄ (FeCN) and their SEM diagrams were given in Figure 1. While CN shows a massive layered structure, FeCN showed a sheet-like structure similar to CN and the addition of iron did not cause any change in the structure of CN. Similar morphologies were reported in the literature (Van et al., 2020; Hu et al., 2019; Ma et al., 2019). BET surface area of FeCN was found as 2.7 m²/g. Bicallo et al. prepared Fe-doped g-C₃N₄ for different weight percentages of Fe and they reported that BET areas of 1%-Fe/CN and 10%-Fe/CN as 36 m²/g and 15 m²/g, respectively (Bicalho et al., 2017). Therefore, it could be deduced that an increase in the Fe amount caused a decrease in the BET area. In literature, it was also reported as the BET area of FeCN (containing 0-1 wt.% Fe) varied between 3.404 and 5.4 m²/g for the different amounts of Fe (Guimei Liu et al., 2020). Consequently, it could be concluded that the BET area of FeCN (20wt.%Fe) is inconsistency with the literature.

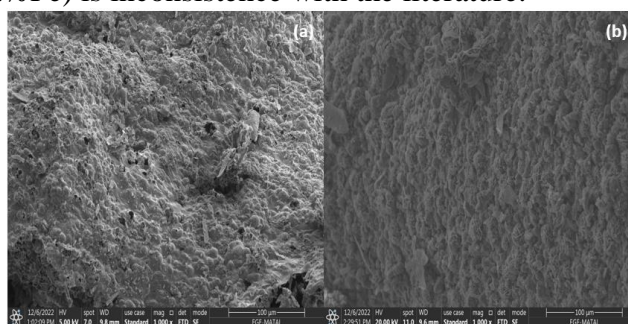


Figure 1. SEM diagrams of CN (a) and FeCN (b)

Degradation and Decolorization of Tartrazine

During the experimental study, all experiments were performed using 20 ppm tartrazine solution for 1 h under solar light irradiation. In this context, firstly, the impact of catalyst amount on the degradation and decolorization of tartrazine was investigated and the results are given in Figure 2. According to the results, very low degradation efficiency was observed at around 8.5% in the absence of FeCN, however, the addition of the catalyst (0.1, 0.2, and 0.4 g/L) enhanced the degradation up to almost 50%. The results showed that the

degradation efficiency reached almost the same values using 0.2 and 0.4 g/L catalyst loading, and thus, to avoid the excess usage of catalyst, 0.2 g/L was chosen as the optimum catalyst loading.

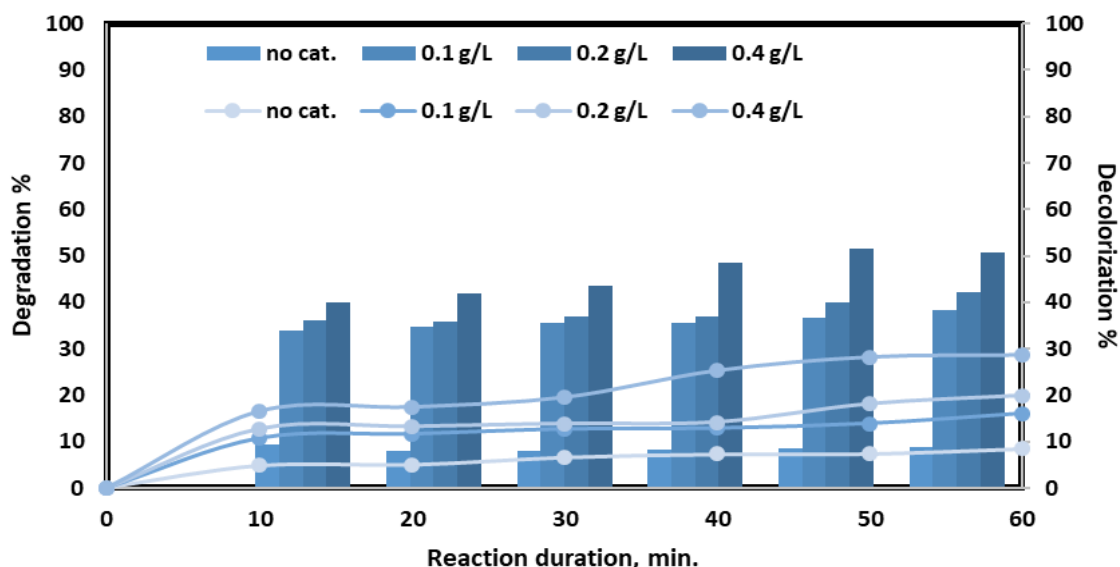


Figure 2. Catalyst amount effect (Reaction conditions: 20 ppm tartrazine, pH 6, 10 mM of HP)

Then, the effect of the initial hydrogen peroxide concentration was investigated and the results are given in Figure 3. The lowest efficiency of degradation and decolorization was observed in the absence of HP. Thanks to the formation of hydroxyl radicals originating from hydrogen peroxide, the breakage of -C-N- in the structures of the dyes may initiate. Therefore, the degradation efficiency of tartrazine can enhance. The usage of 10 mM of HP enhanced the efficiency while 20 mM of HP was used lower efficiency was achieved compared to 10 mM of HP. It could be concluded that the hydroxyl radicals consumed by H₂O₂ and hence, a scavenging effect was observed due to the excess usage of HP (Askarniya et al., 2022). Thus, the optimal HP concentration was selected as 10 mM.

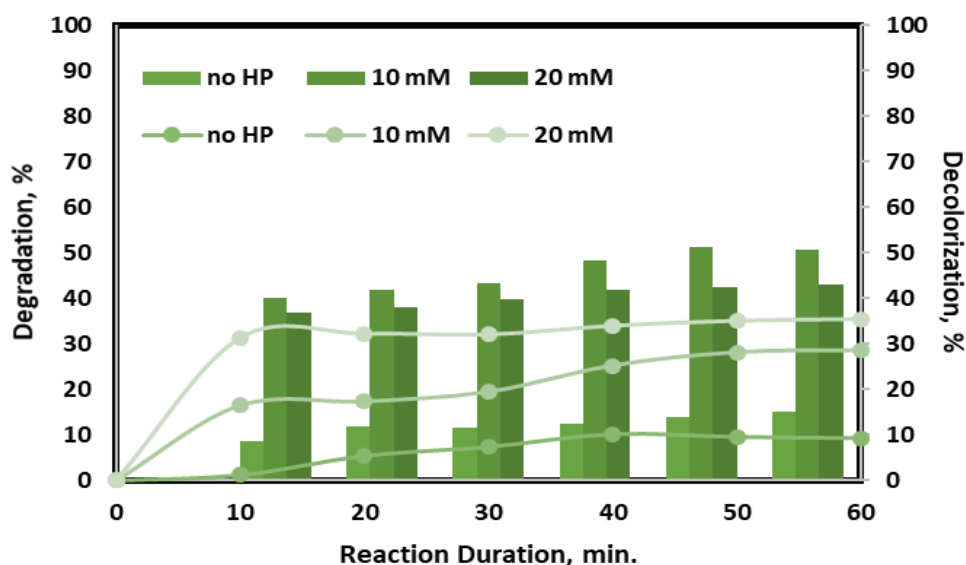


Figure 3. Hydrogen peroxide effect (Reaction conditions: 20 ppm tartrazine, 0.2 g/L catalyst loading, pH 6)

After the determination of the optimum catalyst amount and HP, the experimental study continued with the investigation of the pH effect at pH=3, 6, and 9, and the obtained results are given in Figure 4. The lowest efficiency was achieved at pH 9 whereas the highest degradation (~60%) and almost 90% decolorization were

achieved at pH 3. The attractive force made the negatively charged tartrazine easy to combine with the catalysts at low pH values, whereas the lower degrading efficiency at a high pH value was caused by the electrical repulsion. In literature, Cao et al. used $\text{TiO}_2/\text{g-C}_3\text{N}_4$ nanosheet heterojunctions for the degradation of tartrazine under solar light irradiation, and higher degradation efficiency was observed in acidic reaction media (Cao et al., 2022). Therefore, the optimal pH was selected as 3. Consequently, the optimum reaction conditions were chosen as pH=3, HP=10 mM, and 0.2 of catalyst loading.

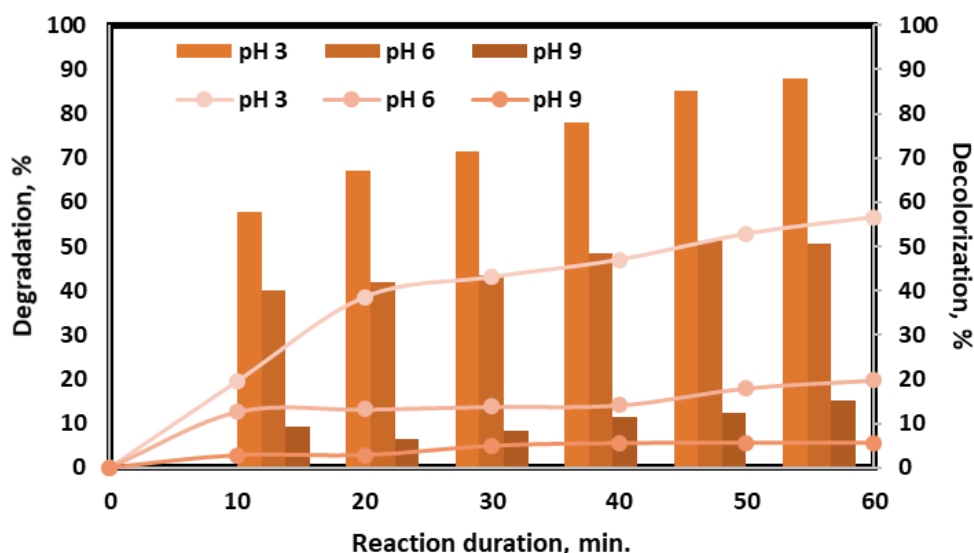


Figure 4. pH effect (Reaction conditions: 20 ppm tartrazine, 0.2 g/L catalyst loading, 10 mM of HP)

After the determination of optimum reaction conditions for tartrazine degradation, a kinetic study was carried out at different reaction temperatures (25, 35, and 45 °C). Based on the results, as the temperature increased the degradation efficiency increased and 85.2 % of tartrazine was degraded at 45 °C. In addition, complete decolorization was observed at this reaction temperature. First and second-order reaction kinetic models were applied to comprehend whether the reaction followed the first-order reaction kinetic model or the second-order kinetic model. The experimental data show well fit to the second-order reaction kinetic model based on the R^2 values. The linearized experimental data are given in Figure 5 and from the graph, the reaction kinetic rate constants were found as 0.0003, 0.0024, and 0.0034 $\text{ppm}^{-1}\text{min}^{-1}$ for 25, 35, and 45 °C, respectively. In addition, the activation energy is calculated as 8.04 kJ/mol (Figure 6, the gas constant $R=8.3145 \text{ J/K mol}$).

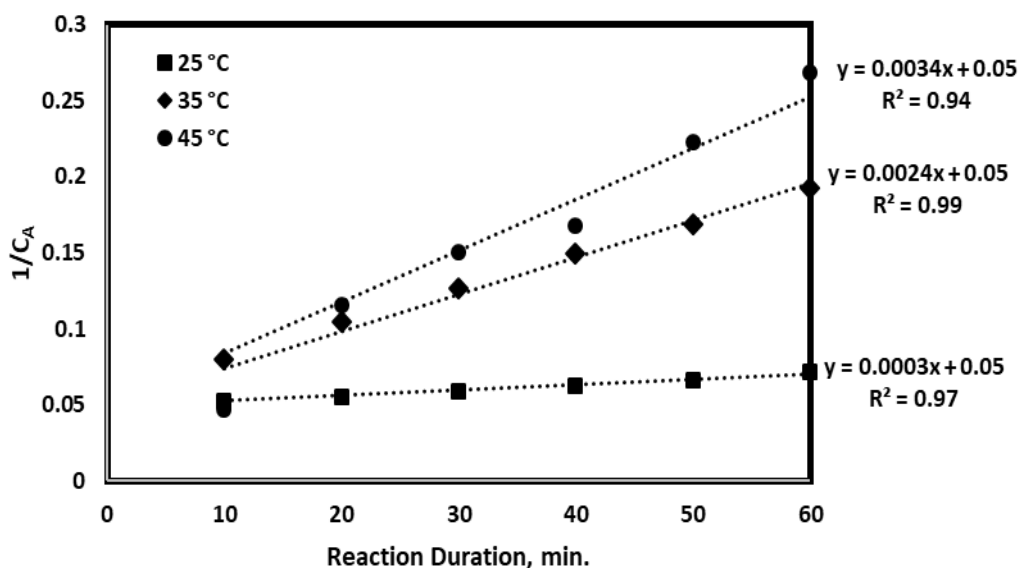


Figure 5. Linearized second-order kinetic plot (Reaction conditions: 20 ppm tartrazine, 0.2 g/L catalyst loading, pH 3, 10 mM of HP)

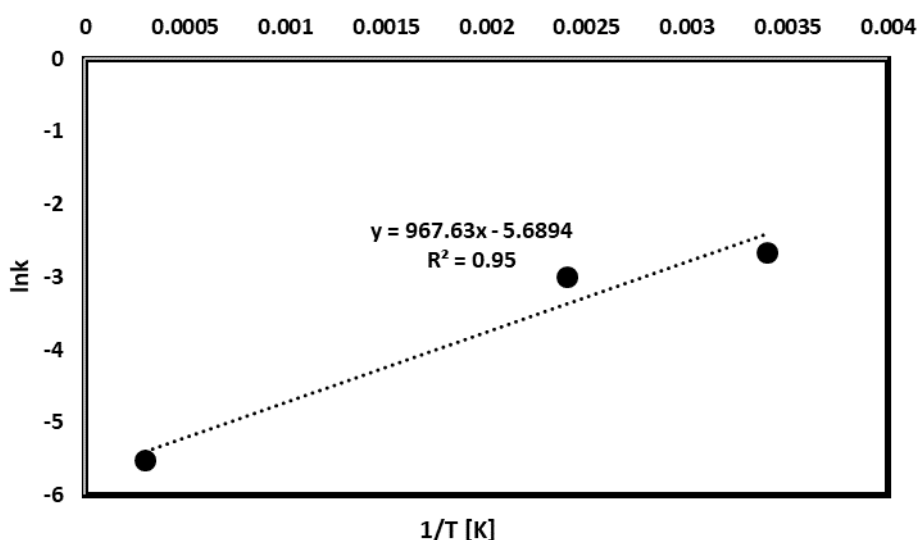


Figure 6. Determination of activation energy

CONCLUSION

Tartrazine, an acidic azo dye, is commonly used as a food additive and because of its common usage, it can be detected in various wastewater streams and hence, it threatens aquatic life because of its toxic feature. In addition, several studies showed that it has allergic, carcinogenetic, and mutagenic effects on humans; thus, it should be treated. In this study, FeCN was used as a solar-driven photocatalyst to treat tartrazine-containing model solution under solar light irradiation. The effective reaction parameters which are the catalyst loading, pH and initial hydrogen peroxide concentration over the degradation of Tartrazine were investigated. The optimum reaction conditions for tartrazine removal were found as 0.2 g/L of FeCN, pH=3, and HP=10 mM, and almost 60 % of tartrazine degradation and 90 % decolorization were achieved at the optimum reaction conditions for one hour of reaction duration under solar light. Therefore, this process could be employed for the degradation of tartrazine. Additionally, a kinetic study was carried out at the three different reaction temperatures (25, 35, and 45 °C) and the highest tartrazine degradation was found as 85.2 % at 45 °C. In addition, complete decolorization was achieved at this reaction temperature. Based on the kinetic study, the degradation of tartrazine followed the second-order reaction kinetic model, and reaction kinetic rate constants

were determined as 0.0003, 0.0024, and 0.0034 ppm⁻¹min⁻¹ for the reaction temperatures of 25, 35, and 45 °C, respectively. The activation energy for the observed reaction was calculated as 8.04 kJ/mol.

REFERENCES

1. Askarniya, Z., Baradaran, S., Sonawane, S. H. and Boczkaj, G., A Comparative Study on the Decolorization of Tartrazine, Ponceau 4R, and Coomassie Brilliant Blue Using Persulfate and Hydrogen Peroxide Based Advanced Oxidation Processes Combined with Hydrodynamic Cavitation, *Chemical Engineering and Processing - Process Intensification*, vol. 181, November 1, 2022. DOI: 10.1016/j.cep.2022.109160
2. Banerjee, S. and Chattopadhyaya, M. C., Adsorption Characteristics for the Removal of a Toxic Dye, Tartrazine from Aqueous Solutions by a Low Cost Agricultural by-Product, *Arabian Journal of Chemistry*, vol. 10, pp. S1629–38, May 1, 2017. DOI: 10.1016/j.arabjc.2013.06.005
3. Bicalho, H. A., Lopez, J. L., Binatti, I., Batista, P. F. R., Ardisson, J. D., Resende, R. R. and Lorençon, E., Facile Synthesis of Highly Dispersed Fe(II)-Doped g-C₃N₄ and Its Application in Fenton-like Catalysis, *Molecular Catalysis*, vol. 435, pp. 156–65, 2017. DOI: 10.1016/j.mcat.2017.04.003
4. Cao, Y., Yuan, G., Guo, Y., Hu, X., Fang, G. and Wang, S., Facile Synthesis of TiO₂/g-C₃N₄ Nanosheet Heterojunctions for Efficient Photocatalytic Degradation of Tartrazine under Simulated Sunlight, *Applied Surface Science*, vol. 600, October 30, 2022. DOI: 10.1016/j.apsusc.2022.154169
5. Gao, J., Wang, Y., Zhou, S., Lin, W. and Kong, Y., A Facile One-Step Synthesis of Fe-Doped g-C₃N₄ Nanosheets and Their Improved Visible-Light Photocatalytic Performance, *ChemCatChem*, vol. 9, no. 9, pp. 1708–15, 2017. DOI: 10.1002/cctc.201700492
6. Hu, J., Zhang, P., An, W., Liu, L., Liang, Y. and Cui, W., In-Situ Fe-Doped g-C₃N₄ Heterogeneous Catalyst via Photocatalysis-Fenton Reaction with Enriched Photocatalytic Performance for Removal of Complex Wastewater, *Applied Catalysis B: Environmental*, vol. 245, pp. 130–42, May 15, 2019. DOI: 10.1016/j.apcatb.2018.12.029
7. Jiang, Y., Ran, J., Mao, K., Yang, X., Zhong, L., Yang, C., Feng, X., and Zhang, H., Recent Progress in Fenton/Fenton-like Reactions for the Removal of Antibiotics in Aqueous Environments, *Ecotoxicology and Environmental Safety*, May 1, 2022.
8. Lin, J., Tian, W., Guan, Z., Zhang, H., Duan, X., Wang, H., Sun, H., Fang, Y., Huang, Y., and Wang, S., Functional Carbon Nitride Materials in Photo-Fenton-Like Catalysis for Environmental Remediation, *Advanced Functional Materials*, June 1, 2022.
9. Liu, G., Dong, G., Zeng, Y., and Wang, C., The Photocatalytic Performance and Active Sites of G-C₃N₄ Effected by the Coordination Doping of Fe(III), *Chinese Journal of Catalysis*, 2020.
10. Liu, X., Ma, R., Zhuang, L., Hu, B., Chen, J., Liu, X. and Wang, X., Recent Developments of Doped G-C₃N₄ Photocatalysts for the Degradation of Organic Pollutants, *Critical Reviews in Environmental Science and Technology*, vol. 51, no. 8, pp. 751–90, from <https://doi.org/10.1080/10643389.2020.1734433>, 2021. DOI: 10.1080/10643389.2020.1734433
11. Li, Z., Kong, C. and Lu, G., Visible Photocatalytic Water Splitting and Photocatalytic Two-Electron Oxygen Formation over Cu- and Fe-Doped g-C₃N₄, *Journal of Physical Chemistry C*, vol. 120, no. 1, pp. 56–63, January 21, 2016. DOI: 10.1021/acs.jpcc.5b09469
12. Ma, T., Shen, Q., Xue, B. Z. J., Guan, R., Liu, X., Jia, H. and Xu, B., Facile Synthesis of Fe-Doped g-C₃N₄ for Enhanced Visible-Light Photocatalytic Activity, *Inorganic Chemistry Communications*, vol. 107, September 1, 2019. DOI: 10.1016/j.inoche.2019.107451
13. Monser, L. and Adhoum, N., Tartrazine Modified Activated Carbon for the Removal of Pb(II), Cd(II) and Cr(III), *Journal of Hazardous Materials*, vol. 161, no. 1, pp. 263–69, January 15, 2009. DOI: 10.1016/j.jhazmat.2008.03.120
14. Van, M. N., Mai, O. L. T., Do, C. P., Thi, H. L., Manh, C. P., Manh, H. N., Thi, D. P. and Danh, B. do, Fe-Doped g-C₃N₄: High-Performance Photocatalysts in Rhodamine b Decomposition, *Polymers*, vol. 12, no. 9, pp. 1–13, September 1, 2020. DOI: 10.3390/polym12091963

A NEW DEEP LEARNING MODEL FOR CHRONIC KIDNEY DISEASE PREDICTION

Resul Özdemir

ORCID: 0000-0003-3678-812X

Murat Taşyürek

ORCID: 0000-0001-5623-8577

Veysel Aslantaş

ORCID: 0000-0002-0952-0315

ABSTRACT

Chronic Kidney Disease (CKD) is a life-threatening disease. Early diagnosis of mortal illnesses is of utmost importance. Utilizing historical data for the prediction of future health conditions is the easiest, less costly and non-invasive way. This approach yields to early detection of diseases as well. Machine Learning (ML) and Deep Learning (DL) models are the most common technics for intelligent estimations. In this paper, we proposed a new 1D-CNN deep learning model to predict CKD problems. The proposed model is compared with K-Nearest Neighbour (KNN), Decision Tree (DT), Support Vector Machine (SVM) and Random Forest (RF) algorithms. Hyperparameters affect the model performances of ML and DL algorithms. In this study, hyperparameter optimization is employed for all models using the Grid Search CV optimization algorithm. In order to improve model quality, 10-fold cross-validation is conducted for all ML models. The comparison metrics, accuracy, precision, recall and F1 score are utilized for performance evaluations. The accuracy metric is compared for both training and test data sets. The remaining metrics, precision, recall and F1 score, are calculated for only the test data set. The proposed 1D-CNN model achieved competitive results among all machine learning models. We have reported 98.93% accuracy for both training and test data sets. Moreover, 98.93% precision is calculated for the test data set. The recall metric value is 98.93% for the test data set. Finally, the F1 score is calculated as 98.93%, which is the best achievement among all ML models in this study.

Keywords: chronic kidney disease, machine learning, deep learning, hyperparameter optimization

INTRODUCTION

Kidneys are the organs located on the lateral parts and toward the back of the human body. The main purpose of kidneys is to segregate toxins and water by filtering blood. In addition to the fact that the kidneys have an important role in the human body, they also cause vital illnesses. Chronic Kidney Disease (CKD) is a life-threatening issue worldwide. Approximately 14% of the world population suffers from this disease, and it brings about more deaths than prostate and breast cancer Ekanayake and Herath (2020).

Prediction of CKD is a life-saving action that leads to early detection of illness. There have been many measurements to classify CKD, such as age, blood pressure, amounts of sodium, potassium, haemoglobin, etc. Rubini et al. (2015). In order to create a relationship between these measurements and disease, Machine Learning (ML) and Deep Learning (DL) models are utilized.

In the literature, K-Nearest Neighbour (KNN), Decision Tree (DT), Support Vector Machine (SVM), and Random Forest (RF) algorithms are popular ML algorithms. Convolutional Neural Networks (CNN) is a DL method which has better performance for two-dimensional and three-dimensional data, especially image data Arslan and Tasyurek (2022), Ozturk et al. (2023), Moustapha et al. (2022), Tasyurek and Ozturk (2022), Ulutas and Aslantas (2023), Akbulut and Aslantas (2023). On the other hand, the One-Dimensional Convolutional Neural Networks (1D-CNN) method is an effective DL technic for one-dimensional data sets. In this study, since the CKD data set is a tabular data set, we implemented a 1D-CNN deep learning model. The proposed DL method has competitive results among powerful ML algorithms.

RELATED WORKS

Islam et al. (2020) have studied CKD risk factor prediction using three different ML algorithms. In the study, ML algorithms Naïve Bayes (NB), Random Forest (RF), and Simple Logistic Regression (SLR) are compared.

The accuracy values are compared in this study. The NB, RF and SLR algorithms have achieved 93.91%, 98.89%, and 94.77% accuracy values, respectively. RF algorithm has the best performance in this study.

Arulanthu and Perumal (2019) have compared four different ML algorithms to predict CKD. Jrip, NB, Sequential Minimal Optimization (SMO) and K-Nearest Neighbor (KNN) algorithms were evaluated in this study. The obtained accuracy scores are 98.80%, 95.00%, 97.75% and 95.75%, respectively. The Jrip model has achieved the best performance among the four ML models.

Revathy et al. (2019) have compared machine learning models for CKD prediction. SVM, DT and RF models were employed for the prediction. RF algorithm has the best performance in terms of accuracy metrics among all algorithms.

Pasadana et al. (2019) have studied different decision tree models for CKD problems. Random forest, DecisionStump, HoeffdingTree, J48, CTC, J48graft, LMT, NBTree, RandomTree, REPTree, and SimpleCart models were utilized for the CKD data set. The random forest model achieved the best performance among tree-based models.

Lambert and Perumal (2021) performed Feature Selection (FS) for CKD prediction. Metaheuristic optimization techniques were utilized for the FS process. In the study, Ant Colony Optimization (ACO) algorithm, Genetic Algorithm (GA) and Particle Swarm Optimization (PSO) algorithms were compared. The ACO-FS approach has produced the best solution for CKD prediction.

Nishanth and Thiruvaran (2017) have proposed an FS method based on KNN and Linear Discriminant Analysis (LDA). In the study, the obtained precision values are over 95% for the data set that emerged after the LDA-based feature selection process. LDA-based solutions have been reported to be much more successful than KNN-based solutions in this paper.

Apart from the estimation of CKD risk factors, studies suggest a suitable diet program for patients Maurya et al. (2019). In this study, three new features, which were Safe, Caution and Danger, were derived according to the amount of potassium in the data set. A system design for a diet program with newly released features is proposed.

In addition, Arulanthu and Perumal (2021) have another study that emphasizes the importance of CKD. This literature review study projects on the benefits of early prediction of CKD.

In this study, we have proposed a new 1D-CNN deep learning model. Moreover, the performances of KNN, DT, RF, SVM and the proposed 1D-CNN model are compared.

BASIC CONCEPT

In this section, the data used in this study is explained with all features and data types. Furthermore, the machine learning algorithms are explained to predict the chronic kidney disease classes.

Data

The features in the Chronic Kidney Disease dataset Rubini et al. (2015), which has been published in UCI Machine Learning Repository, are introduced. Table 1 lists the feature names, short descriptions of the relevant features, and the data type of each field in the dataset. The dataset contains 400 sample data and 25 features. There has been a Class feature, the target field for disease prediction. The remaining 24 features include 11 numerical and 14 categorical data types. In Table 1, the numerical features are listed with metrics. Likewise, the categorical features are shown with possible category options.

Table 1. Feature Description of Chronic Kidney Disease Data Set

Feature Name	Description	Data Type
Age	Age in years	Numeric
Blood Pressure	Amount of blood pressure in mm/Hg	Numeric
Specific Gravity	Specific gravity (1.005,1.010,1.015,1.020,1.025)	Categorical
Albumin	Albumin category (0,1,2,3,4,5)	Categorical
Sugar	Sugar category (0,1,2,3,4,5)	Categorical
Red Blood Cells	Red blood cells category (normal,abnormal)	Categorical
Pus Cell	Puss cell category (normal,abnormal)	Categorical
Pus Cell Clumps	Pus cell clumps category (present,notpresent)	Categorical
Bacteria	Bacteria category (present,notpresent)	Categorical

Blood Glucose Random	Amount of blood glucose random (mgs/dl)	Numeric
Blood Urea	Amount of blood urea (mgs/dl)	Numeric
Serum Creatinine	Amount of serum creatinine (mgs/dl)	Numeric
Sodium	Amount of sodium (mEq/L)	Numeric
Potassium	Amount of potassium (mEq/L)	Numeric
Hemoglobin	Amount of hemoglobin (gms)	Numeric
Packed Cell Volume	Amount of packed cell volume	Numeric
White Blood Cell Count	Count of white blood cells (cells/cumm)	Numeric
Red Blood Cell Count	Count of red blood cells (millions/cmm)	Numeric
Hypertension	Status of hypertension (yes,no)	Categorical
Diabetes Mellitus	Status of Diabetes Mellitus (yes,no)	Categorical
Coronary Artery Disease	Status of coronary artery disease (yes,no)	Categorical
Appetite	Status of appetite (good,poor)	Categorical
Pedal Edema	Status of pedal edema (yes,no))	Categorical
Anemia	Status of anemia (yes,no)	Categorical
Class	Target feature for classification (ckd,notckd)	Categorical

Methods

In this paper, the most popular ML algorithms, which are K-Nearest Neighbour (KNN), Support Vector Machine (SVM), Random Forest (RF), Decision Tree (DT) and 1D Convolutional Neural Network (1D-CNN), are introduced to classify CKD problem.

K-Nearest Neighbour (KNN)

KNN was proposed by Bay to solve classification problems of supervised learning Bay (1999). The basic concept of the algorithm is to find out the similarities between features and target classes. There is a parameter k that defines checking the number of the nearest data samples in the whole data set. The algorithm calculates the distances for all data samples in an iterative way and makes a decision about the target class among k neighbours.

Support Vector Machine (SVM)

SVM has been proposed by Cortes and Vapnik (1995) as a classification algorithm in the realm of machine learning. SVM calculates the margin size with hyper-planes that determine the classes in the given data set. The hyper-planes create a hidden layer that all the data set features are projected to this layer by a kernel function. This kernel function generates the boundary of the data set features to segregate the classes in the model.

Decision Tree (DT)

A decision tree is built to create a model for the classification operation in ML applications. The tree structure makes decisions with respect to features in the data set. The decisions are made from the root and leaves of the tree by calculation methods that reduce uncertainty. Loh (2011) has proposed the decision tree approach for classification and regression problems.

Random Forest (RF)

Random forest is a powerful ML algorithm originating from the decision tree approach. RF brings together decision trees to build a prediction model. All sub-models generate an estimation, and the RF algorithm ends up with the final decision according to the results of these sub-classifiers. Breiman (2001) proposed the RF algorithm.

1D Convolutional Neural Networks (1D-CNN)

Convolutional Neural Networks are deep learning methods to generate high-quality features of given data sets. Generally, CNN models are successful and popular methods in the realm of image-related operations. On the other hand, 1D-CNN models are the special forms of CNN models for one-dimensional data sets. 1D-CNN models generate deep features before neural network classification operations to stage better performance. There have been several studies regarding DL in the literature Arslan and Tasyurek (2022) Ozturk et al. (2023) Moustapha et al. (2022) Tasyurek and Ozturk (2022) Ulutas and Aslantas (2023) Akbulut and Aslantas (2023).

PROPOSED 1D-CNN MODEL

The architectural structure of the proposed 1D-CNN is illustrated in Figure 1. There have been six convolutional layers to obtain deeper features from inputs. The filter size of each convolutional layer is 16, 32, 16, 16, 8 and 4, respectively. There have been 24 features in the data set, and we determine the filter sizes with respect to the feature size accordingly. Rather than keeping the number of filters large and adding fewer layers, the number of filters is determined less and more layers are preferred in the proposed network design. The kernel size is set to 3 for all convolutional layers. The activation function of all convolutional layers is determined as Tanh function for this structure. All convolutional layers are followed by an activation layer which contains ReLU activation function. The Max Pooling layer is employed after convolutional layers. The pool size is set to 2 for this layer. Then, the flatten layer carries out the feature extraction for the neural network classifier. The neural network layer receives the inputs from the flatten layer. This layer contains 64 nodes with ReLU activation function. Finally, the proposed 1D-CNN network generates results with a SoftMax layer.

EXPERIMENTAL RESULTS

The data set is divided into two parts which are training and test data sets. The training set contains 70% of the original data set. On the other hand, the rest 30% of the data set is separated as the test set. In addition, a random 10% of the training set is allocated as the validation for hyperparameter optimization. In order to obtain the optimum parameter, set for all ML algorithms, the Grid Search CV algorithm is employed for hyperparameter optimization. Due to the fact that the data set contains a limited number of records, 10-fold cross-validation is utilized for better performance.

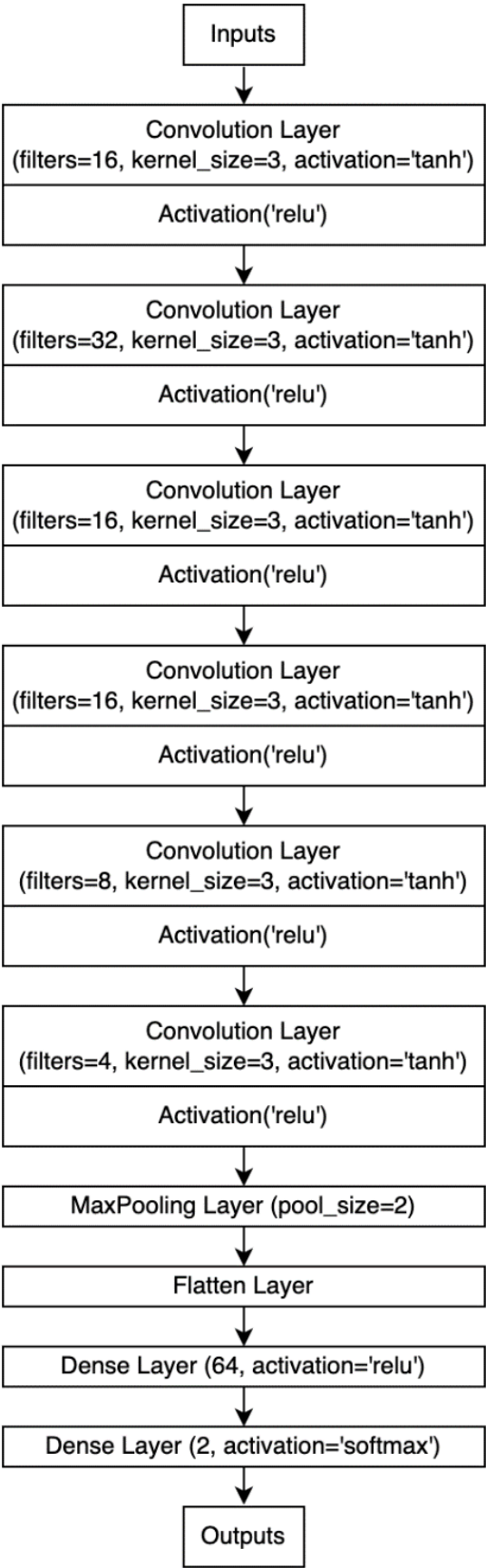


Figure 1 The proposed ID-CNN model architecture

Hyperparameter Optimization

The hyperparameters to be optimized for 1D-CNN, KNN, SVM, RF and DT algorithms are listed in Table 2. The parameters, optimizer, epoch and batchSize are optimized for the 1D-CNN model. The kernel, gamma and C parameters of the SVM algorithm are optimized. The parameters optimized for the RF algorithm are nEstimators, maxDepth, maxFeatures, minSamplesSplit and minSamplesLeaf. The parameters nNeighbors, metric and weights are optimized in the KNN algorithm. Finally, the maxDepth, minSamplesSplit, minSamplesLeaf and criterion parameters of the DT algorithm are optimized.

Table 2: ML Algorithms and Hyperparameters to be optimized

Algorithm	Hyperparameters
1D-CNN	optimizer, epoch, batchSize
SVM	kernel, gamma, C
KNN	nNeighbors, metric, weights
RF	nEstimators, maxDepth, maxFeatures, minSamplesSplit, minSamplesLeaf
DT	maxDepth, minSamplesSplit, minSamplesLeaf, criterion

The list of optimum hyperparameters obtained as a result of the optimization is listed in Table 3. According to results in this table, for 1D-CNN, optimizer is determined as Adam, epoch is 200 and batchSize is 100. The parameter kernel in the SVM algorithm is set as rbf. The gamma is set to 1 and C value is 2. The value of nNeighbors for the KNN algorithm is set to 4, metric value is minkowski, and weights parameter is determined as uniform. The value of nEstimators for the RF algorithm is 30, maxDepth is set to 10, maxFeatures is auto, minSamplesSplit is 2, and minSamplesLeaf is 1. Finally, for the DT algorithm, maxDepth is set to 10, minSamplesSplit is 6, minSamplesLeaf is 1, criterion is determined as entropy.

Table 3: ML Algorithms and Optimized Parameters with Values

Algorithm	Hyperparameters
1D-CNN	optimizer: Adam , epoch: 200 , batch Size: 100
SVM	kernel: rbf , gamma: 1 , C: 2
KNN	nNeighbors: 4 , metric: minkowski , weights: uniform
RF	nEstimators: 30 , maxDepth: 10 , maxFeatures: auto , minSamplesSplit: 2 , minSamplesLeaf: 1
DT	maxDepth: 10 , minSamplesSplit: 6 , minSamplesLeaf: 1 , criterion: entropy

Comparison Metrics

Various comparison metrics are used according to the type of problem to examine the performance of ML and DL methods. In classification problems, accuracy, recall, precision, and F1 Score are commonly used metrics Ozturk et al. (2023).

These metrics are calculated as presented in Eq. 1.

$$\begin{aligned}
 Accuracy &= \frac{TP + TN}{TP + FP + TN + FN} \\
 Recall &= \frac{TP}{TP + FN} \\
 Precision &= \frac{TP}{TP + FP} \\
 F_1 - score &= \frac{2 \times Precision \times Recall}{Precision + Recall}
 \end{aligned} \tag{1}$$

In Eq. 1, when the metrics are analyzed respectively, accuracy shows the percentage of successfully classified samples, recall shows how many of the true positives were successfully predicted, precision refers how many positively predicted values are positive, and f1 score is a measure of the model's precision and robustness. In order to calculate these metrics, TP (true positive), TN (true negative), FP (false positive), and FN (false negative) values should be obtained. TP indicates the number of correctly predicted detections. Thus, this means kidney disease detection to anyone who has kidney disease. TN means a class cannot be detected when a class is not present. In other words, if a person does not have kidney disease, the disease is not detected here. FP is class detection when a class does not exist. Accordingly, when a person does not have the illness, this means kidney disease to that person. FN is that when it belongs to a class, that person's class cannot be detected. In other words, although the person has kidney disease, the disease cannot be detected.

Experiments

The results obtained in the experiments are listed in Table 4. The best results, according to the metrics, are highlighted in bold style. The highest accuracy value for the training dataset is 100%, obtained by the RF algorithm. The SVM algorithm has 99.29%, and the 1D-CNN algorithm has a 98.93% accuracy value. The accuracy values for the test data set are 98.33% for all the 1D-CNN, SVM and RF algorithms. KNN and DT algorithms have 97.50% and 96.67% accuracy values for the test data set, respectively. When we shed light on Precision values, the highest RF and SVM algorithms have reached 100% value. The highest recall value is 98.33% which belongs to the 1D-CNN model. Similarly, the F1 Score value reached the highest value of 98.33% in the 1D-CNN model.

Table 4: ML and DL Models Training and Test Results

Algorithm	Acc.(Training)%	Acc.(Test)%	Precision%	Recall%	F1 Score%
1D-CNN	98.93	98.33	98.33	98.33	98.33
SVM	99.29	98.33	100	95.8	97.87
RF	100	98.33	100	95.8	97.87
KNN	98.21	97.50	97.87	95.8	96.84
DT	99.29	96.67	95.83	95.83	95.83

Furthermore, the confusion matrix of the obtained results is also given for each method. Figure 2 belongs to the 1D-CNN model. Figure 3 is the confusion matrix of the SVM model. Figure 4 depicts RF confusion matrix results. Also, the confusion matrix of the KNN model and DT model are illustrated in Figure 5 and Figure 6.

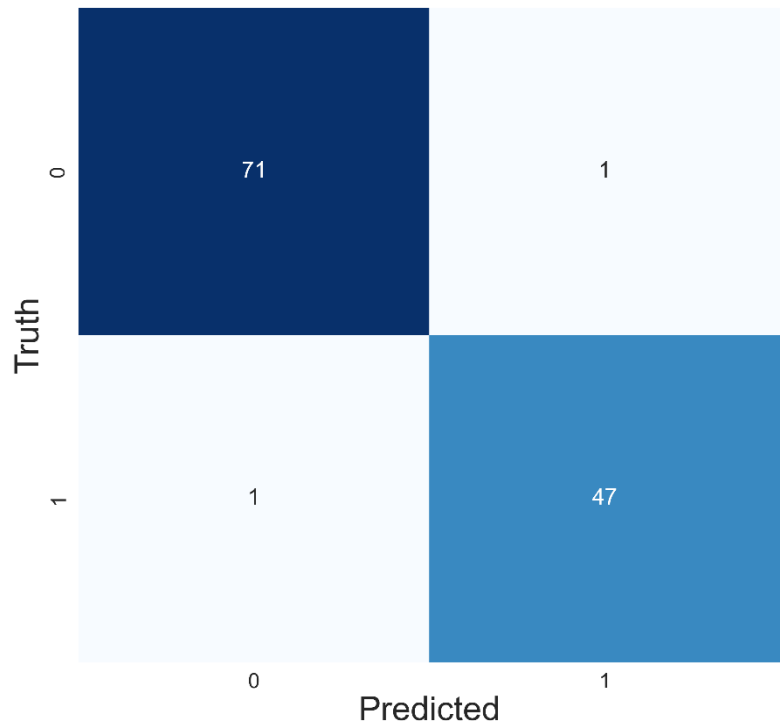


Figure 2 Confusion Matrix of 1D-CNN Model

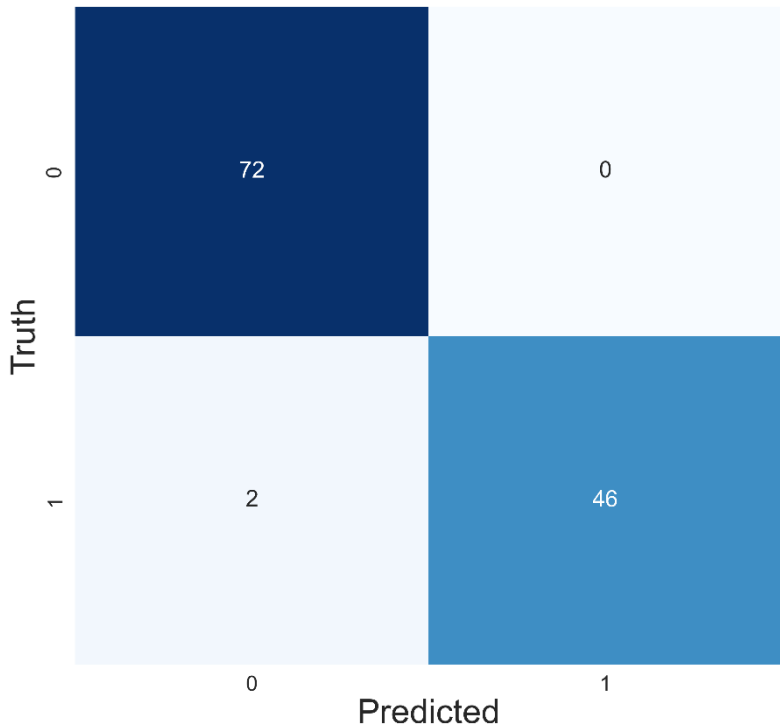


Figure 3 Confusion Matrix of SVM Model

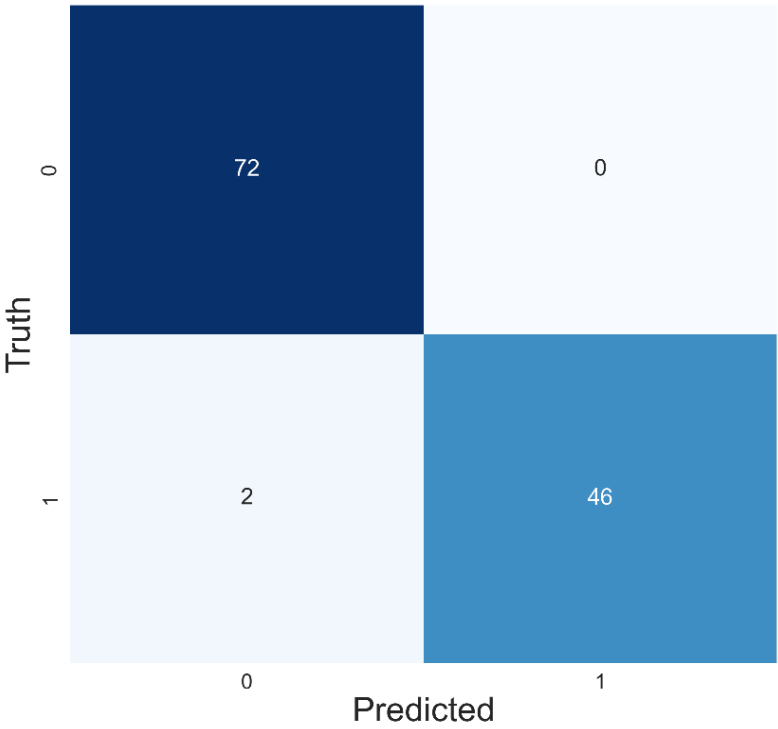


Figure 4 Confusion Matrix of RF Model

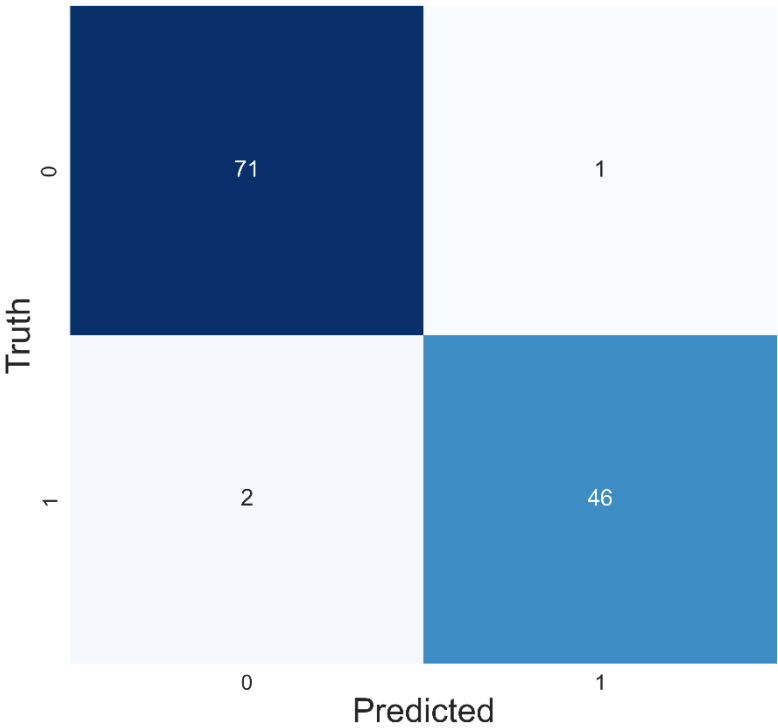


Figure 5 Confusion Matrix of KNN Model

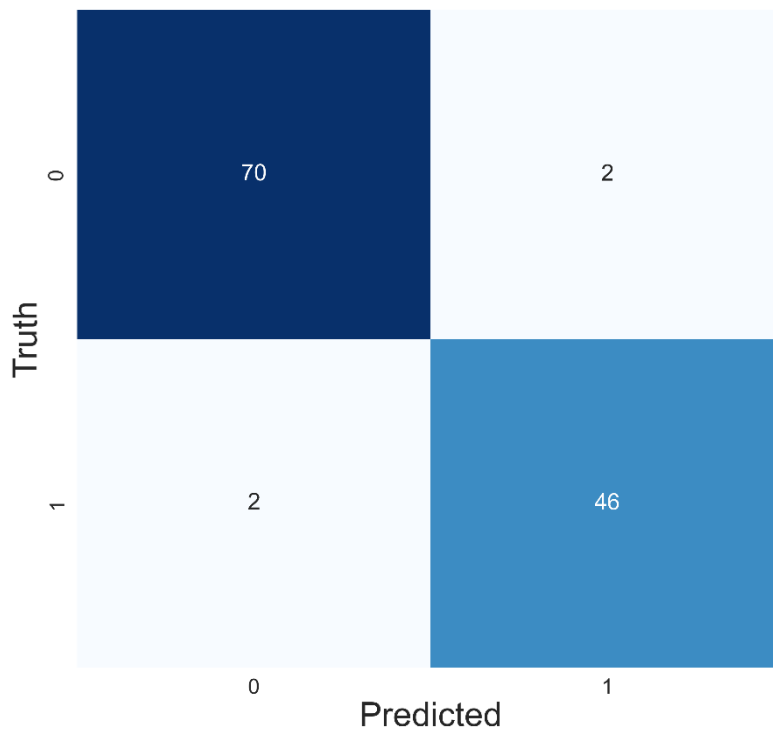


Figure 6 Confusion Matrix of DT Model

CONCLUSION

In this study, a new 1D-CNN deep learning model is proposed for the CKD prediction problem. Moreover, RF, SVM, DT and KNN machine learning methods are compared with the proposed DL method. At the first stage of this study, hyperparameters of all models are determined and optimized. The best parameter set of algorithms is employed for the same training and test data sets. Then, the models are built, and performance evaluation metrics values are obtained for performance comparison. The best accuracy performance for the training set belongs to the RF algorithm. On the other hand, the proposed 1D-CNN model, SVM and RF have the same accuracy value, which is the best performance. SVM and RF algorithms scored the best precision value. The proposed 1D-CNN model has the best scores in terms of recall and F1 score performance metrics. The proposed method produces competitive results with powerful ML algorithms in the literature.

REFERENCES

1. Akbulut, H. and Aslantaş, V. Evrişimli sinir ağı kullanarak çoklu-pozlamalı görüntü birleştirme. *Gazi Üniversitesi Muhendislik Mimarlık Fakültesi Dergisi*, 38(3):1439–1452.
2. Arslan, R. S. and Tasyurek, M. (2022). Amd-cnn: Android malware detection via feature graph and convolutional neural networks. *Concurrency and Computation: Practice and Experience*, 34(23): e7180.
3. Arulanthu, P. and Perumal, E. (2019). Predicting the chronic kidney disease using various classifiers. In 2019 4th international conference on electrical, electron- ics, communication, computer technologies and optimization techniques (ICEEC- COT), pages 70–75. IEEE.
4. Arulanthu, P. and Perumal, E. (2021). Risk factor identification, classification and prediction summary of chronic kidney disease. *Recent Advances in Computer Science and Communications (Formerly: Recent Patents on Computer Science)*, 14(8):2551–2562.
5. Bay, S. D. (1999). Nearest neighbor classification from multiple feature subsets. *Intelligent data analysis*, 3(3):191–209.
6. Breiman, L. (2001). Random forests. *Machine learning*, 45:5–32.
7. Cortes, C. and Vapnik, V. (1995). Support-vector networks. *Machine learning*, 20:273–297.

8. Ekanayake, I. U. and Herath, D. (2020). Chronic kidney disease prediction using machine learning methods. In 2020 Moratuwa Engineering Research Conference (MERCon), pages 260–265. IEEE.
9. Islam, M. A., Akter, S., Hossen, M. S., Keya, S. A., Tisha, S. A., and Hossain, S. (2020). Risk factor prediction of chronic kidney disease based on machine learning algorithms. In 2020 3rd international conference on intelligent sustainable systems (ICISS), pages 952–957. IEEE.
10. Lambert, J. R. and Perumal, E. (2021). Optimal feature selection methods for chronic kidney disease classification using intelligent optimization algorithms. *Recent Advances in Computer Science and Communications (Formerly: Recent Patents on Computer Science)*, 14(9):2886–2898.
11. Loh, W.-Y. (2011). Classification and regression trees. *Wiley interdisciplinary reviews: data mining and knowledge discovery*, 1(1):14–23.
12. Maurya, A., Wable, R., Shinde, R., John, S., Jadhav, R., and Dakshayani, R. (2019). Chronic kidney disease prediction and recommendation of suitable diet plan by using machine learning. In 2019 International Conference on Nascent Technologies in Engineering (ICNTE), pages 1–4. IEEE.
13. Moustapha, M., Tasyurek, M., and Ozturk, C. (2022). A novel yolov5 deep learning model for handwriting detection and recognition. *International Journal on Artificial Intelligence Tools*.
14. Nishanth, A. and Thiruvanan, T. (2017). Identifying important attributes for early detection of chronic kidney disease. *IEEE reviews in biomedical engineering*, 11:208–216.
15. Ozturk, C., Tasyurek, M., and Turkdamar, M. U. (2023). Transfer learning and fine-tuned transfer learning methods' effectiveness analyse in the cnn-based deep learning models. *Concurrency and Computation: Practice and Experience*, 35(4): e7542.
16. Pasadana, I., Hartama, D., Zarlis, M., Sianipar, A., Munandar, A., Baeha, S., and Alam, A. (2019). Chronic kidney disease prediction by using different decision tree techniques. In *Journal of Physics: Conference Series*, volume 1255, page 012024. IOP Publishing.
17. Revathy, S., Bharathi, B., Jeyanthi, P., and Ramesh, M. (2019). Chronic kidney disease prediction using machine learning models. *International Journal of Engineering and Advanced Technology*, 9(1):6364–6367.
18. Rubini, L. J., Eswaran, P., and Soundarapandian, P. (2015). Chronic kidney disease data set. UCI Machine Learning Repository, CA, USA.
19. Tasyurek, M. and Ozturk, C. (2022). Ddl: A new deep learning based approach for multiple house numbers detection and clustering. *Journal of the Faculty of Engineering and Architecture of Gazi University*, 37(2).
20. Ulutas, H. and Aslantas, V. (2023). Design of efficient methods for the detection of tomato leaf disease utilizing proposed ensemble cnn model. *Electronics*, 12(4):827.

EVALUATION OF AGGREGATES IN THE REGIONS OF AZERBAIJAN IN TERMS OF ALKALI-SILICA REACTION

Sabira Shahmarova
Samid Shahmarov
Rasim Bayramli

ABSTRACT

Alkali Silica Reaction (ASR) of aggregates is harmful influence to the concrete. ASR reaction can be eliminated by the application of low alkaline content of cement and non-reactive aggregates, usage of pozzolan additives or based on lithium chemical additives in concrete.

In this research, different source of aggregates from the regions of Azerbaijan were investigated. Accordingly, natural sand from Imishli, Shamakhi and Lankaran cities; crushed river-gravel from Guba, Imishli, Shamakhi and Lankaran cities; granodiorite from Shamkir were tested by the potential alkali reactivity mortar-bar method according to the ASTM C1260 test method. CEM II/A-P 42,5R type cement was used for it. The physical, mechanical and chemical properties of cement, and chemical properties of different source of local aggregates were determined. Water to cement ratio of the mortar mixture: 0.47 (by mass %). 25×25×285 mm sample were prepared. 10% by mass were taken from Fr (2.36-4.75) mm, 25% by mass were taken from Fr (2.36-1.18) mm, Fr (1.18-0.6) mm, Fr (0.6-0.6) mm, 15% by mass were taken Fr (0.3-0.15) mm for the test. 6 samples were prepared, and average result were determined. These samples were kept in 80°C temperature NaOH solution. Changes in the length of the samples were measured after 3rd, 7th, 10th, and 14th days. Based on the analyses results, these aggregates showed nearly similar performance in the mortar-bar method according to the ASTM C1260. The changes in the lengths after 14 days were only identified at the samples of the natural sand and crushed river-gravel from Lankaran city by 0.48% and 0.17%, respectively.

Keywords: potential alkali reactivity, natural sand, crushed river gravel, granodiorite.

INTRODUCTION

Concrete is a crucial building material for our life and concrete deteriorates from environment and chemical factors by time. One of the harmful factors for concrete is alkali silica reaction (ASR). Chemical reaction between alkalis which inside in cement and silicates which inside in aggregate as a result occur Na_2SiO_3 gel and this gel is hygroscopic. This hygroscopic gel happens in humidity condition and swells by time. Swelling hygroscopic gel harmful effect to the concrete face and internal surfaces and decrease the durability of concrete by time [1,2,3]. Other researchers have added additive 0, 8%, 10%, 12% and 14% silica fume from Turkey to OPC and have followed expansion value after 3, 7 and 14 days. The findings suggest that it may even be possible to use a dosage of between 8 and 10% silica fume to control reactive aggregates with values of 0.60 to 0.80%, reducing that expansion down to below 0.1% [5].

[4] have investigated alkali silica reactivity of aggregates in Thailand according to ASTM C1260 standard. From the study, conclusions are two types of sedimentary rocks, Greywacke, and limestone from some sources in eastern region of Thailand, as well as an igneous rock, rhyolitic tuff, from the central region, showed the potential reactivity as the root of ASR problem in the future. Greywacke from the different sources were almost similar in compositions, but significantly different features have been observed in thin section analysis. GRA and CTGW were coarse grained greywacke composed of quartz, feldspar, and rock fragments but REA had different granularity than the other two, with high weathering chlorite with a matrix of subgrained quartz, rock fragments and clay/graphite, deformed by tectonic forces. The ASR risk is increased significantly from subgraining of the microstructure. The highest expansion of REA agreed well with the microstructure analysis. –The microstructure investigation of volcanic rock aggregate, rhyolitic tuff showed slight weathering and the expansion result indicated potential reactivity. –The high silica content found in the limestone sample studied and the expansion higher than the limit suggested potential alkali reactivity.

The purpose of this work, used local different source of aggregates from different factories like natural sand from Imishli, Shamakhi and Lankaran cities, crushed river gravel from Guba, Imishli, Shamakhi and Lankaran cities, granodiorite from Shamkir city investigate due to ASR reaction in aggregates.

MATERIALS AND METHODS

2.1. Alkali-silica reaction according to ASTM C1260 standard

In this research, CEM II/A-P 42,5R cement and different source of aggregates like natural sand from Imishli, Shamakhi and Lankaran cities, crushed river gravel from Guba, Imishli, Shamakhi and Lankaran cities, granodiorite from Shamkir city were used.

CEM II/A-P 42,5R meets standard requirements. Because for creating the alkali silicium gel, Alkali/Oxide Ratio ($\text{Na}_2\text{O}+0,658\text{K}_2\text{O}$) should be more than 0,06 % in alkali silica reaction (ASR). In this work, Alkali/Oxide Ratio 0,89% CEM II/A-P 42,5R cement were used. Chemical properties of cement and aggregates are mentioned in Table 1 and 2, respectively. The aggregates were coded as **1, 2, 3, 4, 5, 6, 7 and 8**. Here, **1**: Natural Sand – Imishli city, **2**: Natural Sand – Shamakhi city, **3**: Natural Sand – Lankaran city, **4**: Crushed River Gravel – Guba city, **5**: Crushed River Gravel – Imishli city, **6**: Crushed River Gravel – Shamakhi city, **7**: Crushed River Gravel – Lankaran city, **8**: Granodiorite-Shamkir city

Table 1. Chemical properties of cement.

	Unit	CEM II/A-P 42.5R Cement
SiO_2	%	25,14
Al_2O_3	%	3,86
Fe_2O_3	%	3,78
CaO	%	58,96
MgO	%	1,45
SO_3	%	3,18
Na_2O	%	0,49
K_2O	%	0,61
LOI	%	1,6
$\text{Na}_2\text{O}+0.658\text{K}_2\text{O}$	%	0,89

Table 2. Chemical Properties of Different Source of Aggregates.

Test	Unit	Natural Sand – Imishli	Natural Sand – Shamakhi	Natural Sand – Lankaran	Crushed River Gravel - Guba
SiO_2	%	61.04	37.01	53.53	35.93
Al_2O_3	%	14.61	5.01	16.61	5.33
Fe_2O_3	%	4.95	2.70	7.28	2.87
CaO	%	6.13	28.30	7.11	28.79
MgO	%	2.30	0.81	4.01	0.91
SO_3	%	0.10	0.08	0.06	0.11
Na_2O	%	3.16	1.08	2.99	1.05
K_2O	%	2.44	0.69	3.60	0.67

15th INTERNATIONAL CONFERENCE ON ENGINEERING & NATURAL SCIENCES

March 04-06, 2023 Muş, TÜRKİYE

TiO ₂	%	0.59	0.30	0.91	0.26
P ₂ O ₅	%	0.20	0.08	0.41	0.12
Mn ₂ O ₃	%	0.08	0.27	0.11	0.16
SrO	%	0.10	0.07	0.14	0.05
ZnO	%	0.01	0.01	0.01	0.01
Cr ₂ O ₃	%	0.03	0.00	0.07	0.01
LOI	%	4.11	23.52	3.01	23.69

Test	Unit	Crushed River Gravel - Imishli	Crushed River Gravel - Shamakhi	Crushed River Gravel - Lankaran	Granodiorite - Shamkir
SiO ₂	%	60.08	28.11	52.90	61.92
Al ₂ O ₃	%	16.02	3.30	18.23	15.59
Fe ₂ O ₃	%	5.50	1.69	7.15	2.65
CaO	%	6.12	35.35	6.68	5.14
MgO	%	2.05	0.63	2.82	2.82
SO ₃	%	0.16	0.11	0.31	0.06
Na ₂ O	%	3.89	0.83	3.57	3.59
K ₂ O	%	2.63	0.52	3.41	1.77
TiO ₂	%	0.68	0.22	0.83	0.58
P ₂ O ₅	%	0.24	0.10	0.46	0.13
Mn ₂ O ₃	%	0.11	0.23	0.13	0.08
SrO	%	0.08	0.03	0.13	0.05
ZnO	%	0.01	0.01	0.01	0.02
Cr ₂ O ₃	%	0.01	0.01	0.01	0.01
LOI	%	2.27	28.43	3.16	2.50

Physical and mechanical properties of cement are shown in Table 3.

Table 3. Physical and Mechanical Properties of Cement

	CEM II/A-P 42.5R Cement
Fineness (residue over 40μ), %	5.6
Specific density, g/cm ³	3.06
Blaine, cm ² /g	3654

15th INTERNATIONAL CONFERENCE ON ENGINEERING & NATURAL SCIENCES

March 04-06, 2023 Muş, TÜRKİYE

Water demand (EN 197-1), %	28.4
Initial setting time, min.	175
Final setting time, min.	320
2 days compressive strength, MPa	31.0
7 days compressive strength, MPa	45.0
28 days compressive strength, MPa	60.1

The map of Azerbaijan which are the cities demonstrated due to test samples taken with red color are shown in Figure 1.

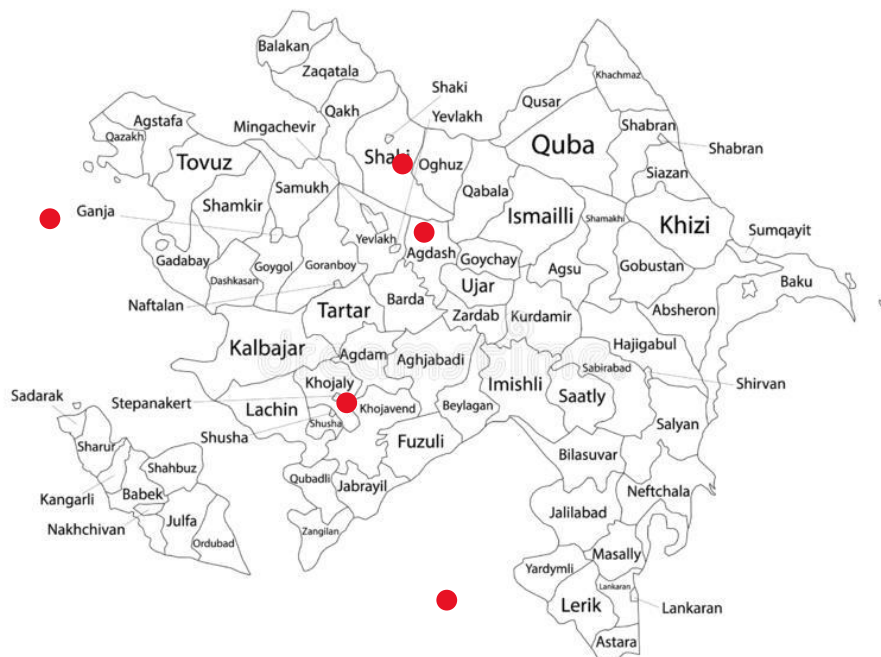


Figure 1. The map of Azerbaijan and the marks showing the sources of the aggregate tested

Test Result for Potential Alkali Reactivity of Aggregates

- Mortar-bar method according to ASTM C1260

Material properties and testing:

Aggregates were in oven dry condition. Sieve analyses of different source of aggregates for ASR test are shown in Table 4.

Table 4. Sieve Analyses of Different Source of Aggregates for ASR.

Sieve Size		Mass, %
Passing	Retained on	
4.75 mm (No. 4)	2.36 mm (No. 8)	10

15th INTERNATIONAL CONFERENCE ON ENGINEERING & NATURAL SCIENCES

March 04-06, 2023 Muş, TÜRKİYE

2.36 mm (No. 8)	1.18 mm (No. 16)	25
1.18 mm (No. 16)	600 µm (No. 30)	25
600 µm (No. 30)	300 µm (No. 50)	25
300 µm (No. 50)	150 µm (No. 100)	15

CEM II/A-P 42.5R type cement was used. Water to cement ratio of the mortar mixture: 0.47 (by mass %). 25×25×285 mm sample were prepared. 6 samples were prepared and average result were determined. These samples were kept in 80°C temperature NaOH solution. These samples length change were measured after 3, 7 10 and 14 days. Potential alkali reactivity of aggregates mortar-bar ASTM C1260 are shown in Table 5 and Figure 2.

Table 5. Potential Alkali Silica Reactivity of Aggregates Mortar-Bar ASTM C 1260.

Name of Aggregate Source	Day	Length Change, %						
		Samp le 1	Samp le 2	Samp le 3	Samp le 4	Samp le 5	Samp le 6	Average
Natural Sand – Imishli	0	0.04	0.04	0.03	0.04	0.04	0.01	0.03
	3	0.06	-0.07	0.05	0.04	0.03	0.03	0.02
	7	0.07	-0.08	0.07	0.05	0.03	0.05	0.03
	10	0.07	-0.08	0.07	0.06	0.04	0.05	0.03
	14	0.08	-0.09	0.09	0.06	0.05	0.06	0.04
Natural Sand – Shamakhi	0	0.03	0.04	0.12	0.04	0.16	0.04	0.07
	3	0.03	0.02	0.03	0.02	0.01	0.01	0.02
	7	0.08	0.09	0	0.09	-0.04	0.11	0.06
	10	0.11	0.10	0.02	0.13	-0.05	0.12	0.07
	14	0.10	0.13	0.04	0.16	-0.01	0.14	0.09
Natural Sand – Lankaran	0	0.04	0.04	0.04	0.03	0.02	0.03	0.03
	3	0.09	0.09	0.09	0.09	0.08	0.08	0.09
	7	0.09	0.11	0.12	0.11	0.10	0.10	0.11
	10	0.29	0.39	0.35	0.32	1.01	0.29	0.44
	14	0.33	0.43	0.41	0.35	1.03	0.32	0.48
Crushed River Gravel – Guba	0	0.04	0.02	0.02	0.02	0.12	0.02	0.04
	3	0.04	0.06	0.05	0.05	-0.05	0.04	0.03
	7	0.05	0.06	0.06	0.05	-0.06	0.04	0.03
	10	0.08	0.07	0.07	0.06	-0.09	0.04	0.04

15th INTERNATIONAL CONFERENCE ON ENGINEERING & NATURAL SCIENCES

March 04-06, 2023 Muş, TÜRKİYE

	14	0.08	0.07	0.07	0.07	-0.09	0.03	0.04
Crushed River Gravel – Imishli	0	0	0.01	0	0	-0.01	0.01	0
	3	0.01	0.01	0.02	0.01	-0.01	-0.02	0
	7	0.03	0.02	0.04	0.02	-0.03	-0.03	0.01
	10	0.04	0.05	0.05	0.04	-0.03	-0.04	0.02
	14	0.05	0.05	0.06	0.05	-0.04	-0.05	0.02
Crushed River Gravel – Shamakhi	0	0.16	0.03	-0.03	-0.08	0.06	0.06	0.03
	3	0	0	0	0	0	0	0
	7	0.02	-0.03	0.03	-0.01	0.01	0.02	0.01
	10	0.03	-0.07	0.05	-0.03	0.04	0.04	0.01
	14	0.04	-0.09	0.07	-0.04	0.05	0.06	0.01
Crushed River Gravel – Lankaran	0	0.01	0.03	0.03	0.01	0.02	0.01	0.02
	3	0.02	0.02	-0.02	0.01	-0.01	-0.19	-0.03
	7	0.14	0.14	0.20	0.16	0.13	0.18	0.16
	10	0.15	0.15	0.23	0.17	0.14	0.16	0.17
	14	0.18	0.17	0.21	0.19	0.16	0.14	0.17
Granodiorite – Shamkir	0	0.04	0.07	0.41	0.02	0.03	0.03	0.10
	3	0.01	0.00	0.01	-0.01	0.01	0.01	0.00
	7	0.02	-0.01	0.02	-0.02	0.01	0.02	0.01
	10	0.03	-0.02	0.02	-0.02	0.01	0.02	0.01
	14	0.03	-0.03	0.03	-0.04	0.02	0.02	0.01

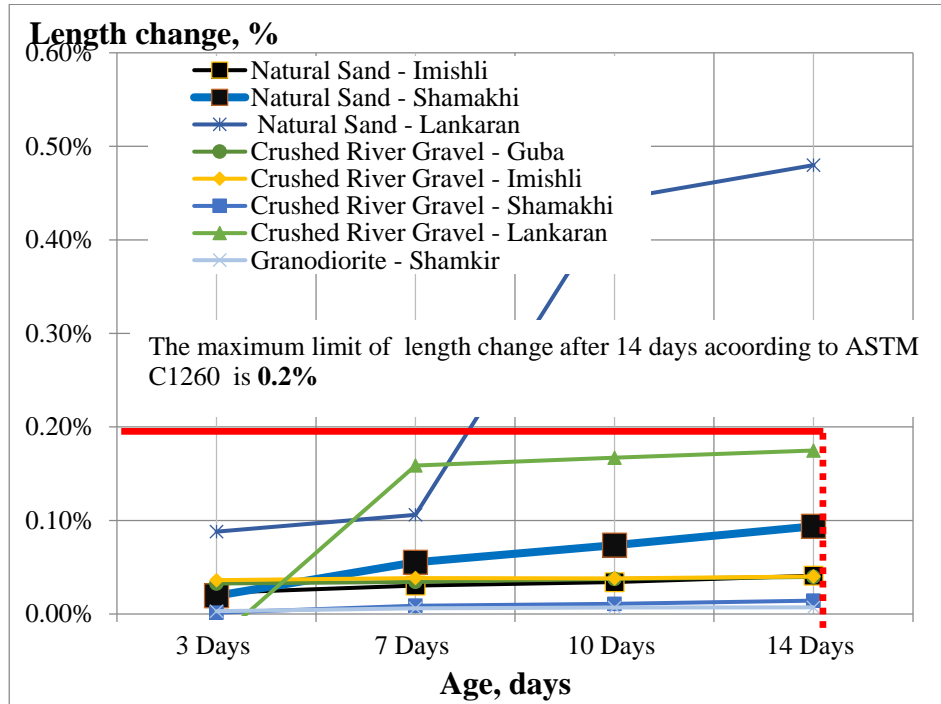


Figure 2. ASTM C1260 Length change development

Based on the results, it can be said that averagely length change, natural sand from Imishli Bahramtapa, crushed river gravel from Guba are the same length after 14 days (0.04%). The length change after 14 days of crushed river gravel from Imishli Bahramtapa is 0.02%. Granodiorite had the best result (0.01%). The length changes after 14 days of natural sand and crushed river gravel from Lankaran are 0.48% and 0.17%, respectively and is not within the standard requirement. The criteria for ASR expansion ratio are listed in Table 6.

Table 6. Expansion Criteria according to ASTM C1260

Criteria	ASTM C1260
Non-reactive	0.0 to 0.1 %
Inconclusive	0.1 to 0.2%
Potentially Reactive	Above to 0.2%

Notes: No cracks or breaks were observed on the specimens after the test.

The pictures of the samples are shown in figure 3 and 4.



Figure 3. The picture of the test samples and test setup



Figure 4. The picture of the test samples

CONCLUSIONS

It can be concluded that, different local source of aggregates is non-reactive according to ASTM C1260 standard requirement, except natural sand from Lankaran city (0.48%). Crushed river stone from Lankaran city (0.17%) test result near to the standard requirement.

The length changes of natural sand and crushed river gravel from Imishli city were 0.04 and 0.02%, respectively and this results within standard requirement.

Although the length change of natural sand from Shamakhi city was 0.09% whereas the length change of

crushed river gravel from Shamkhi city was 0.01% and the test results within the standard requirement. The length change of crushed river gravel from Guba city and Granodiorite from Shamkir city were 0.04% and 0.01%, respectively and the test results within the standard requirement.

Only natural sand from Lankaran city were ASR risk due to the high test result (0.48%) and it is more than standard requirement (0.2%). However, crushed river gravel from Lankaran city (0.17%) near to the standard requirement (0.2%).

CEM II/A-P 42,5R meets standard requirements. Because for creating the alkali silicium gel, Alkali/Oxide Ratio ($\text{Na}_2\text{O}+0,658\text{K}_2\text{O}$) should be more than 0,06 % in alkali silica reaction (ASR). In this work, Alkali/Oxide Ratio 0,89% CEM II/A-P 42,5R cement were used. There is not any standard requirement for silicates in aggregates.

Furthermore, the same aggregates were tested by the TI-B 51 (85) test method. The four samples were prepared in size of 40×40×160 mm and average results were determined. The length of the samples was measuring after 2, 4, 6, 8, 12, 16, 20 weeks and the test continue.

Acknowledgements

The authors would like to thank Norm Cement and its concrete laboratory for the support.

REFERENCES

1. ASTM C1260, Potential Alkali Reactivity of Aggregates (Mortar-Bar Method) Neville, A.M., Properties of Concrete, John Wiley & Sons INC., New York, U.S.A, 1997.
2. Demir, I., Sevim, Ö. (2017). Effect of sulfate on cement mortars containing Li_2SO_4 , LiNO_3 , Li_2CO_3 and LiBr . Construction and Building Materials, 156, 46-55.
3. Demir, I., Sevim, Ö., Kalkan, I. (2018). Microstructural properties of lithium-added cement mortars subjected to alkali-silica reactios. Sadhana, 43 (7), 112.
4. Suvimol Sujjavanich, Krit Won-In, Thanawat Meesak, Watcharagon Wongkamjan and Viggo Jensen. Investigation of potential alkali-silica reactivity of aggregate sources in Thailand. International Journal of Geomate, July, 2017, Vol 13, Issue 35, pp. 108-113.
5. Robert C Lewis and Elif Bayrak, Combating ASR to enable usage of local aggregates in Turkey, 25_Ermco_2015.

APPLICATION OF GRANODIORITE AND CRUSHED RIVER STONE AGGREGATE IN PERVIOUS CONCRETE AND INVESTIGATION OF SOME PROPERTIES

Aminaga Sadıgov
Maharram Şaliyev
Samid Şahmarov

ABSTRACT

In this study, permeable concrete tests were prepared with the use of different aggregate types and fine material aggregates and were determined the permeability coefficient, the amount of voids in the concrete, and the 7 and 28-days compressive strengths. The purpose is when the mixing ratio is different to determine and consider the differences between the void ratio and the permeability coefficients, and to determine the mixing ratio that meets the requirement for the highest strength limit. In the research study, considering two different and different sizes of coarse aggregates, 4 mixture designs were developed and a small amount of fine material was also used. The concrete mixture 1 consists of granodiorite, natural sand and cement, mixture 2 granodiorite and cement, mixture 3 crushed river stone, natural sand and cement, mixture 4 crushed river stone and cement, respectively. Samples were taken to determine the void ratio, permeability and compressive strength, tests were carried out and the results obtained with mathematical equations were evaluated. Experiments have shown that the best average permeability coefficient (4.46) and actual void content (%25.9) is 1 in the granodiorite based and %4.3 sand content mix design. The mix with the best strength index is the 3rd mix design based on crushed river stone and added %4.3 sand (20.4 MPa). CEM II/A-P 42,5N type cement was used for it. The physical and mechanical properties of cement, physical and chemical properties of aggregates were determined.

Keywords: Pervious concrete, void ratio, aggregate type, compressive strength

ÖZET

Bu çalışmada farklı agrega tipi ve ince malzemeli agrega kullanımı ile geçirimli beton deneyleri hazırlanmış ve geçirimsizlik katsayısı, betondaki boşluk miktarı, 7 ve 28 günlük basınç dayanımları belirlenmiştir. Amaç, karışım oranı farklı olduğunda boşluk oranı ve geçirgenlik katsayıları arasındaki farkları belirlemek ve hesaba katmak, en yüksek dayanım sınırı gereksinimini karşılayan karışım oranını belirlemektir. Araştırma kapsamında iki farklı ve değişik boyuttaki iri agrega dikkate alınarak 4 karışım tasarımı geliştirilmiş ve az miktarda ince malzeme de kullanılmıştır. Beton karışımı 1 granodiorit, doğal kum ve çimento, karışım 2 granodiorit ve çimento, karışım 3 kırmataş, kum ve çimento, karışım 4 kırmataş ve çimentodan oluşmuştur. Boşluk oranı, geçirgenlik ve basınç dayanımı belirlenmesi için numuneler alınmış, testler yapılmış ve matematiksel denklemlerle elde edilen sonuçları değerlendirilmiştir. Deneyler, en iyi ortalama geçirgenlik katsayısının (4.46) ve gerçek boşluk içeriğinin (%25.9) granit bazlı ve %4.3 kum içerikli karışım tasarımı 1 olduğunu göstermiştir. En iyi dayanım indeksine sahip karışım, kırma taş esaslı ve %4,3 kum ilave edilen 3. karışım tasarımıdır. Bu testler için CEM II/A-P 42.5N çimento kullanılmıştır. Çimentonun fiziki ve mekaniki, agregaların ise fiziki ve kimyevi özellikleri incelenmiştir.

Anahtar kelimeler: Geçirimli beton, boşluk oranı, agrega tipi, basınç dayanımı

GİRİŞ

Geçirimli beton, büyük hacimli birbirine bağlı boşluklara sahip bir beton türüdür. Geçirimli beton, geleneksel betondan farklı olarak birbirine bağlı boşluklar içeren bir betondur. Çimento, İri agrega ve su karışımından yapılır. Ancak çok az kum içerir veya hiç içermez. Bu, gözenekli bir yapıya sahip bir beton tipi ile sonuçlanır. İnce malzemesi olmayan veya geçirimli beton olarak bilinen geçirimli beton, düşük etkili sürdürülebilir kalkınmanın temel unsurlarından biri olarak iyi tanınan çevre dostu bir kaplama malzemesidir [1].

Geçirimli beton bünyesinde bulunan bir kısmı bağlantılı boşluklardan (%15-35) suyu kolaylıkla geçirebilmesi sayesinde, şiddetli yağışın yüzeysel akışa dönüşme oranını azaltma potansiyeline sahip alternatif bir üst yapı kaplama malzemesidir. Sağladığı drenajla birlikte yeraltı su kaynaklarının beslenmesine

de katkıda bulunmaktadır. Böylece su kaynaklarındaki azalmanın önüne geçilmesi açısından da potansiyel bir kaplama malzemesi olarak düşünülebilir. Geçirimli betonun su geçirgenlik özelliği; tasarımında kullanılan iri agreganın dar bir tane boyut aralığında olması ve ince agrega miktarının minimize edilmesinden (kütlece %10 ve daha az) ileri gelmektedir [2].

Daha önce yapılan çalışmada 1mm'e kadar ince malzeme bazı karışımlarda kullanılmış ve su geçiren betonların geçirimsizlik, yarmada çekme dayanımı gibi özelliklerine bakılmıştır. Bu çalışmada su geçirimsizlik özellikleri ve dayanım özellikleri arasında ters bir ilişki bulunmuştur. Boşluk miktarı arttıkça basınç dayanımı düşmekte ama geçirgenliği artmaktadır [3].

Başka bir çalışmada kullanılan ince malzeme miktarı arttıkça dayanımda artış görülmüştür. İnce malzemenin artmasıyla birlikte dayanımda artış, birim ağırlıkta artış, eğilme dayanımında artış görülmüştür [4].

Bu çalışmanın amacı, iki farklı iri agrega (Granodorit ve Kırmataş) kullanılarak betonda geçirgenlik ve dayanım kriterlerinin araştırılmasıdır. Bu agregalar yerel agrega kaynakları kullanılarak farklı lokasyonlardan yani İmişli şehrinden doğal kum, Guba'dan nehir çakılından Kırmataş, Şemkir şehrinden Granodorit olmak üzere alınmış ve araştırma yapılmıştır.

MATERYAL VƏ YÖNTEMLER

Malzemeler

Deneyisel çalışmada: Granodorit, Kırmataş ve Doğal kum olmak üzere toplamda 3 adet agrega kullanılmıştır. Granodorit agregası Şemkir şehrinden elde edilmiş olup 8 ve 11.2 mm elekten geçirilmesiyle yıkanmadan kullanılmıştır. Temiz Kırmataş ise Guba şehrinde yerleşen Garaçay çayından alınarak 8 ve 11.2 mm lik eleklerden geçirilerek benzer tane boyut dağılımı içinde kalması sağlanmıştır. İncelik modülü 2.2 olan Kum ise İmişli şehrinde yerleşen kaynaktan elde edilmiştir ve yıkanmadan ince malzeme olarak kullanılmıştır. Deneylerde çimento olarak EN 197-1 standartının talebine uygun CEM II/A-P 42.5N tipi Portland çimentosu kullanılmıştır. Çimentoların fiziksel ve mekanik özellikleri Tablo 3-de verilmiştir.

Agregaların özellikleri Tablo 1 ve 2-de verilmiştir.

Tablo 1. Agregaların özellikleri

Agrega tipi	Agrega tane sınıfı	Kil ve Silt İçeriği (%)	Özgül Ağırlık, t/m ³	Su emme (%)
Kırmataş	8-11.2 mm	-	2.70	0.1
Granodorit	8-11.2 mm	-	2.90	0.1
Doğal Kum	2.2 mm	1.5 %	2.55	2.33

Tablo 2. Agregaların kimyevi özellikleri

Kimyasal bileşim	Unit	Doğal Kum (İmişli şehri)	Nehir Çakılından Kırmataş (Guba şehri)	Granodorit (Şemkir şehri)
SiO ₂	%	61.04	34.90	61.80
Al ₂ O ₃	%	14.61	4.85	15.47
Fe ₂ O ₃	%	4.95	2.85	2.64
CaO	%	6.13	27.79	5.13
MgO	%	2.30	0.93	2.81

15th INTERNATIONAL CONFERENCE ON ENGINEERING & NATURAL SCIENCES

March 04-06, 2023 Muş, TÜRKİYE

SO ₃	%	0.10	0.10	0.05
Na ₂ O	%	3.16	1.02	3.58
K ₂ O	%	2.44	0.64	1.76
TiO ₂	%	0.59	0.22	0.57
P ₂ O ₅	%	0.20	0.11	0.15
Mn ₂ O ₃	%	0.08	0.14	0.06
SrO	%	0.10	0.04	0.04
ZnO	%	0.01	0.01	0.02
Cr ₂ O ₃	%	0.03	0.01	0.01
LOI	%	4.11	22.96	2.52

Tablo 3. Çimentonun fiziksel-mekanik özellikleri

	CEM II/A-P 42.5N Çimento
İncelik (40µ üzerinde kalıntı), %	5.5
Özgül yoğunluk, g/cm ³	3.05
Blain, cm ² /g	3653
Su talebi (EN 197-1), %	28.2
Priz başlama süresi, min.	173
Prizin sona erme süresi, min.	319
2 gün basınç dayanımı, MPa	32.0
7 gün basınç dayanımı, MPa	47.0
28 gün basınç dayanımı, MPa	60.1

Geçirimli beton karışım bileşenleri

İki farklı iri agrega ile kum ve kum içermeyen içerikli 4 beton karışımı hazırlanarak testler gerçekleştirilmiştir:

1. Granodorit, Kum və Çimento
2. Granodorit və Çimento
3. Kırmataş, Kum və Çimento
4. Kırmataş və Çimento

Tablo 4'te görüldüğü gibi granodorit ve kırmataş bazında karışımdaki kum miktarı 50 kg'dır (%4,3).

Tablo 4. Karışım hesabı

Karışım	Özgül ağırlık, (kq/m ³)				
	Çimento	Su	Granodorit (D8-10)	Kırmataş (D9,5-12,5)	Kum
№1	300	100	1176	-	50
№2	300	100	-	1226	0
№3	300	100	1176	-	50
№4	300	100	-	1226	0

Granodorit bazlı karışımlarda ilk test, granodorit ve kum bileşimidir. Kum ilavesinin amacı betonun elastisite katsayısını artırmaktır ve aynı zamanda geçirimliliğe olumsuz etkisi olsa bile dayanımı artırmada olumlu rolü olacağını varsaydık. İkinci karışım ise sadece granit bazlıdır. Bu testi yapmak, daha iyi bir sonuç elde etmek için ilk testin, yani kum eklemenin negatif ve pozitif sonuçlarını karşılaştırmaktır. Üçüncü karışım kırmataş ve kumdan oluşuyordu. Kırmataşın seçilme sebebi ise adından da anlaşılacağı gibi Çay taşlarının kırılmasından elde edilen pürüzlü yüzeyin olumlu anlamda bir ek olacağı ve granodorite benzer tane boyutunda (8-11,2 mm) kalması sağlanmıştır. Kırmataş-kum karışımına kum ilavesi, granit esaslı bileşimdeki ile aynı miktardadır. En etkili olanın seçimi, yalnızca kırmataş içeren bileşim ile kırmataş ve kum içeren karışımın sonuçlarının karşılaştırılmasına dayanır. Granodorit ve Kırmataş fraksiyon aralığının 8-11,2 mm olarak seçilmesindeki temel amaç, sıkıştırma sırasında aynı boyuttaki malzemelerin boşluklarını dolduramamasıdır (Şekil 1). Yukarıdakiler göz önüne alındığında, granodorit ve kırmataş bazlı karışım testleri aşağıdaki gibidir:

YAPILAN TESTLER

Boşluk içeriği ölçme testi

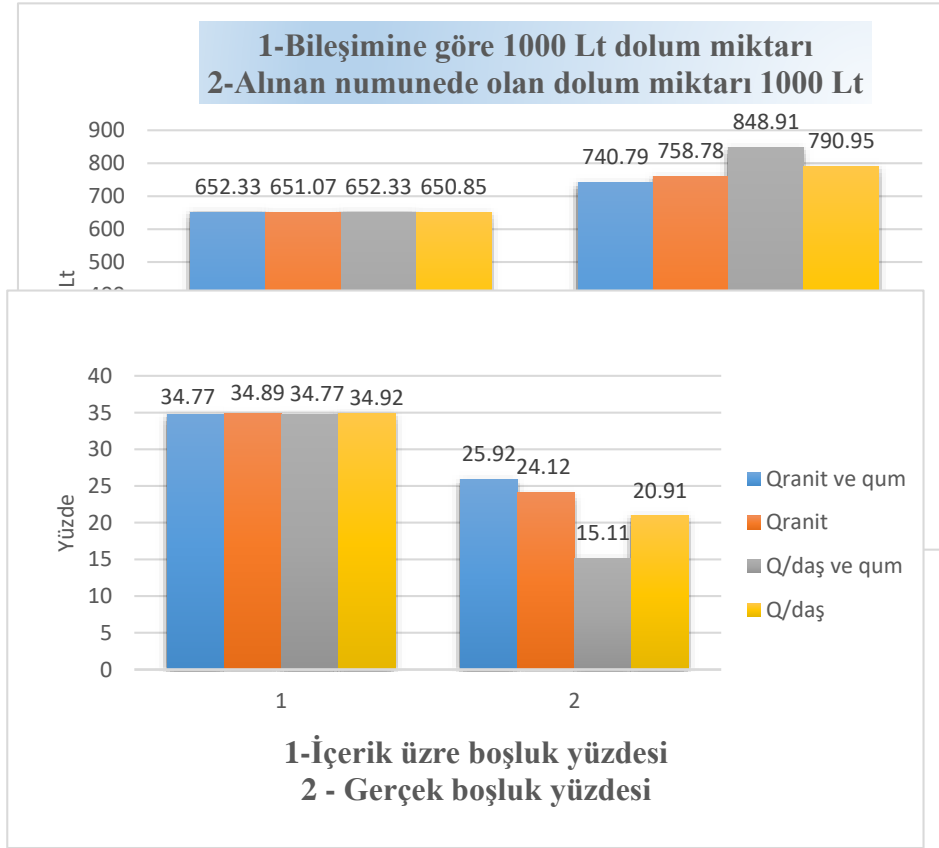
Dolguların hacmini dikkate alarak 1 m³ için gerekli dolgu ağırlıklarını belirledik. Agregaların toplam hacmini 1000 Lt-den çıkararak hazırlanan betondaki boşlukları belirledik. Beton numunelerinden elde edilen test sonuçları Tablo 5'te gösterilmiştir.

Tablo 5. Beton numunelerinden elde edilen test sonuçları

Agregalar	Bileşime göre 1000 litrenin dolum sınırı, kg	Alınan numunede 1000 litrenin dolum limiti, kg	İçerik boşluğu, %	Faktiki boşluk, %	№1 Mukavemet, MPa	№2 Mukavemet, MPa	№3 Mukavemet, MPa	Orta değer, MPa
Granodorit ve qum	652,33	740,79	34,77	25,92	16,3	16,9	18,5	17,2
Granodorit	651,07	758,78	34,89	24,12	12,5	10,5	10,1	11,0
Kırmataş ve qum	652,33	848,91	34,77	15,11	19,2	21,2	19,8	20,4
Kırmataş	650,85	790,95	34,92	20,91	15,5	14,0	15,2	14,9

Aşağıdaki grafiklerden de görüleceği üzere (şekil 1), agregalar farklı olmasından dolayı ağırlık bazında dolum limitleri belirlenmektedir. Şekil 2-de toplam parça hacminden dolgu hacminin çıkarılmasıyla boşluk yüzdeleri belirlendi. Resimlerden de görüleceği üzere (1. resimdeki sol ve sağ grafikler, 2. resimdeki sol ve sağ grafikler) beton karışımının sıkışma derecesi beklenenden daha fazla olmuştur.

Şekil 1. Dolum miktarı



Şekil 2. Boşluk Oranı

Granodorit esaslı karışımlarda, sadece granodorit kullanılan karışımdan alınan numunelerdeki boşluk içeriği, kum ile yapılan granodorit esaslı karışımdan alınan boşluk yüzdesine göre nispeten daha azdı. Sonraki testlerin sonuçlarına göre hangi karışımın daha etkili olduğu belirlenecektir.

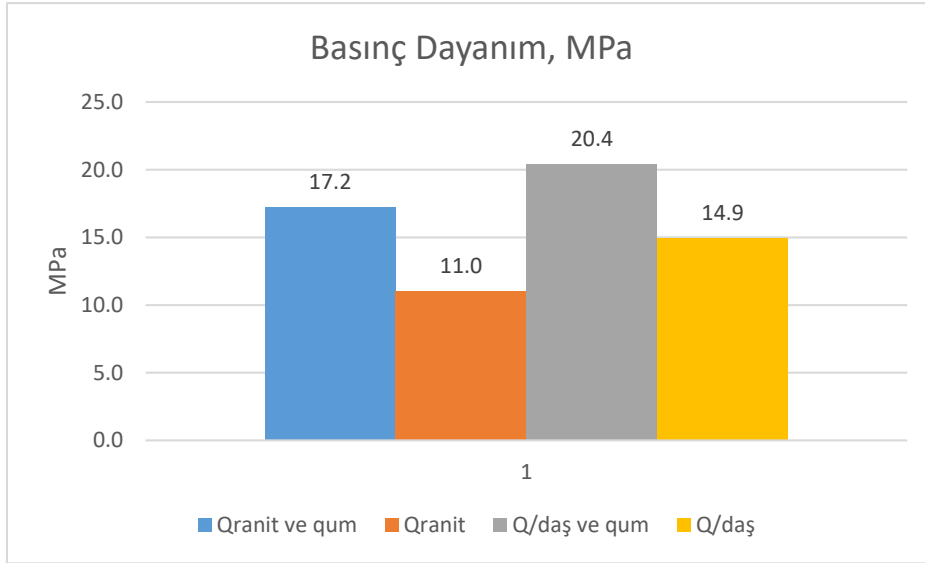
Kırmataş bazlı karışımlarda ise tam tersi sonuçlar elde edilmiştir. Burada sadece kırmataştan yapılan karışım, kumlu kırmataştan yapılan karışıma göre daha boşluklu oldu. Sonuçlara bakıldığında, kırmataş esaslı karışımlardaki boşluk miktarının düşük olması fraksiyon aralığının geniş olmasından kaynaklanabilir. İlk boşluklara göre elde edilen sonuçlardan, daha geçirimli bir beton elde etmek istiyorsak, fraksiyon boyut aralığını en aza indirmemiz gerektiği söylenebilir, örneğin: 8-11,2 mm yerine 8-10 mm veya sadece 10-11,2 mm, yani 11,2 mm elekden geçen ve 10 mm elek üzerinde kalan agregaları kullanmak.

Tablo 4'te görüldüğü gibi, Granodorit esaslı karışımlarda granodorit ve kum karışımının bileşimi toplam ağırlığın 1 m³'ünde 1626 kg, gerçek 1 m³'ünde ise 1846,5 kg'dır. Bahsedilen ağırlıkların oranını katsayı olarak alırsak 0,88'dir. Sadece kırmataştan oluşan kompozisyon baz alınarak ikinci ağırlık 1626 kg olarak aynı tutulsa da 1m³ dolgunun gerçek ağırlığı 1895 kg olmuştur. Buradaki karışımdaki ağırlıkların oranı katsayı olarak 0,858 idi. Katsayılardan da anlaşılacağı üzere sıkıştırma yöntemi standart olmakla birlikte sıkıştırma oranları farklıdır. Sonraki test sonuçlarına göre (tablo 5), sıkıştırma derecesine göre boşluk miktarının sadece granodorit ile hazırlanan karışımda %24,12, granodorit ve kum ile hazırlanan karışımda ise %25,92 olduğunu söyleyebiliriz. Aynı sırayla devam eden dayanım sınırı sonuçları, sıkıştırma derecesine bağlı olarak daha az boşlukla daha düşük dayanım sonuçları vermiştir. Kum ilavesi nedeniyle elastik katsayı artmış, bu da betona özel dayanıklılık kazandırmıştır. Mukavemeti sonucu, daha az boşluk içeren karışımdan daha yüksekti.

Sugeçiricilik

Daha fazla boşluklu granodorit ve kum karışımı, granodorit bazlı karışımlardaki boşluk miktarının doğrudan neden olduğu koşullar nedeniyle daha hızlı sugeçiricilik özelliğine sahiptir. Sonuçlardan da görülebileceği gibi, granodorit bazlı karışım daha düşük değerler göstermiştir.

Şimdi Kırmataş bazlı karışımdan yapılan numunelerin sonuçlarını karşılaştıralım. Kırmataş ve kum içeren karışımda agregaların ağırlığı granodorit karışımındaki 1626 kg/m^3 ile aynı tutulmuş, ancak boşluk miktarının az olması nedeniyle 2116 kg/m^3 agrega kullanılmıştır. Söz konusu ağırlıkların oranı 0,768'dir. Sadece Kırmataş'ta hazırlanan karışımın ağırlığı aynı tutularak sıkıştırma derecesine göre 1m^3 için gerekli dolgu ağırlığı 1976 kg/m^3 olmuştur. Burada elde edilen ağırlıkların oranı katsayı olarak 0,823'tür.



Şekil 3. Basınç Dayanım gelişimi

Bir sonraki testin sonucu tablo 5'dir, kırmataş ve kumdan oluşan karışımda sıkıştırma oranı önceki sıkıştırma prosedürü ile aynı olmasına rağmen sonuç (sıkıştırma oranı) %15,11 olmuştur. Sadece kırmataş ile hazırlanan karışımın boşluk oranı %20,91 ile nispeten daha yüksek olmuştur. Sıkıştırma %'sine bağlı olarak, granodorit bazlı bileşim, basınç dayanım sonuçlarının tersiydi (Şekil 3). Burada sadece kırmataşla yapılan betonun dayanım sınırı 14,8 MPa, kırmataş ve kumla yapılan betonun dayanım sınırı küçük boşluk ve yüksek elastisite katsayısı nedeniyle 20,4 MPa olmuştur.

Kırmataş bazlı karışımlarda kum içeren karışımın boşluk oranı en az 15,11% olmuştur. 4 sonucun boşluk, dayanım sonuçlarına göre sugeçirgenlik katsayılarını belirlemek mümkündür. Elimizdeki imkanlarla standarta göre sugeçirgenlik testleri yaparak sugeçirgenlik katsayılarını her 4 karışıma göre tenliye dayalı olarak tayin ettik:

Tablo 6'dan da görülebileceği gibi, her 4 karışım için 6 silindir numune sonucu elde edilerek geçirgenlik katsayıları belirlenmiştir.

Tablo 6. Su geçirimsizlik katsayısı

Nümunə №	Granodorit və kum		Granodorit		Kırmataş və kum		Kırmataş	
	Zaman, sn.	Geçiricilik katsayısı, mm/san	Zaman, sn.	Geçiricilik katsayısı, mm/san	Zaman, sn.	Geçiricilik katsayısı, mm/san	Zaman, sn.	Geçiricilik katsayısı, mm/san
1.numune	108	4,42	95	3,89	68	2,78	65,5	2,68
2.numune	100	4,09	98	4,01	70	2,86	50	2,05
3.numune	101	4,13	90	3,68	78	3,19	55	2,25
4.numune	110	4,5	100	4,09	65	2,62	60	2,45
5.numune	120	4,91	88	3,68	72	2,95	65	2,66
6.numune	115	4,71	85	3,48	69	2,82	52	2,13
Orta Geçiricilik katsayısı, mm/san	4,46		3,805		2,87		2,37	

Granodorit ve kum karışımı, karışımların bileşimine göre en yüksek geçirgenlik katsayısını vermiştir. Bununla birlikte, diğer sonuçlarda, standardın gerekliliğinin 0,1 mm/sn'den yüksek olduğu için ödenir.

SONUÇLAR

Yol yapımında geçirimli beton kullanılacağı ve yol altyapısında statik yükler olduğu düşünüldüğünde. Bu nedenle geçirimli betonda birincisi geçirgenlik katsayısı, ikincisi ise elastisite katsayısıdır. Bu amaçla çalışmalarımızı kırmataş esaslı karışımlar üzerinde yoğunlaştırsak daha uygun sonuçlar alınabilir. Daha dayanıklı yani dayanım limiti, elastisite katsayısı ve su geçirgenliği açısından kırmataş-kum karışımı beton sonuçları göstermiştir. en yüksek sonuçlar. Bahsedilen sonuçlara göre elde edilen beton cinsinin, Azerbaycan'ın daha çok yağış alan bölgelerinde, kaldırımlarda ve parklarda, ayrıca drenaj sistemi sıkıntısı çeken alanlarda kullanılması uygundur.

Acknowledgements

The authors would like to thank, Gilan Holding Concrete batching plant staff and its concrete laboratory for the support.

KAYNAKÇA

1. Yang, J.; Jiang, G. Experimental study on properties of pervious concrete pavement materials. Cem. Concr. Res. 2003, 33, 381–386. []
2. ACI. 522R–10. Report on Pervious Concrete ACI Committee 522 (2010)
3. Neptune, Andrew I., Putman, Bradley J., “Effect of Aggregate Size and Gradation on Pervious Concrete Mixtures”, ACI Materials Journal, Kasım–Aralık 2010, pp 625-631.
4. Meininger, R., “No Fines Pervious Concrete for Paving”, Concrete International, August 1988, pp 20-27.

NUMERICAL STUDY IN A RECIRCULATION ZONE BETWEEN TWO SUCCESSIVE SPUR DIKES WITH LARGE ROUGHNESS ELEMENTS

Maaz Khan
Ghufran Ahmed Pasha
Sohail Iqbal
Usman Ghani
Afzal Ahmad

ABSTRACT

The recirculation zone formed between two successive spur dikes results in scouring and erosion in spur dike field. The numerical simulations were made to investigate the recirculation zone between two successive spur dikes by changing the different 5 aspect ratios ($\text{aspect ratio} = \frac{\text{Distance between two spur dikes}}{\text{Length of the spur dike}}$) and adding roughness element in spur dike field. Three different measuring locations (L1, L2, and L3) were selected to understand their impact on the flow structure the depth averaged velocity was measured at 3.5 cm of the channel depth. At measuring locations, velocity, turbulent kinetic energy and pressure contours, were examined. The velocity in spur dike field increased from aspect ratio 1 and aspect ratio 2 at three locations. The results shows that aspect ratio 3 having location L3 has the optimum velocity i-e., 30% and T.K.E. in the recirculation zone. The velocity, Turbulence intensity (T.I) and (T.K.E) lower with roughness (12 %) elements in recirculation zone. Therefore, spur dike field along with roughness elements should be preferred to protect the spur dike, and bank from extreme turbulence behaviour of flow during floods and to limit the recirculation zone inside the spur dike field.

Keywords: Spur dike, large roughness elements, Numerical simulation, Flow characteristics.

INTRODUCTION

Spur dikes are hydraulic structures designed to safeguard channel banks against erosion by redirecting the water flow away from them. These structures usually comprise angled vertical walls that divert the flow direction away from the banks by fulfilling their primary objective of protecting the banks. (2) indirectly reducing flow velocity (Pandey, Valyrakis, Qi, Sharma, & Lodhi, 2021). Spur dikes perform their primary function of safeguarding stream banks (Pandey et al., 2021), throughout the globe to improve navigation, strengthen flood protection, and save erodible banks (Iqbal et al., 2021). Because of the complexities involved in the spur arrangement and the stream wise spur extension, spur dike scour behavior has not progressed (Karami, Ardeshir, Behzadian, & Ghodsian, 2011). Hydraulic engineering deals with a very broad and difficult subject while studying the flow mechanism around various spurs.

Large roughness elements are generally used that leads to energy loss in a stream channel causing the hydraulic of the flow in the channel. Roughness elements can be large stone or concrete blocks placed in the channel's bed with a different configuration to impose more resistance (Alwan & Azzubaidi, 2021). Roughness elements in a channel are obstacles or irregularities on the surface of the channel walls that increase friction and decrease water velocity. These elements can include rocks, vegetation, and sediment deposits. The roughness of a channel affects flow patterns, turbulence, and mixing, and is a critical parameter in calculating water flow rates and sediment transport. The roughness elements' size, shape, and distribution are important factors in determining flow resistance and sediment transport rates. (Julien, 2018)

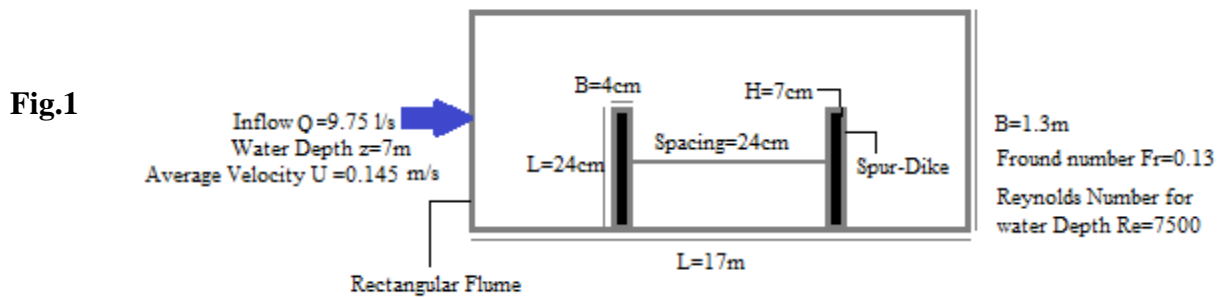
The previous literature review show that the study uses computational fluid dynamics (CFD) simulations to model the flow patterns and recirculation zone behind the spur dike. The results show that the size and shape of the recirculation zone are strongly affected by the height and length of the spur dike. A longer, taller spur dike leads to a larger recirculation zone and more turbulent flow (Gao, Yang, Wang, & Zhao, 2022). The study uses a physical model of an open channel with a single spur dike, and measures flow velocities and turbulence behind the dike for different configurations. The results show that the size and shape of the recirculation zone are strongly affected by the height, length, and spacing of the spur dikes. A taller and longer spur dike creates a larger recirculation zone and stronger turbulence, while a shorter and smaller spur dike has a smaller

recirculation zone and weaker turbulence (Jeon, Lee, & Kang, 2018). The study uses a physical model and flow visualization techniques to observe the flow patterns behind a double spur dike. The results show that the presence of the second spur dike leads to the formation of a second recirculation zone downstream of the first dike. The size and shape of the second recirculation zone are affected by the spacing between the two dikes and the angle between the two walls of the dikes (Razzaghi, 2020). The study found that recirculation zones can form downstream of the dikes, leading to increased turbulence and erosion. The size and shape of the recirculation zone depend on the flow velocity, angle of attack of the flow, and the geometry of the dike (Li, 2013). This study examines the flow hydrodynamics of mixing layers in consecutive vegetated groyne fields using numerical simulations. The results suggest that the presence of vegetation can enhance turbulence and increase mixing within the groynes, leading to improved water quality in rivers (Ke Xiang (向珂), 2020). Various hydraulic structures (river training works) are provided within a river to protect and manage river flow for human protection. The spur is one of the most significant and prevalent hydraulic structures used for river training (Iqbal et al., 2022). In the bed to change the important problems that occur widely in open channels are erosion and sedimentation in their mainstream. These problems have been studied for a long time to find techniques to get rid of it. There are many solutions that are used to control these problems. One of these solutions is increasing resistance of the channel bed by adding large roughness element in the channel (Alwan & Azzubaidi, 2021). Surface roughness elements of boundary layer size and smaller are pervasive and have a significant impact on flow instability and transformation from laminar to turbulent flow. These are the velocity streaks caused by the so-called lift up effect (Wu, Axtmann, & Rist, 2021). Recirculation in a spur dike within a channel can also negatively affect the channel's hydraulic and ecological functioning. The presence of recirculation zones downstream of the dike can lead to the accumulation of fine sediments and organic matter, which can degrade water quality and harm aquatic ecosystems. Additionally, the increased turbulence and mixing associated with recirculation can lead to increased erosion of the channel bed and banks, which can cause channel instability and loss of habitat. Finally, the presence of recirculation zones can also increase the risk of flooding in downstream areas by impeding water flow through the channel. Erosion of the riverbed, changes in water levels, and changes in flow velocity. Therefore, careful consideration of the potential negative impacts of recirculation in spur dikes is necessary to design and manage river systems. However, scour around spur dikes can be a major problem impacting their stability and hydraulic performance. This research examines the flow behavior in recirculation zone by varying space between two successive spur dikes to measure the scouring responsible factors i.e. velocity and turbulence at points L1, L2 & L3 in spur dike field. Hence numerical simulation was conducted for reducing the maximum scouring factor and to minimize the recirculation zone by adding large roughness elements in the spur dikes fields. This study will help in determining scouring factor in upstream and downstream of the spur dikes fields and banks.

METHODOLOGY

Experimental work Description

The present numerical model was validated by comparing it to the experimental data of Brevis et. al (Brevis, García-Villalba, & Niño, 2014) that were conducted at the Institute of Hydromechanics, Karlsruhe Institute of Technology, in Germany. The tilting rectangular flume was 17 meters flume length and 1.3 meters in width. It was imperative that the aspect ratio between the length of a spur dike (K) and the distance that separated two subsequent spur dikes (W) remain constant at one. Particle image velocimetry (PIV) was used to take flow velocity magnitude across a test area that was 24 cm long and 45 cm wide. Within the spur dike field, measuring locations L1, L2, and L3 were evaluated with an identical distance of 6 cm from upstream to downstream in a span wise orientation. For the experimental domain, including its spur dimensions, we provide the full set of hydraulic conditions in Fig.1. All other settings, such as the channel width and the spur dike dimensions, were maintained at their default.



Experimental parameters of (Brevis et al., 2014)

Numerical Model Setup with Boundary Conditions

The numerical domain was reduced to 104 cm in length and 96 cm in breadth by imposing periodic boundary conditions at the flow's entrance and outflow. The channel width and spur dimensions, along with all the other factors, remained constant.

L1, L2, and L3 were the measuring location in the spur dike field for numerical simulation. For the geometry and meshing of the numerical model, Gambit software was used. A *CFD* (computational Fluid Dynamics) in this work, FLUENT was utilized for simulations as well as post-processing. For the simulation, an unstructured tri-pave mesh was used. The chosen mesh had nodes counts of 220, 120, and 60 in the longitudinal, transverse, and vertical dimensions, respectively. This resulted in about 1.6 million grid points with a given value. The mesh independence test was also run to check the correctness of the *CFD* simulations. For the under-relaxation factors and near-wall treatment, the standard values and standard wall function were employed. For turbulence modelling, a Reynolds stress model (*RSM*) was employed, and a Semi-Implicit Method for Pressure Linked Equations (*SIMPLE*) method was used to achieve pressure-velocity coupling. The convergence criteria for all residuals values were set at 1×10^{-6} . The periodic boundary condition was set at both the domain's inlet and outlet. In the channel, the discharge and flow depth were 9.75 L/s and 0.07 cm, respectively. The free surface was assigned the symmetry boundary condition; however, the bed, sidewalls, roughness elements and spur-dikes were allocated using the no-slip condition and conventional wall function as utilized by previous studies.

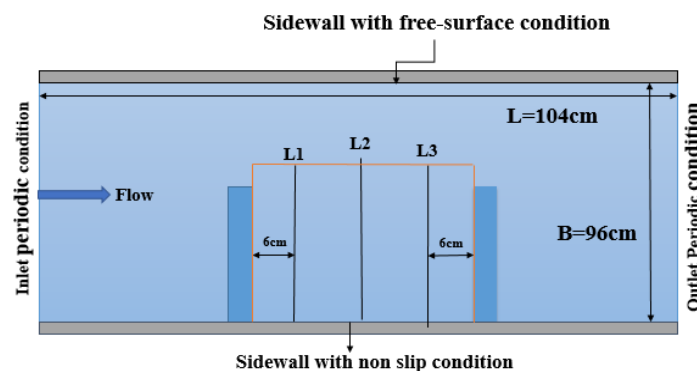


Fig.2 On the top view of the channel Numerical setup for simulation, measuring location at L1, L2, and L3.

Model Validation

The comparison between the experimental findings of Brevis et al. (2014) and the numerical findings of the depth-averaged stream-wise (u) velocity was carried out at three distinct locations (L1, L2, and L3) and is depicted in figure 2. The upstream (u/s) to downstream (d/s) spur may be measured at 6 cm, 12 cm, and 18 cm at three different points. On the x-axis, the span-wise velocity was normalized using the beginning velocity, $U = Q/BZ$. Q stands for discharge, while BZ stands for the area denoted by $\langle u \rangle U$ on the x-axis. By dividing it by the length of the spur dike, the Y-axis (total channel width) becomes dimensionless. On the Y-axis, it is denoted by Y/L . The line separates the mainstream line field ($Y/L = 1-1.6$) from the spur dike field ($Y/L = 0-$

1). There is a good link between the experimental and numerical results, demonstrating the validity of the current numerical model. Compared to the spur dike field, the mean stream-wise velocities at the spur dike head ($Y/L = 0$ to 1) increased at all three points (L1, L2, and L3). The spur dike field and the mainstream are separated by a shear layer. (Weitbrecht, Socolofsky, & Jirka, 2008). The flow velocity gradually increased and reached a maximum value in the mainstream channel ($<Y/L> 1$). This increase in velocity flux at $Y/L = 1$ results from high-speed flow in the mainstream as well as momentum exchange between the spur dike field and the mainstream. Koken and Constantinescu (2009) found a similar change in the velocity profile due to the presence of emerging spur dikes. The validation therefore suggests that the present numerical model may be used to simulate an open channel flow in the presence of spur dikes.

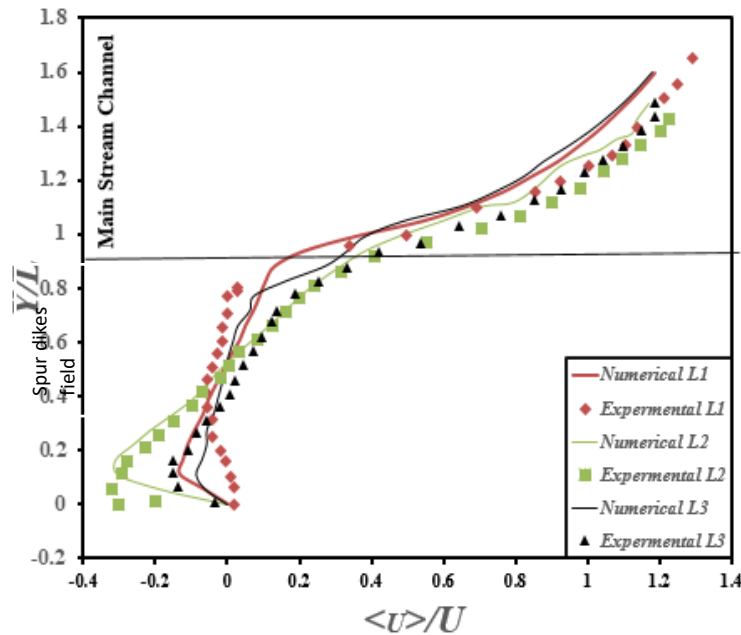


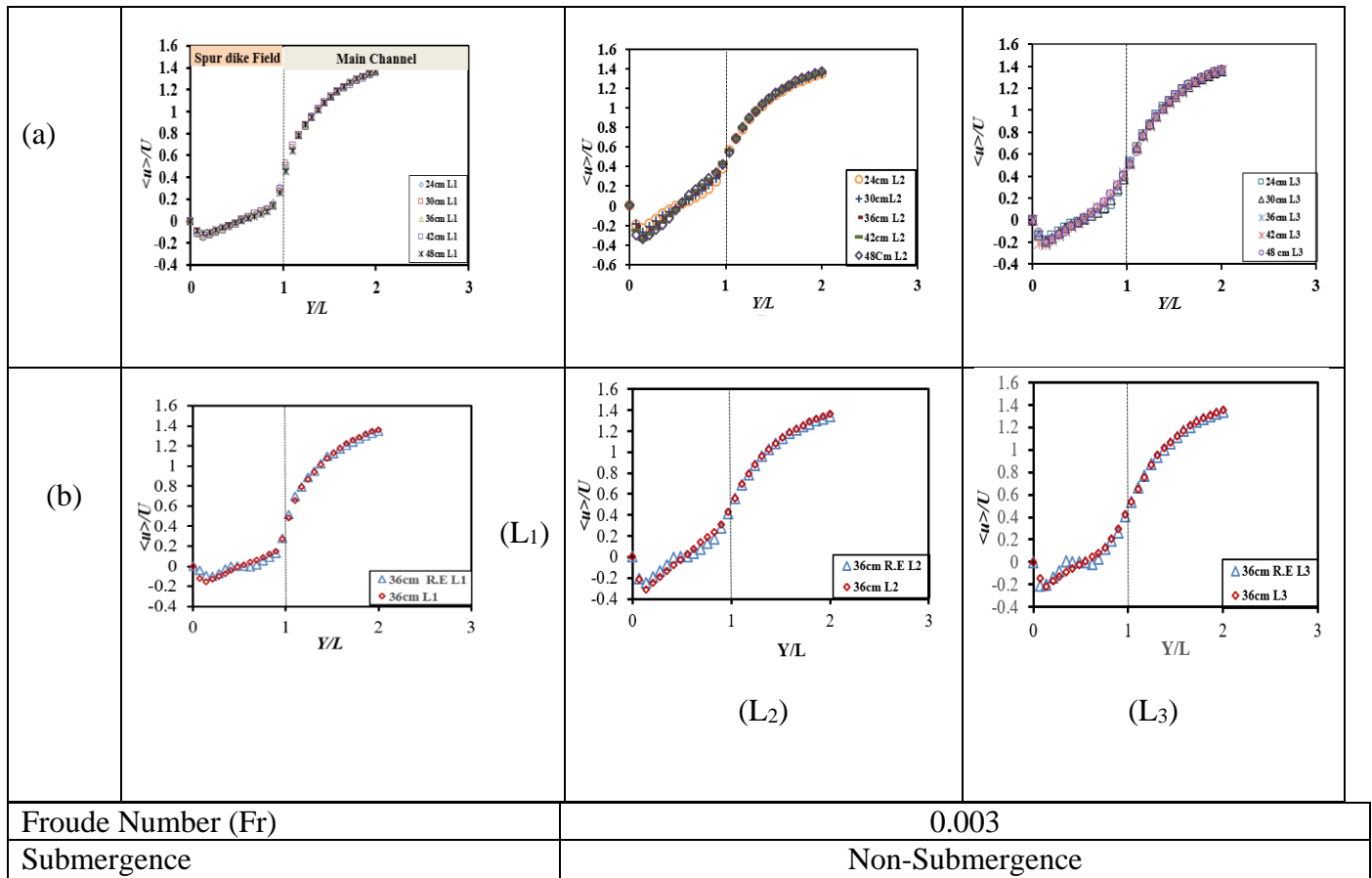
Fig.3 Comparison of numerical and experimental (Brevis et al., 2014) stream-wise velocity $<u>/U$ at L1, L2, and L3. Line separate spur dike field and main stream

Specifications for Numerical Simulation

The computational domain's length and breadth were adjusted to 104 cm and 96 cm respectively for the current numerical simulation shown in fig (2). The domain revealed two rectangular spur dikes. Different spacing's between spur dikes were positioned perpendicular to the mainstream. In addition, Roughness element with the dimensions of $3 \times 4 \times 3.5$ cm added to spur dike filed in case of 2ABC of the computational domain Place upstream, downstream, and middle of in the spur dike field. The external dimensions of the spur dike ($4 \text{ cm} \times 24 \text{ cm} \times 7 \text{ cm}$) were set at the same as in the validation scenario. Numerical simulation was performed using five different spacing between spur dikes and one case placing roughness element in spur dike Field. The diagram for representing the measurement sites L1, L2, and L3 is displayed in Table 1.

Table 1 Simulation conditions in terms of geometry and hydraulic

Cases	S1	S2	S3	S4	S5	2ABC
Spacing	24cm	30cm	36cm	42cm	48cm	36cm
Figure						
Location measurement	L1,L2&L3					
Flow Depth	7cm					
Discharge (Q)	9.75 L/S					
Reynold Number	10,000					
Initial Velocity (U)	0.145m/s					



RESULTS

Description of the Flow's Features

Figure.4 Illustrates the normalized depth-averaged streamwise velocity distribution ($\langle u \rangle / U$) in the span wise direction, where the locations of computation (L1, L2, and L3) play a crucial role in observing flow behaviour in the spur dike field. The span-wise dimension (Y) of the computational domain was normalized with the length of the spur, while the mean streamwise velocity (u) was normalized with the initial velocity (U). The velocity profile (u/U) moves from the right bank to the middle of the channel. The flow in the recirculation zone between spur dikes shows a rise in turbulent kinetic energy and a little velocity in situations S_1 , S_2 , and S_3 . TKE and flow velocity in the recirculation zone between spur dikes decrease in cases S_4 and S_5 , respectively. According to the S_3 simulation outcomes, the recirculation zone seemed to have the maximum velocity and turbulent kinetic energy. The roughness element was added to reduce the kinetic energy of turbulence in the recirculation zone. Because of the recirculation eye that had developed in the middle of the spur dike field, the velocity was shown to be zero magnitude at L2. The recirculation was responsible for the negative values of span wise velocity measured at L3 (Iqbal et al., 2022). The average depth velocity for S_3 was measured to be the highest across all three levels (L1, L2, and L3). At Y/L , the depth-averaged velocity increased up to 14 % for S_3 at L1, while at L2 & L3 was Increased 8.5% and 29.6%. Roughness Elements are added thereafter. For S_3 at L1 the depth-average velocity decreased to 40.2732%, whereas it reduces by 28.439% and 11.453% at L2 and L3 respectively.

Fig.4. Figure (4a) shows the distribution of the mean stream-wise velocity for different aspect ratios. Figure (4b) shows the roughness element within the spur dikes field's mean stream-wise velocity. L1, L2, and L3 measuring location

Turbulent Kinetic Energy

At L1, L2, and L3, the depth average Turbulent Kinetic Energy (TKE) along the point is indicated. TKE was divided with U^2 to make it non-dimensional. TKE exhibited greater values for the S_3 at the spur field. TKE, on the other hand, provided the same inflation trend for S_1 - S_3 . When compared to the maximum value of S_3 ,

The average depth velocity for S3 was measured to be the highest across all three levels (L1, L2, and L3). At Y/L, The turbulence kinetic energy increased up to 69.574% for S3 at L1, while at L2 & L3 was Increased 447% and 181%.. Roughness elements are added thereafter. For S3 at L1, the Turbulent Kinetic Energy decreased to 19.544% whereas it reduced by 69.16% and 10.53% at L2 and L3, respectively

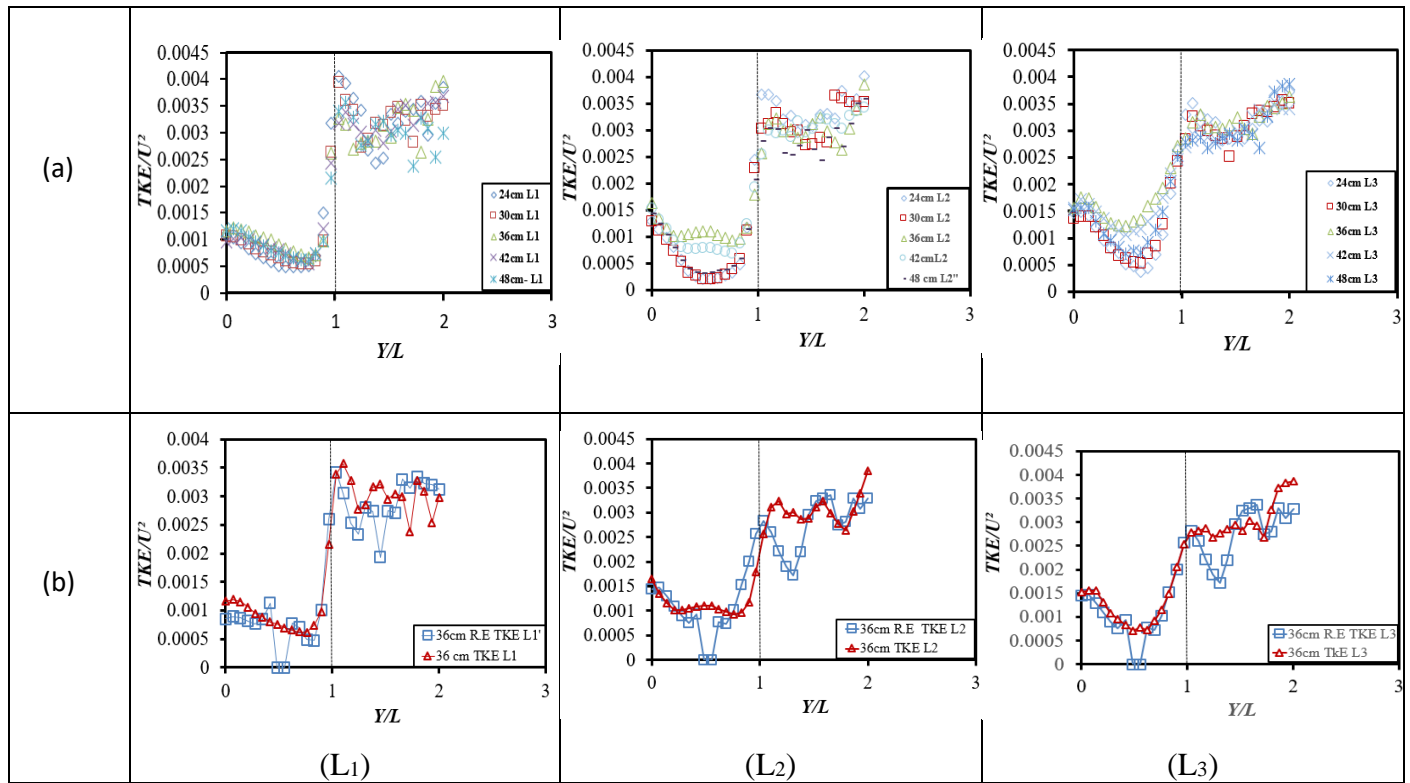
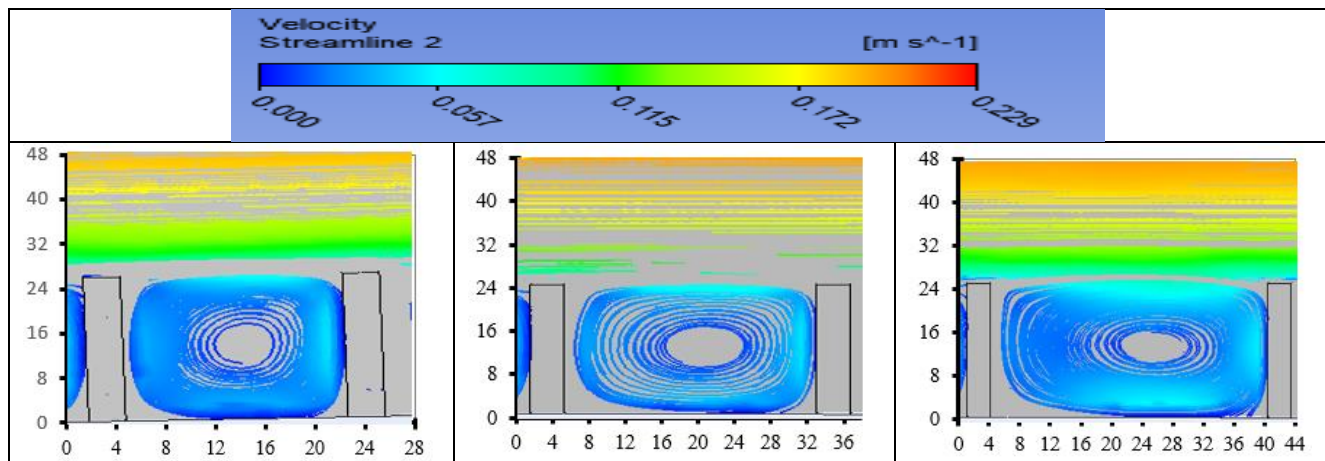


Fig.5. Figure (5a) shows the distribution of depth-averaged (TKE) for different aspect ratios. Figure (5b) shows the roughness element within the spur dikes field's depth-averaged (TKE). L1, L2, and L3 measuring locations

Mean Stream-wise velocity Stream line
The figure shows the average velocity of water flow in the x-y direction at a depth of 3.5cm (half of the water depth). The contour lines indicate the velocity distribution from the right bank to the middle of the channel. The red color indicates a high-velocity region where the streamlines are uniformly distributed across the width of the channel. In the case of S3, the mean velocity in the recirculation zone between the dikes at location L3 was 29.6% higher compared to the other cases. This means that the water flow was faster in this region in case S3 than in the other cases. In case 2ABC, roughness elements were added to the spur dike field, which caused the velocity to decrease by 11.45%. This means that the roughness elements dampened the water flow, resulting in slower velocities in this case compared to the other cases.



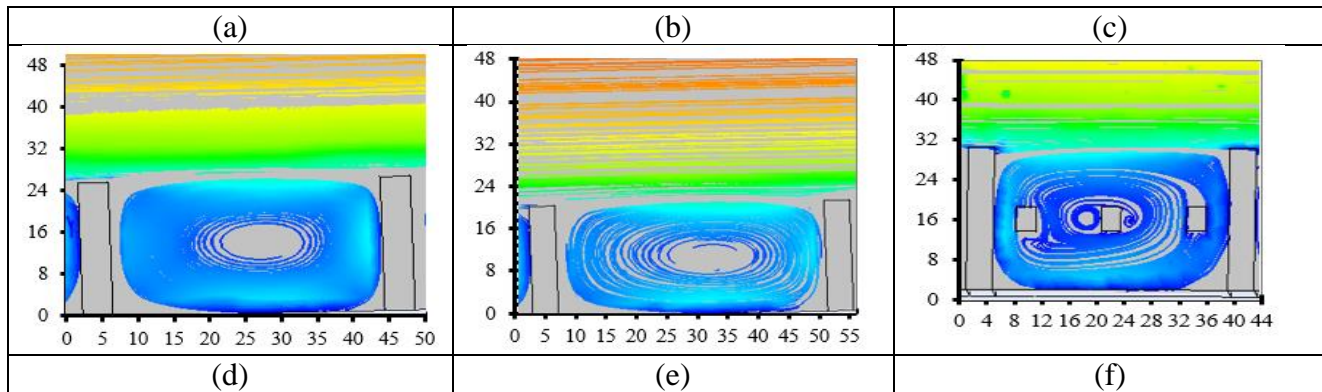


Fig.6.Mean Velocity in recirculation zone in spur dike in horizontal plane at $Z_h=3.5\text{cm}$ (a)24cm spacing b/w spur dikes, (b) 30cm spacing b/w spur dikes, (c)36cm spacing b/w spur dikes,(d) 42cm spacing b/w spur dikes,(e) 48 spacing b/w spur dikes,(f) Roughness Element added middle of spur dike field

Conclusion

The study investigated the impact of **aspect ratio** = $\left(\frac{\text{Distance between two spur dikes}}{\text{Length of the spur dike}} \right)$ and roughness elements on the recirculation zone in spur dike fields. The recirculations contain high-intensity flow, which begins to erode the bank and spur dikes that surround the recirculations. The present study concluded that, The results shows that aspect ratio 3 having location L3 has the optimum velocity i-e., 30% and T.K.E. in the recirculation zone. Adding roughness elements to the recirculation zone lowered scour responsible factors i.e., the velocity, turbulence intensity, and turbulent kinetic energy. Using spur dike fields with roughness elements can protect against extreme turbulence during floods and limit erosion in the recirculation zone, making it a preferred option for protecting spur dikes and banks.

REFERENCES

1. (Bahrami-Yarahmadi, Pagliara, Yabarehpour, & Najafi, 2020)
2. Alwan, I. A., & Azzubaidi, R. Z. J. A. o. A. U. J. o. E. S. (2021). Investigations on Large-Scale Geometric Roughness Elements in Open Channels with Different Heights. 28(1), 07-14.
3. Bahrami-Yarahmadi, M., Pagliara, S., Yabarehpour, E., & Najafi, N. J. K. J. o. C. E. (2020). Study of scour and flow patterns around triangular-shaped spur dikes. 24(11), 3279-3288.
4. Brevis, W., García-Villalba, M., & Niño, Y. J. E. F. M. (2014). Experimental and large eddy simulation study of the flow developed by a sequence of lateral obstacles. 14(4), 873-893.
5. Gao, Y., Yang, H., Wang, L., & Zhao, M. J. P. o. F. (2022). Three-dimensional numerical investigation on flow behaviors around a diversion dike. 34(12), 125119.
6. Iqbal, S., Pasha, G. A., Ghani, U., Ahmed, A., Farooq, R., & Haider, R. J. T. v. (2022). Investigation of Flow Dynamics Around a Combination of Different Head Shapes of Spur Dikes. 29(6), 2111-2120.
7. Iqbal, S., Pasha, G. A., Ghani, U., Ullah, M. K., Ahmed, A. J. A. J. f. S., & Engineering. (2021). Flow Dynamics Around Permeable Spur Dike in a Rectangular Channel. 46(5), 4999-5011.
8. Jeon, J., Lee, J. Y., & Kang, S. J. W. R. R. (2018). Experimental investigation of three-dimensional flow structure and turbulent flow mechanisms around a nonsubmerged spur dike with a low length-to-depth ratio. 54(5), 3530-3556.
9. Julien, P. Y. (2018). *River mechanics*: Cambridge University Press.
10. Karami, H., Ardeshtir, A., Behzadian, K., & Ghodsian, M. J. J. o. h. r. (2011). Protective spur dike for scour mitigation of existing spur dikes. 49(6), 809-813.
11. Ke Xiang (向珂), Z. Y. 杨., 1. (2020). Flow hydrodynamics of the mixing layer in consecutive vegetated groyne fields. *Physics of Fluids*.
12. Li, J., Chen, Z., & Chen, S. (2013). (2013). Numerical simulation of local scouring around spur dikes in open channels. *Journal of Hydrodynamics, Ser. B*, 25(1), 107-115.
13. Pandey, M., Valyrakis, M., Qi, M., Sharma, A., & Lodhi, A. S. J. I. J. o. S. R. (2021). Experimental assessment and prediction of temporal scour depth around a spur dike. 36(1), 17-28.

15th INTERNATIONAL CONFERENCE ON ENGINEERING & NATURAL SCIENCES

March 04-06, 2023 Muş, TÜRKİYE

14. Razzaghi, A., & Kavianpour, M. R. (2020). Experimental investigation of the effect of a double spur dike on recirculation zone characteristics in open channel flow. *Environmental Fluid Mechanics*, 20(3), 483-498.
15. Wu, Y., Axtmann, G., & Rist, U. J. J. o. F. M. (2021). Linear stability analysis of a boundary layer with rotating wall-normal cylindrical roughness elements. 915.

FARKLI SARIM YÖNLERİNDEKİ KARBON ELYAF TAKVİYELİ KOMPOZİT BORULARIN TORNALAMA YÖNTEMİ İLE İŞLENEBİLİRLİĞİ ÜZERİNE İNCELEME AN INVESTIGATION ON THE MACHINABILITY OF CARBON FIBER REINFORCED COMPOSITE PIPES IN DIFFERENT WINDING DIRECTIONS BY TURNING METHOD

Merve Yılmaz Arıcı

ORCID: 0000-0001-7120-4850

Mert Kılınçel

ORCID: 0000-0001-7057-4390

Şenol Şirin

ORCID: 0000-0002-3629-9003

ÖZET

Polimer matrisli kompozit malzemeler; yüksek mukavemet, yüksek darbe dayanımı, esneklik ve hafiflik özellikleri sayesinde denizcilik, uzay, havacılık, motor sporları, enerji ve savunma sanayisi gibi birçok endüstride kullanılmaktadır. Ancak polimer matrisli kompozit malzemeler düşük işlenebilirlik özelliğine sahiptirler. Polimer matrisli kompozitlerin işlenmesi sonrasında düşük yüzey kalitesi ve kesici takım aşınması gibi sorunlarla karşılaşmaktadır. Bu çalışmada karbon takviyeli polimer matrisli kompozitlerin tornalanmasında; kesici takım ucu, elyaf oryantasyonu (sarım yönü ve açısı), kesme hızı ve kuvveti, ilerleme hızı, talaş miktarı ve talaş derinliği parametrelerinin işlenen malzemedeki yüzey kalitesi ve kullanılan kesici takım aşınması miktarına etkisi üzerine yapılan çalışmalar araştırılmıştır. Araştırma sonucunda karbon elyafın sarım yönü ve açısı değiştiğinde, tornalama sonrasında talaş tipi, talaş miktarları ve kesici takım ucundaki aşınma oranının da etkilendiği görülmüştür. Özellikle ilerleme ve kesme hızı etkisinin işlenen malzemedeki yüzey pürüzlülüğü ve kullanılan takım aşınması üzerindeki etkisinin büyük ölçekli olduğu ortaya konulmuştur.

Anahtar Kelimeler: Yüzey pürüzlülüğü, Karbon elyaf, Polimer matrisli kompozitler, İşlenebilirlik, Kesici takım aşınması

ABSTRACT

Composite materials with polymer matrix; Thanks to its high strength, high impact resistance, flexibility, and lightness properties, it is used in many industries such as maritime, space, aviation, motorsports, energy, and defence. However, polymer matrix composite materials have low machinability properties. After processing polymer matrix composites, problems such as poor surface quality and cutting tool wear are encountered. In this study, in the turning of carbon-reinforced polymer matrix composites; In this study, the effects of cutting tool tip, fiber orientation (winding direction and angle), cutting speed and force, feed rate, chip amount, and depth of cut parameters on the surface quality of the processed material and the amount of cutting tool wear were investigated. As a result of the research, it was observed that when the wind direction and angle of the carbon fibers change, the chip type, chip amounts, and the wear rate on the cutting tool tip are also affected after turning. In particular, it has been revealed that the effects of feed and cutting speed on the surface roughness of the machined material and the wear of the tool used are large-scale.

Keywords: Surface roughness, Carbon fiber, Polymer matrix composites, Machinability, Cutting tool wear

INTRODUCTION

Composite Materials

Composite material is classified according to structure, type of reinforcement element, and matrix types; It is classified according to the structure, type of reinforcement element, and matrix type. Composite material is a new type formed by combining at least two or more of the same or different materials due to suitable combinations and shows better properties according to the area of use [1]. High strength, lightness, non-flammability, high fatigue strength and wear resistance, low electrical conductivity, design flexibility, good fracture resistance, dimensional stability, high thermal resistance, and high corrosion resistance are the most important properties of composite materials. The structure of composite materials consists of reinforcement

and matrix phases [2]. The reinforcement phase provides strength to the material and protects it against load, while the matrix phase keeps the reinforcement phase together and protects the material from environmental effects [3]. Matrix materials are divided into three groups metal, ceramic, and polymer matrix composite materials, according to the intended use of the composite material. As a reinforcement element, glass, carbon, or aramid fiber is preferred by the area of use [4].

Carbon Fiber Fabric Types

Woven, knitted fabrics are knits produced by passing yarns in 0° and 90° directions over each other and holding on to each other without a third material. Of these yarns, the 0° orientation is called the warp, and the 90° orientation is called the weft (warp). The way the yarns pass through each other is determined according to the need and usage, and the types are named accordingly. The most commonly used weaving types in composite production are plain, twill, and satin weaving [5]. According to the way how the fibers settle into the tissue during manufacturing, composite types are shown in Figure 1.

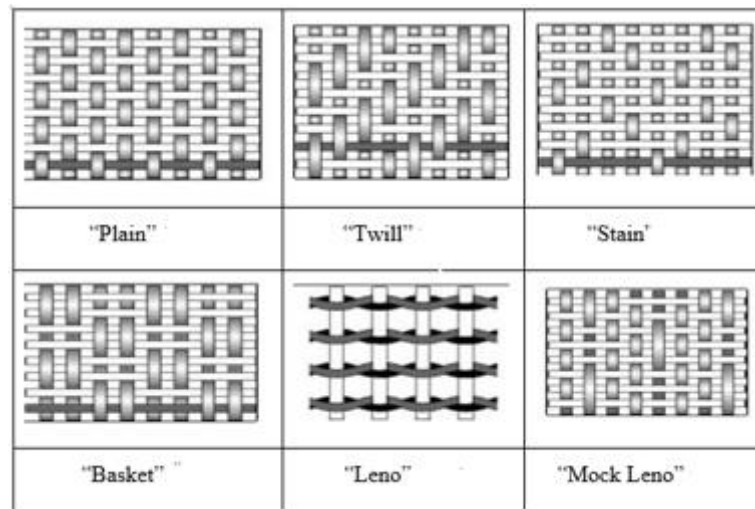


Figure 1. Composite types are according to how the fibers settle into the tissue [6].

Composite Structured Pipes

The primer is used as a mold release agent to facilitate post-process separation. Composite pipes are mostly from inside to outside; They consist of three basic layers: lining, prepreg structure, and outer film. When high pressure acts on the inner parts of open-ended composite pipes, stresses occur in the pipe in the circumferential and axial directions. However, when these stresses are caused by internal pressure, the stress values in the axial direction are accepted as "0" in the calculations. During manufacturing, many different types of stress can be observed on the composite pipe, apart from environmental and axial stresses. The calculations of all these stresses and the discontinuities that may occur due to them in the composite structure should be performed by assuming that the outer film is absent. These advantages have led scientists to research CFRP pipe manufacturing, and many studies continue to be conducted in this area.

Composite pipes, created by combining different pipe types, provide high efficiency and usage advantages; It is used in piping systems such as sewer lines, water transport channels, and drainage lines. In addition, composite pipes are frequently used due to their high resistance to chemicals, resistance to calcification and corrosion, low losses during assembly, and providing fast and serial assembly [7].

Composite pipes, defined as Advanced Engineering Products, can be produced using three different manufacturing methods: pultrusion, fiber wrapping, and rolling and wrapping. In the carbon fiber pipe pultrusion production method, carbon fiber roving's in the longitudinal direction and continuous form pass through the thermoset resin pool, pass through the mold for the desired form, and are heated to cure and form. Carbon fiber makes pipes susceptible to shear loads. For this reason, the fixing points that load at the connection points should be designed to distribute the load [8].

Pultrusion manufacturing has the most common use among these methods. However, in this method, an increase in weight is observed due to the presence of unidirectional reinforcement elements and the higher

resin density due to the dipping process. The fact that the reinforcement material is in one direction in the structure provides high strength in this direction, but products with low performance under compression and torsion emerge. Compared to the other two methods, products that can be automated and have much lower costs can be manufactured with this method in a short time. [9]. The visual in Figure 2 summarizes the construction phase of the pultrusion process.

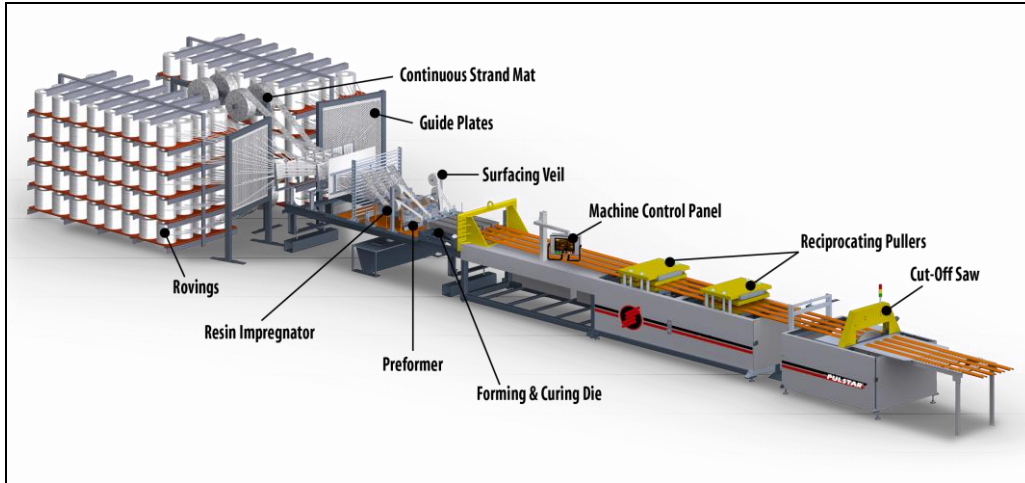


Figure 2. Pultrusion process [10].

Since this method has no unidirectional fiber placement, materials that are resistant to bending and torsion can be produced if requested. In the fiber winding process, the continuous fibers are passed through resin baths, wound on the rotating mandrels at desired angles, and hardened. However, different winding techniques cannot be used simultaneously in the inner structure since winding can be done in a single knitting type. Very large pipe productions can be realized quickly in the fiber winding process, which is carried out with a high degree of automation. In Figure 3, the open fiber winding machine visually represents the continuous fiber winding machine [11].

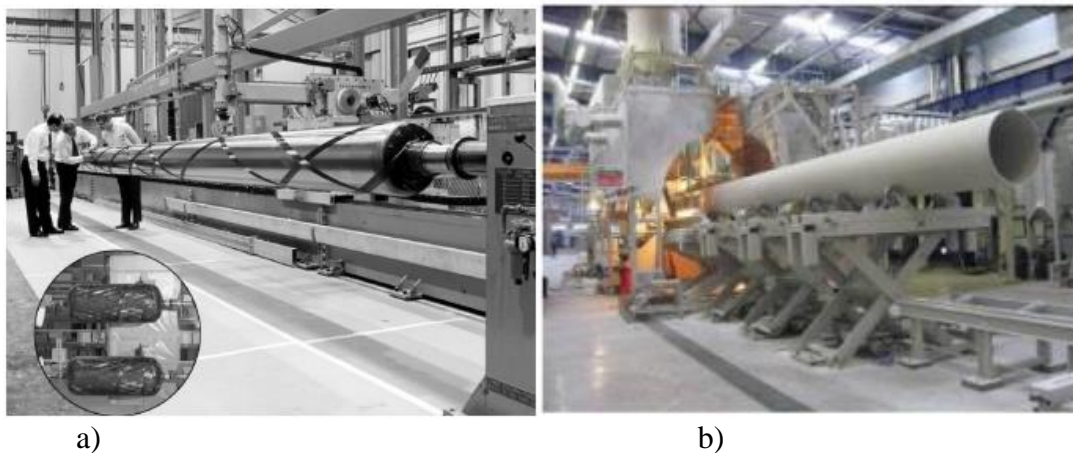


Figure 3. a) Angled fiber winding method, b) Continuous fiber winding machine [11].

Sayman has created a new method for determining the stresses on polymer matrix composite pipes of different thicknesses under the influence of hydrothermal forces. Composite layers were selected in fiber orientations $[0^\circ/90^\circ]$, $[30^\circ/-30^\circ]$, $[45^\circ/-45^\circ]$, and $[60^\circ/-60^\circ]$. [12].

Kalaycıoğlu et al., $[90^\circ, \pm 55^\circ, 90^\circ]$ symmetrical and $[\pm 55^\circ, 90^\circ, 90^\circ]$ asymmetrical 650 mm long, 65 mm diameter, and 1.7 mm thick; They produced CFRP pipes and evaluated their burst resistance [13].

Machinability of Composite Materials

In this review article, research was made on the machinability of polymer matrix composites. Optimum machining parameters were investigated to ensure low cutting tool wear and surface roughness after machining.

Composite materials need machining to remove roughness on their surfaces, remove burrs, drill holes, and improve surface quality to be ready for use after being produced by various methods. Although some materials such as glass, carbon, boron, alumina, and silicon carbide used as reinforcement in composites are quite sensitive and hard, machining is used. Because reinforcing elements are brittle materials, brittle fracture occurs instead of plastic deformation in the workpiece during machining. Due to the hard and abrasive properties of the reinforcement elements used in composite materials, the choice of cutting tool material is of great importance to minimize the wear of the cutting tool [14].

The processing of composite materials depends on the properties of the reinforcement and matrix phase, the composition of the composite, and its response in the processing process [14]. In the review article, the effect of fiber orientation (winding angle), cutting speed, feed rate, cutting tool type, mechanical properties of the processed material on the surface roughness of the material after processing, and the amount of wear of the cutting tool used during processing were examined in detail. In Figure 1 and Figure 2 below, the images of different winding angles of carbon fibers taken under an SEM microscope and fiber weaving types are added as sample images.

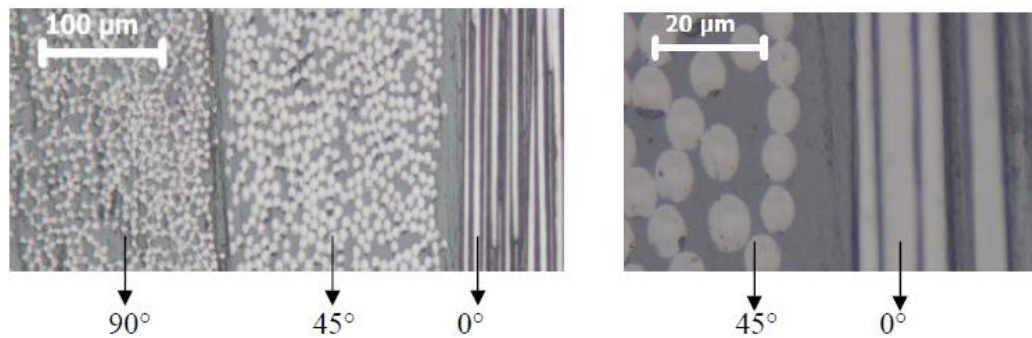


Figure 4. SEM images of carbon fiber composite material [15].

Machining in Fiber Reinforced Composites

Fiber-reinforced plastic composites are composite materials preferred for processing due to their high heat-resistant tensile and compression strengths. Although the number of layers is high in terms of suitability for machining, drilling has a significant place in terms of the machinability of these composite materials [16].

Ekici and Işık; conducted research on the surface damage that occurs while drilling glass fiber-reinforced material as reinforcement. Drilling was carried out using 2, 3, and 4-fluted HSS drills with 60°, 90°, and 120° tip angles. As a result of their experiment, it was revealed that the surface damage decreased with the enlarge in the cutting speed, and the surface damage increased with the increased feed rate [17].

Phadnis et al.; investigated the effects of cutting parameters on thrust force and torque while drilling carbon fiber-reinforced polymer epoxy composite materials. They stated that low feed rates and high cutting speeds are ideal for drilling carbon and epoxy laminates [18].

R. Vinayagamorthy et al.; investigated the effect of speed in the cutting process and cutting speed in the feed direction, which is other cutting parameters, on ease of processing to reduce the processing time and cost. However, the cutting force in fiber-reinforced plastic materials is less. By conducting extensive research on the effects of production methods and processing parameters, they came up with conclusions about the optimum conditions for processing. They investigated the surface roughness of glass fiber-reinforced plastic pipes during drilling by filament winding method. They concluded that high spindle speed, depth of cut, and low spindle speed would be used for drilling at low surface roughness [19].

Naresh et al., Using the Taguchi method, aimed to reveal the most appropriate parameter values for cutting speed and surface roughness in glass fiber-reinforced composites. As a result of their research, they concluded that the factor in values such as surface roughness, shear force, and delamination is the fiber angle. They

concluded that the surface roughness and delamination increase with the increase in the cutting angle and feed rate of the cutting tool and that the fiber angle affects the surface roughness the most [20].

In this study, Jinguang Du et al. mainly review the research on the machining status of carbon fiber-reinforced ceramic matrix composites, including carbon fiber-reinforced polymer matrix composites, in terms of conventional processing and non-traditional processing method. Traditional processing methods have advantages such as production convenience and reduced equipment investment with developing technology. It has advantages. However, tool wear is particularly severe when carbide tools are used. As a hard cutting point, it rubs directly against the tool's cutting edge, causing the cutting edge to wear. Cutting heat occurs with cutting the matrix, separating the fibers by breaking, and the friction between the cutting edge, the chips formed, and the machined surface. The cutting heat mainly concentrates near the tool's cutting edge, causing wear of the surface material on the tool and reducing the tool's cutting performance. PCD and CBN-type cutting tools have excellent properties suitable for machining ceramic matrix composites in the conventional processing of carbon fiber reinforced composites, which have low interlayer bond strength and whose shear force exceeds the bond strength between layers during vertical fiber stacking, tearing, burrs, etc. Many processing errors occur. Delamination defects occur during processing. During the drilling processes of these composites, due to the force effect in the axis direction, the material in the outermost part is deformed and withdrawn, which causes delamination, that is, the plate damage that occurs at the hole entrance and exits from each other. [21].

Hintze et al.; researched the effect of the amount of delamination formed during the milling of carbon fiber-reinforced composite material on surface damage and fiber angles. As a result of their studies, they observed that the surface damage increased with the cutting tool with a large tip radius value. They showed that the surface damage rate is reduced when low fiber angle carbon fiber reinforced material is used [22].

Senthil Kumar et al.; investigated the effects on tool wear by drilling plastic and titanium alloy layered materials with carbon fiber reinforcement at different drilling parameters. As the number of holes increases, the amount of wear enlarges, and they concluded that the chip is better removed from the surface and tool wear is less in drills with a tip angle of 130° compared to drills with a tip angle of 118° [23].

Durão et al.; In their study, different drill bit geometries and feed rates were compared in the drilling process of carbon fiber-reinforced laminated composites. Their study compared the compressive force after drilling, the roughness of the perforated wall surface, and the delamination values after drilling. They stated that a low feed rate reduces thrust force and delamination factor. They noted that the most suitable drills for high feed rate are helical drills with 120° tip angle and step drills, and they could not reach a valid conclusion due to the scattered hole surface roughness measurements [24].

Turning of Carbon Fiber Reinforced Composite Materials

Turning; It is called chip removal, using a fixed cutting tool over a cylindrical rotating workpiece. Turning is among the most preferred operations in industrial sectors among traditional and modern machining methods. Abrasion on the cutting tool surface during chip removal causes roughness on the part surface [25]. Wear on the tool's surface is undesirable because it shortens the life of the tool and causes damage to the surface quality of the part. In this case, factors such as the cutting speed of the cutting tool, the feed rate, the tip of the cutting tool, the type of material preferred at the tip of the cutting tool, and the winding angle of the composite material play an active role.

K. Abhishek et al.; highlights the application potential of a multi-response optimization path by integrating nonlinear regression modelling, fuzzy inference system (FIS), and JAYA optimization algorithm for optimal machining parameter selection during the turning process of carbon fiber reinforced plastic materials. Experiments were carried out considering spindle speed, feed rate, and depth of cut as process control parameters of fiber-reinforced epoxy matrix composites. The metal removal rate, the surface roughness average, and the cutting force are considered unique features of the machining. With the baseline experimental research, it has been observed that the JAYA algorithm provides reliable results with less computational effort and time.

They considered metal removal rate, roughness average, and resulting cutting force as critical output responses and noted other process responses, such as tool life and extent of tool wear. These include the dimensional

accuracy of machine tool vibration and different roughness parameters of the machined product [26]. Figure 3 shows the composite pipes subjected to the turning process with different winding types and feed rates.



Figure 5. Turned composite pipes [26].

K. Vijay Kumar et al.; The effects of machining parameters on the material properties of hybrid composite pipes produced by hand lay-up were analyzed. The turning process was carried out on carbon and aramid fiber composite materials. They brought the minimum cutting speed and surface roughness values to the optimum level. Depending on the experimental results, they modelled the analysis results mathematically. The study used bisphenol as the resin, and bidirectional mixed composite material consisting of carbon and aramid fibers as the reinforcement element. The parameters used in the experiment; were spindle speed, feed rate, and depth of cut. As a result of this study, it was concluded that the cutting force increased with the increase in cutting speed, the surface roughness decreased, the cutting force decreased with the rising feed rate, and the surface roughness decreased when it started to advance [27].

Azmi et al.; Turning operations were carried out on two fiber-reinforced composite materials to determine the power and specific energy constants and evaluate their effects due to differences in machining conditions. The study discusses the durability, metal removal rate, and specific cutting energy of pultruded carbon fiber reinforced plastic composites (CRFP) and carbon fiber composite pipes during the turning process at different parameter settings. According to the test results, the effects of the parameters used for the turning process on the chip removal and specific cutting energies of the fiber composites were determined. The increase in shear is due to the MRR, as the experimental results show a positive linear relationship, and the shear strength (R^2) is very close to 1.0, regardless of the type of CFRP composites used. In addition to the experimental results, it was revealed that the specific shear energy of both fiber composites was significantly affected by the feed rate. The specific energy constant can be reduced according to the feed rate, especially for pultruded CFRP composite and CFRP composite pipe. The relationships between the specific cutting energy and the feed rate in the study revealed that it was in good agreement with the theoretical specific cutting force model [28]. Table 1 and Figure 6 express the linear relationship between cutting power and metal removal rate.

Table 1. Parameter values are considered for the cutting process [28].

Depth of cut, a_p (mm)	feed rate, f (mm/rev)	V_c (m/min)	Condition
0.2	0.15, 0.30, 0.45, 0.60	20, 40, 60, 80, 100	Dry
0.1	0.10, 0.20, 0.40, 0.50	50, 100, 150, 200, 250	Dry

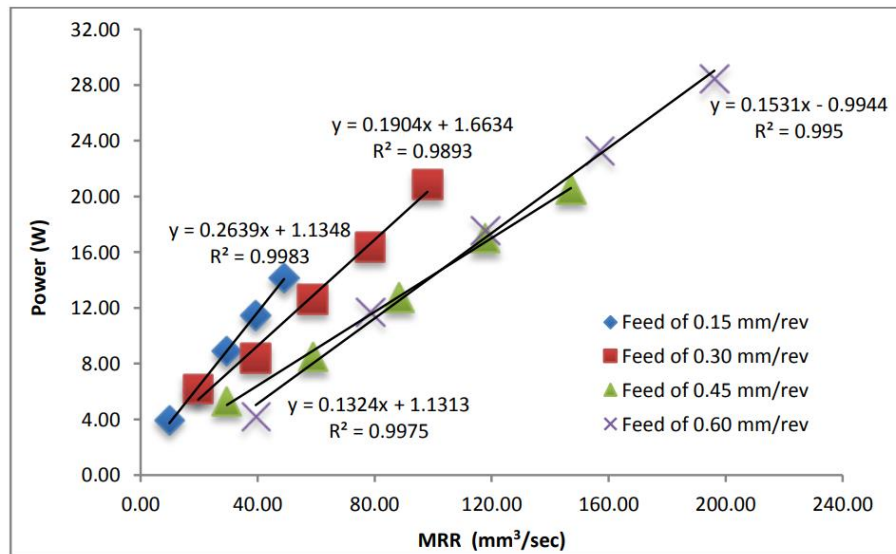


Figure 6. Power and material removal rates at different feed rates [28].

In their study by N. Duboust et al., The surface roughness value was found using a non-contact optical method for the commercial aspect and compared with a most preferred stylus profilometer. The edges of the unidirectional and multidirectional carbon fiber plates are trimmed, slotted, and milled. The change in surface roughness value was compared with the difference in the type of tool used, with different fiber placements and separate cutting parameters. Surface damage and shear mechanisms were evaluated using scanning electron microscope images, and the suitability of roughness parameters such as surface area (Sa), skewness, and kurtosis was also analyzed. The optical system allowed accurate roughness calculation of individual plies on a versatile composite plate with different fiber orientations. Also, research results have proven that the optical system, including the use of areal roughness values, can improve the accuracy of the roughness measurement of machined fiber composite surfaces and is less accurate in terms of position during measurement than the stylus. The results obtained in the study, a new optical method was used to measure the surface roughness and damage of the machined composite surfaces. The results confirmed that fiber orientation is important in the stock removal mechanism and surface damage. 135° fiber orientation was the critical fiber orientation for surface damage and roughness measurement. The parameters of kurtosis and curvature are useful and represent surface quality and damage, including the presence of cracks, pits, and protruding fibers. Statistical methods: showed that feed rate and tool variation had the most significant effect on surface quality, and fiber placements varied most with changes in feed. The non-contact optical method is a useful research method for measuring the surface roughness of processed composites. More importantly, it allows the characterization of roughness or damage in single-ply layers of a machined versatile composite plate in a way that is impossible with a stylus. This technique eliminates the insecurity issues associated with measuring surface roughness with a stylus, thereby enabling a wider exclusivity of the profile and the complex damage mechanisms seen in engineered fiber composite plates. [29].

Ki Soo Kim et al. Experimentally investigated the machinability of high-strength carbon fiber epoxy composite materials for the turning process was experimentally investigated. Chip formation structures and tool wear constants of the Taylor method were determined. In addition, surface roughness values were measured according to cutting speeds and feed rates. Surface roughness depends more on feed and fiber wrap angle than cutting speed. In the study, the results of the turning of carbon fiber-epoxy composite materials; the cutting tool's edge wear increases with the fiber wrap angle increase. Also, the larger the fiber wrap angle, the greater the dependence of tool wear on the cutting speed. Regarding edge wear and surface roughness of the tungsten carbide cutting tool type, the cutting speed and feed rate are 20-40 m/min, respectively. And 0.2 mm/rev is recommended [30].

Ramesh et al.; investigated the effect of cutting parameters on surface roughness in the turning of Grade 5 titanium alloys at different cutting parameters with CVD (TiN, TiCN, Al₂O₃) coated hard carbide cutting tool tips. They concluded that the feed rate is the most critical parameter affecting the surface roughness, the

surface roughness increases significantly with the increase in feed rate and the depth of cut, and the surface roughness value decreases with the increase in cutting speed [31].

Material Type and Properties in Machining of Composite Materials

Carbon fiber-reinforced composites cause brittle fractures depending on the winding direction and angle of the fibers and may form chips with high abrasiveness during machining. Although the effect of the matrix phase on the cutting force in composite materials is not as much as the reinforcement element, its impact on chip formation is high. Due to the orientation of the fibers in the composite materials, the high strength increases the shear force. Carbon fibers are materials with high thermal conductivity. Therefore, the heat generated during machining moves away from the machining area, reducing cutting tool wear. However, the heat-affected zone in the material increases. Glass and aramid fibers are materials with low thermal conductivity. Therefore, the heat generated during machining cannot move away from the machining area, and tool wear increases.

Due to the different thermal expansion coefficients of the fiber and reinforcement elements in composite materials, stresses occur, and deformations are observed due to the expansion difference between the matrix and the fiber. In addition, if the strength between the layers is low, chip breaking and layer separation can be seen in the material [32].

R. Teti researched various subjects on processing metal-ceramic and polymer matrix composites. He emphasized that the processing of composite materials requires different properties in terms of geometry and wear resistance of the cutting tool. The wear mechanisms in the cutting tool are primarily related to the physical and mechanical properties of the fiber difference in the matrix structures. Glass and carbon fibers show a strong abrasive behavior due to their abrasive properties and structure. On the other hand, Aramid fibers can cause deterioration in the cutting tool due to their low thermal conductivity and ductile properties. Adhesive wear occurs when carbonized or molten matrix deposits build up on tool surfaces. The machinability of metal matrix composites is critically affected by reinforcement and matrix hardness, with higher hardness significantly shortening tool life. CBN and diamond-tipped (PCD) tools show better wear resistance than carbide tools. While Carbide coated tools can be used economically in roughing operations, while PCD tools should be used in finishing operations due to their long tool cycles. Coating carbide tools with high wear-resistant TiN does not improve tool life, but the proper diamond coating is the best tool technology for tools with complex geometry [14].

Effect of Cutting Tool on Machinability of Composite Materials

While the tool material is important in composite materials where high-strength carbon fiber reinforcement material is used, the choice of tool geometry is a more critical factor in composite materials where low-strength reinforcement material is used.

The coating process applied to the cutting tools is a method to increase the performance of the cutting tool. Diamond-coated tools with high hardness coating and high abrasion resistance are preferred when processing composite materials. Tool wear decreases as the particle size of the cutting tool material decreases. Sintered carbide and PCD tools with fine grain size are used to process composites with increased strength with glass fibers and carbon fibers.

Dipti Kanta Das et al.; The wear of the cutting tool was investigated during the turning of ceramic-reinforced aluminum matrix composites. It has been shown that the tool wear mechanism is mainly affected by the edge wear of the tool life during the turning of these composites. As the reinforcements strengthening agent size or power-to-weight ratio weight increased, the cutting speed, feed rate, cutting depth, and the cutting tools edge wear increased. Cutting speed and feed rate are the most important parameters affecting edge wear. The effect of the depth of the shear surface on flank wear is limited. PCD cutting tools outperformed HSS, WC, ceramic, CVD diamond-coated WC, and CBN cutting tools in terms of tool wear and life, even in the higher range of cutting parameters when turning ceramic-reinforced aluminum matrix composites. They concluded that tool wear increases with increasing particle size or weight ratio of reinforcement while turning ceramic-reinforced aluminium matrix composites [33].

Celik et al.; conducted research on cutting tool materials, wear mechanisms, cutting forces, and surface roughness in the machining of titanium and alloys by machining. As a result, they emphasized that the depth

of cut should be low in turning and milling operations and cutting tools with high wear resistance and chemical stability should be preferred. Pressurized coolants with lubricating properties should be preferred [34].

Xu et al.; In their study, they investigated the cutting performance of carbon fiber-reinforced polymer epoxy composites by using polycrystalline diamond "PCD" drills in the drilling process. The PCD wedge drill revealed more thrust than the PCD helical drill. They concluded that although greater thrust forces were produced for PCD wedge drill cutting, they had lower surface roughness, smaller surface burrs, and less delamination damage [35].

RESULTS

- Some of the conclusions drawn from the research are as follows:
- The cutting tool type and tip angle must be carefully selected and attached to the machine to minimize cutting tool wear.
- Processing a composite; depends on the mechanical properties of the reinforcing material and the matrix materials, the structure contained in a small amount of the composite material, as well as the reaction of the material in the processing process.
- Glass fibers and carbon fibers exhibit a strong abrasive behaviour as they are naturally hard and highly abrasive. Aramid fibers, on the other hand, disrupt the structure of cutting tools due to their low thermal conductivity and ductility.
- Carbide tools, coated (diamond) carbide tools, and PCD tools show good results in tool wear and tool life when machining glass fiber-reinforced composites and carbon fiber-reinforced composites. However, the wear of these cutting tool materials is quite different from each other. Diamond carbide and PCD tools have higher wear resistance than plain carbide tools.
- Ceramic-tipped cutting tools (CBN) are unsuitable because their low strength and high brittleness make them susceptible to impacts. Their low thermal conductivity does not allow the machining heat to dissipate.
- When the surface roughness of the glass fiber-reinforced plastic pipes during the drilling process with the filament winding method was examined, it was concluded that low surface roughness was obtained when high spindle speed, depth of cut, and low spindle speed were applied.
- After processing, the surface roughness of bidirectional composite materials consisting of carbon and aramid fibers as matrix material, bisphenol resin reinforcement element, was investigated. As the cutting speed increases, the cutting force increases, and the surface roughness decreases; It was concluded that with the increase of feed rate, the cutting force decreased, and the surface roughness increased initially and decreased when it started to feed rate.
- In turning carbon fiber-reinforced epoxy matrix composite materials, the edge wear on the cutting tool increases in direct proportion to the increase of the fiber wrap angle. When the fiber wrap angle is large, the tool wear depends more on the cutting speed. In addition, surface roughness depends more on feed rate and fiber wrap angle than cutting speed.
- In machining carbon fiber-reinforced ceramic matrix composites, PCD and CBN-type cutting tools are suitable for machining ceramic matrix composites and have very low tool edge wear properties. Delamination defects occur during the processing of carbon fiber-reinforced ceramic matrix composites, which have low interlayer bond strength and whose shear force exceeds the bond strength between layers during vertical fiber stacking. Many processing errors occur. Tearing, burrs, etc. After processing.
- During the drilling of carbon fiber reinforced ceramic matrix composites, the edge material is deformed and withdrawn due to the movement of the axially loaded column, which causes the plates to separate from each other, with a defect such as wear. The matrix fibers are pulled from the surface for burr formation.

REFERENCES

1. Ü.G. Başçı, "Al₂O₃ Partikül Takviyeli Al-Cu Esaslı Metal Matrisli Kompozit Malzeme Üretimi," Yüksek lisans tezi, İstanbul Üniversitesi, İstanbul, Türkiye, 1999.
2. İ. Uygur ve H. Saruhan, "Mechanical behavior of aluminum-based metal matrix composites," Sakarya Üniversitesi Fen Bilimleri Enstitüsü Dergisi, c. 8, sayı 1, ss. 167-174, 2004.
3. <http://kompozithayalleri.com/matris-nedir/>
4. M. Sönmez, "Polimer Matrisli Kompozitlerin Endüstri Ürünleri Tasarımında Önemi ve Geleceği: Türkiye'den Dört Örnek Firma Üzerine Bir İnceleme," Yüksek lisans tezi, İstanbul Teknik Üniversitesi, İstanbul, Türkiye, 2009.
5. METYX Composites, Reinforcement Brochure, <http://www.metyx.com/Brochure>
6. M. Kara, "Düşük hızlı darbe sonrası yama ile tamir edilmiş filaman sarım CTP boruların iç basınç altındaki hasar davranışı," Doktora tezi, Makine Mühendisliği, Fen Bilimleri Enstitüsü, Selçuk Üniversitesi, Konya, Türkiye, 2012.
7. E. Gücüyen, R. T. Erdem, E. Kantar, "Kompozit Boru Kesitlerinin Çarpma Etkisi Altında Deneysel ve Nümerik Olarak İncelenmesi", Fırat üniversitesi mühendislik bilim dergisi, c.30 sayı 1, ss. 139-149, 2018.
8. <https://www.kompozitshop.com/karbon-fiber-elyaf-pultruzyon-borular-nasil-uretilir>
9. A.M. Bahar, "Pultruzyon Yöntemiyle Ctp Üretimi ve Üretim Parametrelerinin Malzeme Nihai Özelliklerine Etkisi", Yıldız Teknik Üniversitesi, Yüksek lisans tezi, 2009.
10. <https://www.strongwell.com/about/the-pultrusion-process/>
11. D. Kaya, S. Subaşı, A. Subaşı, "Elyaf Sarma Tekniği ile Üretilen Kompozit Borularda Reçine ve Cam Elyaf Türünün İç Basınç Dayanımına Etkisi", Düzce Üniversitesi mühendislik fakültesi ISITES Valencia -Spain, 2015.
12. O. Sayman, Ü. Esendemir, A. Öndürücü, "Serbest Ucundan Tekil Yüke Maruz Ankastre Metal Matrisli Kompozit Kirişin Elasto-Plastik Çözümü", Pamukkale University Journal of Engineering Sciences, c.7, s.3, ss. 313-312, 2001.
13. S. K. Mazumdar, Composite Manufacturing Materials, Product and Process Engineering, Florida, USA: CRC Press LLC, 2002.
14. R. Teti, "Machining of Composite Materials," CIRP Annals, c. 51, sayı 2, ss. 611-634, 2002.
15. Ş. Bayraktar, "Karbon Elyaf Takviyeli Polimer Kompozit Malzemelerin Frezeleme İşleminde İşlenebilirliğinin Deneysel Araştırılması," Yüksek Lisans Tezi, Gazi Üniversitesi, 2011.
16. F. Karaca, "Cam Elyaf Takviyeli Plastik Kompozitlerde Delme Parametrelerinin Deformasyon Faktörüne Etkisinin Araştırılması", Fırat Üniversitesi Mühendislik Bilim Dergisi, c.28, sayı 2, ss.23-27, 2016.
17. E. Ekici, "Cam Elyaf Takviyeli Polimer Kompozit Malzemenin Delinmesi Esnasında Oluşan Yüzey Hasarının Deneysel Olarak İncelenmesi", Uluslararası İleri Teknolojiler Sempozyumu (IATS), ss.1-6, 2009.
18. V. A Phadnis, F. Makhdom, A. Roy ve V. Silberschmidt, "Drilling in Carbon/Epoxy Composites", Experimental Investigations and Finite Element Implementation, Composites: c. 47, ss 41-51, 2013.
19. R. Vinayagamoorthy, "A review on the machining of fiber-reinforced polymeric laminates," Journal of Reinforced Plastics and Composites, c. 37, sayı 1, ss. 49-59, 2018.
20. N. Naresh., K. Rajasekhar, P.V.B. Reddy, "Parametric analysis of GFRP composites in CNC milling machine using Taguchi method", IOSR Journal of Mechanical and Civil Engineering C. 6, sayı 1, ss.102-111, 2013.
21. J. Du, H. Zhang, Y. Geng, W. Ming, W. He, J. Ma, Y. Cao, X. Li ve Kun Liu, "A review on machining of carbon fiber reinforced ceramic matrix composites," Ceramics International, c. 45, sayı 15, ss. 18155-18166, 2019.
22. W. Hintze, D. Hartmann, C. Schütte, "Occurrence and propagation of delamination during the machining of carbon fiber reinforced plastics", Composites Science and Technology, c. 71, sayı 15, ss. 1719-1726, 2011.

23. M. Senthil Kumar, A. Parabukarathi, V. Krishnaraj, Study on tool wear and chip formation during drilling carbon fiber reinforced polymer (CFRP)/titanium alloy (Ti-6Al-4V) stacks, *Procedia Engineering*, c.64, ss. 582-592, 2013.
24. L.M. Durão, D. Gonçalves, J. Tavares, V. Albuquerque, A. Vieira ve A. Marques, "Drilling Tool Geometry Evaluation for Reinforced Composite Laminates", *Composite Structures*, c. 92, ss. 1545-1550, 2010.
25. E. Kılıçkap, Y. H. Çelik, A. Yardımeden, "Karbon elyaf takviyeli plastik kompozitlerin tornalanmasında yüzey pürüzlülüğü ve takım aşınmasına etki eden parametrelerin araştırılması," *Dicle Üniversitesi, Mühendislik Dergisi*, c.8, sayı 1, ss. 175-180, 2017.
26. K. Abhishek, V. R. Kumar, S. Datta ve S. S. Mahapatra, "Application of JAYA algorithm for the optimization of machining performance characteristics during the turning of CFRP (epoxy) composites: comparison with TLBO, GA, and ICA," *Engineering with Computers*, c.33, ss.457-475, 2017.
27. K. V. Kumar, A. N. Sait ve K. Panneerselvam, "Machinability study of hybrid-polymer composite pipe using response surface methodology and genetic algorithm," *Journal of Sandwich Structures and Materials*, c. 16, sayı 4, ss. 418-439, 2014.
28. I. Azmi, A. Z. Syahmi, M. Naquib, T. C. Lih, A F. Mansor ve A. N. M. Khalil, "Effects of machining conditions on the specific cutting energy of carbon fiber reinforced polymer composites," *Journal of Physics: Conference Series*, c. 908, 2017.
29. N. Duboust, H. Ghadbeigi, C. Pinna, S. Ayvar-Soberanis, A Collis, R. Scaife ve K. Kerrigan, "An optical method for measuring surface roughness of machined carbon fiber reinforced plastic composites," *Journal of Composite Materials*, c. 51, sayı 3, ss. 289-351, 2016.
30. K. S. Kim, D. G. Lee, Y. K. Kwak ve S. Namgung, "Machinability of carbon fiber-epoxy composite materials in turning," *Journal of Materials Processing Technology*, c. 32, sayı 3, ss. 553-570, 1992.
31. S. Ramesh, L. Karunamoorthy, K. Palanikumar, "Surface roughness analysis in the machining of titanium alloy", *Materials and Manufacturing Processes*, c.23, ss.174-181, 2008
32. Özgür BİÇER, "Karbon Fiber Takviyeli Kompozitlerin İşlenebilirliği ve Vidalı Birleştirme Yeteneklerinin İncelenmesi," *Yüksek Lisans Tezi*, Necmeddin Erbakan Üniversitesi, 2017.
33. D. K. Das, P. C. Mishra, S. Singh ve R. K. Thakur, "Tool wear in turning ceramic reinforced aluminum matrix composites—A review," *Journal of Composite Materials*, c. 49, sayı 24, ss. 1-13, 2014.
34. Y. H. Çelik, E. Kılıçkap, "Titanyum Alaşımlarından Ti-6Al-4V'nın İşlenmesinde Karşılaşılan Zorluklar", *Gazi University Journal of Science*, c.6, sayı 1, ss. 163-175, 2018.
35. J. Xu, Q. An ve M. Chen, "A Comparative Evaluation of Polycrystalline Diamond Drills in Drilling High Strength T800s/250f CFRP", *Composite Structures*, c. 117, ss. 71-82, 2014.

MODIFIED METHOD OF DEFERRED MOIRÉ PATTERNS TO MEASURE DISPLACEMENT

Vladimir Saveljev
ORCID: 0000-0003-2187-704X

ABSTRACT

Measuring displacement with a digital camera using the moiré effect has certain advantages over direct measurements. Previously, we proposed a method to measure the linear displacement of distant objects based on the moiré effect.

To date, we have implemented the software and developed some improvements in the method. In particular, we made simultaneous measurements of displacements in two directions. We have shown the use of an approximate grid instead of a conventional linear grid with almost the same output readings. In addition, we have converted the deliberately delayed original method into a real-time procedure.

Keywords: moiré effect, moiré measurements, phase measurement, moiré magnifier, public safety.

INTRODUCTION

The moiré is an optical effect we can meet all around us, see Figure 1.



Figure 1. Examples of the moiré effect.

The moiré effect is the formation of patterns of longer periods caused by interference between similar periodic structures of shorter periods plus averaging.

A useful application of the moiré effect is to measure the linear displacement (movement) of distant objects. The moiré measurement is based on two principles: moiré magnification (Hutley et al., 1994) and phase proportionality (Amidror, 2000). In terms of linear measurements, the magnified phase of the patterns means the displacement. At each moment, the position of the oscillating grid is compared with the static computer-generated reference grid, see Figure 2.

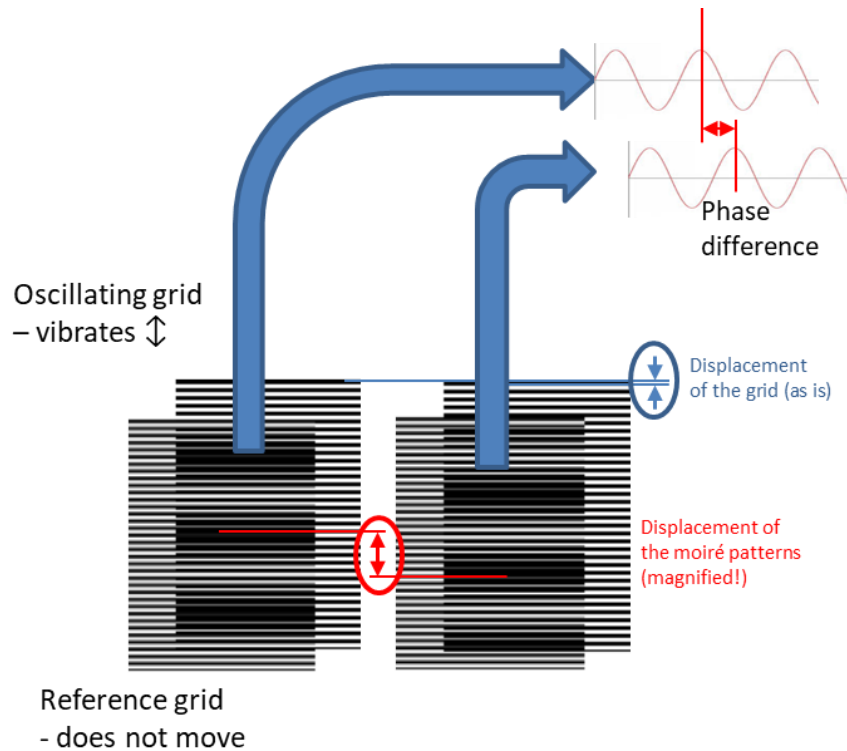


Figure 2. Principle of measurements.

Measuring displacement with a digital camera using the moiré effect (with magnified phase) has advantages over direct measurements (roughly speaking, counting pixels in camera images).

Previously (Saveljev et al., 2023), we proposed the deferred moiré method for measuring the linear displacement of distant objects. Data processing is intentionally divided in two separate parts: data acquisition and data processing. The first one is implemented as a video recording of a vibrating (displacing) object in the field (“in vivo”), the second as the processing of that video in the lab (“in vitro”) any time later. The parts are almost independent, which gives some flexibility in practical measurements.

RESEARCH AND FINDINGS

To date, we have developed some improvements. In particular, we made simultaneous measurements, demonstrated the use of an approximate grid, transformed the deliberately delayed original method into a real-time procedure, and implemented the real-time software.

The vertical and horizontal oscillations were measured in a parked car. To excite the vibration, the car was pushed horizontally (the door to the side) and vertically (the hood down). For measurements, two perpendicular gratings were attached to the car, as shown in Figure 3.



Figure 3. Layout of simultaneous measurements.

The accuracy of measurements at the distance of 2.5 m was 10 pixels per mm, i.e., the minimal measured displacement was about 0.1 mm.

In some cases, we might not install the regular grid on an object, while other almost similar structures might exist. Therefore, we consider approximate grids, as in (Saveljev at al., 2020). An example is shown in Figure 4.

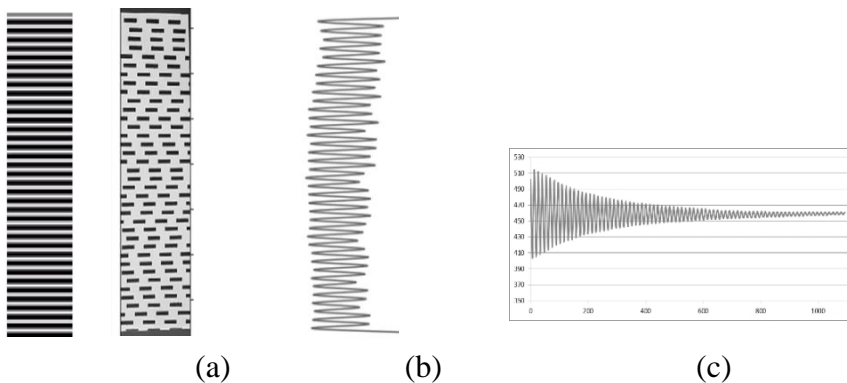


Figure 4. (a) Regular and approximate grids, (b) their profile, (c) output signal.

In the test of damped oscillations of a plastic rod, except for the amplitude, the period and the exponential decay rate were measured: 0.503 vs. 0.501 sec, 0.099 vs. -0.098 sec⁻¹, both parameters practically identical for both regular line grid and the randomized approximate grid.

In a monitoring system, the data should be sent to a data collection unit regularly without interruption. In this case, we need to implement all the processing algorithms in real time; otherwise, some information could be lost, which is unacceptable in a real-time monitoring system. There are two separate hardware parts in the real-time system: (1) the grid on the object and (2) the camera + processor, see Figure 5.

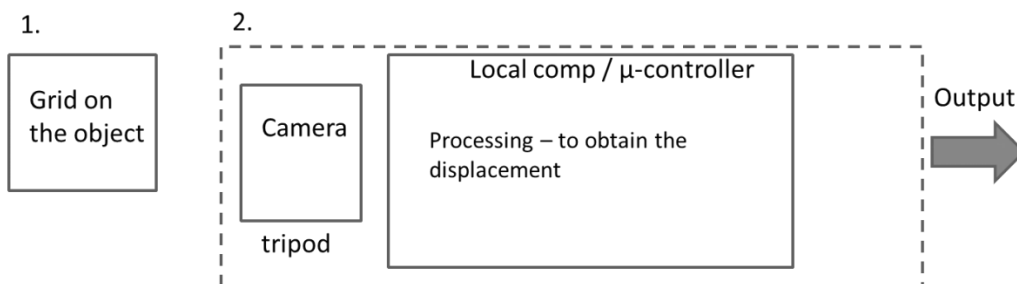


Figure 5. Flowchart of real-time system.

The results of the real-time measurements were displayed in two options: in the command line and in a separate window. In parallel, the measured data are recorded (and processed later, probably, in a different way).

CONCLUSION

Simultaneous measurements of displacements in two directions were carried out. At a short distance of 2.5 m, the accuracy of measurements was about 0.1 mm.

We have demonstrated the usage of an approximate grid. The results are practically identical for both grids (regular and approximate).

We have implemented a real-time moiré measurement algorithm that does not need intermediate data storage. All calculations (including two-stage unwrap) are performed in one pass, within the time interval between the successive camera frames (30 msec at 30 FPS). The accuracy was 0.2 mm at distances up to 20 m.

The results can be applied in various fields: measuring vibrations in bridges and vehicles, detecting cracks in structures, as well as for medical purposes (respiratory rate).

REFERENCES

1. Amidror, I. (2000), *The theory of the moiré phenomenon*, Springer.
2. Hutley, M.C., Hunt, R., Stevens, R.F., and Savander, P. (1994), Moiré magnifier, *Pure and Applied Optics: Journal of the European Optical Society Part A*, vol. 3, No 2, pp. 133–142.

15th INTERNATIONAL CONFERENCE ON ENGINEERING & NATURAL SCIENCES

March 04-06, 2023 Muş, TÜRKİYE

3. Saveljev, V., Kim, J., Son, J.-Y., Kim, Y., and Heo, G. (2020), Static moiré patterns in moving grids, *Scientific Reports*, vol. 10, article number: 14414.
4. Saveljev, V., Son, J.-Y., Lee, H., and Heo, G. (2023), Non-contact measurement of vibrations using deferred moiré patterns, *Advances in Mechanical Engineering* (in press).

GEÇİRİMSİZ YÜZEYLERİN YAĞMUR SUYU YÖNETİMİNE ETKİSİ EFFECT OF IMPERMEABLE SURFACES ON STORM WATER MANAGEMENT

Pelin Sertyesilisik
ORCID: 0000-0003-4047-3614

ÖZET

Uzun süreli ve sık yağış olayları ve nüfus artışı, sel gibi kentsel su yönetimini olumsuz etkileyebilir. Kentsel alanlarda yüzey taşkınlarının yıkıcı sonuçları olabilir. Kentsel alanlarda, geçirimsiz yüzeylerin sayısının artması nedeniyle drenaj sistemlerini yönetmek zor olabileceğinden, drenaj sistemlerinden yoğun su çıkışları olabilir. Drenaj sistemlerinin girdileri yağış, içme suyu ve atık su olabilir. Bu çalışma, gelişmekte olan bölgelerde yağmur suyunun yönetimine odaklanmaktadır. EPA SWMM ile yağmur suyu modellemesi yapılmıştır. EPA SWMM, yağmur suyu drenaj sistemindeki su seviyesini görüntülemek için kullanıldı. 1boyutlu drenaj ağı modeli, kanal, bağlantı ve alt havza özelliklerini içermektedir. Başlıca en önemli veri olan Dijital Yükseklik Modeli (DEM) ile havzadaki eğim, akış yönü ve çıkış noktası tespit edildi. DEM, LiDAR ve Sokak görünümü giriş verileri, Arc MAP yazılımı ve Google Earth aracılığıyla incelenmiştir. Bu çalışmada geçirimsiz yüzeyin yüzey akışı üzerindeki etkisi gözlenmiştir. Araştırma sahası gelişme potansiyeli olan Afyon Meslek Yüksekokulunun bulunduğu alan seçilmiştir. Bu çalışma, araştırma alanının yağış olaylarına karşı yüzey taşkın riskini ve drenaj sistemi tasarım parametrelerini incelemektedir. Bu araştırmanın sonuçları, yeşil çatılar veya geçirgen kaldırımlar gibi çeşitli düşük etkili kentleşme uygulaması kontrol stratejileri uygulanarak, kentsel drenaj sistemlerini iklim değişikliğine ve kentleşmeye karşı iyileştirmek için kullanılabilir.

Anahtar Kelimeler: Kentsel Taşkın Riski, Yağmur Suyu Modellemesi, EPA-SWMM.

ABSTRACT

The prolonged and frequent rainfall events and population growth can adversely impact urban water management, such as surface flooding. Surface flooding in urban areas can have devastating consequences. In urban areas, the surface overflow can be the outflows from drainage systems because it can be challenging to manage drainage systems due to the increased number of impermeable surfaces. The inputs of the drainage systems can be rainfall, drinking, and wastewater. This study focuses on managing stormwater in developing areas. Stormwater modelling was done via EPA SWMM. The EPA SWMM was used to display the water level in the stormwater drainage system. The 1D drainage network model includes conduit, junction, and sub-catchment characteristics. The primary input data, The Digital Elevation Model (DEM), was used to determine the slope, flow direction, and outflow point. The DEM, LiDAR, and Street view input data were studied via the Arc MAP tool and Google Earth. The impact of the impermeable surface on the surface runoff was observed in this study. The research site is Afyon Vocational School which has a potential developing area. This study examines the research area's surface flood risk against rainfall events and drainage system design parameters. The outcomes of this research can be used to improve urban drainage systems against climate change and urbanisation by implementing various Low impact development (LID) control strategies, such as green roofs or permeable pavements.

Keywords: Urban Flood Risk, Storm Water Modelling, EPA-SWMM.

GİRİŞ

Kentsel taşkınlar, küresel iklim değişikliği, nüfus artışı ve kentleşme nedeniyle drenaj sistemlerinin bu durumlara adapte olamayışı sebebiyle görülebilmektedir (Öner, 1997; Schmitt vd., 2004; Liu vd., 2022). Kentsel alt yapı sistemleri ile atıksu, içme suyu ve yağmur suyu taşınabilmektedir bu su çeşitleri yaşamın devamı için önem taşımaktadır. Bu sebeple özellikle temiz su sistemleri ve kirli su sistemlerinin tasarım ve bakımına önem verilmelidir. Tasarım kısmının en önemli olduğu durumlardan biride yeni yerleşmelerin görüleceği yerler olabilir. Özellikle, geçirimli yüzeyler geçirimsiz yüzeyler dönüştürülmesi ile yağmur sularının topraktan sızmasının azaldığı, yüzey akışının arttığı bilinmektedir. Bununla beraber iklim değişikliği ile yağış olayları ani ve şiddetli olarak görülebilmektedir (Wang & Zhou, 2005).

Tüm bu sebeplerden ötürü bu çalışmada gelişme bölgelerindeki yağmur suyu yönetimine katkı olması amaçlanmıştır.

ARAŞTIRMA VE BULGULAR

Metot

Çalışmanın metodu şu adımlardan oluşmaktadır.

1. Çalışma alanının yükselti, eğim, toprak yapısı, yüzey kullanım alanlarının tespiti,
2. Çalışma alanının da ki yağış olaylarının tespiti,
3. Yağmur suyu yönetimi boru sisteminin modellenmesi

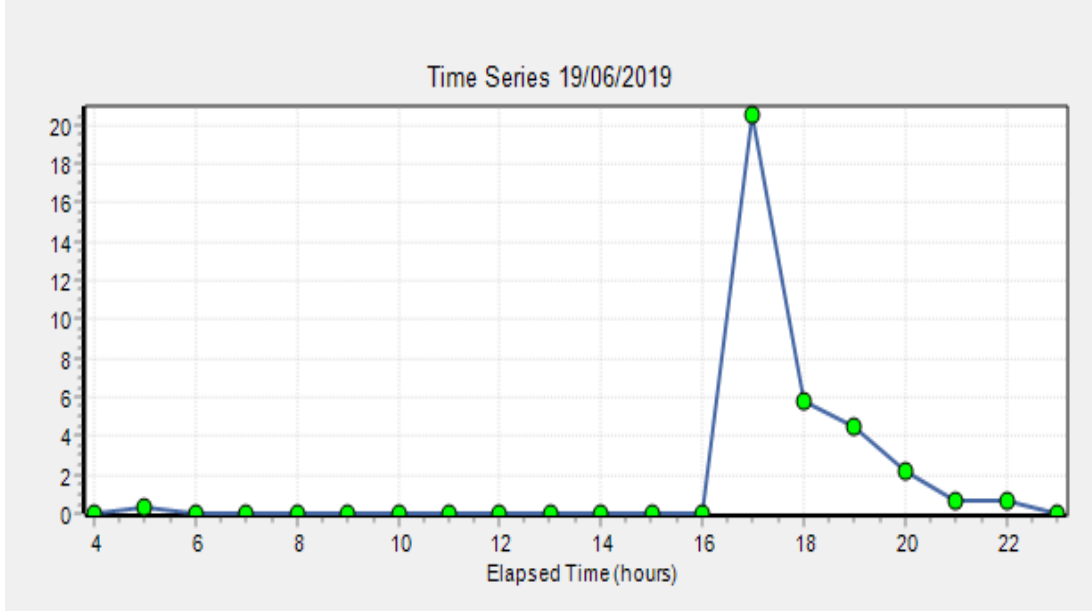
Araştırma alanımız Şekilde 2.1(Google Earth, 2022) de belirtilen kırmızı kare içindeki alandır. Bu alana düşen yağışın EPA-SWMM programıyla simülasyonu ile yağmur suyu drenaj sisteminin incelenmesi yapılmıştır (US-EPA, 2009; Rossman &Simon, 2022).



Şekil 2.1. Çalışma Alanı Afyon Meslek Yüksekokulu

Bu çalışmada EPA-SWMM programı Dinamik Dalga Analizi yöntemi seçilerek kullanılmıştır. Süreklilik ve momentum formülleri kullanılmaktadır. Bu denklemlerin türetilmesi, Henderson (1966), Cunge vd (1980) ve French (1985) gibi standard metinler de bulunulabilmektedir.

EPA-SWMM modeline girilmesi gereken eğim (%) değerleri, ArcGIS programına girilen DEM verisiyle elde edilmiştir (US-EPA, 2009; Rossman & Simon, 2022). Bir diğer önemli veride yağmur suyu verisidir.



Şekil 2.2 19.06.2019 gününde görülen yağış yükseklikleri (mm)/zaman (saat)

19.06.2019 gününde görülen yağış yükseklikleri (mm) /zaman (saat) Şekil 2.2 de görülmektedir. Bu yağmur olayının seçilmesinin sebebi ani bir şiddetli yağış görülmesidir.

Çalışma alanı iki ana alt havzaya ayrıldı bu alt havzanın özellikleri Tablo 2.1'den görülebilir. Bu iki alt havzaya düşen yağışlar Tablo 2.2 ve Tablo 2.3 de gösterilen özelliklerdeki altyapı sistemleri ile taşınmaktadırlar.

Tablo 2.1. Kullanılan alt havzaların özellikleri

Özellikler	S-C1	S-C2
Alan (m ²)	9554	10390
Genişlik (m)	93.18	85.16
% Eğim	2.5	2.5
% Geçirimsiz alan	93	87
N-Imperv	0.011	0.011
N-Perv	0.41	0.41
Dstore- Imperv	0.07	0.07
Dstore-Perv	0.15	0.15
%Zero-Imperv	25	25

Tablo 2.2. Akar kot

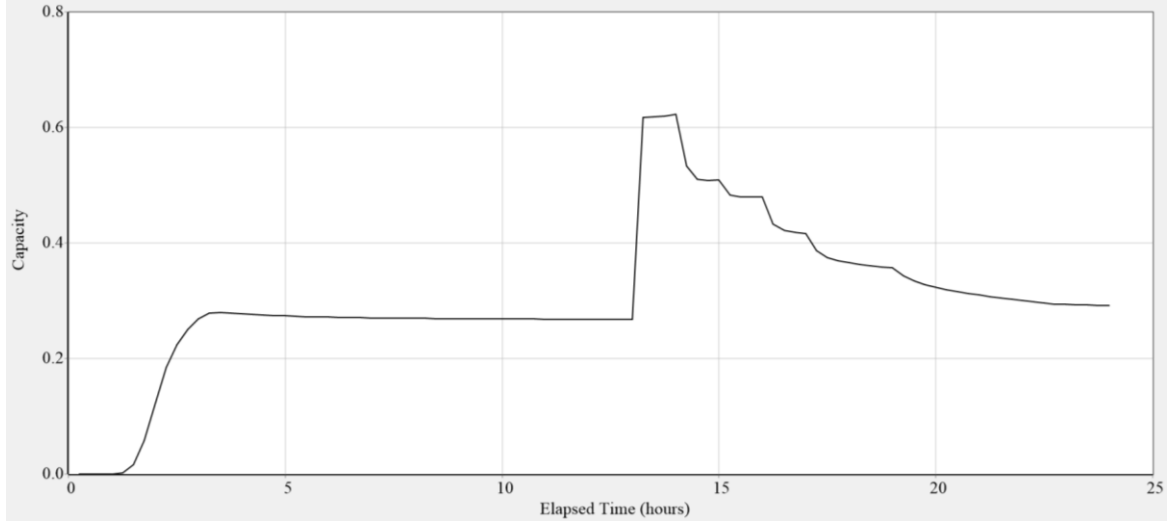
Bağlantı Noktaları	Akar kot (m)
J1	1009,20
J2	1008,92
J3	1009,17
Çıkış	1007,59

Tablo 2.3. Yağmursuyu Borularının Özellikleri

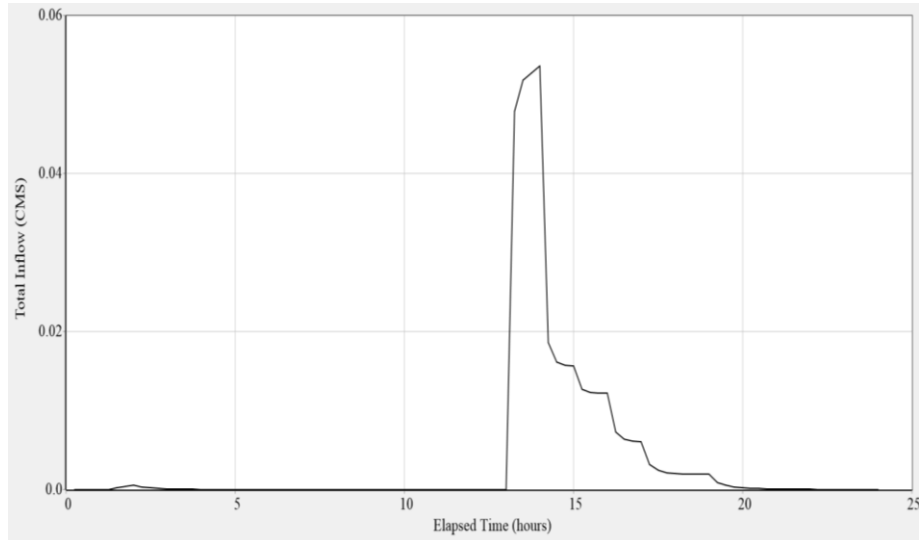
Yağmursuyu Boruları	Uzunluk (m)	Materyal	Sürtünme katsayısı	Max. Derinlik (m)
Con 1	74	Korige	0.02	0.4
Con 2	45,75	Korige	0.02	0.4
Con 3	17,21	Korige	0.02	0.4

Deneysel sonuçlar ve değerlendirmeleri

Tablo 2.1,2.2 ve 2.3 ve Şekil 2.2'deki veriler programa aktarılıp program çalıştırıldığında analiz sonuçları Şekil 2.3'de yer almaktadır.

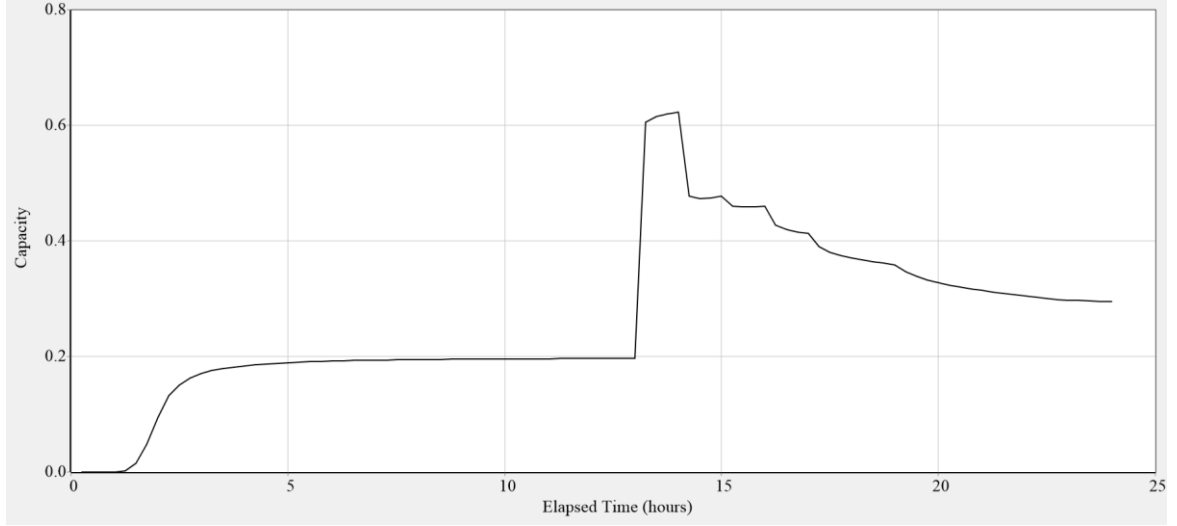


Şekil 2.2 Alt havza 2 ye ait yağmur suyu borusundaki kapasite

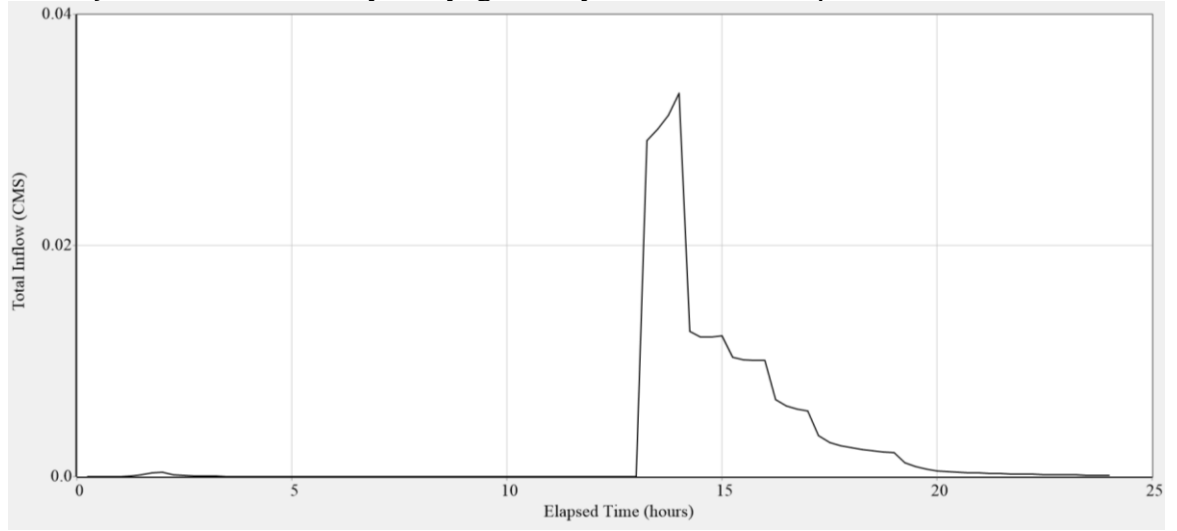


Şekil 2.3 Alt havza 2 ye ait yağmur suyu borusundaki toplam giriş debisi

Alt havza 2 ye ait yağmur suyu borusundaki toplam giriş debisi 0.05 cms değerinde ve kapasite 0.7 değerine yaklaşmaktadır. Bu boru hattında yeni yapılaşmalarla, ileride daha fazla su girdileri olabileceği için planlama yapılırken bu borunu su kapasitesini etkileyen faktörler net belirlenmeli. Bu sebeple alt havza 2'nin geçirimsizlik yüzdesi %87 den 50 ye düşürüldü ve model tekrar çalıştırıldı.

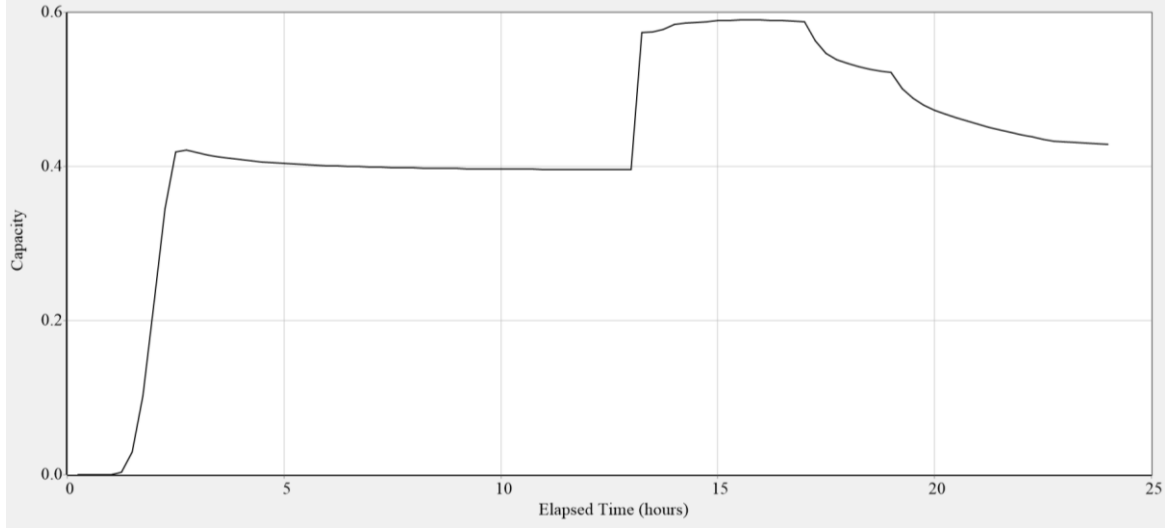


Şekil 2.4 Alt havza 2 ye ait yağmur suyu borusundaki kapasite



Şekil 2.5 Alt havza 2 ye ait yağmur suyu borusundaki toplam giriş debisi

Şekil 2.4'te görüldüğü üzere geçirimsizlik yüzdesi düşürüldüğünde borunun kapasite doluluk oranı başlangıçta azalmaktadır. Benzer şekilde (Şekil 2.5) yağmur suyu borusundaki toplam giriş debisinde de azalma görülmüştür. Bu durum geçirimli alanın doygunluğa ulaşmasından etkilemiş olabilmektedir. Bir diğer analizde boru tam doluluk yaşanmadığı için pik derinlik 0,4 m'den 0,3 m ye indirildi ve maliyetin azaltılması amaçlandı.



Şekil 2.6. Alt havza 2 ye ait yağmur suyu borusundaki kapasite

Şekil 2.6 da görüldüğü üzere borunun maksimum derinliği 0,4 m'den 0,3 metre indirildiğinde kapasitesindeki doluluk değeri maksimum değere yaklaşmaktadır.

SONUÇ

- Bu çalışma, gelişmekte olan bölgelerde yağmur suyunun yönetimine odaklanmaktadır.
- EPA SWMM, yağmur suyu drenaj sistemindeki su seviyesini görüntülemek için kullanıldı. Bir boyutlu drenaj ağı modeli, kanal, bağlantı ve alt havza özelliklerini içermektedir.
- Bu çalışma sürdürülebilir kentsel altyapı tasarımına katkı amaçlı yapılmaktadır.
- Alt havzanın geçirimsizlik yüzdesini çatıdaki yağmur suyunun ayrıca toplanıp direkt kanalizasyon sistemine verilmesinden etkilemektedir.
- Alt havzanın geçirimsizlik yüzdesinin artırılıp topraktan yağmur suyunun verimli bir şekilde sızdırılması boru maliyetini ve taşkın riskini düşürebilir.
- İklim değişikliği sebebiyle görülen ani kısa süreli ama yoğun yağışların kanalizasyon sistemine olan ani yüklerini ve yağmursuyu debisini azaltıcı yeşil çatı, su depoları, geçirimli kaldırımlar gibi uygulamalar yapılmalıdır.
- Suyun akış yolunu ve süresini düzenleyici yöntemler geliştirilmelidir.
- Bununla birlikte eğiminde çıkış debisine belirgin etkisi bulunmaktadır.

KAYNAKÇA

1. Cunge, J. (1980). Practical aspects of computational river hydraulics. *Pitman Publishing Ltd. London, (17 CUN), 1980, 420.*
2. EPA SWMM, available at: <https://www.epa.gov/water-research/storm-water-management-model-swmm>, last access: 07 November 2022.
3. French, R. H. (1985). *Open-channel hydraulics* (p. 705). New York: McGraw-Hill.
4. Google Earth. (2022). Afyon Vocational School. Maxar Technologies. Imagery Date 7/16/2022.
5. Henderson, F. M. (1966). Open channel flow Mac Millan Publishing Co. Inc., New York 1966, 288-324.
6. Liu, B., Xu, C., Yang, J., Lin, S., & Wang, X. (2022). Effect of Land Use and Drainage System Changes on Urban Flood Spatial Distribution in Handan City: A Case Study. *Sustainability, 14*(21), 14610.

15th INTERNATIONAL CONFERENCE ON ENGINEERING & NATURAL SCIENCES

March 04-06, 2023 Muş, TÜRKİYE

7. Öner, S.S. (1997). *The Use of SWMM simulation model in urban storm water management* [Master Thesis, Dokuz Eylül University]. Ulusal Tez Merkezi Repository. <https://tez.yok.gov.tr/UlusalTezMerkezi/65574/>
8. Rossman, L. A. (2017). Storm Water Management Model Reference Manual Volume II – Hydraulics. U.S. Environmental Protection Agency, Washington, DC, EPA/600/R-17/111.
9. Rossman, L. A. and Simon, M.A. (2022). Storm water management model user's manual, version 5.2 (p. 424). Cincinnati: National Risk Management Research Laboratory, Office of Research and Development, US Environmental Protection Agency.
10. Schmitt, T. G., Thomas, M., & Ettrich, N. (2004). Analysis and modelling of flooding in urban drainage systems. *Journal of hydrology*, 299(3-4), 300-311. <https://doi.org/10.1016/j.jhydrol.2004.08.012>.
11. US-EPA. (2009). *Storm Water Management Model*, Applications Manual.

ANALOG pH SENSÖRÜN ESP8266 TABANLI MİKRODENETLEYİCİ DEVRESİNDE FARKLI KABLO UZUNLUKLARI PERFORMANS KARŞILAŞTIRMASI PERFORMANCE COMPARISON OF DIFFERENT CABLE LENGTHS IN ESP8266 BASED MICROCONTROLLER CIRCUIT OF ANALOG pH SENSOR

Kamil Aykutaalp Gündüz
ORCID: 0000-0002-2290-5447
Fatih Başçiftçi
ORCID: 0000-0003-1679-7416
Züleyha Yılmaz Acar
ORCID: 0000-0002-4488-478X

ÖZET

pH algılayıcılar sıvıların kalitesini ölçme işlemlerinde kullanılırlar. Su ve başka çözeltilerdeki asitlik ve bazik durumları tespit ederler. pH algılayıcılar endüstrinin birçok alanında, hem sıvı gıdaların üretim aşamalarında hem de kimyasal laboratuvarlarda kalite ve verimliliğin iyileştirilmesinde kullanılırlar. Genellikle fabrika çıkışlı kalibrasyona sahip ve farklı kablo uzunluklarına sahip olarak üretimleri yapılır. Kalibrasyon işlemi, seri üretimi yapılan sensörlerin kendi entegre devreleri üzerinden gerçekleştirilir. Bu çeşit algılayıcılar, kendi üzerlerinde bulunan dijital göstergeler sayesinde sonuçları gösterdiklerinden, verilerin uzaktan takibi ve izlenmesi mümkün olmamaktadır. Bu çalışmada, piyasada uygun fiyatlı olarak satılan ve birçok bilimsel araştırmalarda kullanılan analog pH algılayıcıların fabrika çıkışlı kablo uzunlukları değiştirilerek, pH verilerinin karşılaştırmaları yapılmıştır. Nesnelerin İnterneti (Internet of Things, IoT) teknolojisi ile dünyayı gözlemleme yeteneğine sahip, veri işleyebilen, verileri analiz edebilen ve karar verme işlemleri gerçekleştirebilen, kablosuz algılayıcılar yardımıyla canlı cansız nesneleri tanımlayabilen sistemler geliştirilmeye başlanmıştır. IoT destekli cihazlar, internet üzerinden birbirleriyle konuşabilir ve böylece kendi aralarında veri aktarımı yapabilirler. Bu özelliğinden dolayı IoT teknolojilerinin verdiği olanaklarla, akıllı şehir, akıllı ev, akıllı trafik, akıllı tarım ve biyomedikal sistemlerinin yanı sıra akıllı çiftlik ve hayvancılık alanlarında da kullanımı günden güne artmaktadır. Bu çalışmada IoT uyumlu ESP8266 tabanlı iki farklı mikrodnetleyici ile analog pH algılayıcıdan veriler kablosuz olarak kayıt altına alınıp karşılaştırmaları yapılmıştır. Seçilen mikrodnetleyiciler, IoT (Internet of Things) projelerinde kullanılabilir modellerden seçilmiştir. Böylece analog pH algılayıcıların fabrika çıkışlı yapıları değiştirilerek, kablosuz ağlarla oluşturulan projelerde kullanımlarının uygunluğu incelenmiştir. Çalışmada farklı pil besleme üniteleri kullanılarak karşılaştırmaları yapılmıştır. Aynı özelliklere sahip analog pH algılayıcıların ve mikrodnetleyicilerin kablo uzunluk performans sonuçları ölçülmüştür. Sensörlerin fiziksel değişimleri, Esp8266 tabanlı donanımsal devre tasarımları ve yazılım yazarlar tarafından geliştirilmiştir.

Anahtar Kelimeler: Algılayıcı, Analog pH, ESP8266, IoT, Kablo.

ABSTRACT

pH sensors are used to measure the quality of liquids. They detect acidity and basicity in water and other solutions. pH sensors are used in many areas of industry, both in the production stages of liquid foods and in chemical laboratories to improve quality and efficiency. They are usually produced with factory calibration and with different cable lengths. They are usually produced with factory calibration and with different cable lengths. The calibration process is carried out on the sensors own integrated circuits. Since these kinds of sensors show the results thanks to the digital indicators on them, it is not possible to monitor and monitor the data remotely. In this study, comparisons of pH data were made by changing the factory cable lengths of analog pH sensors used in many scientific researches and sold at affordable prices in the market. With the Internet of Things (IoT) technology, systems that have the ability to observe the world, process data, analyze data and perform decision-making processes, and identify living and inanimate objects with the help of wireless sensors have begun to be developed. IoT supported devices can talk to each other over the internet and thus transfer data among themselves. Due to this feature, the use of smart city, smart home, smart traffic, smart agriculture and biomedical systems, as well as smart farm and animal husbandry, is increasing day by

day with the opportunities provided by IoT technologies. In this study, data from two different IoT compatible ESP8266-based microcontrollers and analog pH sensors were wirelessly recorded and compared. Selected microcontrollers are selected from models that can be used in IoT (Internet of Things) projects. Thus, the ex-factory structures of analog pH sensors were changed and the suitability of their use in projects created with wireless networks was examined. In the study, comparisons were made using different battery supply units. The cable length performance results of analog pH sensors and microcontrollers with the same characteristics were measured. Physical changes of sensors, hardware circuit designs based on Esp8266 and software have been developed by the authors.

Keywords: Analog pH, Cable, ESP8266, IoT, Sensor.

GİRİŞ

Endüstri 4.0 ile birlikte ilerleyen teknolojik gelişmeler, internete bağlanan insan ve makine sayısının artmasına neden olmaktadır. Bu rakamlara göre, 2023 yılında dünya üzerindeki internete bağlı cihazların %34'ünü M2M ve IoT cihazlarının oluşturacağı öngörülmektedir (CISCO VNI, 2023). IoT (Internet of Things), akıllı ev sistemleri, e-sağlık, ekolojik sistemler, tarım, hayvancılık, enerji, şehirler, ölçümler, endüstriyel kontrol, güvenlik ve acil durumlar, alışveriş, lojistik gibi birçok alanda kullanılır (Gökrem, 2016).

Danimarkalı bir kimyagerin 1909 yılında tanımlamasıyla pH kavramı kullanılmaya başlanmıştır (Keskin, 2010). pH değerleri ölçümlerinin önemli olduğu alanlardan bazıları ise; gıda, atık madde, tarım, hayvancılık, biyoteknoloji, galvanizasyon, yüzme havuzları, osmosis tesisleridir (Ölmez, 2009). IoT çalışmalarında rol alan nesnelerin karmaşık yapıda olması sebebiyle bu cihazların haberleşmesinde de çeşitli iletişim yöntem ve teknolojileri kullanılır. Wi-fi, IEEE 802.15.4, Bluetooth, Z-wave, LTE ve LPWAN bu teknolojilere örnek olarak gösterilebilir (Khalil & Özdemir, 2018). Amaç, sistem gereksinimlerine göre uygun bağlantı türünü seçmek, işlene verilerin etkin halde işletilmesini sağlamaktır (Bozdoğan, 2015).

IoT'nin gerçekleşmesi için temelde nesnenin internet ağına bağlanıp, üzerindeki en az bir sensör ile alınan değerlerin sunucu ortamına veya başka bir ağ cihazına aktarılması gerekir. Bunun için gerekli aşamalar; besleme ünitesi, mikroişlemci, sensörler ve internet bağlantısıdır. Bu çalışmada geliştirilen IoT cihazı, Esp8266 modüle sahip mikrodenetleyici üzerinde bulunan analog pH sensöründen ölçülen veriler incelenmiştir. Fabrika çıkışlı pH algılayıcıdan BNC konnektörüne bağlanmayı sağlayan kablo uzunluğunun farklı algılayıcı ve farklı mikrodenetleyicilere göre karşılaştırması yapılmıştır.

ARAŞTIRMA VE BULGULAR

Donanım Çalışmaları

Sanayide pH ölçümü, ölçümü yapılan çözelti veya katı nesnenin içindeki asit veya bazik değerlerinin ölçümlenmesinde kullanılan ölçerler tarafından gerçekleştirilir. pH, bir sıvı çözeltisinin asitlik veya baziklik derecesini gösteren bir terimdir. 0'dan 14'e kadar olan bir aralıkta ölçülür (Koçak, 2018). pH terimindeki p harfi, eksi logaritmanın matematiksel gösteriminden, H harfi ise hidrojenin kimyasal formülünden türetilmişlerdir (Yarba, 2019). Saf suyun pH değeri 7,0'dır. Şekil 2.1'de farklı model analog pH ölçerler gösterilmiştir.

Şekil 2.1. Analog pH sensörleri



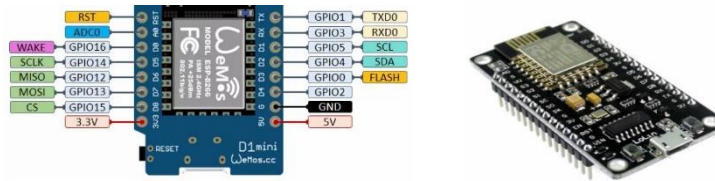
Tablo 2.1’de kullanılan pH ölçerin ve fabrika çıkışlı konektörün teknik özellikleri listelenmiştir.

Tablo 2.1. pH sensörü teknik özellikleri

Tanım	Teknik Özellik
Güç Modülü	+5,0V
Modül Boyutu	43mm x 32mm
Ölçüm Aralığı	0-14pH
Sıcaklık Ölçüm Aralığı	0-60 derece
Doğruluk:	$\pm 0,1$ pH (25 santigrat derecede)
BNC konektörü	pH sensörü bağlanır
PH2.0 Arabirimi	(3-pin SMD)
Pot	Kazanç ayarı

IoT nesnesinin mikrodnetleyici modülü olan Wi-fi 802.11b/g/n standartlarını destekleyen ESP8266EX tabanlı mikrodnetleyiciler kullanılmıştır. Şekil 2.2’de modelin pin bilgileri ve görseli gösterilmiştir. Küçük boyutlu ve Arduino ile uyumlu olarak çalışabilen, düşük güç tüketen bir mikrodnetleyicidir. Bunların yanı sıra teknik özellikleri; ESP-8266EX modeli, 3,3V çalışma gerilimine, 4MB flash belleğe, 68,6 mm x 53,4 mm boyutlarına ve 25gr ağırlığa sahiptir.

Şekil 2.2. Esp8266 modüllü mikrodnetleyiciler



Cihaz Geliştirme Çalışmaları

Cihaz, ölçülen sıvının pH ve sıcaklık bilgisini kablosuz olarak internet bağlantısı üzerinden bilgisayar ortamına gönderme işlemini gerçekleştirmektedir. Cihazın kaplanmadan önceki geliştirme aşamaları Şekil 2.3’de gösterilmiştir. Cihazda kullanılan materyaller Tablo 2.2’de gösterilmiştir.

Tablo 2.1. Birinci cihazda kullanılan materyaller ve özellikleri

Materyal	Özellik ve fonksiyonu
Wemos d1 mini	Mikrodnetleyici / IoT cihazı
pH sensörü	Analog / pH değeri ölçümü
Analog-dijital dönüştürücü	Sinyal dönüştürücü / interpolasyon
DS18B20 sıcaklık sensör	Su geçirmez / sıcaklık ölçümü
Anahtar	Su geçirmez / pil kontrolü
18650 Li-on pil	3000mah / Güç ünitesi

Şekil 2.3. Geliştirme aşamaları



a) 1. aşama bağlantıları



b) 2. aşama bağlantıları



c) 3. aşama bağlantıları



d) 4. aşama bağlantıları

Deneysel Sonuçlar

Besleme ünitesi olan 3,7V 3000mah batarya, işlem döngüsü çerçevesinde yaklaşık olarak her 15 dakikada bir derin uyku moduna geçerek pil ömrünün 10 kat daha uzun ömürlü olmasını sağlamaktadır. Pil ömrü hesaplaması yapılırken Wemos d1 mini mikrodnetleyicisinin normal modda çalışırken, ağa bağlanıp verileri gönderirken ve derin uyku modunda çalışırken pilden çektiği akım ölçülmüştür. Cihazın çektiği akım normal ve derin uyku modundaki durumları Tablo 2.3'te karşılaştırılmıştır.

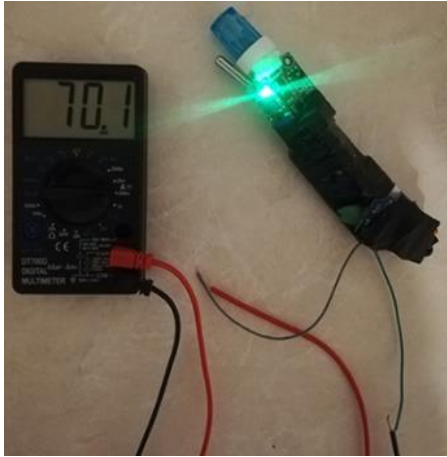
Tablo 2.2. Esp8266 modüllü mikrodnetleyici modları çalışma akımları

Wemos d1 mikrodnetleyici	Ölçülen (mah)
Derin Uyku Mod	5-6mah
Normal Mod	75-80mah

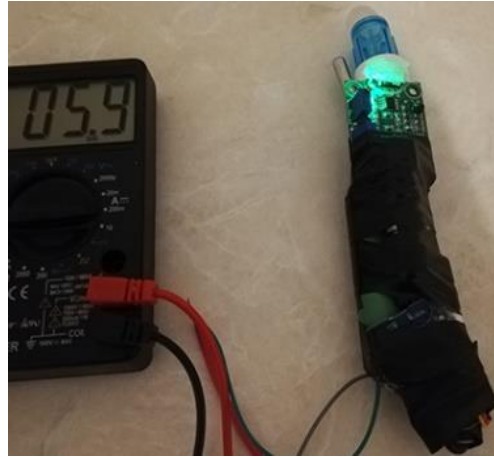
NodeMCU	Ölçülen (mah)
Derin Uyku Mod	9-10 mah
Normal Mod	110-120 mah

Cihazın bir saat içinde pilden çektiği akımı hesaplamak için hem normal modda iken hem derin uyku modunda iken çektiği akımlar ölçülerek kaydedilmiş, Şekil 2.4'te ölçümler ve Tablo 2.4'te ortalama akımlar gösterilmiştir.

Şekil 2.4. Cihazın modlarına göre akım durumları



Derin uyku mod



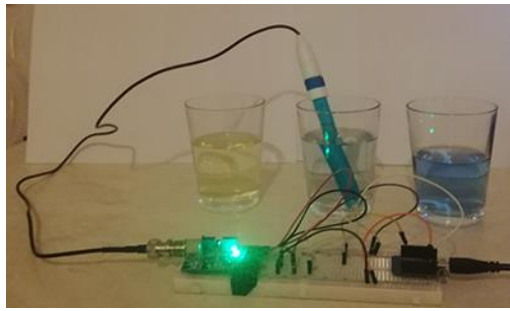
Normal mod

Tablo 2.3. Mikrodenetleyicinin ortalama harcadığı akım tablosu

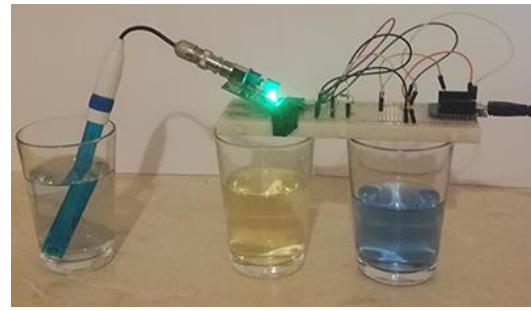
	<i>Derin Uyku Mod (mah)</i>	<i>Normal Mod (mah)</i>
<i>Her 5 dk'da bir 12 saat boyunca her saatteki düzenli akım ortalamaları ölçümleri</i>	5,9	75,7
	6,0	74,2
	5,9	73,7
	5,9	73,6
	5,9	73,6
	6,0	70,1
	5,9	70,6
	6,0	69,4
	5,9	69,5
	5,9	69,5
	6,0	70,0
		69,3
		72,2
		69,5
		71,48
<i>Ortalama</i>	5,93	

Kullanılan pH sensöründen BNC konnektörüne kadar olan sinyali taşıyan kablo uzunluğunun ölçüm sonuçlarına olan etkisi düzenli ölçümler yapılarak gözlemlenmiştir. İki aynı marka ve model pH probunun, kablo uzunluğu değiştirilerek, aynı mikrodenetleyici ve besleme üniteleriyle birlikte tasarlanmış, gönderdiği veriler kayıt altına alınmıştır. Farklı kablo uzunluklarına sahip cihazların solüsyon üzerindeki testleri Şekil 2.5'te gösterilmiştir.

Şekil 2.5. pH probu kablo uzunluk karşılaştırması



a) Kablo uzunluğu = 30cm



b) Kablo uzunluğu = 3 cm

Tüm diğer özellikleri aynı tutulan iki ayrı devrede sadece pH probundan çeviriciye gelen kablonun uzunluklarının değiştirilmesi ile gerçekleştirilen ölçümler Tablo 2.5'te gösterilmiştir.

Tablo 2.5. Farklı uzunluktaki kablolar ile gerçekleştirilen ölçümler

Ölçüm sayısı	Kablo uzunluğu 30cm (ölçülen pH)	Kablo uzunluğu 3cm (ölçülen pH)
1	6,84	6,87
2	6,85	6,85
3	6,84	6,85
4	6,89	6,81
5	6,89	6,89
6	6,84	6,84
7	6,87	6,87
8	6,87	6,89
9	6,89	6,85
10	6,85	6,87
Ortalama	6,863	6,859

*Ölçümler 150dk boyunca her 15dk'da bir yapılmıştır.

SONUÇ

7,01 pH değerindeki bir solisyonun her 15dk'da bir yaklaşık olarak 3 saatlik bir sürede alınan 10 ölçüm sonucunda pH probuna ait olan fabrika çıkışlı kablo uzunluğu ile alınan ölçümler ile kablonun 10 kat kısaltılması sonucunda alınan ölçümler karşılaştırılıp sonuçları incelenmiştir. Bu inceleme sonucunda kablonun kısaltılmış olması ölçüm doğruluğu açısından hata kabul edilebilir bir farkın oluşmadığını göstermektedir. Ölçümler oda sıcaklığında ($\approx 26^{\circ}\text{C}$) ölçülmüş olup eşit şartlarda ölçüm ortamı sağlanmıştır. Arduino uyumlu olmayan ve endüstriyel olarak üretilmiş analog pH algılayıcılarında direkt olarak kablo uzunluğu ölçümleri etkilemektedir. IoT uyumlu mikrodenetleyiciler üzerinde pH ölçümleri yapılırken seçilen algılayıcı önem taşımaktadır.

Kablonun fiziksel değişimi aşamasında kesilen uca yine aynı kalitede başka bir BNC konnektörü bağlanarak ölçümler gerçekleştirilmiştir. Farklı analog sensörler kullanıldığında, BNC konnektörün uyumsuz seçilmesi durumunda ise tutarsız pH değerlerinin alındığı gözlenmiş, ayrıca dijital çevirici üzerinde bulunan buffer ışığının yeşil ışık yerine kırmızı yandığı gözlenmiştir.

KAYNAKLAR

1. Bozdoğan, Z. (2015), Nesnelerin interneti için mimari tasarımı, Yüksek Lisans Tezi, Düzce Üniversitesi Fen Bilimleri Enstitüsü, Düzce.
2. CISCO VNI., (2023), Cisco Visual Networking Index: Forecast and Trends, 2018–2023 [online], <https://www.cisco.com/c/en/us/solutions/collateral/executive-perspectives/annual-internet-report/white-paper-c11-741490.html> [Ziyaret Tarihi: 12 Şubat 2023].
3. Gökrem L., Bozuklu M., (2016), Nesnelerin interneti: yapılan çalışmalar ve ülkemizdeki mevcut durum, *Gaziosmanpaşa Journal of Scientific Research*, 13, 47–68.
4. Keskin, B., Tutak, D. & Köse, E. (2010). Ofset Baskıda Nemlendirme Suyu Ph'nın Kalıptaki Tram Nokta Kayıplarına Etkisi. *Politeknik Dergisi*, 13 (1), 43-47.
5. Khalil E.A., Özdemir S., (2018), Nesnelerin internetine genel bir bakış: kavram, özellikler, zorluklar ve fırsatlar, *Pamukkale University Journal of Engineering Sciences*, 24 (2), 311–326.
6. Koçak, Z. (2018). İçme Suyunun Kimyasal Analiz Parametrelerinin Uzaktan Online Takibi, Gaziosmanpaşa Üniversitesi Fen Bilimleri Enstitüsü, Yüksek Lisans Tezi, Tokat.
7. Ölmez, M., Saraç, D. (2009). Su Ürünleri İçin pH'nın Önemi. *Ziraat Mühendisliği*, (353), 12-17.
8. Sözüdoğru, O., Günaslan, S. & Fil, B. A. (2022). Mezbaha Atık sularından Elektrooksidasyon Sistemi ile KOİ ve Renk Giderilmesi Üzerine pH ve Akım Yoğunluğunun Etkisi. *Avrupa Bilim ve Teknoloji Dergisi*, ICAENS May 2022, 106-110.
9. Yarba, M.M. (2019). Antalya İli Kesme Çiçek Üretim Alanlarında Görülen Bitki Paraziti Nematodlar ve Mücadelesi, Kahramanmaraş Sütçü İmam Üniversitesi Fen Bilimleri Enstitüsü, Doktora Tezi, Kahramanmaraş.

RECENT APPLICATIONS OF THERMOELECTRIC COOLING DEVICES: A REVIEW OF PERFORMANCE PARAMETERS

E. Cuce

ORCID: 0000-0003-0150-4705

P. M. Cuce

ORCID: 0000-0002-6522-7092

T. Guclu

ORCID: 0000-0002-5864-3864

ABSTRACT

Thermoelectric coolers have become a frequently preferred technology in the refrigeration industry, especially in the last decade. In general, a circuit is formed by connecting two different semiconductor materials electrically in series and thermally in parallel between two ceramic plates. When a current is applied to this circuit, one of the ceramic plate surfaces starts to heat up and the other cools. This phenomenon is called the Peltier effect, and thermoelectric coolers are also specifically called Peltier. In particular, their silent and vibration-free operation, not containing any fixed parts, and being suitable for automation are the most important reasons for preference compared to traditional cooling technologies. On the other hand, they are not ideal for large cooling loads due to their poor performance compared to conventional cooling technologies. For this reason, they are mostly preferred in portable cooling applications and low volume cooling loads such as in-car refrigerators, minibars, organ and drug transport boxes. In recent years, new models and designs have been developed to increase the performance of thermoelectric coolers. In these studies, it is generally aimed to increase the cold side performance of the thermoelectric cooler by controlling the hot side temperature. For this reason, fluid-cooled systems on the hot surface have been tried and significant improvements have been achieved in the performance of thermoelectric devices.

Keywords: Thermoelectric cooling, COP, cooling power

INTRODUCTION

Throughout the world, there is a rapid transition period from fossil-based energy sources to environmentally friendly renewable energy sources. This rapid transition is not only limited to the use of renewable energy sources instead of fossil-based energy, but also important studies are carried out to increase the efficiency of existing technologies (P. M. Cuce et al. 2021; Shoeibi et al. 2022). As a result of scientific studies, significant improvements are achieved in the efficiency of many energy sources and devices. Regarding energy efficiency, it is essential to increase the efficiency of cooling, heating, and ventilation systems, which constitute a significant part of the energy consumed worldwide. In this context, new technologies have been developed to replace systems containing environmentally harmful refrigerants, and studies continue in this area today. One of these technologies is thermoelectric devices (TEDs) (Sun et al. 2022).

In general, TEDs consist of two different semiconductor materials, P-type and N-type, arranged in thermally parallel and electrically series between two ceramic plates. TEDs can be used for cooling-heating or electricity generation according to the effect applied (Guclu and Cuce 2019). TEDs used for electricity generation are called thermoelectric generators (TEG) and work according to the so-called Seebeck effect. In this operating setup, a temperature difference is created between the surfaces of the TED and the semiconductors are connected to a circuit. As a result of the electron movement caused by the temperature difference, current is observed in the circuit (Chen et al. 2022). TEDs used for cooling are called thermoelectric coolers (TEC) and work according to the so-called Peltier Effect. When the ends of the semiconductors are connected to a circuit and current is applied to the circuit, one surface of the TEC starts to heat up and the other surface starts to cool. Thus, with the help of TEC, the cooling process is carried out by extracting heat from the environment (Fan, Rezaia, and Gao 2022). A schematic representation of a typical TED is shown in Figure 1 (Bucher and Amrouch 2022).

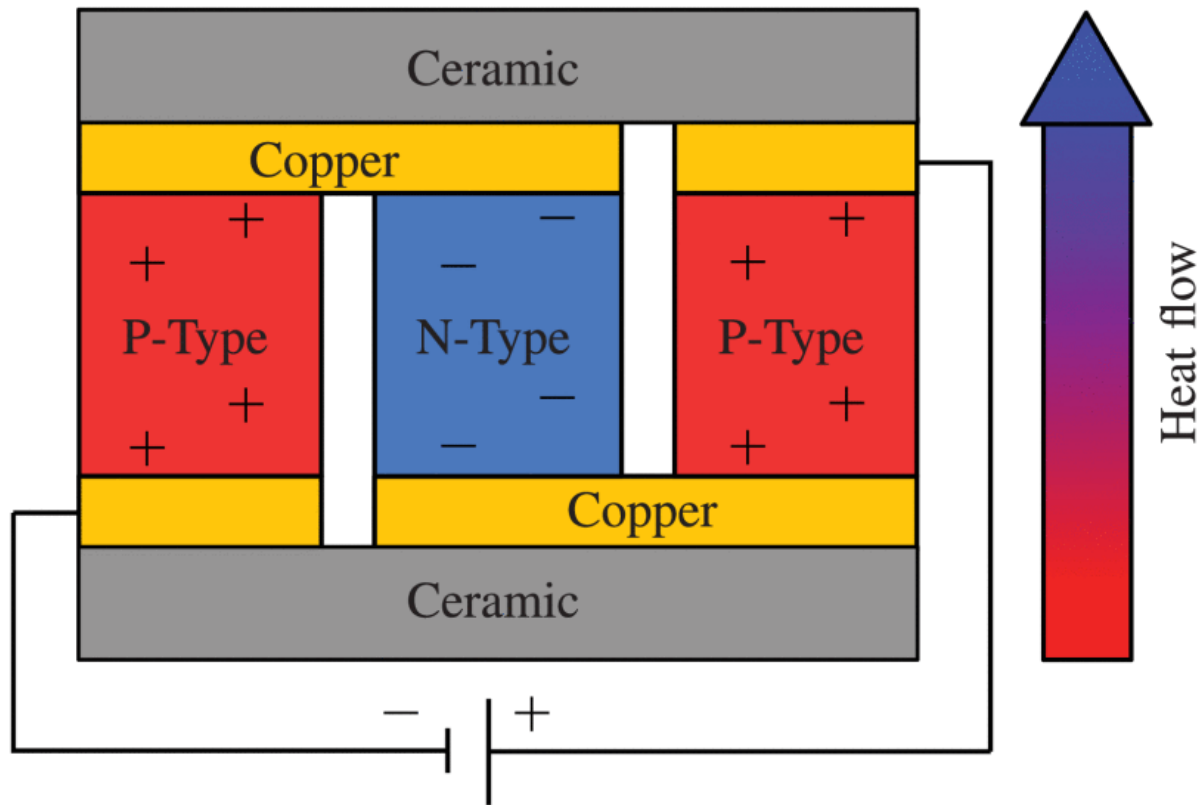


Figure 1. Schematic description of TED (Bucher and Amrouch 2022)

In addition to their long life, TEDs are vibration-free and quiet, have no moving parts, can be produced in any size and are suitable for automation. They are also suitable for applications requiring instant temperature control thanks to their fast response times (Park et al. 2022). On the other hand, since they have low coefficient of performance (COP) values compared to conventional cooling systems, they are not preferred in large scale cooling or heating applications. Applications such as microprocessor cooling, in-car refrigerators, mini bars, organ and drug transport boxes are the most preferred applications of TECs (Al-Bahrani et al. 2022). TEGs are generally used to increase efficiency in hybrid systems.

RECENT DEVELOPMENT AND APPLICATIONS

The efficiency of TEDs depends on the size of the temperature difference between the surfaces. For example, the lower the hot side temperature of TECs can be kept, the lower the cold side temperature decreases. For this reason, liquid cooling processes are applied on these surfaces in order to increase the amount of heat removed from the hot surface of the TEC (Gökçek and Şahin 2017). Cuce et al. (E. Cuce, Guclu, and Cuce 2020) investigated the effect of cooling with fluid on the hot surface on the cooling power of TECs experimentally. They aimed to further increase the amount of heat transfer by using various nanofluids instead of pure water as a refrigerant, and used various nanofluids for this purpose. According to the results obtained from the study, it was seen that the temperature difference between cold and hot surfaces could be increased up to 55% in the case of using 1% mixture ratio Al_2O_3 -water nanofluid. In another study, which is a continuation of the study, hybrid nanofluids were tested as refrigerants and it was observed that the temperature difference between hot and cold surfaces increased (Mert et al. 2022). In another study, electrical consumption values were compared, and it was observed that not only the temperature difference between hot and cold surfaces increased with the use of nanofluids, but also the temperature of the cooler cabinet decreased faster, thus reducing the electricity consumption values (P. M. Cuce, Guclu, and Cuce 2022). In recent years, hybrid systems have been created by using TEDs together with renewable energy sources, thus providing energy efficiency (Wehbi et al. 2022). Zhang et al. (Zhang, Huang, and Chen 2022) compared the performances of a single-photovoltaic (PV) system and a hybrid system consisting of PV-TEG-TEC in their numerical study. It has been observed that with the hybrid system they developed, a 3.97% increase in energy

efficiency can be achieved compared to the single-PV system. Singh et al. (Singh et al. 2022) investigated performance improvements in PV modules with a hybrid cooling system developed using phase change material (PCM) and TEC. A hybrid cooling system has been designed to prevent electrical efficiency reductions caused by overheating PV modules. PCM is used on the back surface of the PV module, and the cold surface of the TECs is contacted with the surface of the PCM. Aluminum fins were also used to remove the heat from the hot side of TCE. The results obtained from the study showed that it is possible to obtain a 19.32% increase in electrical efficiency in the case of using a hybrid cooling system. Liu et al. (Liu et al. 2022) conducted a study to monitor the thermal performance of high-temperature batteries by providing temperature control with a hybrid cooling system consisting of PCM and TECs. TECs were used to prevent PCMs from melting rapidly due to the heat absorbed from the batteries, and liquid-cooled blocks were used to remove the heat from the hot side of the TEC. The optimum fin thickness (FT) was investigated during the study by changing the fin thickness between PCM and TEC. According to the results, when the FT is increased to 8 mm, the temperature control time is extended by 12%, while the temperature difference increases by 13.7%. On the other hand, when the applied current intensity was increased up to 6A, it was observed that the temperature control time increased up to 87.42% while the COP values decreased. The optimum FT was determined as 4 mm and the optimum current intensity was determined as 3A.

CONCLUSION

TEDs are especially used in small space cooling and electronic cooling applications, thanks to their advantages such as their compact structure, suitability for automation, long-term operation without maintenance and not containing harmful fluids. On the other hand, it is a technology still under development due to its low COP values. One of the most important improvements made for this purpose is the use of liquid-cooled blocks on the hot surface. In addition, TEDs can be used with other systems to create hybrid cooling or electricity generation systems. The efficiency of hybrid systems using TEDs is better than single-systems. For this reason, its use with energy sources such as PV systems, biofuel systems, PCM-integrated systems is becoming more common day by day.

REFERENCES

1. Al-Bahrani, Mohammed, Hasan Shakir Majdi, Azher M. Abed, and Alistair Cree. 2022. "An Innovated Method to Monitor the Health Condition of the Thermoelectric Cooling System Using Nanocomposite-Based CNTs." *International Journal of Energy Research* 46(6): 7519–28.
2. Bucher, Tim, and Hussam Amrouch. 2022. "Modeling TPU Thermal Maps Under Superlattice Thermoelectric Cooling." *IEEE Access* 10: 21970–78.
3. Chen, Wen Yi, Xiao Lei Shi, Jin Zou, and Zhi Gang Chen. 2022. "Thermoelectric Coolers for On-Chip Thermal Management: Materials, Design, and Optimization." *Materials Science and Engineering R: Reports* 151(August): 100700.
4. Cuce, Erdem, Tamer Guclu, and Pinar Mert Cuce. 2020. "Improving Thermal Performance of Thermoelectric Coolers (TECs) through a Nanofluid Driven Water to Air Heat Exchanger Design: An Experimental Research." *Energy Conversion and Management* 214(February): 112893. <https://doi.org/10.1016/j.enconman.2020.112893>.
5. Cuce, Pinar Mert, Erdem Cuce, Tamer Guclu, and Veysel Demirci. 2021. "Energy Saving Aspects of Green Facades: Current Applications and Challenges." *Green Building & Construction Economics*: 1–11.
6. Cuce, Pinar Mert, Tamer Guclu, and Erdem Cuce. 2022. "The Effect of Nanofluid Usage on Electricity Consumption in Thermoelectric Refrigeration Application: An Experimental Study." *GAZİ JOURNAL OF ENGINEERING SCIENCES* 8: 228–36.
7. Fan, Shifa, Alireza Rezaei, and Yuanwen Gao. 2022. "Thermal-Electric and Stress Analysis of Thermoelectric Coolers under Continuous Pulse Input Current." *Applied Thermal Engineering* 214(February): 118910.
8. Gökçek, Murat, and Fatih Şahin. 2017. "Experimental Performance Investigation of Minichannel Water Cooled-Thermoelectric Refrigerator." *Case Studies in Thermal Engineering* 10(February): 54–

- 62.
9. Guclu, Tamer, and Erdem Cuce. 2019. "Thermoelectric Coolers (TECs): From Theory to Practice." *Journal of Electronic Materials* 48(1): 211–30.
10. Liu, Xun et al. 2022. "Thermal Performance of Battery Thermal Management System Using Fins to Enhance the Combination of Thermoelectric Cooler and Phase Change Material." *Applied Energy* 322(May): 119503. <https://doi.org/10.1016/j.apenergy.2022.119503>.
11. Mert, Pinar et al. 2022. "Effect of Using Hybrid Nanofluids as a Coolant on the Thermal Performance of Portable Thermoelectric Refrigerators." *Sustainable Energy Technologies and Assessments* 53(PC): 102685. <https://doi.org/10.1016/j.seta.2022.102685>.
12. Park, Sang J. et al. 2022. "Adaptive Thermoelectric Cooling System for Energy-Efficient Local and Transient Heat Management." *Applied Thermal Engineering* 216(March): 119060.
13. Shoeibi, Shahin et al. 2022. "A Review on Using Thermoelectric Cooling, Heating, and Electricity Generators in Solar Energy Applications." *Sustainable Energy Technologies and Assessments* 52(PB): 102105.
14. Singh, Deeksha et al. 2022. "Performance Improvement of Solar PV Module through Hybrid Cooling System with Thermoelectric Coolers and Phase Change Material." *Solar Energy* 241(April): 538–52. <https://doi.org/10.1016/j.solener.2022.06.028>.
15. Sun, Wei, Wei Di Liu, Qingfeng Liu, and Zhi Gang Chen. 2022. "Advances in Thermoelectric Devices for Localized Cooling." *Chemical Engineering Journal* 450(P4): 138389.
16. Wehbi, Zahra et al. 2022. "Hybrid Thermoelectric Generators-Renewable Energy Systems: A Short Review on Recent Developments." *Energy Reports* 8(May): 1361–70. <https://doi.org/10.1016/j.egyr.2022.08.068>.
17. Zhang, Xiaona, Yewu Huang, and Zhuo Chen. 2022. "A Hybrid System Integrating Photovoltaic Module and Thermoelectric Devices for Power and Cooling Cogeneration." *Solar Energy* 239(May): 350–58. <https://doi.org/10.1016/j.solener.2022.05.011>.

THE EFFECT OF PELTIER POSITION ON COOLING PERFORMANCE IN THERMOELECTRIC COOLERS

E. Cuce

ORCID: 0000-0003-0150-4705

P. M. Cuce

ORCID: 0000-0002-6522-7092

T. Guclu

ORCID: 0000-0002-5864-3864

ABSTRACT

Thermoelectric devices have significant advantages such as silent and vibration-free operation, long life, no moving parts, being suitable for automation and compact structure. Thanks to these advantages, it is a frequently preferred method, especially for small-scale cooling and heating loads. Thermoelectric devices are formed by connecting P and N-type semiconductors electrically in series and thermally in parallel between two ceramic plates and work with the so-called Peltier and Seebeck effect. If a circuit is formed with two different semiconductors and an electric current is applied, one surface of the semiconductor starts to heat up and the other surface starts to cool. This phenomenon is called the Peltier effect and constitutes the working principle of thermoelectric coolers. Likewise, if no current is applied to the circuit and a temperature difference is created between the surfaces, a current rise is observed in the circuit. This effect is called the Seebeck effect and forms the working principle of thermoelectric generators. The COP values of thermoelectric coolers are low compared to conventional cooling systems. Therefore, they are not suitable for large cooling loads. In recent years, studies have been carried out to increase the performance of these devices. In this study, the effect of the Peltier position on cooling performance in thermoelectric coolers will be investigated experimentally. For this purpose, a small-volume insulated cabinet was selected and its performance was observed by placing the Peltier assembly on the top and bottom surfaces of the cabinet.

Keywords: Thermoelectric cooling, COP, cooling power

INTRODUCTION

Thermoelectric devices (TEDs) are devices that provide thermal energy using electrical energy or generate electrical energy by utilizing the temperature difference (Sajid, Hassan, & Rahman, 2017). Generally, the structure of TEDs consists of P-type and N-type semiconductor materials arranged between two ceramic plates. TEDs are divided into two groups; thermoelectric generators (TEGs) and thermoelectric coolers (TECs) (Zhao & Tan, 2014). TEGs work according to the called Seebeck effect. The seebeck effect, if a temperature difference is created between the surfaces and the ends of the semiconductors are connected to a circuit, a current is seen in the circuit (Champier, 2017). TECs, on the other hand, work according to the Peltier effect, which is the opposite of this effect, and these devices are also called Peltier. In the Peltier effect, if the ends of the semiconductors arranged between two ceramic plates are connected to a circuit and current is applied, one of the surfaces starts to cool and the other to heat up. Thus, cooling processes are carried out with the help of the cold side (Guclu & Cuce, 2019). The schematic representation of a typical Peltier is as in Figure 1 (URL-1).

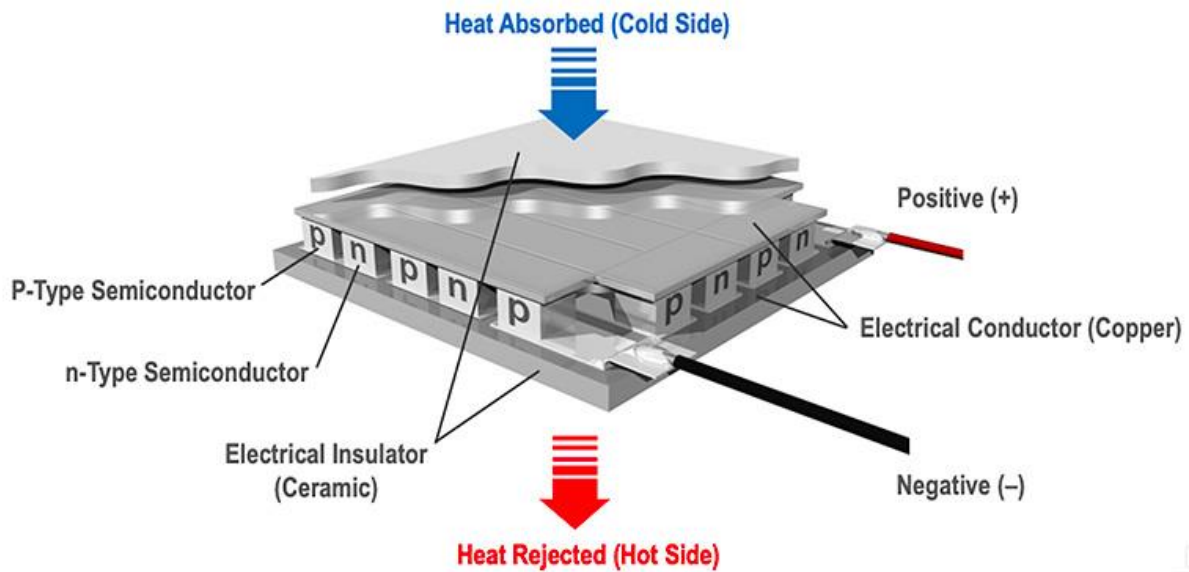


Figure 1. Schematic description of Peltier (URL-1).

As for the advantages of thermoelectric coolers, they are quiet and still, compact in structure, suitable for automation, and long-lasting and low maintenance costs (Yu & Wang, 2009). In addition, TECs are used in a wide range of areas, such as mini refrigerators, in-car coolers, drug transport boxes, electronic cooling, and military and space research (Choi, Han, Cho, & Lee, 2018). On the other hand, TECs have low COP values when compared to conventional cooling systems (Hermes & Barbosa, 2012). For this reason, studies to increase the performance of TECs continue. In this context, one of the methods applied is to apply liquid cooling on this surface in order to keep the hot side temperature of the Peltier at lower values (E. Cuce, Guclu, & Cuce, 2020; P. M. Cuce, Guclu, & Cuce, 2022; Mert, Cuce, Guclu, Shaik, & Alshahrani, 2022). In this study, the effect of the Peltier position on the cooling power of a small-volume thermoelectric refrigerator is investigated. For this purpose, a mini refrigerator was designed, and manufactured and experimental studies were carried out.

MATERIAL AND METHOD

During the experiments, a cabinet with a 3.5 L internal volume made of 60 mm thick insulation material was used as the cooling cabinet. A 12 V 4 A Peltier was used by combining aluminum fins on its hot and cold surfaces. A fan is used on the hot side fin to remove the heat faster. In order to better observe the effects of natural convection and Peltier position, no fan was used on the cold surface. The Peltier assembly is placed in the cabinet through the space opened in the middle of one surface of the cooler cabinet. Four K-type thermocouples were used to measure cold and hot surface temperatures, outdoor and indoor temperatures. The experimental setup is shown in Figure 2 and schematic description is shown in Figure 3.



Figure 2. Experimental setup

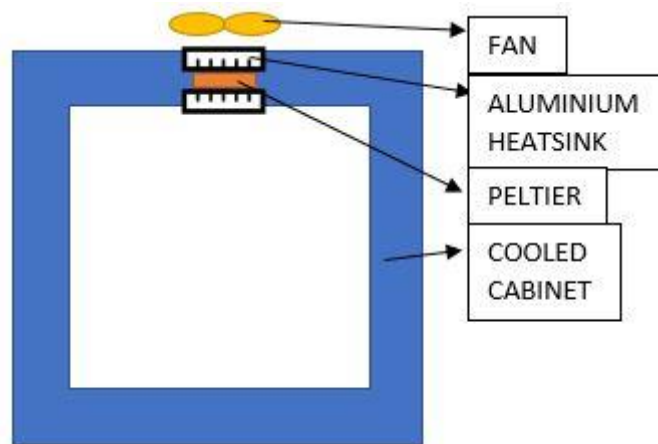


Figure 3. Schematic description

After the experimental setup was prepared, the cooling cabinet was positioned so the Peltier setup was on the upper side and the measurements started. Then, the cooler cabinet was turned upside down and measurements were taken again while the Peltier assembly was in the lower position of the cabinet. The experiments were carried out under the same conditions and outdoor temperature. Experiment times were determined as the steady state of the cold heatsink temperature.

CONCLUSION

In this study, the effect of the Peltier position on cabinet cooling performance was investigated in a small-volume thermoelectric refrigerator. For this purpose, a cooling cabinet made of 60 mm thick insulation material was used. The Peltier assembly was operated in two different situations, with the lower and upper surfaces of the cooling cabinet, and the results were compared.

First, measurements were taken with the Peltier assembly in the upper position. After 2400 seconds, it was observed that the temperature of the cooler cabin decreased from 24.8 °C to 17.7 °C. Meanwhile, the cold-side heatsink temperature converged to -3.5 degrees. The results obtained are shown in Figure 4.

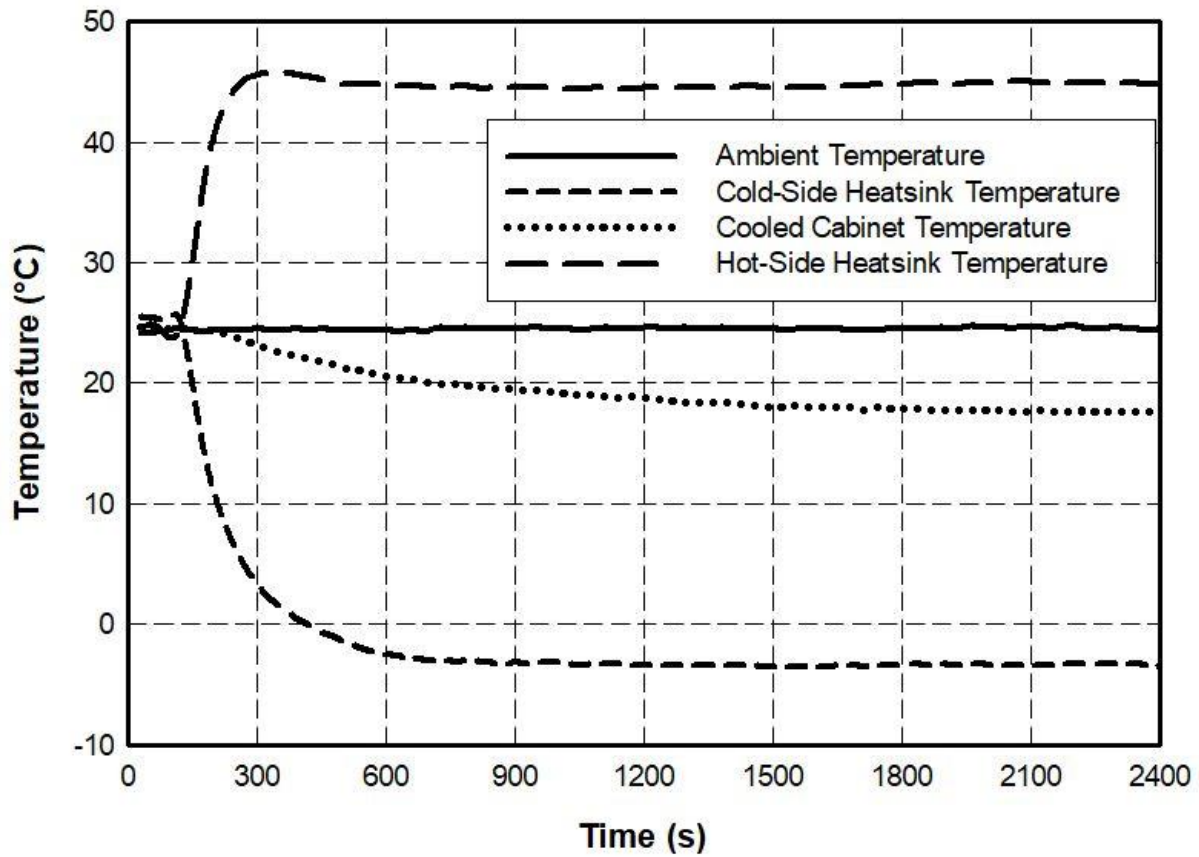


Figure 4. Temperature values when the Peltier is in the upper position.

Then, the Peltier assembly was adjusted to the lower position of the cooling cabinet and tested under the same conditions for the same time. At the end of 2400 seconds, it was observed that the temperature of the cooling cabinet decreased from 25 °C to 21.5 °C, and the temperature of the cold-side heatsink from 30 C to -4.7 °C as shown in Figure 5.

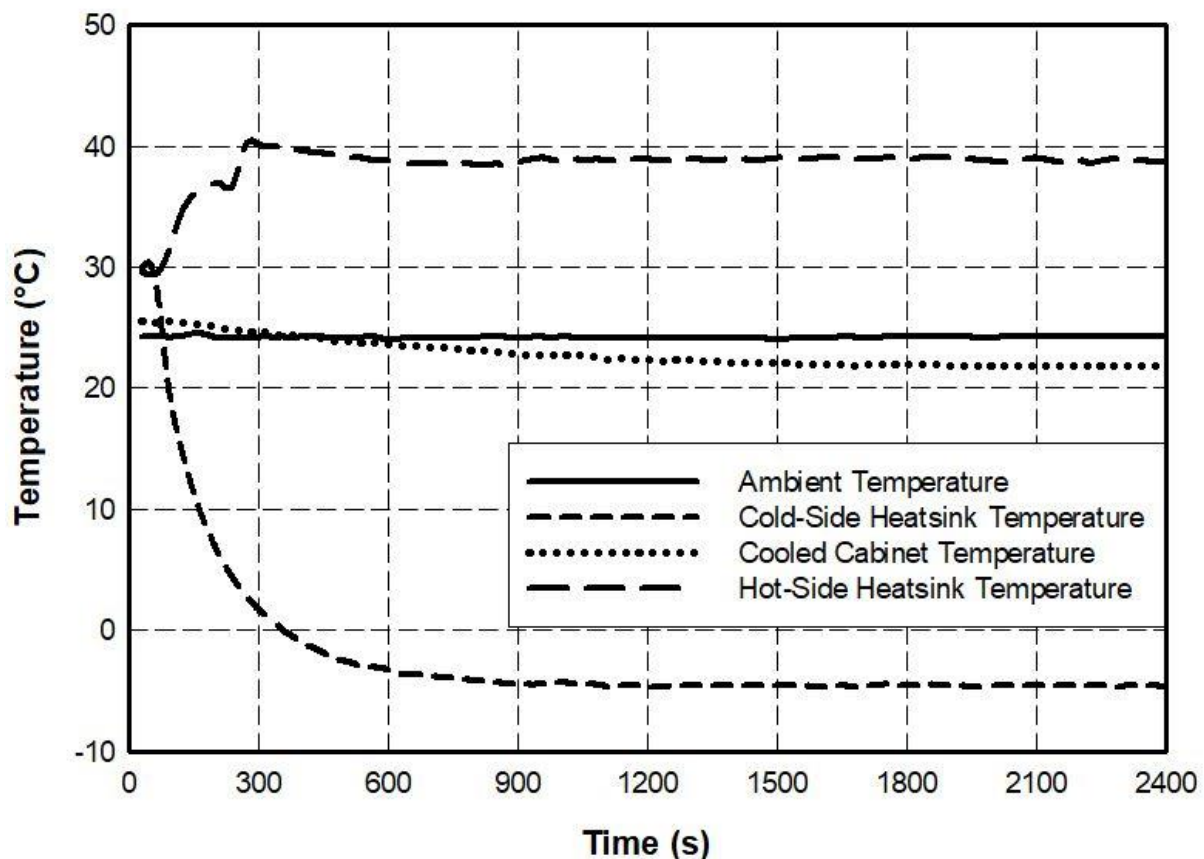


Figure 5. Temperature values when the Peltier is in the lower position.

It has been observed that in the upper position of the Peltier, the cooled ambient temperature reaches 3.8 °C lower values at the end of the same period compared to the lower position. The results obtained from the study showed that the Peltier position has an effect on the cooling performance when the forced air movement is not applied with a fan on the cold surface in thermoelectric refrigerator applications.

REFERENCES

- Champier, D. (2017). Thermoelectric generators: A review of applications. *Energy Conversion and Management*, 140, 167–181. <https://doi.org/10.1016/j.enconman.2017.02.070>
- Choi, S., Han, U., Cho, H., & Lee, H. (2018). Review: Recent advances in household refrigerator cycle technologies. *Applied Thermal Engineering*, 132, 560–574. <https://doi.org/10.1016/j.applthermaleng.2017.12.133>
- Cuce, E., Guclu, T., & Cuce, P. M. (2020). Improving thermal performance of thermoelectric coolers (TECs) through a nanofluid driven water to air heat exchanger design: An experimental research. *Energy Conversion and Management*, 214(February), 112893. <https://doi.org/10.1016/j.enconman.2020.112893>
- Cuce, P. M., Guclu, T., & Cuce, E. (2022). The Effect of Nanofluid Usage on Electricity Consumption in Thermoelectric Refrigeration Application: An Experimental Study. *GAZİ JOURNAL OF ENGINEERING SCIENCES*, 8, 228–236. <https://doi.org/10.30855/gmbd.0705006>
- Guclu, T., & Cuce, E. (2019). Thermoelectric Coolers (TECs): From Theory to Practice. *Journal of Electronic Materials*, 48(1), 211–230. <https://doi.org/10.1007/s11664-018-6753-0>
- Hermes, C. J. L., & Barbosa, J. R. (2012). Thermodynamic comparison of Peltier, Stirling, and vapor compression portable coolers. *Applied Energy*, 91(1), 51–58. <https://doi.org/10.1016/j.apenergy.2011.08.043>
- Mert, P., Cuce, E., Guclu, T., Shaik, S., & Alshahrani, S. (2022). Effect of using hybrid nanofluids as a coolant on the thermal performance of portable thermoelectric refrigerators. *Sustainable Energy*

- Technologies and Assessments*, 53(PC), 102685. <https://doi.org/10.1016/j.seta.2022.102685>
8. Sajid, M., Hassan, I., & Rahman, A. (2017). An overview of cooling of thermoelectric devices. *Renewable and Sustainable Energy Reviews*, 78(October 2015), 15–22. <https://doi.org/10.1016/j.rser.2017.04.098>
 9. URL-1. (n.d.). Retrieved from <https://www.medicaldesignandoutsourcing.com/thermoelectric-cooler-solutions-for-medical-applications/>
 10. Yu, J., & Wang, B. (2009). Enhancing the maximum coefficient of performance of thermoelectric cooling modules using internally cascaded thermoelectric couples. *International Journal of Refrigeration*, 32(1), 32–39. <https://doi.org/10.1016/j.ijrefrig.2008.08.006>
 11. Zhao, D., & Tan, G. (2014). A review of thermoelectric cooling: Materials, modeling and applications. *Applied Thermal Engineering*, 66(1–2), 15–24. <https://doi.org/10.1016/j.applthermaleng.2014.01.074>

ANOMALİ TESPİTİ TEKNİKLERİ VE UYGULAMA ALANLARI ANOMALY DETECTION TECHNIQUES AND APPLICATIONS

Ayhan Dükkancı

ORCID: 0000-0003-1196-2072

Ismail Kırbaş

ORCID: 0000-0002-1206-8294

ÖZET

Anomali tespiti, geçmiş yüzyılın başlarından itibaren araştırılmaya başlanmış ve günümüzde yapay zeka algoritmalarında meydana gelen gelişmeler ile birlikte çeşitli uygulama alanlarında daha kapsamlı yer almaya başlamış bir konudur. Bu alanda birçok teknik belirli alanlar için özel olarak geliştirilmişken diğerleri daha geneldir. Konuyla ilgili araştırmaya yapılandırılmış bir genel bakış sağlayan anomali tespiti üzerine bir derleme yapılmıştır. Mevcut teknikler, her bir teknik tarafından benimsenen temel yaklaşıma dayalı olarak farklı kategorilerde gruplandırılmıştır. Her kategori için, teknikler tarafından normal ve anormal davranış arasında ayırım yapmak için kullanılan temel varsayımlar belirtilmiştir. Bu varsayımlar, etkinliğini değerlendirmek için belirli bir alana bir teknik uygularken kılavuz olarak kullanılabilir. Çalışmada her kategori için temel bir anomali saptama teknikleri açıklanmış ve o kategoride var olan farklı tekniklerin temel tekniğin varyantları oldukları gösterilmiştir. Ek olarak, anomali tespit tekniklerinin uygulama alanları için zorlukları tanımlanmıştır. Bu çalışmada ayrıca, gerçek dünya uygulama alanlarında önemli bir sorun olan tekniklerin hesaplama karmaşıklığından da bahsedilmiştir. Bu derleme çalışmasında, konuyla ilgili temel bilgi verilmesi amaçlanarak farklı alanlarda nasıl uygulanabileceğinin daha iyi anlaşılmasının sağlanacağı umulmaktadır.

Anahtar kelimeler: anomali tespiti, aykırı değer tespiti, makine öğrenmesi, sinyal işleme

ABSTRACT

Anomaly detection is a subject that has been started to be researched since the beginning of the last century and has begun to take a more comprehensive place in various application areas with the developments in artificial intelligence algorithms today. Many techniques in this area have been developed specifically for specific areas, while others are more general. A review was made on anomaly detection, which provides a structured overview of the research on the subject. The available techniques are grouped into different categories based on the basic approach taken by each technique. For each category, the main assumptions used by the techniques to distinguish between normal and abnormal behavior are specified. These assumptions can be used as a guide when applying a technique to a particular area to evaluate its effectiveness. In the study, a basic anomaly detection techniques were explained for each category and it was shown that the different techniques in that category were variants of the basic technique. In addition, the difficulties for the application areas of anomaly detection techniques are defined. In this study, the computational complexity of the techniques, which is an important problem in real world application areas, is also mentioned. In this review study, it is hoped that it will provide a better understanding of how it can be applied in different fields by aiming to give basic information about the subject.

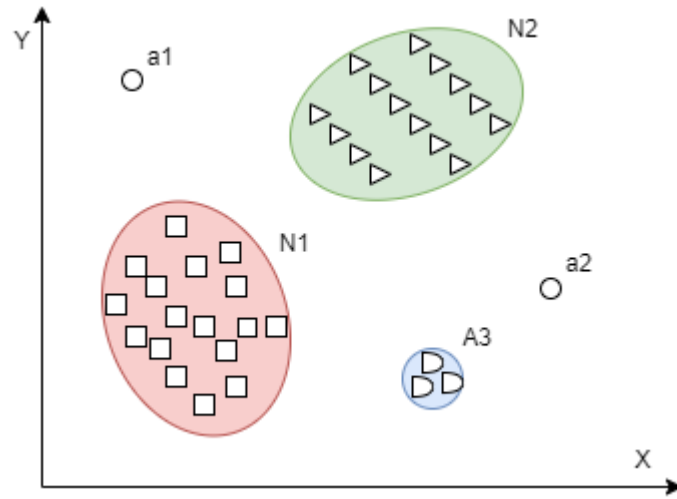
Keywords: anomaly detection, machine learning, outlier detection, signal processing

GİRİŞ

Anomali tespiti, verilerde beklenen davranışa uymayan kalıpları bulma problemini ifade eder. Bu uyumsuz modeller genellikle farklı uygulama alanlarında anomaliler, anormallikler, aykırı değerler, uyumsuz gözlemler, istisnalar, sapmalar, sürprizler, tuhaflıklar veya kirleticiler olarak adlandırılır. Bunlardan anomaliler ve aykırı değerler, anomali tespiti bağlamında en sık kullanılan iki terimdir. Anomali tespiti, kredi kartları, sigorta veya sağlık hizmetleri için dolandırıcılık tespiti, siber güvenlik için izinsiz giriş tespiti, güvenlik açısından kritik sistemlerde arıza tespiti, endüstriyel sistem ve makinelerde üretim hataları, arıza kestirimi ve düşman faaliyetleri için askeri gözetim gibi çok çeşitli uygulamalarda geniş kullanım alanı bulmaktadır. Anomali tespitinin önemi, verilerdeki anormalliklerin çok çeşitli uygulama alanlarında önemli ve genellikle kritik, eyleme geçirilebilir bilgilere dönüşmesi gerçeğinden kaynaklanmaktadır.

Örneğin, bir bilgisayar ağındaki anormal bir trafik modeli, saldırıya uğramış bir bilgisayarın hassas verileri yetkisiz bir hedefe gönderdiği anlamına gelebilir (Kumar 2005). Anormal bir MRI görüntüsü, kötü huylu tümörlerin varlığını gösterebilir (Spence, Parra, ve Sajda 2001). Kredi kartı işlem verilerindeki anormallikler, kredi kartı veya kimlik hırsızlığına işaret edebilir (Aleskerov', t.y.). Bir uzay aracı sensöründen gelen anormal okumalar, uzay aracının bazı bileşenlerinde bir arızaya işaret edebilir (Fujimaki, Yairi, ve Machida 2005). Verilerdeki aykırı değerlerin veya anormalliklerin saptanması, istatistik camiasında 19. yüzyılın başlarında incelenmiştir (Stigler 1978). Zamanla, çeşitli araştırma topluluklarında çeşitli anomali tespit teknikleri geliştirilmiştir. Bu tekniklerin çoğu, belirli uygulama alanları için özel olarak geliştirilmiştir, diğerleri ise daha geneldir. Bu çalışma, anormallik tespitine ilişkin araştırmaya yapılandırılmış ve kapsamlı bir genel bakış sağlamaya çalışır. Bu konuda araştırmaların yapıldığı farklı yönlerin ve bir alanda geliştirilen tekniklerin başlangıçta amaçlanmayan alanlarda nasıl uygulanabileceğinin daha iyi anlaşılmasını kolaylaştıracakı umulmaktadır.

Anomaliler, iyi tanımlanmış bir normal davranış kavramına uymayan verilerdeki kalıplardır. Şekil 1, basit bir iki boyutlu veri setindeki anormallikleri göstermektedir. Verilerin N1 ve N2 olmak üzere iki normal bölgesi vardır, çünkü çoğu gözlem bu iki bölgede yer alır. Bu bölgelerden yeterince uzakta olan noktalar, örneğin a1 ve a2 noktaları ve A3 bölgesindeki noktalar anomali'dir.



Şekil 1. İki boyutlu bir veri setindeki basit bir anomali örneği.

Verilerde anormallikler, örneğin kredi kartı dolandırıcılığı, siber izinsiz giriş, terörist faaliyet veya bir sistemin bozulması gibi kötü niyetli faaliyetler gibi çeşitli nedenlerle ortaya çıkabilir, ancak tüm nedenlerin ortak özelliği, analist için ilgi çekici olmalarıdır.

Anomalilerin ilginçliği veya gerçek yaşamla ilgili olması, anomali tespitinin önemli bir özelliğidir. Anomali algılama, gürültü giderme ile ilişkilidir, ancak bundan farklıdır (Tang vd. 2002) ve gürültü uyumu (Rousseeuw ve Leroy 1987), her ikisi de verilerdeki istenmeyen gürültüyle ilgilenir. Gürültü, verilerde analistin ilgisini çekmeyen ancak veri analizine engel teşkil eden bir fenomen olarak tanımlanabilir ve gürültü giderme, herhangi bir veri analizi yapılmadan önce istenmeyen nesnelerin çıkarılması ihtiyacından kaynaklanır. Gürültü uyumu, anormal gözlemlere karşı istatistiksel bir model tahmininin bağışlaştırılması anlamına gelir (Huber 1981).

Anomali tespiti ile ilgili bir diğer konu da yenilik tespitidir (Markou ve Singh 2003), örneğin bir haber grubundaki yeni bir tartışma konusu gibi verilerde daha önce gözlemlenmemiş (ortaya çıkan, yeni) kalıpları tespit etmeyi amaçlar.

Yeni modeller ve anormallikler arasındaki fark, yeni modellerin tipik olarak tespit edildikten sonra normal modele dahil edilmesidir. Bu ilgili sorunlara yönelik çözümlerin genellikle anomali tespiti için kullanıldığı ve bunun tersinin de dikkate alınması gerekir ve bu nedenle bu incelemede de tartışılmaktadır.

Anomaliler, beklenen normal davranışa uymayan bir model olarak tanımlanır. Bu nedenle, basit bir anomali tespit yaklaşımı, normal davranışı temsil eden bir bölge tanımlamak ve bu normal bölgeye ait olmayan

verilerdeki herhangi bir gözlemi bir anormallik olarak beyan etmektir. Ancak birkaç faktör, görünüşte basit olan bu yaklaşımı çok zorlaştırıyor:

Mümkün olan her normal davranışı kapsayan normal bir bölge belirlemek çok zordur. Ek olarak, normal ve anormal davranış arasındaki sınır genellikle kesin değildir. Bu nedenle, sınıra yakın bir anormal gözlem aslında normal olabilir ve bunun tersi de geçerlidir.

Anormallikler kötü niyetli eylemlerin sonucu olduğunda, kötü niyetli düşmanlar genellikle anormal gözlemlerin normal görünmesini sağlamak için kendilerini uyarlayabilir ve böylece normal davranışı tanımlama görevini daha zor hale getirir.

Birçok alanda normal davranış gelişmeye devam ediyor ve mevcut bir normal davranış kavramı gelecekte yeterince temsil edilemeyebilir.

Anomali kavramı, farklı uygulama alanları için farklıdır. Örneğin, tıp alanında normalden küçük bir sapma (örneğin, vücut sıcaklığındaki dalgalanmalar) bir anormallik olabilirken, borsa alanında benzer bir sapma (örneğin, bir hisse senedinin değerindeki dalgalanmalar) normal olarak kabul edilebilir. Bu nedenle, bir alanda geliştirilen bir tekniği diğerine uygulamak kolay değildir.

Anomali tespit teknikleri tarafından kullanılan modellerin eğitimi/doğrulanması için etiketlenmiş verilerin mevcudiyeti genellikle önemli bir sorundur.

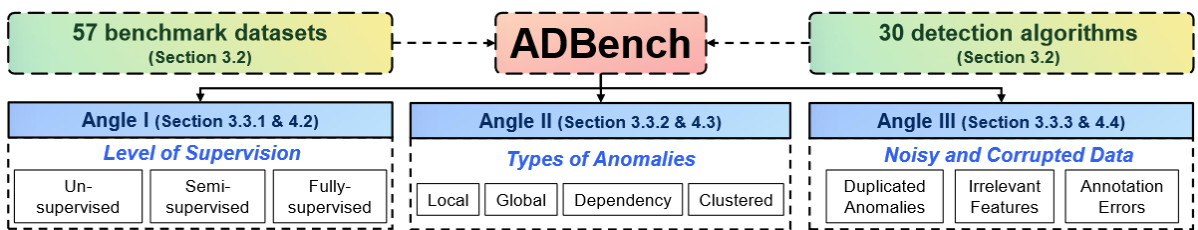
Genellikle veriler, gerçek anomalilere benzer olma eğiliminde olan ve bu nedenle ayırt edilmesi ve ortadan kaldırılması zor olan gürültü içerir.

Bu zorluklar nedeniyle, en genel şekliyle anomali tespit probleminin çözülmesi kolay değildir. Aslında, mevcut anormallik tespit tekniklerinin çoğu, sorunun belirli bir formülasyonunu çözer. Formülasyon, verilerin doğası, etiketlenmiş verilerin mevcudiyeti, tespit edilecek anormalliklerin türü ve benzeri gibi çeşitli faktörler tarafından tetiklenir. Genellikle bu faktörler, anormalliklerin tespit edilmesi gereken uygulama alanı tarafından belirlenir. Araştırmacılar, istatistik, makine öğrenimi, veri madenciliği, bilgi teorisi, spektral teori gibi farklı disiplinlerden kavramları benimsemiş ve bunları belirli problem formülasyonlarına uygulamışlardır.

Bu sınırlamaları ele almak için, ADBench adlı en kapsamlı tablosal anormallik algılama karşılaştırmalı değerlendirmesini tasarlamışlardır. Sektördeki hem araştırma ihtiyaçlarını hem de dağıtım gereksinimlerini analiz ederek, deneyleri anormallik tespitinde üç ana kategoride ele almışlardır. Şekil 2, ADBench'e genel bir bakış sunar.

Şekil 2. ADBench'in tasarımı.(Han vd., t.y.)

Anomali Kategorileri



Anomali tipi bir anormallik saptama tekniğinin önemli bir yönü, istenen anomalinin doğasıdır. Anomaliler aşağıdaki üç kategoride sınıflandırılabilir:

Nokta Anomalileri: Tek bir veri örneği, verilerin geri kalanına göre anormal olarak kabul edilebilirse, bu örnek bir nokta anomalisi olarak adlandırılır. Bu, en basit anomali türüdür ve anomali tespiti üzerine yapılan araştırmaların çoğunun odak noktasıdır.

Örneğin, Şekil 1'de a1 ve a2 noktaları ile A3 bölgesindeki noktalar normal bölgelerin sınırlarının dışında yer alır ve bu nedenle normal veri noktalarından farklı oldukları için nokta anomalileridir.

Bağlamsal Anomaliler: Bir veri örneği, belirli bir bağlamda anormalse, ancak başka türlü değilse, o zaman bağlamsal anormallik olarak adlandırılır (koşullu anormallik olarak da anılır)(Chandola, Banerjee, ve Kumar 2009).

Bağlam kavramı, veri kümesindeki yapı tarafından tetiklenir ve problem formülasyonunun bir parçası olarak belirtilmesi gerekir. Her veri örneği, aşağıdaki iki özellik kümesi kullanılarak tanımlanır:

(1) Bağlamsal nitelikler. Bağlamsal nitelikler, söz konusu örnek için bağlamı (veya mahalleyi) belirlemek için kullanılır. Örneğin, mekansal veri kümelerinde, bir konumun boylamı ve enlemi bağlamsal niteliklerdir. Zaman serisi verilerinde zaman, bir örneğin tüm dizi üzerindeki konumunu belirleyen bağlamsal bir özneliktir.

(2) Davranışsal özellikler. Davranışsal nitelikler, bir örneğin bağlamsal olmayan özelliklerini tanımlar. Örneğin, tüm dünyanın ortalama yağışını açıklayan bir mekansal veri setinde, herhangi bir yerdeki yağış miktarı davranışsal bir özelliktir.

Kolektif Anomaliler: İlgili veri örneklerinden oluşan bir koleksiyon, tüm veri setine göre anormal ise, buna toplu anormali denir. Kolektif bir anomalideki bireysel veri örnekleri, kendi başlarına anormal olmayabilir, ancak bunların bir koleksiyon olarak bir arada bulunmaları anormaldir.

Şekil 3, bir insan elektrokardiyogram çıktısını gösteren bir örnektir (Song vd. 2007). Vurgulanan bölge bir anormalliği gösterir çünkü aynı düşük değer anormal derecede uzun bir süre boyunca mevcuttur (bir Atriyal Erken Kasılmaya karşılık gelir). Bu düşük değer kendi başına bir anormallik değildir.

Şekil 3. Bir insan elektrokardiyogram çıktısında Atriyal Erken Kasılmaya karşılık gelen toplu anormali.

Anomali Tespit Yöntemleri

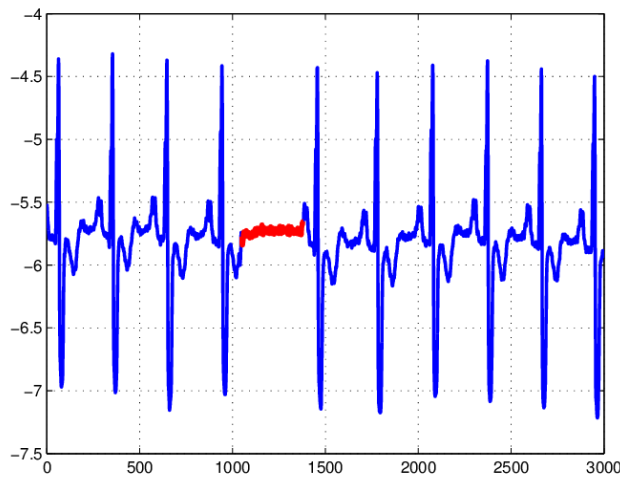
Bir veri örneğiyle ilişkilendirilen etiketler, o örneğin normal mi yoksa anormal mi olduğunu belirtir. Doğru ve her tür davranış temsil eden etiketli verileri elde etmenin genellikle engelleyici derecede pahalı olduğu unutulmamalıdır. Etiketleme genellikle bir insan uzman tarafından manuel olarak yapılır ve bu nedenle etiketlenmiş eğitim veri setini elde etmek için önemli çaba gerekir. Tipik olarak, tüm olası anormal davranış türlerini kapsayan etiketlenmiş bir anormal veri örnekleri seti elde etmek, normal davranış için etiketler almaktan daha zordur. Ayrıca, anormal davranış doğası gereği genellikle dinamiklidir; örneğin, etiketli eğitim verisi olmayan yeni tip anormallikler ortaya çıkabilir.

Hava trafik güvenliği gibi belirli durumlarda, anormal durumlar katastrofik olaylara dönüşebilir ve bu nedenle çok nadirdir.

Etiketlerin ne ölçüde mevcut olduğuna bağlı olarak, anormallik algılama teknikleri aşağıdaki üç moddan birinde çalışabilir:

Denetimli Anormallik Tespiti (Supervised Anomaly Detection)

Denetimli modda eğitilen teknikler, normal ve anormal sınıfları için örnekleri etiketleyen bir eğitim veri setinin kullanılabilir olduğunu varsayar. Bu gibi durumlarda tipik bir yaklaşım, normale karşı anormal sınıfları için tahmine dayalı bir model oluşturmaktır. Herhangi bir görünmeyen veri örneği, hangi sınıfa ait olduğunu belirlemek için modelle karşılaştırılır.



Denetimli anormallik tespitinde ortaya çıkan iki ana sorun vardır.

İlk olarak, eğitim verilerindeki anormal örnekler normal örneklerle kıyasla çok daha azdır. Dengesiz sınıf dağılımları nedeniyle ortaya çıkan sorunlar, veri madenciliği ve makine öğrenimi literatüründe ele alınmıştır (Joshi ve Agarwal, t.y.; Phua, Alahakoon, ve Lee, t.y.; Vilalta ve Sheng Ma 2002).

İkincisi, özellikle anomali sınıfı için doğru ve temsili etiketler elde etmek genellikle zordur. Etiketli bir eğitim veri seti elde etmek için normal bir veri setine yapay anormallikler enjekte eden bir dizi teknik önerilmiştir (Theiler ve Cai 2003; Abe, Kearns, ve Sato 2006; Steinwart, Hush, ve Scovel, t.y.). Bu iki sorun dışında, denetlenen anormallik algılama sorunu, tahmine dayalı modeller oluşturmaya benzer.

Yarı Denetimli Anormallik Tespiti (Semi Supervised Anomaly Detection): Yarı denetimli modda çalışan teknikler, eğitim verilerinin yalnızca normal sınıf için örneklerini etiketlediğini varsayar. Anomali sınıfı için etiket gerektirmedikleri için denetimli tekniklerden daha yaygın olarak uygulanabilirler.

Örneğin, uzay aracı arıza tespitinde, bir anormallik senaryosu, modellenmesi kolay olmayan bir kazaya işaret eder. Bu tür tekniklerde kullanılan tipik yaklaşım, normal davranışa karşılık gelen sınıf için bir model oluşturmak ve bu modeli test verilerindeki anormallikleri belirlemek için kullanmaktır. Eğitim için yalnızca anomali örneklerinin kullanılabilirliğini varsayan sınırlı bir anormallik tespit teknikleri seti mevcuttur. Bu tür teknikler, öncelikle verilerde meydana gelebilecek her olası anormal davranışı kapsayan bir eğitim veri seti elde etmenin zor olması nedeniyle yaygın olarak kullanılmaz.

Denetimsiz Anormallik Tespiti (Unsupervised Anomaly Detection): Denetimsiz modda çalışan teknikler, eğitim verisi gerektirmez ve bu nedenle en yaygın şekilde uygulanabilir. Bu kategorideki teknikler, test verilerinde normal örneklerin anormalliklerden çok daha sık olduğu varsayımını ima eder. Bu varsayım doğru değilse, bu tür teknikler yüksek yanlış alarm oranlarına sahiptir. Pek çok yarı denetimli teknik, eğitim verisi olarak etiketlenmemiş veri kümesinin bir örneğini kullanarak denetimsiz bir modda çalışacak şekilde uyarlanabilir. Bu tür bir uyarılama, test verilerinin çok az anormallik içerdiğini ve eğitim sırasında öğrenilen modelin bu birkaç anormalliğe karşı dayanıklı olduğunu varsayar.

Anomali Tespit Teknikleri

Sınıflandırma tabanlı anomali tespit teknikleri: Sınıflandırma, bir dizi etiketli veri örneğinden (eğitim) bir model (sınıflandırıcı) öğrenmek ve ardından öğrenilen modeli (test) kullanarak bir test örneğini sınıflardan birine sınıflandırmak için kullanılır. Sınıflandırmaya dayalı anomali tespit teknikleri, benzer bir iki fazlı şekilde çalışır. Eğitim aşaması, mevcut etiketli eğitim verilerini kullanarak bir sınıflandırıcı öğrenir. Test aşaması, sınıflandırıcıyı kullanarak bir test örneğini normal veya anormal olarak sınıflandırır. Sınıflandırmaya dayalı anomali tespit teknikleri verilen özellik uzayında normal ve anormal sınıfları ayırt edebilen bir sınıflandırıcı öğrenilebilir varsayım altında çalışır.

Eğitim aşaması için mevcut olan etiketlere bağlı olarak, sınıflandırmaya dayalı anormallik tespit teknikleri iki geniş kategoriye ayrılabilir: çok sınıflı ve tek sınıflı anormallik tespit teknikleri.

En yakın komşu tabanlı anomali tespit teknikleri: En yakın komşu analizi kavramı, birkaç anomali tespit tekniğinde kullanılmıştır. Bu tür teknikler normal veri örnekleri yoğun komşuluklarda meydana gelirken, anormallikler en yakın komşularından uzakta meydana gelir varsayımına dayanmaktadır.

En yakın komşu tabanlı anormallik tespit teknikleri, iki veri örneği arasında tanımlanmış bir mesafe veya benzerlik ölçüsü gerektirir. İki veri örneği arasındaki mesafe (veya benzerlik) farklı şekillerde hesaplanabilir. Sürekli öznitelikler için Öklid mesafesi popüler bir seçimdir, ancak başka ölçüler de kullanılabilir [19]. Kategorik nitelikler için genellikle basit bir eşleştirme katsayısı kullanılır, ancak daha karmaşık mesafe ölçüleri de kullanılabilir. Çok değişkenli veri örnekleri için, mesafe veya benzerlik genellikle her özellik için hesaplanır ve ardından birleştirilir.

Kümeleme tabanlı anomali tespit teknikleri: Kümeleme, benzer veri örneklerini kümeler halinde gruplandırmak için kullanılır. Kümeleme, yarı denetimli kümeleme olsa da, öncelikle denetimsiz bir tekniktir ve son zamanlarda araştırılmıştır. Kümeleme ve anormallik tespiti temelde birbirinden farklı görünse de, birkaç kümeleme tabanlı anormallik tespiti tekniği geliştirilmiştir. Kümeleme tabanlı anomali tespit teknikleri üç kategoriye ayrılabilir. Kümelemeye dayalı tekniklerin ilk kategorisi şu varsayımına dayanır: Varsayım. Normal veri örnekleri, verilerdeki bir kümeye aitken, anormallikler herhangi bir kümeye ait değildir. Bu varsayımına dayanan teknikler, bilinen bir kümeleme tabanlı algoritmayı veri kümesine uygular ve herhangi bir kümeye ait olmayan herhangi bir veri örneğini anormal olarak ilan eder.

İstatistiksel anomali tespit teknikleri: Herhangi bir istatistiksel anormallik tespit tekniğinin altında yatan ilke şudur: "Bir anormallik, varsayılan stokastik model tarafından üretilmediğinden kısmen veya tamamen ilgisiz olduğundan şüphelenilen bir gözlemdir". İstatistiksel anormallik tespit teknikleri aşağıdaki temel

varsayıma dayanmaktadır: Varsayım. Normal veri örnekleri, stokastik modelin yüksek olasılık bölgelerinde meydana gelirken, stokastik modelin düşük olasılık bölgelerinde anormallikler meydana gelir.

İstatistiksel teknikler, verilen verilere istatistiksel bir model (genellikle normal davranış için) uydurur ve ardından görünmeyen bir örneğin bu modele ait olup olmadığını belirlemek için bir istatistiksel çıkarım testi uygular. Uygulanan test istatistiğine göre, öğrenilen modelden üretilme olasılığı düşük olan örnekler, anormallik olarak ilan edilir.

Bilgi teorik anomali tespit teknikleri: Bilgi teorik teknikleri, Kolomogorov Karmaşıklığı, entropi, görelî entropi vb. gibi farklı bilgi teorik ölçümleri kullanarak bir veri kümesinin bilgi içeriğini analiz eder. Bu tür teknikler aşağıdaki temel varsayıma dayanmaktadır: Varsayım. Verilerdeki anormallikler, veri setinin bilgi içeriğinde düzensizliklere neden olur.

Spektral anomali tespit teknikleri: Spektral teknikler, verideki değişkenliğin büyük kısmını yakalayan öz niteliklerin bir kombinasyonunu kullanarak verinin yaklaşık bir değerini bulmaya çalışır.

Bu tür teknikler aşağıdaki temel varsayıma dayanmaktadır: Varsayım. Veriler, normal örneklerin ve anormalliklerin önemli ölçüde farklı görüldüğü daha düşük boyutlu bir alt uzaya gömülebilir. Bu nedenle, spektral anomali tespit tekniklerinin benimsediği genel yaklaşım, anormal durumların kolayca tanımlanabileceği bu tür alt uzayları (gömmeler, çıkıntılar, vb.) belirlemektir. Bu tür teknikler, denetimsiz ve yarı denetimli bir ortamda çalışabilir.

Bağlamsal anomalilerin işlenmesi teknikleri: Şimdiye kadar bahsediler anomali tespit teknikleri, öncelikle nokta anomalilerini tespit etmeye odaklanır.

Bu bölümde, bağlamsal anomalileri ele alan anomali algılama tekniklerini tartışacağız.

Bağlamsal anormallikler, verilerin bir dizi bağlamsal öz niteliğe (bir bağlamı tanımlamak için) ve bir dizi davranışsal öz niteliğe (bir bağlam içindeki anormallikleri saptamak için) sahip olmasını gerektirir.

Bağlamsal niteliklerin tanımlanabileceği yollardan bazıları şunlardır:

Mekansal Veriler: bir veri örneğinin konumunu ve dolayısıyla bir uzamsal komşuluğu tanımlayan uzamsal niteliklere sahiptir. Bağlam tabanlı bir dizi anormallik saptama tekniği mekansal veri içeren veriler için önerilmiştir.

Grafikler: Düğümleri birbirine bağlayan kenarlar, her düğüm için komşuluğu tanımlar. Bağlamsal anormallik algılama teknikleri, Sun ve diğerleri tarafından grafiğe dayalı verilere uygulanmıştır.

Sıralı: Veriler sıralıdır: bir veri örneğinin bağlamsal niteliği, onun sıradaki konumudur. Zaman serisi verileri, bağlamsal anormallik tespiti kategorisinde kapsamlı bir şekilde araştırılmıştır [28]. Anomali tespit tekniklerinin geliştirildiği sıralı verilerin başka bir biçimi, her olayın bir zaman damgasına sahip olduğu olay verileridir (örneğin, işletim sistemi çağrı verileri veya Web verileri). Zaman serisi verileri ile olay dizileri arasındaki fark, ikincisi için ardışık olaylar arasındaki varışlar arası sürenin eşit olmamasıdır.

Profil: Çoğu zaman veriler açık bir uzamsal veya sıralı yapıya sahip olmayabilir, ancak yine de bir dizi bağlamsal öz nitelik kullanılarak bileşenler halinde bölümlere ayrılabilir veya kümelenebilir. Bu öz nitelikler tipik olarak, cep telefonu dolandırıcılığı tespiti gibi etkinlik izleme sistemlerinde kullanıcıları profillemek ve gruplandırmak için kullanılır, CRM veritabanları ve kredi kartı dolandırıcılığının tespiti. Kullanıcılar daha sonra kendi grupları içinde anormallikler açısından analiz edilir.

Anomali Tespit Uygulama Alanları

İzinsiz giriş tespiti: İzinsiz giriş tespiti, bilgisayarla ilgili bir sistemdeki kötü amaçlı etkinliklerin (hırsızlıklar, sızmalar ve diğer bilgisayar kötüye kullanımı biçimleri) saptanması anlamına gelir. Bu kötü amaçlı faaliyetler veya izinsiz girişler, bilgisayar güvenliği açısından ilgi çekicidir. Bir izinsiz giriş, sistemin normal davranışından farklıdır ve bu nedenle, izinsiz giriş tespit alanında anormallik tespit teknikleri uygulanabilir.

Dolandırıcılık Tespiti: Dolandırıcılık tespiti, bankalar, kredi kartı şirketleri, sigorta acenteleri, cep telefonu şirketleri, borsa vb. ticari kuruluşlarda meydana gelen suç faaliyetlerinin tespitini ifade eder. Kötü niyetli kullanıcılar, kuruluşun gerçek müşterileri olabilir veya kendilerini müşteri olarak tanıtır (kimlik hırsızlığı olarak da bilinir). Dolandırıcılık, bu kullanıcıların kuruluş tarafından sağlanan kaynakları yetkisiz bir şekilde tüketmesi ile ortaya çıkar. Kuruluşlar, ekonomik kayıpları önlemek için bu tür dolandırıcılıkların derhal tespit edilmesiyle ilgileniyor.

Tıbbi ve Halk Sağlığı Anomali Tespiti: Tıp ve halk sağlığı alanlarındaki anormallik tespiti, genellikle hasta kayıtlarıyla çalışır. Anormal hasta durumu, enstrümantasyon hataları veya kayıt hataları gibi çeşitli nedenlerle verilerde anormallikler olabilir.

Çeşitli teknikler ayrıca belirli bir alandaki hastalık salgınlarını tespit etmeye odaklanmıştır.

Bu nedenle, anomali tespiti bu alanda çok kritik bir problemdir ve yüksek derecede doğruluk gerektirir. Veriler tipik olarak hastanın yaşı, kan grubu ve kilosu gibi birkaç farklı özellik türüne sahip olabilecek kayıtlardan oluşur. Verilerin ayrıca zamansal ve mekansal bir yönü olabilir. Bu alandaki mevcut anomali tespit tekniklerinin çoğu, anormal kayıtları (nokta anomalileri) tespit etmeyi amaçlamaktadır. Tipik olarak etiketlenmiş veriler sağlıklı hastalara aittir, dolayısıyla tekniklerin çoğu yarı denetimli bir yaklaşımı benimser.

Endüstriyel Hasar Tespiti: Endüstriyel üniteler, sürekli kullanım ve normal aşınma ve yıpranma nedeniyle hasar görür. Daha fazla aşınmayı, yüklenmeyi ve dolayısı ile kayıpları önlemek için bu tür hasarların erken tespit edilmesi gerekir (Principi vd. 2017). Bu alandaki veriler, farklı sensörler kullanılarak kaydedildiği ve analiz için toplandığı için genellikle sensör verileri olarak adlandırılır (Popescu ve Mahnot 2009). Anormallik tespit teknikleri, bu tür hasarları tespit etmek için bu alanda kapsamlı bir şekilde uygulanmıştır. Endüstriyel hasar tespiti ayrıca iki alanda sınıflandırılabilir; biri motorlar, motorlar vb. mekanik bileşenlerdeki kusurlarla ilgilenirken diğeri fiziksel yapılarıdaki kusurlarla ilgilenir. Önceki etki alanı, sistem sağlığı yönetimi olarak da adlandırılır (Marchi vd. 2017).

Görüntü İşleme: Anomali saptama teknikleri, görüntülerle ilgili olarak ya bir görüntüde zaman içinde meydana gelen değişikliklerle (hareket algılama) ya da statik görüntüde anormal görünen bölgelerle ilgilenir. Bu alan uydu görüntülerini içerir, rakam tanıma, spektroskopi, mamografik görüntü analizi ve video izleme. Anormallikler hareketten veya yabancı bir nesnenin sokulmasından veya enstrümantasyon hatalarından kaynaklanır. Verilerin mekansal ve zamansal özellikleri vardır. Her veri noktasının renk, açıklık, doku vb. gibi birkaç sürekli özelliği vardır. İlginç anomaliler, görüntülerdeki anormal noktalar veya bölgelerdir (nokta ve bağlamsal anomaliler). Bu alandaki en önemli zorluklardan biri, girdinin büyük boyutudur. Video verileriyle uğraşırken, çevrimiçi anormallik tespit teknikleri gereklidir (Dunning 2014).

Metin Verilerinde Anormallik Tespiti: Bu alandaki anormallik tespit teknikleri, öncelikle yeni konuları veya olayları veya bir belge veya haber makaleleri koleksiyonundaki haberleri tespit eder. Anormallikler, yeni bir ilginç olay veya anormal bir konudan kaynaklanır. Bu alandaki veriler tipik olarak yüksek boyutlu ve çok seyrekler. Belgeler zaman içinde toplandığından verilerin zamansal bir yönü de vardır. Bu alandaki anormallik tespit teknikleri için bir zorluk, bir kategoriye veya konuya ait belgelerdeki büyük farklılıkları ele almaktır.

Sensör Ağları: Sensör ağları son zamanlarda önemli bir araştırma konusu haline gelmiştir; çeşitli kablolu sensörlerden toplanan sensör verilerinin birkaç benzersiz özelliği olduğundan, veri analizi açısından daha fazla işlem gerektirirler (Dunning 2014). Bir sensör ağından toplanan verilerdeki anormallikler, bir veya daha fazla sensörün arızalı olduğu veya analistlerin ilgisini çekecek olayları (izinsiz girişler gibi) tespit ettikleri anlamına gelebilir. Bu nedenle, sensör ağlarındaki anormallik tespiti, sensör hatası tespitini veya izinsiz giriş tespitini veya her ikisini birden yakalayabilir. Tek bir sensör ağı, ikili, ayrık, sürekli, ses, video vb. gibi farklı türde verileri toplayan sensörlerden oluşabilir. Veriler akış modunda oluşturulur. Çoğu zaman, çeşitli sensörlerin yerleştirildiği ortam ve iletişim kanalı, toplanan verilerde gürültüye ve eksik değerlere neden olur. Sensör ağlarında anormallik tespiti, bir dizi benzersiz zorluk ortaya çıkarır (Cooper vd. 2020). Anormallik tespit tekniklerinin çevrimiçi çalışması için gereklidir. Ciddi kaynak kısıtlamaları nedeniyle, anormallik tespit tekniklerinin hafif olması gerekir. Diğer bir zorluk ise, verilerin dağıtılmış bir şekilde toplanması ve dolayısıyla onu analiz etmek için dağıtılmış bir veri madenciliği yaklaşımının gerekli olmasıdır. Ayrıca, sensörden toplanan verilerde gürültünün varlığı, artık ilginç anormallikler ile istenmeyen gürültü/eksik değerleri ayırt etmesi gerektiğinden, anormallik tespitini daha da zorlaştırır. Grafikler: Düzgümleri (veri örnekleri) birbirine bağlayan kenarlar, her düğüm için komşuluğu tanımlar.

SONUÇ

Günümüzde sensör teknolojilerinin gelişmesi ile fiziksel ortamlarda veri toplamak daha kolay ve ilginç hale gelmiştir. Biriken bu verilerin işlenmesi ve yorumlanması için kullanılan yapay zeka destekli makine öğrenimi algoritmaların çoğalması ve etkin hale gelmesi veri işlemeyi kolaylaştırmıştır. İşlenen bu veriler ile iletişim, endüstriyel üretim, sensör ağları, tıp ve hatta tarım ve hayvancılık gibi alanlarda kritik durumlarda anomali

olarak tanımladığımız beklentimiz dışındaki verilerin tespiti ve ortaya çıkartılmasını olanaklı hale getirmektedir. 1900'lü yılların başlarından beri çalışılan anomali tespiti konusu günümüzde çok çalışılmış bir konu haline gelmiştir.

Bu çalışma ile anomali tespiti üzerine çalışmak isteyen araştırmacılar için temel bir literatür özeti verilmiştir. Ayrıca bu alanda karşılaşılabilecek zorluklar, teknikler ve uygulama alanlarından da bahsedilmiştir.

Etkili anormallik tespitinin neyin normal olmadığını keşfetmek için neyin normal olduğunu modelleme temel konseptine dayandığını unutulmamalıdır. Bunu yapmanın en etkili yolu uyarlanabilir olasılık modelleriyle başlanması önerilmektedir.

KAYNAKÇA

1. Abe, Takashi, Charles F. Kearns, ve Yoshiaki Sato. 2006. "Muscle Size and Strength Are Increased Following Walk Training with Restricted Venous Blood Flow from the Leg Muscle, Kaatsu-Walk Training". *Journal of Applied Physiology* 100 (5): 1460-66. <https://doi.org/10.1152/japplphysiol.01267.2005>.
2. Aleskerov', Emin. t.y. : "A Neural Network Based Database Stern for Credit Card Fraud Detection".
3. Chandola, Varun, Arindam Banerjee, ve Vipin Kumar. 2009. "Anomaly Detection: A Survey". *ACM Computing Surveys* 41 (3): 1-58. <https://doi.org/10.1145/1541880.1541882>.
4. Cooper, Clayton, Jianjing Zhang, Robert X. Gao, Peng Wang, ve Ihab Ragai. 2020. "Anomaly Detection in Milling Tools Using Acoustic Signals and Generative Adversarial Networks". *Procedia Manufacturing* 48: 372-78. <https://doi.org/10.1016/j.promfg.2020.05.059>.
5. Dunning, Ted. 2014. *Practical Machine Learning: A New Look at Anomaly Detection*. First edition. Beijing: O'Reilly.
6. Han, Songqiao, Xiyang Hu, Hailiang Huang, Minqi Jiang, ve Yue Zhao. t.y. "ADBench: Anomaly Detection Benchmark".
7. Huber, Peter J. 1981. *Robust Statistics*. Wiley Series in Probability and Mathematical Statistics. New York: Wiley.
8. Joshi, Mahesh V, ve Ramesh C Agarwal. t.y. "Predicting Rare Classes: Can Boosting Make Any Weak Learner Strong?"
9. Kumar, V. 2005. "Parallel and Distributed Computing for Cybersecurity". *IEEE Distributed Systems Online* 6 (10): 1541896. <https://doi.org/10.1109/MDSO.2005.53>.
10. Marchi, Erik, Fabio Vesperini, Stefano Squartini, ve Björn Schuller. 2017. "Deep Recurrent Neural Network-Based Autoencoders for Acoustic Novelty Detection". *Computational Intelligence and Neuroscience* 2017: 1-14. <https://doi.org/10.1155/2017/4694860>.
11. Markou, Markos, ve Sameer Singh. 2003. "Novelty Detection: A Review—Part 1: Statistical Approaches". *Signal Processing* 83 (12): 2481-97. <https://doi.org/10.1016/j.sigpro.2003.07.018>.
12. Phua, Clifton, Daminda Alahakoon, ve Vincent Lee. t.y. "Minority Report in Fraud Detection: Classification of Skewed Data".
13. Popescu, M., ve A. Mahnot. 2009. "Acoustic Fall Detection Using One-Class Classifiers". İçinde *2009 Annual International Conference of the IEEE Engineering in Medicine and Biology Society*, 3505-8. Minneapolis, MN: IEEE. <https://doi.org/10.1109/IEMBS.2009.5334521>.
14. Principi, Emanuele, Fabio Vesperini, Stefano Squartini, ve Francesco Piazza. 2017. "Acoustic Novelty Detection with Adversarial Autoencoders". İçinde *2017 International Joint Conference on Neural Networks (IJCNN)*, 3324-30. Anchorage, AK, USA: IEEE. <https://doi.org/10.1109/IJCNN.2017.7966273>.
15. Rousseeuw, Peter J., ve Annick M. Leroy. 1987. *Robust Regression and Outlier Detection*. Wiley Series in Probability and Mathematical Statistics. New York: Wiley.
16. Song, Xiuyao, Mingxi Wu, Christopher Jermaine, ve Sanjay Ranka. 2007. "Conditional Anomaly Detection". *IEEE Transactions on Knowledge and Data Engineering* 19 (5): 631-45. <https://doi.org/10.1109/TKDE.2007.1009>.
17. Spence, C., L. Parra, ve P. Sajda. 2001. "Detection, Synthesis and Compression in Mammographic Image Analysis with a Hierarchical Image Probability Model". İçinde *Proceedings IEEE Workshop*

- on *Mathematical Methods in Biomedical Image Analysis (MMBIA 2001)*, 3-10. Kauai, HI, USA: IEEE Comput. Soc. <https://doi.org/10.1109/MMBIA.2001.991693>.
18. Steinwart, Ingo, Don Hush, ve Clint Scovel. t.y. “A Classification Framework for Anomaly Detection”.
 19. Stigler, Stephen M. 1978. “Francis Ysidro Edgeworth, Statistician”. *Journal of the Royal Statistical Society. Series A (General)* 141 (3): 287. <https://doi.org/10.2307/2344804>.
 20. Tang, Jian, Zhixiang Chen, Ada Wai-chee Fu, ve David W. Cheung. 2002. “Enhancing Effectiveness of Outlier Detections for Low Density Patterns”. İçinde *Advances in Knowledge Discovery and Data Mining*, editör Ming-Syan Chen, Philip S. Yu, ve Bing Liu, 2336:535-48. Lecture Notes in Computer Science. Berlin, Heidelberg: Springer Berlin Heidelberg. https://doi.org/10.1007/3-540-47887-6_53.
 21. Theiler, James P., ve D. M. Cai. 2003. “Resampling Approach for Anomaly Detection in Multispectral Images”. İçinde , editör Sylvia S. Shen ve Paul E. Lewis, 230. Orlando, FL. <https://doi.org/10.1117/12.487069>.
 22. Vilalta, R. ve Sheng Ma. 2002. “Predicting Rare Events in Temporal Domains”. İçinde *2002 IEEE International Conference on Data Mining, 2002. Proceedings.*, 474-81. Maebashi City, Japan: IEEE Comput. Soc. <https://doi.org/10.1109/ICDM.2002.1183991>.

FIRSATLAR VE RİSKLERİ İLE CHATGPT CHATGPT WITH OPPORTUNITIES AND RISKS

Tarık Kabak

ORCID: 0000-0002-1206-8294

İsmail Kırbaş

ORCID: 0000-0002-2187-3746

ÖZET

Bu çalışmada, günümüzde Yapay Zeka (Artificial Intelligence-AI) alanındaki önemli ilerlemeler sonucunda birçok tartışmalara, kaygılara, hatta komplo teorilerine konu olan ChatGPT (Generative Pre-Trained Transformer-GPT-Önceden Eğitilmiş Üretken Dönüştürücü) olarak adlandırılan büyük dil modeli (Large Language Model-LLM) konusundaki gelişmelere ve sağlayabilecekleri faydalara veya yol açabilecekleri sorunlara dair bir değerlendirme sunulmaktadır. Son yıllarda Google, Microsoft ve Apple gibi teknoloji devleri ve daha birçok firma ya da kurum belirli amaçlar için yapay zeka modellerini kullanmakta ve geliştirmeye devam etmektedir. Uzun ve çeşitli eğitim yöntemleri kullanılarak sürekli olarak eğitilen farklı yapay zekalar, belirli amaçlara yönelik özelleştirilerek o alanlarda fayda sağlamaları amacıyla hizmet vermektedir. Bu çalışmamıza konu olan ve OpenAI firması tarafından geliştirilmekte olan ChatGPT-3 isimli sohbet botu; teknoloji ile etkileşimimizi önemli ölçüde değiştirebilecek potansiyele sahiptir. ChatGPT-3 sohbet botunun en önemli becerisi; eğitimi sırasında işlediği çok büyük miktarda verinin de yardımıyla yüksek doğrulukta, hatta neredeyse insana yakın denebilecek ölçüde metinleri anlayıp yeni metinler üretebilmesidir. Bu sayede de doğal dil işleme (Natural Language Processing-NLP) ve doğal dil anlama (Natural Language Understanding-NLU) alanlarında devrimsel olasılıklar sunmaktadır. GPT dil modeli üzerine inşa edilen ChatGPT'nin sunduğu bu olasılıklar içerisinde hukuktan tıpa, matematikten finansa, akademik makale yazımından kod yazımına, sosyal medya ilişkilerinden dil tercüme işlemlerine hatta güvenlik açıklarının tespitine kadar geniş bir yelpaze bulunmaktadır.

Anahtar Kelimeler: Büyük Dil İşleme, ChatGPT, Doğal Dil İşleme, GPT, sohbet, Yapay Zekâ.

ABSTRACT

In this paper, we present a review of the developments in the Large Language Model (LLM) known as ChatGPT (Generative Pre-Trained Transformer), which has been the subject of many discussions, concerns, and even conspiracy theories as a result of today's significant advances in Artificial Intelligence (AI), and the benefits or concerns they can cause. Today, technology giants like Google, Microsoft, Apple, and numerous other businesses and organizations are constantly implementing artificial intelligence for specific purposes. Various artificial intelligences are customized for specific purposes and serve to provide benefits in those areas after being continuously trained through several different trainings. The subject of this study, ChatGPT-3 language model, which is being developed by OpenAI, has the potential to significantly change the way we interact with technology. The most important capability of ChatGPT-3 language model is its ability to understand texts and generate new texts with high accuracy, almost human-like, using the massive amount of data it processes during training. As a result, it provides revolutionary opportunities in the fields of Natural Language Processing (NLP) and Natural Language Understanding (NLU). Capabilities of ChatGPT-3 language model, range from law to medicine, mathematics to finance, academic article writing to code writing, social media relations to language translation, and even security vulnerability detection.

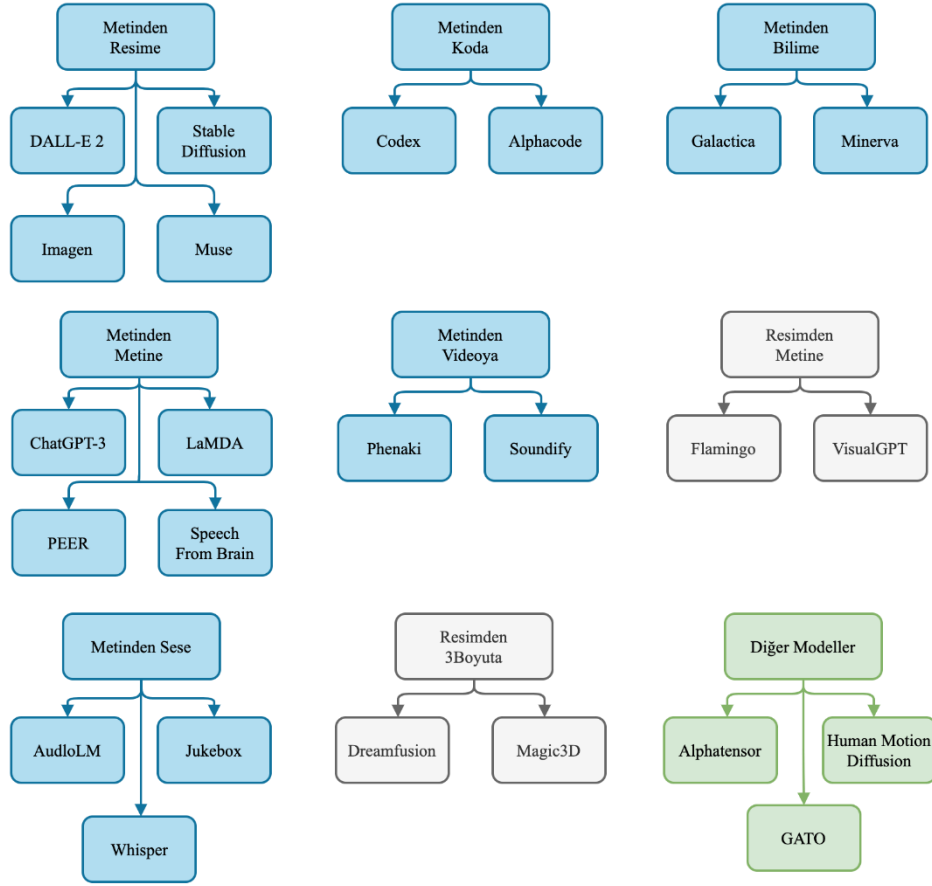
Keywords: Artificial Intelligence, chatbot, ChatGPT, Large Language Model, Natural Language Processing.

GİRİŞ

Bu çalışma, günümüzün en akıllı yapay zeka modellerinden biri kabul edilen ve birçok tartışmayı da beraberinde getiren ChatGPT özelinde, dil modelleri hakkında genel bir çerçeve çizmek, dil modellerinden biri olan büyük dil modelini kullanan ChatGPT'nin sergilediği yetenekleri incelemek, limitlerini anlamak ve finans, eğitim, sağlık, hukuk, kodlama hatta akademik yazım gibi alanlardaki sunduğu potansiyele odaklanmasının yanında benzer veya farklı alanlarda beraberinde getirebileceği risklere de değinmektedir.

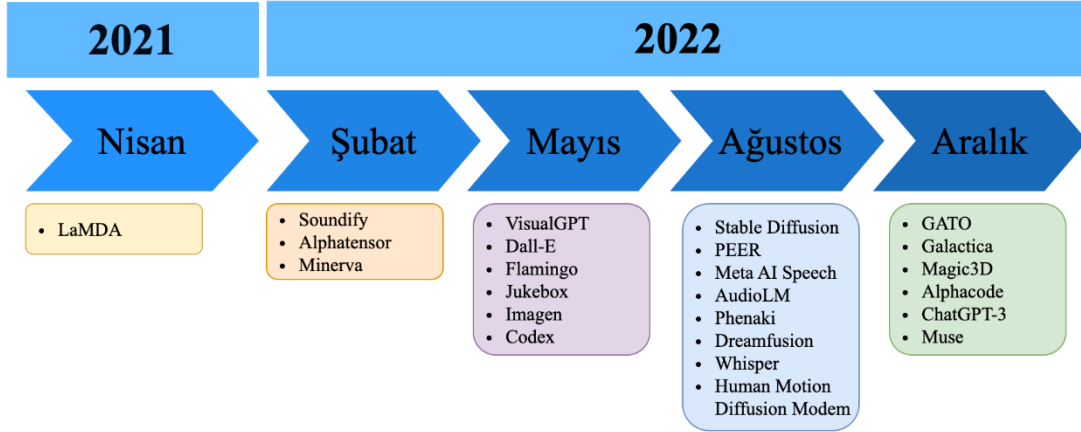
Günümüzde yapay zeka alanındaki artan gelişmeler beraberinde müthiş bir potansiyelin yanında bazı konularda kaygıları da gün yüzüne çıkarmaktadır. Yapay zeka modellerinin yapabildikleri ve yapabilecekleri düşünüldüğünde değerlendirilen her iki sonuç da yadsınamaz durumdadır. Örneğin, yapay zeka modellerinin, eğitim alanındaki işgücüne olan etkisi gelecek nesillere ne öğretileceği ve nasıl öğretileceği konularında endişeler yaratmaktadır(Zhai 2021). Bunun yanı sıra yapa zekalar son yıllarda, akademik yazım, kodlama ve sanat gibi genellikle sadece yetenekli profesyoneller tarafından gerçekleştirilen yaratıcı çalışmaları kısmen, bazı durumlarda tam manada ikame etme potansiyelini de göstermişlerdir(Li vd. 2022).

Şekil 1’de farklı amaçlar için oluşturulmuş ve eğitilmiş farklı yapay zeka modelleri görülebilmektedir. Her bir model hedeflendiği işlemleri yerine getirebilmek için çeşitli eğitimlerden geçirilmektedir. Bu eğitimler genel anlamda girdi ve çıktı ilişkisine göre farklılık göstermektedir. Hatta aynı girdi ve çıktı formatları konusunda eğitilen modellerin dahi eğitim süreçleri birbirlerinden farklı olabilmektedir.



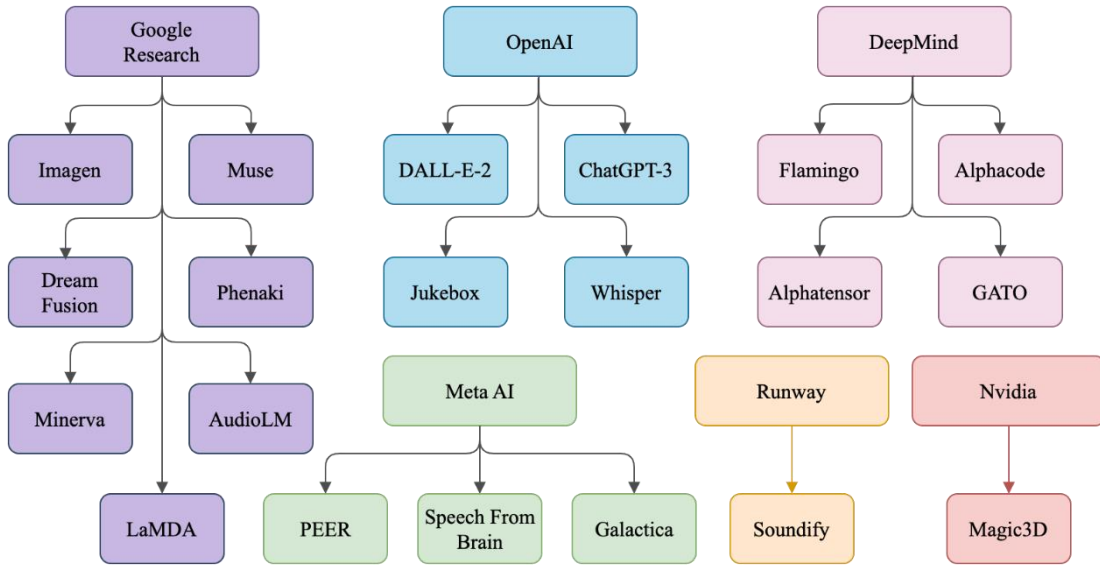
Şekil 1. Girdi ve çıktı formatlarına göre bazı yapay zeka modelleri.

Yapay zeka konusunun alt alanlarından biri de doğal dil işleme olarak adlandırılan alandır. Her geçen gün dünya üzerinde internet kullanımının yaygınlaşması sonucunda kullanıcı sayısının da artmasıyla internet ortamına yüklenen veri miktarı da günden güne artmaktadır. Bu durumun kaçınılmaz sonucu olarak da büyük veri kümelerinin çoğalması, yaygınlaşması ve bu veri kümelerine erişimin kolaylaşması ile araştırmacılar, rahatça erişebildikleri bu veri kümelerinin yardımıyla eğittikleri sohbet temelli yanıtlar sunabilen yapay zeka modelleri geliştirmişlerdir. Günümüzde birçok farklı geliştirici tarafından farklı amaçlarla farklı şekillerde eğitilerek piyasaya sürülmüş onlarca yapay zeka modeli mevcuttur. Şekil 2’de piyasaya sürülme tarihlerine göre en bilinen yapay zeka modelleri gösterilmiştir.



Şekil 2. Piyasaya sürülme tarihlerine göre yapay zeka modellerinden bazıları

Google, Apple, Nvidia, OpenAI gibi teknoloji firmaları da kendi hedefleri doğrultusunda farklı amaçlar için farklı yapay zeka modelleri eğitmektedir. Şekil 3’te popüler yapay zeka modellerinin hangi firmalar tarafından geliştirildiği gösterilmektedir.



Şekil 3. Geliştiricilerine göre düzenlenmiş bazı yapay zeka modelleri.

Dil eğitimleri için farklı modeller kullanılmakla birlikte en yaygın kullanılan modellerden birisi de büyük dil modelidir. Büyük dil modelinin becerisi; metinleri okumak, anlamak gerektiğinde tercüme etmek ve cümlede yazılacak sonraki kelimeyi tahmin ederek insanlarınkine benzer şekilde yazma ve anlama işlemleri yapabilmesidir. Bu modeli kullanan belki de en popüler yapay zeka modeli de ChatGPT sohbet botunda kullanılan GPT olarak adlandırılan dil modelidir.

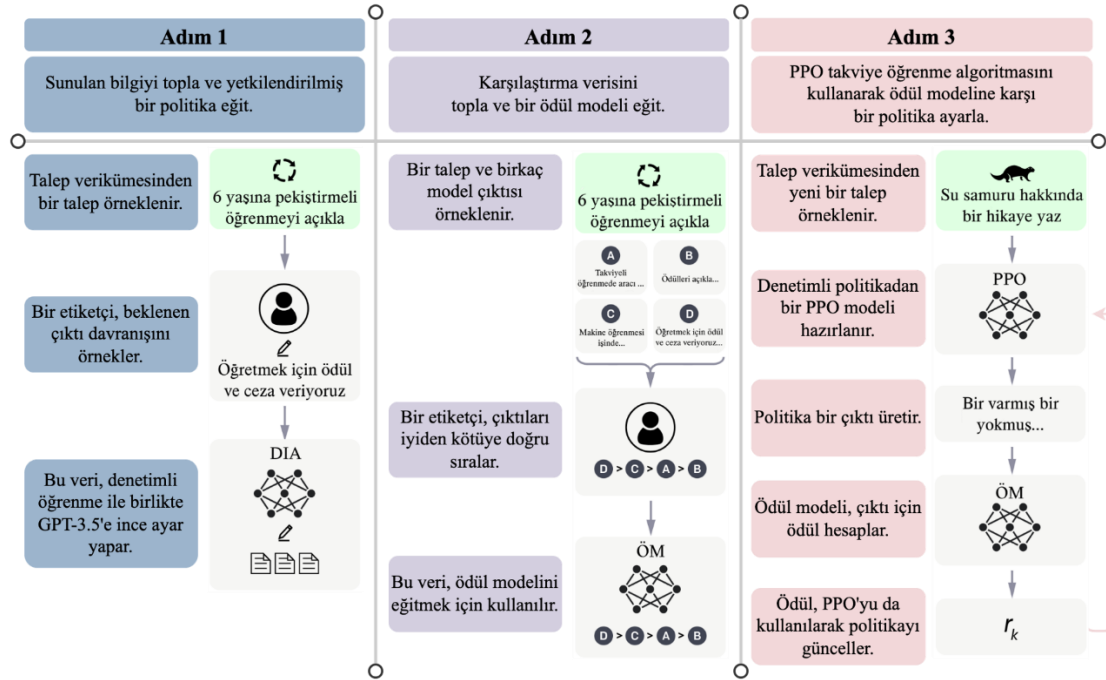
Chatgpt Modeline Yakından Bir Bakış

ChatGPT sohbet botu; OpenAI isimli, 2015 yılında Silikon Vadisi’nde kurulan bir teknoloji firması tarafından, insanlar tarafından oluşturulmuş büyük miktarda metinler kullanılarak büyük dil modeli ile geliştirilen ve 30 Kasım 2022 yayımlanan genel amaçlı bir sohbet botudur(“ChatGPT: Optimizing Language Models for Dialogue” t.y.). ChatGPT 40 terabayttan fazla metin kullanılarak eğitilmiştir. Basit bir matematikle bu miktar, kindle formatında 40 milyona yakın kitaba karşılık gelmektedir(Rudolph, J., Tan, S., ve Tan, S. 2023).



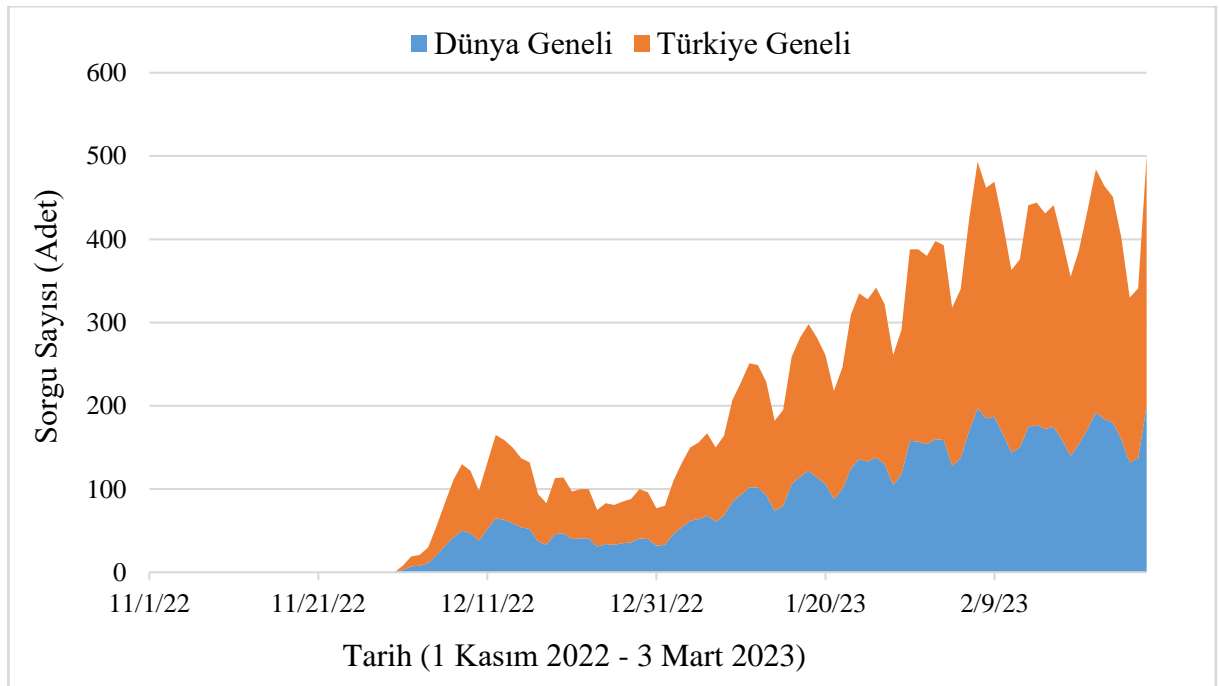
Şekil 4. OpenAI firması ile GPT ve ChatGPT'nin yol haritası("About OpenAI" t.y.).

ChatGPT modeli; belirli girdiler veya sohbet etkisiyle insan benzeri metinler oluşturmak üzere tasarlanmış çok çeşitli konularda doğal sohbetler edebilme becerisine sahiptir [6]. Kendinde önceki dil modelinden farklı olarak eğitiminin bir kısmı insan geribildirimisi sayesinde güçlendirilmiş öğrenme yoluyla yapılmıştır. Bu şekilde Proksimal Politika Optimizasyonu (Proximal Policy Optimization) kullanarak modele ince ayar yapabilmek için yanıtların kalitesi sıralanmıştır. Bu yeni yaklaşım sayesinde ChatGPT takip eden soruları yanıtlayabilir, yanlışlarını kabul edebilir ve uygun olmayan sorguları reddedebilir hale gelmiştir. Şekil 5.'te GPT modelinin eğitim adımları gösterilmiştir. ChatGPT-1 117 milyon parametre içeren model kullanırken ChatGPT-3 için bu rakam 175 milyara ulaşmıştır("ChatGPT: Optimizing Language Models for Dialogue" t.y.). ChatGPT yapay zeka modeli; Şekil 1.'de de görülebildiği üzere metin girdi alıp yine metin çıktısı üretebilen LaMDA, PEER ve Speech From Brain ile birlikte en bilinen modellerden birisidir.



Şekil 5. ChatGPT'nin temeli olan GPT dil modelinin eğitim adımları("ChatGPT: Optimizing Language Models for Dialogue" t.y.).

Son sürümünün piyasaya sürüldüğü tarihten günümüze ChatGPT, sürekli ilgi odağı olan yapay zeka modellerinden birisi olmuştur. Aşağıdaki şekilde Google arama motoru kullanılarak ülkemizden ve dünya genelinde yapılan "chatgpt" ve "chat gpt" kelimelerinin, 1 Kasım 2022 ile 3 Mart 2023 tarihleri arasındaki toplam sorgu sayısının tarihsel dağılımı gösterilmektedir("Google Trendler - Türkiye - 'chat gpt'" t.y.; "Google Trendler - Türkiye - 'chatgpt'" t.y.; "Google Trendler - Dünya Geneli - 'chatgpt'" t.y.; "Google Trendler - Dünya Geneli - 'chat gpt'" t.y.).



Şekil 6. 1 Kasım 2022 ile 3 Mart 2023 tarihleri arasında Türkiye'den ve dünya genelinden Google arama motoru kullanılarak yapılan "chatgpt" ve "chat gpt" sorgu sayılarının toplamının tarihsel dağılımı.

Genel anlamda dil modellerinin becerilerini ve yapabileceklerinin sınırlarını belirleyen en önemli faktör eğitimlerinde kullanılan parametre sayılarıdır. Ne kadar çok parametre kullanılır ise dil modelleri için anlama ve yorumlama yetenekleri o denli yüksek olacaktır. Aşağıdaki tabloda bilinen bazı popüler dil modellerinin eğitimlerinde kullanılan parametre sayıları ve piyasaya sürülme tarihleri gösterilmiştir.

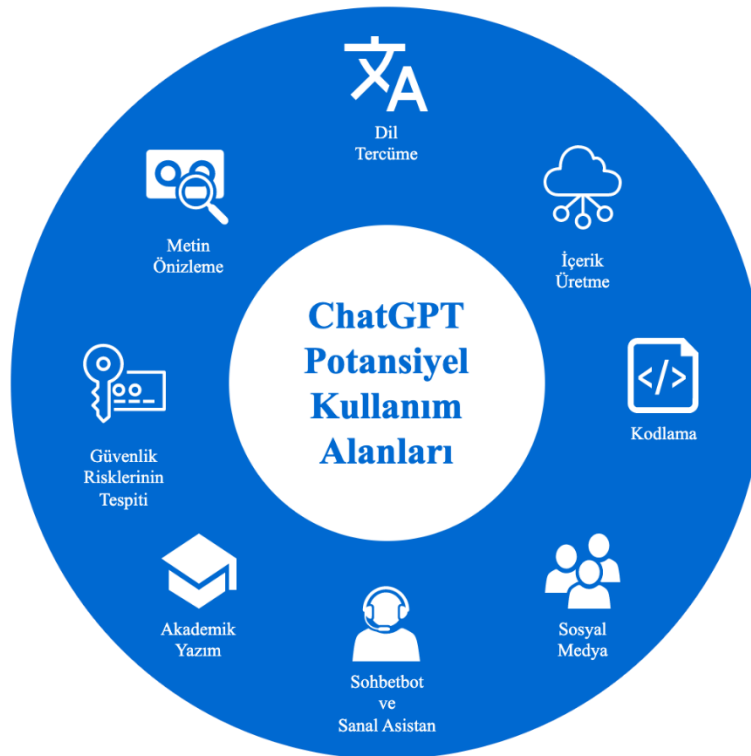
Tablo 1. Farklı büyük dil modellerinin piyasaya sürülme tarihleri ve eğitimleri için kullanılan parametre sayıları.

Model	BERT	RoBERTa	GPT-1	GPT-2	T5	Turing NLG	GPT-3
Parametre Sayıları*	340	354	117	1200	11000	17000	175000
Piyasaya Sürülme Tarihleri	2018	2020	2018	2019	2019	2020	2022

*Milyar adet

ChatGPT'nin Yetenekleri ve Sunduğu Fırsatlar

ChatGPT ve diğer tün yapay zeka modelleri, sonuçta insanların hayatlarını direk ya da dolaylı olarak kolaylaştırmak amacıyla geliştirilmektedirler. Sağlayabileceği fayda ve fırsatları da temelde metinden metine olarak eğitilen bir sohbet botu modeli olması sebebiyle yazılı şekilde olabilecektir. Hangi alanda ne oranda fırsat ve fayda sağlayabileceği henüz tam olarak netleşmemiş olmakla birlikte finans, eğitim, hukuk, sağlık gibi alanlarda ciddi faydalar sağlayabileceğine dair çalışmalar bulunmaktadır.



Şekil 7. ChatGPT yapay zeka modelinin potansiyel kullanım alanlarına bazı örnekler.

Yakın zamanda eğitim alanında yapılan bir çalışmada; ChatGPT dil modelinin yazma yeterliliğinin ortalama bir öğrencinin çok üzerinde olduğu tespit edilmiş ve yazdığı metnin okunabilir ve içerik açısından tutarlı ve (nispeten) doğru olduğu görülmüş, insanlarla karşılaştırıldığında da ihtiyaç duyulan bilgiyi daha verimli bir şekilde bulabildiği gösterilmiştir(Zhai 2022). Hatta ChatGPT, eğitim alanında sunduğu potansiyel fırsatlar açısından oyunun kurallarını değiştirebilecek bir yapay zeka modeli olarak ifade edilmektedir("AI bot ChatGPT writes smart essays — should professors worry?" t.y.). Meta'nın dil aracı PEER veya RoBERTa gibi

diğer yapay zeka dil modelleriyle karşılaştırıldığında ChatGPT "daha yaratıcı" yanıtlar sunmaktadır("ChatGPT is a new AI chatbot that can answer questions and write essays" t.y.).

ChatGPT dil modelinin en büyük sayılabilecek avantajlarından birisi de akademik yazım konusunda araştırmaya yardımcı olma yeteneğidir. ChatGPT, makalelerin özetlerini oluşturabilir, kilit noktaları vurgulayabilir ve hatta alıntılar sunabilmektedir. Bu sayede araştırmacılara önemli miktarda zaman ve emek tasarrufu sağlayarak analiz ve yorumlama gibi daha önemli görevlere odaklanmalarına olanak tanıyabilmektedir(Aljanabi vd. 2023).

ChatGPT gibi yapay zeka modelleri, avukatlık mesleğini icra edenler için de çeşitli faydalar sağlayabilmektedir. Bir avukat ChatGPT yapay zeka modeline bir notun ilk taslağını hazırlatabilir ve daha sonra bu taslağı gerektiği gibi değiştirebilir. ChatGPT yapay zeka modelini ilk argüman grubunu üretmek ve daha sonra bunları en etkili olana kadar elemesini sağlamak amacıyla veya çalışmaların daha verimli hale getirilebilmesi için daha eski yasal belge örneklerini incelemek yoluyla da kullanılabilir. Pedagogik olarak, hukuk fakülteleri, hukuk öğrencilerini bu araçları uygulamalarında en etkili şekilde kullanmaya nasıl hazırlayacaklarını düşünmeli ve aynı zamanda öğrencilere hukuki araştırma ve değerlendirme konularında temel becerilerinin yalnızca dil modellerine devredilemeyeceğini önemle vurgulamalıdır. ChatGPT ve benzeri araçlar bir avukatın daha verimli çalışmasına yardımcı olabilirken, günümüz itibariyle bir avukatın ilgili hukuk kaynaklarını bulma, anlama ve bunlardan akıl yürütme ihtiyacını ikame edebilecek durumda değildir(Choi vd. 2023).

ChatGPT yapay zeka modeli, ekonomik ve finansal verilerin raporlarını ve özetlerini oluşturmak için kullanılabilir, böylece araştırmacıların ve analistlerin bulgularını anlamlandırmalarını kolaylaştırır. Ayrıca, geçmiş verilere dayalı tahminler ve öngörüler oluşturmak için de kullanılabilir, bu da karar verme süreçleri için değerli olabilir(Alshater 2022).

Kodlama konusunda hata düzeltme ile ilgili yapılan standart bir karşılaştırma testinde ChatGPT yapay zeka modeli; Codex ve kendine ait derin öğrenme temelli otomatik yazılım onarma (Automated Program Repair–APR) ile benzer performans sergilemesine karşın 40 hatadan 19 tanesini düzelterek, 7 tanesini düzeltebilen standart otomatik yazılım onarma yöntemlerine kıyasla çok daha başarılı olmuştur. Hatta, hata ile ilgili daha biraz daha bilgi vermek ChatGPT performansını daha da arttırarak %77.5 başarı oranına ulaştırmıştır(Sobania vd. 2023).

Aşağıdaki şekilde QuixBugs'tan("QuixBugs Benchmark | QuixBugs" t.y.) alınan problemler için ChatGPT tarafından verilen cevapların sınıflandırılması görülmektedir.



Şekil 8. ChatGPT yapay zeka modeli tarafından QuixBugs'tan alınan problemlere verilen yanıtların sınıflandırılması(Sobania vd. 2023).

ChatGPT'nin Limitleri ve Doğurabileceği Riskler

ChatGPT yapay zeka modeli, her ne kadar çok büyük miktarda veri kümesi ile eğitilmiş olsa da hala o veri kümesinin sağladığı ölçüde bilgiye beceriye sahip durumdadır. Bu sebeple hala eksik veya yanlış bilgi çıktısı üretebilmektedir. Bazen, çok karmaşık algoritmik problemleri çözebilirken basit matematik sorularına hatalı cevaplar verebilmektedir.

Yakın zamanda yapılan bir çalışmada; ChatGPT yapay zeka modeli, kendisine sorulan programlama sorularının %37,5'ine doğru cevap verebilmiştir. Yanlış cevapların karakteristiği incelendiğinde ise;

- Bilgi eksikliği

- Hatalı varsayım
- Bilgi eksikliği ve hatalı varsayım birlikte

olmak üzere üç ana sebep göze çarpmaktadır(Jalil vd. 2023).

ChatGPT, özellikle çevrimiçi sınavların giderek yaygınlaştığı yükseköğretimde çevrimiçi sınavların bütünlüğüne yönelik önemli bir tehdit oluşturmaktadır. Bu ve benzeri yapay zeka modelleri yüksek derecede eleştirel düşünme becerilerine sahip olmakla birlikte, çok az girdi ile son derece gerçekçi metinler üretebilmekte, bu da öğrencilerin sınavlarda kopya çekmesini mümkün kılmaktadır. Her ne kadar yüzyüze sınavlara geri dönmek çözüm olsa da her zaman mümkün olmamakla birlikte gelişmiş yapay zekâ metin çıktı tespit araçları kullanmak bu sorunun çözümü açısından etkili olabilmektedir. Ancak ne yazık ki bu tarz araçlar da kusursuz çözümler sunmaktan uzaktır. ChatGPT gibi yapay zeka modellerinin etkilerini tam olarak anlamak ve bu araçları kullanarak kopya çekilmesi gibi sorunlarla mücadele edebilme yöntemleri geliştirmek için daha fazla araştırmaya ihtiyaç duyulmaktadır. Eğitimcilerin ve kurumların ChatGPT'nin kopya çekmek için kullanılma riskinin farkında olmaları ve tüm öğrenciler için çevrimiçi sınavların adil olması ve geçerliliğini korumak için bu sorunun ciddi olarak ele alarak gerekli araştırmaları ve önlemleri sunabilmeleri çok önemlidir(Susnjak 2022).

ChatGPT'nin matematiksel becerilerini test etmek amaçlı yapılmış bir çalışmada, medyada yarattığı sansasyonun aksine ChatGPT henüz tutarlı bir şekilde yüksek kaliteli kanıtlar veya hesaplamalar sunmaya hazır olmadığı görülmüştür(Frieder vd. 2023).

Yukarıda bahsettiklerimizden daha da sık dile getirilen ve belki de en önemli risk ya da kaygı; ChatGPT yapay zeka modelinin de bir parçası olduğu her önemli teknolojik gelişme ya da atılım sonrası mevcut mesleklerin bu gelişmelere karşı ne derece duyarlı olduğu konusudur. Geçmişten günümüze kadar defalarca yaşanan bu teknolojik atılımlar her seferinde geniş kitlelerde, teknolojinin er ya da geç insanların yerini alacağı korkusu doğurmuştur. Bu konuda yapılan bir çalışma göstermiştir ki, bu tarz teknolojik gelişmelerin, esas olarak düşük vasıflı işçilerin teknolojiye duyarlı olmayan görevlere, yani yaratıcı ve sosyal zeka gerektiren görevlere atanacaklarını göstermektedir. Ancak insanların bu yarışı kazanabilmeleri için yaratıcı ve sosyal beceriler edinmeleri ya da sahip oldukları bu becerileri geliştirmeleri gerekecektir(Frey ve Osborne 2017).

Yukarıda bahsettiğimiz limitler ve risklerin yanında ChatGPT yapay zeka modeli için öngörülen diğer limit ve riskler aşağıdaki şekilde sıralanabilir.

- Gizlilik sorunları
- Siber güvenlik tehdidi
- Taraflı içerik
- İşten çıkarma
- İntihal
- Aşırı bağımlılık
- Kısıtlı içerik
- Empati eksikliği
- Yaratıcılık eksikliği
- Bağlamsal sınırlamalar

SONUÇLAR VE DEĞERLENDİRME

Bilgiyi işlemenin yanı sıra yapay zekalar, işin yürütülmesi açısından daha güvenilirdir. Bilgiyi toplamak ve sunmak konusunda da oldukça beceriklidirler. Günümüzde bilimsel çalışmalar gün geçtikçe artan bir hızla yapay zeka modellerine sırtını yaslamak durumunda kalmaktadır. Bu bilimsel çalışmaların yürütülebilmesi için de bilim insanları ve mühendisler karmaşık problemleri çözebilmek adına, tahmin, sınıflandırma ve çıkarım yapmak konularında süper bilgisayarlar kullanmaktadır. Yapay zeka modellerinin birer yazılım olması sebebiyle, bu bilgisayar sistemleri ne kadar gelişirse yapay zeka modelleri de daha büyük verileri işleyebilmek, daha hızlı ve kesintisiz hizmet sunabilmek için o derece geniş alana sahip olacaklardır. Bununla birlikte, yapay zeka modellerinin belli alanlardaki öğrenme görevlerine entegre edilmesi insanların gerçek

dünyada karşılaşılabildikleri sorunları nasıl çözdüğünü gösterdiği için yine yapay zeka modellerinin eğitimleri açısından kritik öneme sahiptir.

ChatGPT dil modelinin sunduğu olanaklar neticesinde, insan iletişiminde dil bariyerini ortadan kaldırarak iletişimde çığır açabilmesinin yanı sıra müşteri ilişkileri gibi alanlarda da firmalara ve müşterilere inanılmaz kolaylıklar sağlayabilecektir. Çok kısa denebilecek sürelerde akademik makalelerin ya da kitapların önemli noktalarını tespit ederek özetlerini çıkarabilmesinin ve karmaşık soruları anlayıp basitleştirebilmesi sayesinde de öğrencilere eğitim hayatlarında önemli kolaylıklar sunabilecektir. ChatGPT, akademi ve kütüphaneciliği hem kaygı verici hem de heyecan verici yeni yollarla ilerletmek için önemli bir güce sahiptir(Lund ve Wang 2023).

Eğitimin dışında medikal, matematik, ekonomi ve hukuk gibi alanlarında da ChatGPT yapay zeka modeli önemli sınavların belirli kısımlarını da olsa başarabildiğini göstermiştir. Bazı alanlarda ve konularda oldukça başarılı ancak farklı konularda yetersiz kalan ChatGPT yapay zeka modeli; o konularda kendisine çok daha fazla veri kaynağı sağlanır ve eğitimi de o alanlarda yoğunlaştırılırsa çok daha fazla başarı gösterebilecek yeteneğe sahiptir. Sağlık alanında yapılan farklı bir çalışmada ise klinik süreçlere dahil edilerek basitleştirilmiş radyoloji raporlarının otomatik olarak oluşturulması sağlanarak radyoloji ve diğer tıbbi alanlarda hasta merkezli bakımı iyileştirmek için ChatGPT gibi büyük dil modellerinin kullanılmasında büyük bir potansiyel görülmüştür(Jeblick vd. 2022).

Henüz görece yakın zamanda piyasaya sürülmüş olması sebebiyle neler yapabileceği ve yapabildiği şeyleri ne kadar iyi yapabileceği konusunda tam resmi görebilmek için henüz çok erken demek yanlış olmaz. Yapa zeka modelleri, insan zekasının sınırlarıyla doğru orantılı olarak gelişmeye devam edeceğinden insan zekasının hangi kısımlarının yapay zeka modelleri tarafından ikame edilebileceğini daha iyi anlayabilmek için hem insan zekası hem de yapay zeka modelleri konusunda çok daha fazla araştırmaya ihtiyaç duyulmaktadır(Frey ve Osborne 2017).

Doğasında var olan kısıtlamalara rağmen doğru araçlar ve yaklaşımlarla, yapay zeka ve doğal dil işleme teknolojileri birçok alanda verimliliği ve etkinliği büyük ölçüde artırma potansiyeline sahip olmasıyla yeni keşiflere ve öngörülere yol açarak geleceği şekillendirme gücüne sahiptir(Alshater 2022).

TEŞEKKÜR

Bu çalışma Burdur Mehmet Akif Ersoy Üniversitesi Bilimsel Araştırma Projeleri Komisyonunca desteklenmiştir. Proje No: 0886-YL-23.

KAYNAKÇA

1. “About OpenAI”. t.y. Erişim 21 Şubat 2023. <https://openai.com/about/>.
2. “AI bot ChatGPT writes smart essays — should professors worry?” t.y. Erişim 28 Şubat 2023. <https://www.nature.com/articles/d41586-022-04397-7>.
3. Aljanabi, Mohammad, Mohanad Ghazi, Ahmed Hussein Ali, ve Abas Abed. 2023. “ChatGpt: Open Possibilities”. *Iraqi Journal for Computer Science and Mathematics* 4 (1). <https://doi.org/10.52866/ijcsm.2023.01.01.0018>.
4. Alshater, Muneer. 2022. “Exploring the Role of Artificial Intelligence in Enhancing Academic Performance: A Case Study of ChatGPT”. *SSRN Electronic Journal*. <https://doi.org/10.2139/ssrn.4312358>.
5. “ChatGPT is a new AI chatbot that can answer questions and write essays”. t.y. Erişim 02 Mart 2023. <https://www.cnbc.com/2022/12/13/chatgpt-is-a-new-ai-chatbot-that-can-answer-questions-and-write-essays.html>.
6. “ChatGPT: Optimizing Language Models for Dialogue”. t.y. Erişim 27 Şubat 2023. <https://openai.com/blog/chatgpt/>.
7. Choi, Jonathan H., Kristin E. Hickman, Amy Monahan, ve Daniel B. Schwarcz. 2023. “ChatGPT Goes to Law School”. *SSRN Electronic Journal*. <https://doi.org/10.2139/ssrn.4335905>.
8. Frey, Carl Benedikt, ve Michael A. Osborne. 2017. “The Future of Employment: How Susceptible Are Jobs to Computerisation?” *Technological Forecasting and Social Change* 114 (Ocak): 254-80. <https://doi.org/10.1016/j.techfore.2016.08.019>.

9. Frieder, Simon, Luca Pinchetti, Ryan-Rhys Griffiths, Tommaso Salvatori, Thomas Lukasiewicz, Philipp Christian Petersen, Alexis Chevalier, ve Julius Berner. 2023. "Mathematical Capabilities of ChatGPT". arXiv. <http://arxiv.org/abs/2301.13867>.
10. "Google Trendler - Dünya Geneli - 'chat gpt'". t.y. Erişim 03 Mart 2023. <https://trends.google.com/trends/explore?date=2022-11-01%202023-03-03&q=chat%20gpt>.
11. "Google Trendler - Dünya Geneli - 'chatgpt'". t.y. Erişim 03 Mart 2023. <https://trends.google.com/trends/explore?date=2022-11-01%202023-03-03&q=chatgpt>.
12. "Google Trendler - Türkiye - 'chat gpt'". t.y. Erişim 03 Mart 2023. <https://trends.google.com/trends/explore?date=2022-11-01%202023-03-03&geo=TR&q=chat%20gpt>.
13. "Google Trendler - Türkiye - 'chatgpt'". t.y. Erişim 03 Mart 2023. <https://trends.google.com/trends/explore?date=2022-11-01%202023-03-03&geo=TR&q=chatgpt>.
14. Jalil, Sajed, Suzzana Rafi, Thomas D. LaToza, Kevin Moran, ve Wing Lam. 2023. "ChatGPT and Software Testing Education: Promises & Perils". arXiv. <http://arxiv.org/abs/2302.03287>.
15. Jeblick, Katharina, Balthasar Schachtner, Jakob Dextl, Andreas Mittermeier, Anna Theresa Stüber, Johanna Topalis, Tobias Weber, vd. 2022. "ChatGPT Makes Medicine Easy to Swallow: An Exploratory Case Study on Simplified Radiology Reports". arXiv. <http://arxiv.org/abs/2212.14882>.
16. Li, Yujia, David Choi, Junyoung Chung, Nate Kushman, Julian Schrittwieser, Rémi Leblond, Tom Eccles, vd. 2022. "Competition-Level Code Generation with AlphaCode". *Science* 378 (6624): 1092-97. <https://doi.org/10.1126/science.abq1158>.
17. Lund, Brady D., ve Ting Wang. 2023. "Chatting about ChatGPT: How May AI and GPT Impact Academia and Libraries?" *Library Hi Tech News*, Şubat. <https://doi.org/10.1108/LHTN-01-2023-0009>.
18. "QuixBugs Benchmark | QuixBugs". t.y. Erişim 02 Mart 2023. <https://jkoppel.github.io/QuixBugs/>.
19. Rudolph, J., Tan, S., ve Tan, S. 2023. "ChatGPT: Bullshit Spewer or the End of Traditional Assessments in Higher Education?" *Journal of Applied Learning & Teaching* 6 (1). <https://doi.org/10.37074/jalt.2023.6.1.9>.
20. Sobania, Dominik, Martin Briesch, Carol Hanna, ve Justyna Petke. 2023. "An Analysis of the Automatic Bug Fixing Performance of ChatGPT". arXiv. <http://arxiv.org/abs/2301.08653>.
21. Susnjak, Teo. 2022. "ChatGPT: The End of Online Exam Integrity?" arXiv. <http://arxiv.org/abs/2212.09292>.
22. Zhai, Xiaoming. 2021. "Practices and Theories: How Can Machine Learning Assist in Innovative Assessment Practices in Science Education". *Journal of Science Education and Technology* 30 (2): 139-49. <https://doi.org/10.1007/s10956-021-09901-8>.
23. Zhai, Xiaoming. 2022. "ChatGPT User Experience: Implications for Education". *SSRN Electronic Journal*. <https://doi.org/10.2139/ssrn.4312418>.

AÇILMIŞ E-TİPİ CAM ELYAF TAKVİYELİ EPOKSİ KOMPOZİTLER: YANMA DAYANIMI VE LİF BOY/ÇAP ORANIN İLİŞKİSİ OPENED-UP E-GLASS FIBER REINFORCED EPOXY COMPOSITES: RELATIONSHIP BETWEEN FIBER ASPECT RATIO AND FLAME RESISTANCY

Hayriye Hale Aygün
ORCID: 0000-0002-2812-8079

ÖZET

Lif takviyeli kompozitler, fonksiyonel ve hafif malzeme üretimini mümkün kılmalarından dolayı gelecek vaad eden malzemelerdir. Lif takviyeli kompozitlerin mekanik özelliklerinin geliştirilmesi üzerine sayısız çalışma yapılmıştır ancak yasal zorunluluklar yangının yıkıcı etkisini azaltmak için bu kompozitlerin yanma direncinin artırılmasını da zorunlu kılmaktadır. Kompozitlerin yanma direnci, kompozitin yapısına yanma direnci yüksek malzeme ilavesi yada kompozit yüzeyinin uygun alev itici ile kaplanması sayesinde artırılmaya çalışılmıştır. Bu çalışmada ise kompozit malzemenin yanma direncinin, herhangi bir alev itici uygulama olmaksızın geliştirilmesi üzerine odaklanılmıştır. Bu amaçla üç farklı lif boy/çap oranına sahip kırılmış E-tipi cam elyaf lif açma prosesi sayesinde cam elyaf demetlerine dönüştürülmüş ve epoksi matrisin takviyelendirilmesinde kullanılmıştır. Eşdeğer üretim parametreleri kullanılarak açılmış ve kırılmış cam elyaf takviyeli epoksi matrisli kompozit malzemeler üretilmiş ve bu numunelerin yanma direnci UL94 5VB yanma testi ile test edilmiştir. Elde edilen sonuçlar, açılmış cam elyaf takviyeli epoksi kompozitlerin yanma direncinin kırılmış cam elyaf takviyeli epoksi kompozitlerin direncinden daha iyi olduğunu göstermiştir. Kırılmış cam elyaf takviyeli epoksi kompozitlerde deformasyon ve kararmaya bağlı geniş alan oluşumu gözlenirken, lif boy/çap oranı yüksek kırılmış cam elyafının lif açma işlemine tabi tutulması ile elde edilen açılmış cam elyaf ile takviyelendirilmiş kompozitlerde belirtilen deformasyonlar gözlenmemiştir. Açılmış cam elyaf takviyeli epoksi kompozitlerin yanma direnci, malzeme yüzeyinde oluşan kusurların ortadan kaldırılması için elle yatırma yöntemi yerine daha gelişmiş üretim yöntemlerinin kullanılmasıyla daha etkili bir şekilde artırılabilir.

Anahtar Kelimeler: E-cam elyaf, epoksi, lif boy/çap oranı, lif açma işlemi, yanma direnci

ABSTRACT

Fiber reinforced composites are the most promising materials because of enabling functional and light weight material production. Numerous researches have been performed on improving mechanical properties of fiber reinforced composites but legislative regulations obligate to develop flame resistancy of these composites in order to minimize hazardous effect of fire destruction. Flame resistancy of composites have been improved either with adding flame resistant material in composite structure or coating composite surface with appropriate flame retardant. This study focused on improving flame resistancy of composite material without any flame retardant application. For this aim, chopped E-glass fibers with three different fiber aspect ratio were reformed to glass fiber bundles by fiber opening process and used for reinforcement of epoxy matrix. Epoxy composites with opened-up or chopped glass fibers were produced with identical manufacturing parameters and their flame resistancy were tested by UL94 5VB burning test. Results showed that flame resistancy of epoxy composites with opened-up glass fibers were higher than those of chopped ones. Hole occurrence and large darkening area were available after burning test in chopped glass fiber reinforced composites but not in composites with opened-up glass fiber having high aspect ratio. Flame resistancy of opened-up glass fiber epoxy composites can be improved by better manufacturing process instead of hand lay-up process in order to eliminate surface imperfections.

Keywords: aspect ratio, E-glass fiber, epoxy resin, flame resistance, fiber opening process

INTRODUCTION

Glass fibers are manufactured from homogeneous melts with different compositions. The primary component is silica and the other components are variable by means of their types and amounts. Variability in composition lead to production of different types of glass fibers for meeting technical demands in industrial applications. Among these different types of glass fibers, the mostly used type is E-glass fibers and they are also known as commercial purpose glass fibers. Due to extreme usage of E-glass fibers, they are marketted in various forms such as; chopped, mat, direct rovings and assembled rovings. Chopped glass fibers are obtained by different production lines but the most versatile one is direct chopping because of low labor cost and uninterrupted production. In direct chopping, E-glass melt is forced to bushing, the outputs of bushing process, namely monofilaments, are gathered in form of multifilament, multifilament is coated with appropriate sizing agent and sized multifilament is conducted to chopper [1, 2]. Figure 1 illustrates different forms of chopped glass fiber-based products.

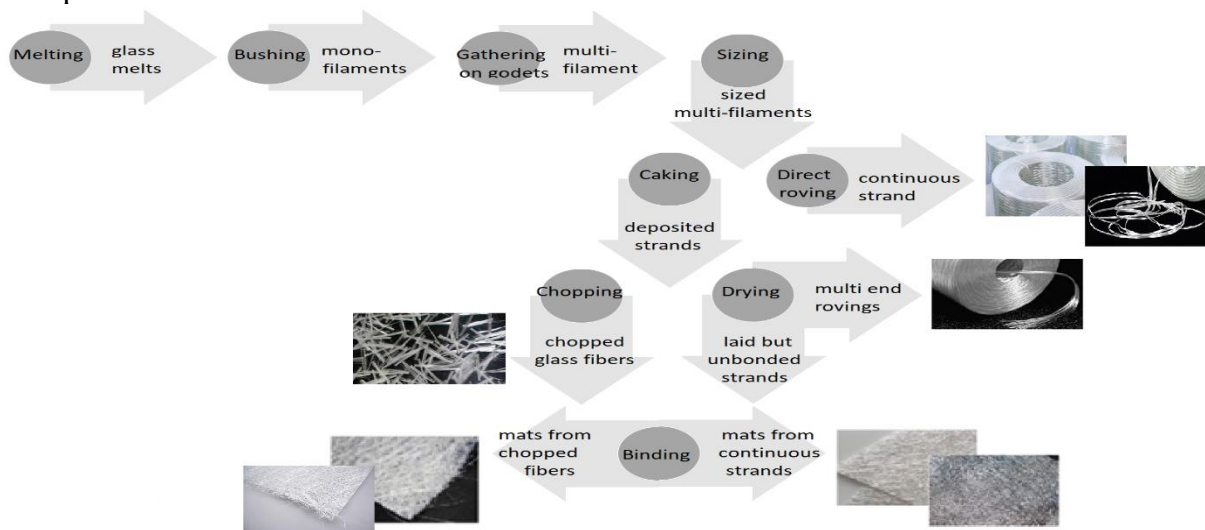


Figure 1. Flow diagram of glass fiber manufacturing and by-/end-products

Composite material production is one of the most popular field in which different forms of E-glass fibers are used. In fiber reinforced composites, mechanical properties of end product strictly depend on manufacturing technique, fiber orientation and proportion for strong bonding of fiber into matrix element in fiber/matrix interphase [3,4]. Generally, reinforcement of glass fiber with convenient matrix element results in production of composite material with high mechanical strength. Epoxy is the widely used matrix element in glass fiber reinforced composites due to its low shrinkage, high water resistance, good impregnation, ease of processing and high mechanical strength [5]. Especially, flexural and tensile strengths of E-glass fiber reinforced epoxy composites increase with increase in fiber/epoxy matrix proportion for randomly oriented fiber reinforcement and fiber concentration in epoxy composite can be up to 50-60% [6]. Following studies are performed for examining mechanical properties of epoxy composites with chopped E-glass fiber reinforcement. Mubarak et al. (2020) studied on mechanical and microstructural properties of chopped E-glass fiber/epoxy composites. They manufactured composites by hand lay-up technique and reported that tensile strength and hardness of composites with E-glass at 10 % in w were higher than those of other samples. Voids and dislocation were available in studied samples due to manufacturing technique [6]. Ozsoy et al. (2017) investigated mechanical and tribological characteristics of chopped E-glass fiber/epoxy composites. Composites were manufactured by mixing epoxy resin and fiber with fiber proportion of 10, 30 and 50 w%. They claimed that decrease in tensile strength and negligible changes in bending strength were observed with increase in reinforcement but impact strength and hardness of composites were developed [7]. Gupta and Siddhartha (2012) compared mechanical properties of epoxy composites reinforced with randomly or bi-directionally oriented chopped E-glass. They resulted that randomly oriented E-glass fiber reinforced epoxy composites showed better impact and wear resistance by increasing fiber loading [8]. Hemanth et al. (2017) compared mechanical properties of coconut and chopped E-glass fiber reinforced epoxy composites. They manufactured composites by hand lay-

up technique by keeping fiber lengths at 5-6 mm and fiber loading concentration at 18 w%. They reported that E-glass reinforced epoxy composites showed better mechanical strength at than those of coconut reinforced ones [9]. Matei et al (2016) examined mechanical properties of kevlar pulp and chopped E-glass fiber reinforced composites with different types of epoxy resin. They concluded that tensile, impact and flexural strengths of chopped E-glass fiber reinforced epoxy composites increased by increasing fiber loading and were higher for all different types of epoxy resin than kevlar pulp reinforced composites. Better tensile and flexural properties were observed with T 19-38/700 epiloxx resin for glass fiber containing composites [10]. Nayak et al. (2018) manufactured chopped strand mat reinforced composites with matrix mixture of cashew nut shell liquid and epoxy. They reported that micro hardness, tensile strength and flexural strength were increased by increasing fiber content and composite material production had improved functional properties than those of neat polymers, namely for individual matrix element [11].

Flammability is a characteristic property resulting possible hazardous effect and defines as ability of a material to ignite easily and burn rapidly in case of being exposed to a flame. Due to regulations governed by laws, flammability of materials has been considered as a significant topic and researchers have focused on increasing flame resistancy of materials [12]. Glass fiber reinforced epoxy composites has been used in numerous industrial fields due to high mechanical properties. However minimal fire resistivity or high flammability of epoxy cause drawbacks for application of glass fiber reinforced epoxy composites in some fields due to potential fire hazard [13, 14]. Thereby it is an oblique to improve flame retardancy or resistancy of glass fiber reinforced epoxy or other polymeric composites. Zhao et al (2017) examined the flammability properties of glass fiber/epoxy composites treated with phenylphosphonate and they concluded that flammability of composites was decreased significantly with respect to untreated composites and self-extinguishing ability of composite were developed [15]. Lin et al. (2018) investigated the flame retardancy and mechanical properties of glass fiber reinforced polycarbonate composites modified with different flame retardants. They reported that treating with blending of SiR and SiKSS flame retardants improved flame retardancy property without decreasing mechanical performance of composites [16]. Chen et al (2019) studied on flame retardancy and mechanical properties of glass fiber reinforced polyethylene composites filled with intumescent flame retardant and they concluded that composites treated with 30 wt% flame retardant decreased fire hazard significantly and doping with flame retardant contributed fiber-matrix interfacial strength [17]. Chang et al. (2012) manufactured epoxy/glass fiber hybrid composites with clay and flame retardant; namely DBDPO, and they reported that a loading of 50 wt% of flame retardant developed inflammability and thermal behaviors of composites [18]. Walters and Lyon (2008) reported that woven glass/epoxy composites manufactured with bisphenol-C cyanate ester BPCCE satisfied fire performance requirements for panels in commercial aircraft and structural polymer composites for ships [19].

From the literature survey, many of these studies focus on developing mechanical properties of chopped glass fiber reinforced epoxy composites. By means of flammability, there are some experimental attempts for increasing flame resistancy of chopped glass fiber reinforced epoxy composites with flame retardant addition. In this study, chopped glass fibers were opened-up for mimicking bundle form of natural fibers, epoxy composites with different opened-up glass fiber proportions were manufactured by hand lay-up technique and flammability of composites were examined without any flame retardant loading. The aim was to observe the effect of fiber opening-up process on flammability behavior of composites.

EXPERIMENTAL PROCEDURE

Material and Method

Chopped E-glass fibers with different fiber aspect ratio were obtained from Cam Elyaf A.Ş. Epoxy resin (Comp A) and hardener (Comp B) were supplied from Mar Yapı Ltd Şti. Properties of materials are given in Table 1.

Table 1. Properties of chopped E-glass fibers

	PP ₄	PBT ₂	PH ₂
Glass type	E	E	E
Fiber diameter (μ)	13	10.5	13
Chopping length (mm)	4.5	4.5	3
Moisture regain (%)	Max 0.07	Max 0.07	Max 0.07

Fiber opening process

5 grams of chopped E-glass fibers were put into a PE barrel. Lid of barrel was firmly closed and pressurized air with 60 PSI was applied into barrel from the hole on lid at certain intervals. By the help of pressurized air, chopped glass fibers were crashed to each other and inner walls of barrel and chopped glass fibers were opened up and reshaped into bundle form by courtesy of friction and static electricity occurrence [20]. Figure 2 shows the views of E-glass fibers before and after fiber opening process.



Figure 2. Views of E-glass fibers; (a) chopped E-glass fiber (PH₂) before fiber opening, (b) opened-up E-glass fiber (PH₂) after fiber opening, (c) opened-up E-glass fiber (PBT₂)

Composite manufacturing

Glass fibers were added into epoxy resin (Comp A) with 5%, 10% and 15 % in w and mixed for 2 h with mechanical stirrer. Then hardener (Comp B) was added with Comp A/ Comp B ratio of 3:1 and mixed for 5 min. Mixture was hand laid up to 15 cm x 15 cm x 4 mm molds and waited for 24 hours for casting.

Characterization

Flame resistance of composite samples were tested according to UL94 5VB standard in which test criteria of plaque or bar specimens was identified. UL-94 5VB flammability test was performed on samples with dimensions of 15 cm x 15 cm x 4 mm (length x width x thickness). Source with flame height of 125 mm was positioned under the sample at vertical angle of 20°. Samples were exposed to flame at 5 min intervals and this procedure were repeated 5 times for each sample [21]. Test criteria of UL-94 standard is given in Table 2.

Table 2. Burning criteria of bar and plaque samples for UL-94 vertical rating

Test criteria	UL 94 V	
	94-5VA	94-5VB
Afterflame time plus afterglow time after fifth flame application for each individual bar specimen (s)	≤ 60	≤ 60
Cotton indicator ignited by flaming particles or drops from any bar specimen	No	No
Burn-through (hole) of any plaque specimen	No	Yes

RESULTS AND DISCUSSION

Total time (afterflame time and afterglow time after fifth flame application) was measured low than 60 s for all opened-up glass fiber reinforced composites. Ignition of different samples at fourth or fifth flame application and extinguishing as removing flame from sample showed that surface imperfections and cavities were

available in composite structures due to manufacturing technique. These faults lead to increase in total burning times of chopped glass fiber reinforced composites produced by identical fiber proportion and manufacturing technique. Total burning times were 95 s and less than 60 s for chopped- and opened-up PBT₂ composites with 10 w% fiber loading. For 10% PH₂ samples, total burning times were 65 s and 50 s for chopped and opened-up fiber reinforcement, respectively. The difference in total times can be explained that reinforcement with glass bundles caused better fiber distribution in epoxy matrix. Thereby, flame resistancy of samples increased and total burning time decreased.

Flammability of materials is related with heat release which defines heat dissipation per unit volume. Based on this definition, it is seen that material thickness has great importance on flammability of tested material. It is reported that heat dissipates fastly on composites with thickness of less than 8 mm at low fiber loading, matrix is dominant element on flammability of composite structure and burning rate is strictly based on reinforcing fiber type. Increasing fiber loading in glass fiber reinforced composites lead to decrease in heat dissipation and heat release was measured as 35 J/m³ ve 22 J/m³ for glass fiber/epoxy composites with 2,5 mm and 5mm thickness, respectively [22, 23]. In this study, epoxy composites with 4 mm thickness were manufactured by identical manufacturing parameters such as; randomly oriented fiber distribution, fiber loading and production method. The form of reinforcing fiber were the only variable for each group in composite manufacturing as well. By means of fiber form, opened-up fiber loading developed flame resistancy of composites. Besides, PH₂ loaded composites were more flame resistant than other groups, namely composites with PBT₂ or PP₄. In Figure 4, surface and strictrual deformations of different samples are compared. Aspect ratio of PH₂ (13 : 3) was higher than that of PBT₂ (10.5 : 4.5) and PP₄ (13 : 4.5). This case can be correlated with flammability behaviors of composites that usage of opened-up fiber with high aspect ratio improves flame resistance of epoxy composites.

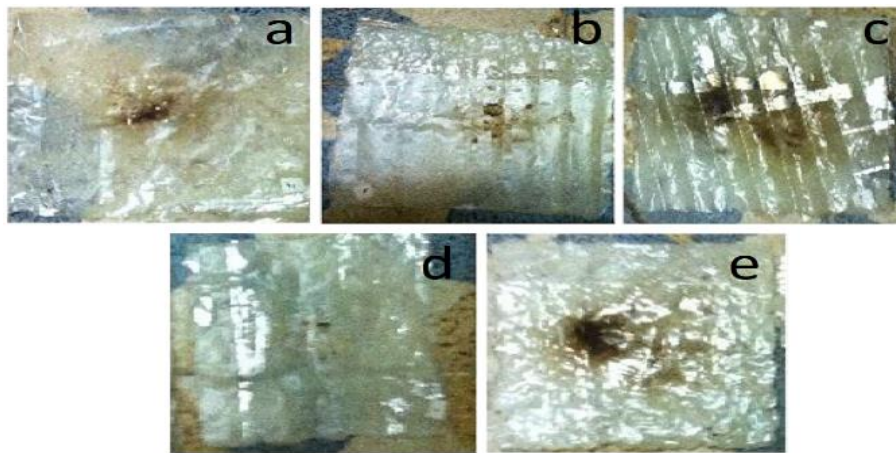


Figure 4. Views of epoxy composites with opened-up glass fibers after burning test; (a) 5 % PBT₂, (b) 10 % PBT₂, (c) 15 % PBT₂, (d) 15 % PH₂ and (e) 15 % PP₄

Ignition of cotton indicator was observable in chopped PP₄ composites with 5 % and 15 % loading. In any of opened-up fiber loaded composites, cotton indicator did not ignite during different stages of flame applications. By considering surface breakdown of composites after flame applications, hole occurrence was available in all PBT₂ composites (opened-up and chopped ones), all chopped-PP₄ composites and 5% chopped fiber loaded PH₂ composites. Surface breakdown due to hole occurrence was not observable in none of the opened-up fiber loaded composites. By means of fiber aspect ratio used in this study, composites with PBT₂ fiber having low aspect ratio (10.5 : 4.5) were significantly affected from the damage of flame damage and all samples with this fiber revealed surface breakdown either in opened-up or chopped reinforcements.

It is known that darkening on surface is result of excess smoke evolution during flame application or self-burning. Excess smoke evolution refers to disorientation in structure of material and this means that material suffers from damage of flame and slogs to withstand deteoration [22, 23]. Figure 5 shows that darkening is larger due to high heat dissipation in chopped fiber loaded composites but not in opened-up loaded ones.

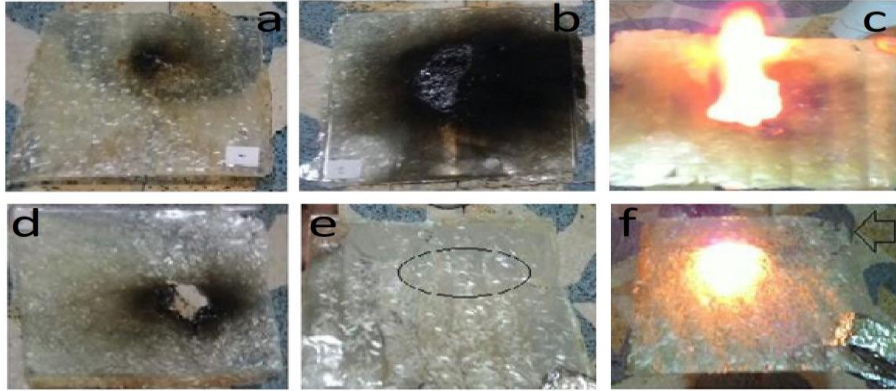


Figure 5. Epoxy composites with chopped glass fibers after burning test; (a) 5 % PBT₂, (b) 10 % PBT₂, (c) burning of 15 % PBT₂, (d) 5 % PH₂, (e) cracking of 5 % PP₄ sample at second flame application and (f) cracking of 15 % PP₄ sample at fourth flame application

Table 3. Vertical burning test results of epoxy composites

			Total time after fifth flame application	Ignition of cotton indicator	Burn-through (hole occurrence)	Other observations
PBT ₂	Chopped	5%	≥60 sn	No	Yes	Ignition at third or fourth flame application, extinguished, low darkening
		10%	≥60 sn	No	Yes	Ignition at fourth flame application, burned, high darkening
		15%	≤60 sn	No	Yes	Ignition at fifth flame application, burned, high darkening
	Opened-up	5%	≤60 sn	No	Yes	Ignition at fifth flame application, extinguished, low darkening
		10%	≤60 sn	No	Yes	Ignition at third, fourth or fifth flame application, extinguished, high darkening
		15%	≤60 sn	No	Yes	No ignition, low darkening
PH ₂	Chopped	5%	≥60 sn	No	Yes	Inginition at fourth or fifth flame application, extinguished, low darkening
		10%	≥60 sn	No	No	Inginition at fifth flame application, extinguished, high darkening
		15%	≤60 sn	No	No	No ignition, low darkening
	Opened-up	5%	≤60 sn	No	No	Inginition at fifth flame application, extinguished, high darkening
		10%	≤60 sn	No	No	No ignition, low darkening
		15%	≤60 sn	No	No	No ignition, low darkening
PP ₄	Chopped	5%	≤60 sn	Yes	Yes	Cracking, no ignition, low darkening
		10%	≤60 sn	No	Yes	Cracking, no ignition, low darkening
		15%	≤60 sn	Yes	Yes	Cracking, ignition at fourth or fifth flame application, extinguished, low darkening
	Opened-up	5%	≤60 sn	No	No	Ignition at fourth or fifth flame application, extinguished, low darkening
		10%	≤60 sn	No	No	Ignition at fifth flame application, extinguished, low darkening
		15%	≤60 sn	No	No	Ignition at fifth flame application, extinguished, low darkening

CONCLUSION

In this experimental research, flame resistancy of chopped E-glass fiber reinforced epoxy composites are compared to those of composites with opened-up E-glass fiber. Firstly, chopped E-glass fibers were exposed to fiber opening process via pressurized air in a closed barrel and then epoxy composites with opened-up glass fibers in bundle form were casted by hand lay-up technique. The effect of reinforcement as bundle instead of chop on flammability of epoxy composites was examined. Based on the results of UL94 5VB burning test, followings were concluded.

In chopped-PBT₂ and -PP₄ composites, hole occurrences are observed at different stages of flame applications even in high fiber proportions but not in opened-up PP₄ composites. There is no ignition of cotton indicators during burning test of opened-up E-glass fiber composites. Total time for each individual sample of chopped-PBT₂ and -PP₄ composites is higher than 60 s in 5 % and 10 % fiber loading. Fiber opening process lead to decrease in darkening for all samples and inhibit cracking occurrence observed in PP₄ samples. PH₂ glass fibers contribute flame resistancy of composites due to its high fiber aspect ratio. Contribution of corresponding fiber increases by reforming chopped to bundle form via fiber opening-up process because distribution of fiber in matrix is enhanced. Composites with opened-up PH₂ glass fibers are the most flame resistant ones among manufactured samples. These samples exhibit desired behaviors for criteria of flammability test standard, even at low fiber loading. Generally, fiber opening process improves flame resistant characteristics of samples. Flame resistancy of samples can be improved with better manufacturing conditions for better surface characteristics.

ACKNOWLEDGEMENT

This study was funded by TÜBİTAK with Project number of 214M280.

REFERENCES

1. Wallenberger FT, Bingham PA. Fiberglass and glass technology. New York: Springer 2010.
2. Cevahir A. Glass fibers. In: Seydibeyoğlu MÖ, Mohanty AK, Misra M, Eds. Fiber technology for fiber reinforced composites. Amsterdam: Woodhead publishing 2017; pp. 99-121.
3. Lee D. Local anisotropy analysis based on the Mori-Tanaka model for multiphase composites with fiber length and orientation distributions. Compos B Eng 2018; 148: 227-234.
4. Nugroho A, Abdurrohman K, Kusmono K, Hestiawan H, Jamasri J. Effect of manufacturing method to tensile properties of hybrid composite reinforced by natural (agel leaf fiber) and glass fibers. J Phys Conf Ser 2018; 1005(1): 012004.
5. Jeencham R, Suppakarn N, Jarukumjorn K. Effect of flame retardants on flame retardant, mechanical, and thermal properties of sisal fiber/polypropylene composites. Compos Part B: Eng 2014; 56: 249-253.
6. Singh S, Kumar P, Jain SK. An experimental and numerical investigation of mechanical properties of glass fiber reinforced epoxy composites. Adv Mat Lett 2013; 4(7): 567-572.
7. Mubarak EMM, Al-Kalali RHM, Husein EA, Mahdi BS. Mechanical properties of chopped e-glass fiber reinforced epoxy resin. J Mech Eng Res Dev 2020; 43(2): 247-256.
8. Ozsoy N, Ozsoy M, Mimaroglu A. Mechanical and tribological behaviour of chopped e-glass fiberreinforced epoxy composite materials. Acta Phys Pol A 2017; 132(3): 852-856.
9. Gupta K, Siddhartha S. Mechanical and abrasive wear characterization of bidirectional and chopped E-glass fibre reinforced composite materials. Mater Des 2012; 35: 467-479.
10. Hemanth RD, Kumar MS, Gopinath A, Natrayan L. Evaluation of mechanical properties of E-glass and coconut fiber reinforced with polyester and epoxy resin matrices. Int J Mech Prod Eng Res Dev 2017; 7(5): 13-20.
11. Matei S, Stoicasnescu M, Crisan A. Composites with short fibers reinforced epoxy resin matrix. Procedia Tech 2015; 22: 174-181.
12. Nayak SY, Heckadka SS, Thomas LG, Baby A. Tensile and flexural properties of chopped strand E-glass fibe mat reinforced CNSL-epoxy composites. MATEC Web Conf 2018; 144: 02025.

13. Lyon RE, Demario J, Walter RN, Crowley S. Flammability of glass fiber reinforced polymer composites. In Proc. of 4th International Conference on Composites in Fire 2005; pp 1-18.
14. Fan Z, Santare MH, Advani SG. Interlaminar shear strength of glass fiber reinforced epoxy composites enhanced with multi-walled carbon nanotubes. *Compos Part A Appl Sci Manuf* 2008; 39: 540-554.
15. Kandola BK, Horrocks AR, Myler P, Blair D. Mechanical performance of heat/fire damaged novel flame retardant glass-reinforced epoxy composites, *Compos Part A: Appl Sci Manuf* 2003; 34 (9): 863-873.
16. Zhao X, Yang L, Martin FH, Zhang XQ, Wang R, Wang DY. Influence of phenylphosphonate based flame retardant on epoxy/glass fiber reinforced composites (GRE): Flammability, mechanical and thermal stability properties. *Compos Part B: Eng* 2017; 110: 511-519.
17. Lin J, Li J, Li X, Guan Y, Chen L. Flame retardancy and toughening modification of glass fiber-reinforced polycarbonate composites. *Polym J* 2019; 51(7): 1-9.
18. Chen J, Wang J, Ding A, Ni A, Chen H. Flame retardancy and mechanical properties of glass fibre reinforced polyethylene composites filled with novel intumescent flame retardant. *Compos Part B: Eng* 2019; 179:107555.
19. Chang L, Jaafar M, Chow WS. Thermal behavior and flammability of epoxy/glass fiber composites containing clay and decabromodiphenyl oxide. *J Thermal Anal Calorim* 2012; 112(3): 1157-1164.
20. Walters RN, Lyon RE. Flammability of polymer composites, Technical report. US Department of Transportation 2008; p 22.
21. Aygün HH. Effect of fiber opening process on mechanical and insulating properties of glass fiber reinforced epoxy composites. *Teks ve Muhendis* 2020; 27(118): 75-83.
22. UL-94 standard: Test for flammability of plastic materials for parts in devices and appliances
23. Mouritz AP. Post-fire flexural properties of fibre reinforced polyester, epoxy and phenolic composites. *J Mater Sci* 2002, 37: 1377-1386.
24. Mouritz AP, Gibson AG. Fire properties of polymer composite materials. Berlin: Springer Science and Business Media 2007.

GÜNEŞ BACASI GÜÇ SANTRALLERİNDE KOLEKTÖR YÜKSEKLİĞİNİN ETKİSİNİN SAYISAL ANALİZİ NUMERICAL ANALYSIS OF THE EFFECT OF COLLECTOR HEIGHT IN SOLAR CHIMNEY POWER PLANTS

E. Cuce

ORCID: 0000-0003-0150-4705

P. M. Cuce

ORCID: 0000-0002-6522-7092

H. Sen

ORCID: 0000-0003-3089-8678

ÖZET

Güneş enerji sistemleri sürdürülebilir ve temiz çevre için kaçınılmazdır. Özellikler artan insan nüfusu ile enerji tüketimindeki fazlalaşma fosil yakıtların kullanımı açısından tehlikeli boyuta ulaşmıştır. Güneş bacası güç santralleri hem düşük bakım maliyetleri hem de CO₂ salınımının düşük olması bakımından popülerliğini arttırmaktadır. Yüksek bacası sayesinde oluşturduğu basınç farkı elektrik üretimi için itici güç oluşturmaktadır. Ayrıca geniş toplayıcı ile üzerine düşen güneş ışınımını bünyesine alarak altındaki sistem havasının kinetik enerjisini artırır. Kinetik enerjisi artan sistem havası, türbin aracılığıyla elektrik üretir. Bu çalışma ilk prototip olan Manzanares güç santralini referans alarak toplayıcı yüksekliğindeki değişimin sistem havası üzerindeki etkisini yorumlamayı amaçlar. 3 boyutlu CFD modeli oluşturularak deneysel ve literatür verileri ile doğrulanır. Tüm çözümlemeler sürekli koşullar altında sabit 300 K çevre sıcaklığı ve 1000 W/m² güneş ışınım şiddetinde elde edilir. 1,85 m yüksekliğe sahip olan pilot tesisin ideal toplayıcı yüksekliğinin daha az olması gerektiği, düşük toplayıcı yüksekliklerinde sistemin performansının arttığı görülmektedir. Ayrıca toplayıcı yüksekliğindeki artış ile sistemin debisinde belirgin bir yükselme olduğu tespit edilir. Maksimum hava akış hızının düşük toplayıcı yüksekliklerinde daha yüksek olduğu, bunun nedeninin sisteme giren toplam enerjinin sabit olmasına rağmen hava debisindeki azalmadan kaynaklandığı belirlenir.

Anahtar Kelimeler: Güneş bacası güç santralleri, Toplayıcı yüksekliği, Toplayıcı etkisi

ABSTRACT

Solar energy systems are indispensable for a sustainable and clean environment. Especially with the increasing human population, the increase in energy consumption has reached a dangerous level in terms of the use of fossil fuels. Solar chimney power plants are gaining popularity due to low maintenance costs and CO₂ emissions. The pressure difference created by its high chimney creates a driving force for electricity generation. In addition, it increases the kinetic energy of the system air under it by absorbing the solar radiation falling on it with its large collector. System air with increased kinetic energy generates electricity through the turbine. This study aims to interpret the effect of the change in collector height on the system air concerning the first prototype Manzanares power plant. A 3D CFD model is created and verified with experimental and literature data. All analyzes are obtained under continuous conditions at a constant ambient temperature of 300 K and a solar irradiance of 1000 W/m². It is seen that the ideal collector height of the pilot plant, which has a height of 1.85 m, should be less, and the system's performance increases at low collector heights. In addition, it is determined that there is a significant increase in the system's flow rate with the rise in the collector height. It is determined that the maximum air flow rate is higher at low collector heights due to the decrease in the air flow rate even though the total energy entering the system is constant.

Keywords: Solar chimney power plant, collector height, collector effect

INTRODUCTION

The rapidly increasing human population in the world in the last century has caused energy consumption to reach incredible levels. Especially with the technological developments, the increase in energy dependency has revealed multi-faceted effects. The energy need for a short-term solution has been met from fossil fuels for many years. As this situation increased environmental pollution and harmful gas emissions, the search for

clean energy was born. The best source for this quest is renewable energy sources. Renewable energy sources are indispensable for the continuity of our planet, as they do not have harmful gas emissions and are environmentally friendly. Geothermal, solar, hydroelectric and wind energy are among the most common renewable energy sources. Of these, solar energy has an unlimited potential for humanity. Although solar energy has a wide usage area, it is widely used for space heating, hot water production and electricity generation. Solar energy can be used directly or indirectly to generate electricity. PV modules are used to generate electricity directly. PV modules can convert the solar radiation falling on them directly into electricity (Cuce et al., 2017). Indirectly, an intermediate fluid is needed to generate electricity from solar energy. Solar energy is first transferred to a fluid through some systems, and then electricity is produced from the kinetic energy of the fluid through a turbine (Cuce et al., 2022). One of the solar energy systems working with this technique is solar chimney power plants (SCPP). These systems, which receive solar energy with the semi-permeable feature of the large-scale collector, do not have harmful gas emissions. It creates a vacuum effect with the pressure difference at the inlet and outlet of the high chimney, which is the other structural element. This vacuum effect forces the system air, whose temperature and kinetic energy increase in the collector center, to upward movement. This results in the system air accelerating into the chimney and rising. In the meantime, the kinetic energy of the system air is converted into electricity with the turbine inside the chimney. SCPP systems are first installed in Manzanares, Spain in the 1980s. The system with a chimney height of 194.6 m had a collector with a diameter of 244 m and it was shown by experimental measurements that it gave a power output of 50 kW (Haaf et al., 1983). In the next process, researchers do different studies to improve the performance of the system. In general, studies can be classified under two headings as climatic and geometric parameters. Environmental temperature and solar radiation intensity are climatic parameters. For the Manzanares pilot plant, it is claimed by researchers that an increase in ambient temperature decreases the performance of the system, while an increase in solar radiation intensity increases performance (Cuce et al. 2020a). Geometric parameters can be evaluated as chimney height and diameter, collector height and diameter. The size of the collector is important as it directly affects the energy entering the system. Li et al. (2012) in their 3D CFD study for the Manzanares pilot plant, they claim that the power output is approximately 54 kW in the reference case, and if the collector radius is doubled, the power output will exceed twice that of 120 kW. The height of the chimney also affects the performance of the system like the collector. Cuce et al. (2020b) They analyze the effect of chimney height on the system with the 3D CFD model they created over the Manzanares pilot facility. They emphasize that the power output, which is 54 kW at the reference height, will increase to 134 kW if the chimney height is 500 m. It is claimed by researchers that the chimney is the driving force of the system and can provide continuous power output (Sen and Cuce, 2020).

When the studies are evaluated, it is seen that there is intense work on the collector size and chimney height, but the collector height is not adequately interpreted. In studies on the collector height, it is neglected that the air under the collector shows turbulent flow, especially after a certain height. In this study, the outputs of the system are compared by accepting both turbulent flow and laminar flow for different values of the collector height.

RESEARCH AND FINDINGS

In this study, in which the effect of collector height on the performance of the SCPP system is evaluated, a 3D CFD model is created with the student version of ANSYS engineering commercial software. The created 3D model is converted into a 90° model for economy and solved in the FLUENT interface using the boussinesq approach under constant climatic conditions. 3D CFD design, the visual and mesh image of the 90° model are given in Figure1.

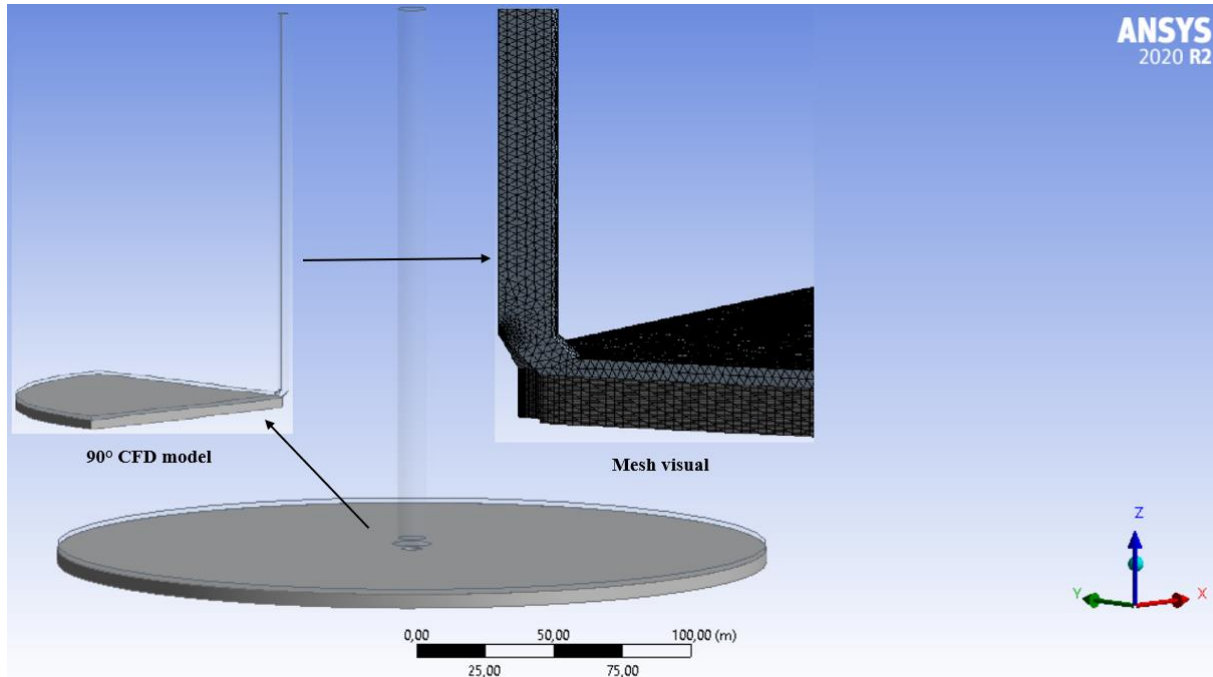


Figure 1. Images of 3D CFD model, 90° model and mesh image.

In the analysis, mesh-independent solution is performed to reach the ideal number of cells. The detailed comparison of the mesh independent solution is given in Table 1. When the table is examined, since the % change in the number of elements for 0.8 m element size is negligible, it is considered sufficient for the solution. CFD and geometric data of the system are given in Table 2. For the mesh-independent solution, the maximum air flow rate (V_{max}) in the system is taken as reference.

Table 1. Mesh independence solution and details.

Element size (m)	Element numbers	V_{max} (m/s)	%change
1	367857	15.145	-
0.9	482518	14.311	-5.506
0.8	625305	14.223	-0.614
0.7	838257	14.301	0.548

Table 2. Gometric data of the system and CFD details (Haaf, 1984).

Collector height (m)	0.5 – 2.5	Collector Radius (m)	122
Chimney height (m)	194.6	Chimney diameter (m)	10
Air density (kg/m^3)	1.176	Atmospheric pressure (Pa)	92930
Ambient temperature (K)	300	Solar radiation (W/m^2)	1000

In the CFD model, 5 m is considered sufficient since the temperature does not change in the experimental data from a depth of 1 m on the ground (Haaf, 1984). Soil and gravel mixture is used as the ground material based on the pilot plant. The floor and chimney are defined as opaque and the collector as semi-permeable. Material properties are given in Table 3. In the solvent options, coupled is used for pressure-velocity analysis, PRESTO! for pressure discretization, and a 2nd order solution for other discretizations. The convergence criterion is taken as 10^{-6} for all cases.

Table 3. Material properties used in the CFD model (Pandey et al., 2021; Abdelmohimen and Algarni, 2018).

Material/Properties	Density (kg/m^3)	Heat cap. (J/kgK)	Thermal con. (W/mK)
---------------------	-----------------------------	------------------------------	--------------------------------

Ground	2160	750	1.15
Glass	2700	840	0.78
Chimney	2100	880	1.4

After determining the applicability of the CFD model with the mesh-independent solution, experimental data and literature are used to validate the model. In the study based on the pilot plant, it is seen that the maximum air flow rate (V_{max}) is 14.223 m/s and the power output is 53.6 kW. These results are consistent with experimental data. Detailed comparison is given in Table 4.

Table 4. Verification of the CFD model with the literature (Schlaich et al., 2005).

	Experimental	CFD	% Error
Maximum velocity (V_{max}) (m/s)	15	14.223	5.18
Power output (P) (kW)	50	53.6	7.2

The solutions are repeated by changing the collector height in the range of 0.5 – 2.5 m with the verified model. In all analyses, the flow is considered turbulent. It is seen that reducing the height of the ball increases the performance of the system in general. In the reference case, the maximum air flow rate in the system at 1.85 m collector height is 14.223 m/s, while if the collector height is 0.5 m, it is seen that the maximum air flow rate increases by 70% and exceeds 24 m/s. The same is true for the mean pressure difference at the turbine position. It is seen that the average pressure difference, which is 106,623 Pa for the reference situation at the turbine position, increases by 160% to 277,721 Pa when the collector height is made 0.5 m. There is no similar situation for mass flow. It is seen that the mass flow rate, which is 1108.6 kg/s at the reference height, decreases by 43% and becomes 631.46 kg/s if the collector height is made 0.5 m. The power output graph of the system at different collector heights is given in Figure 2. It is noteworthy that the power output decreases with the collector height. Reducing the collector height after a point may affect the flow characteristics and cause the conversion from turbulent flow to laminar flow. In this case, the air flow rate in the system will decrease, so the power output will also decrease. For this, the performance data of the system for both laminar and turbulent flow at low collector heights are evaluated. Detailed data are given in Table 5.

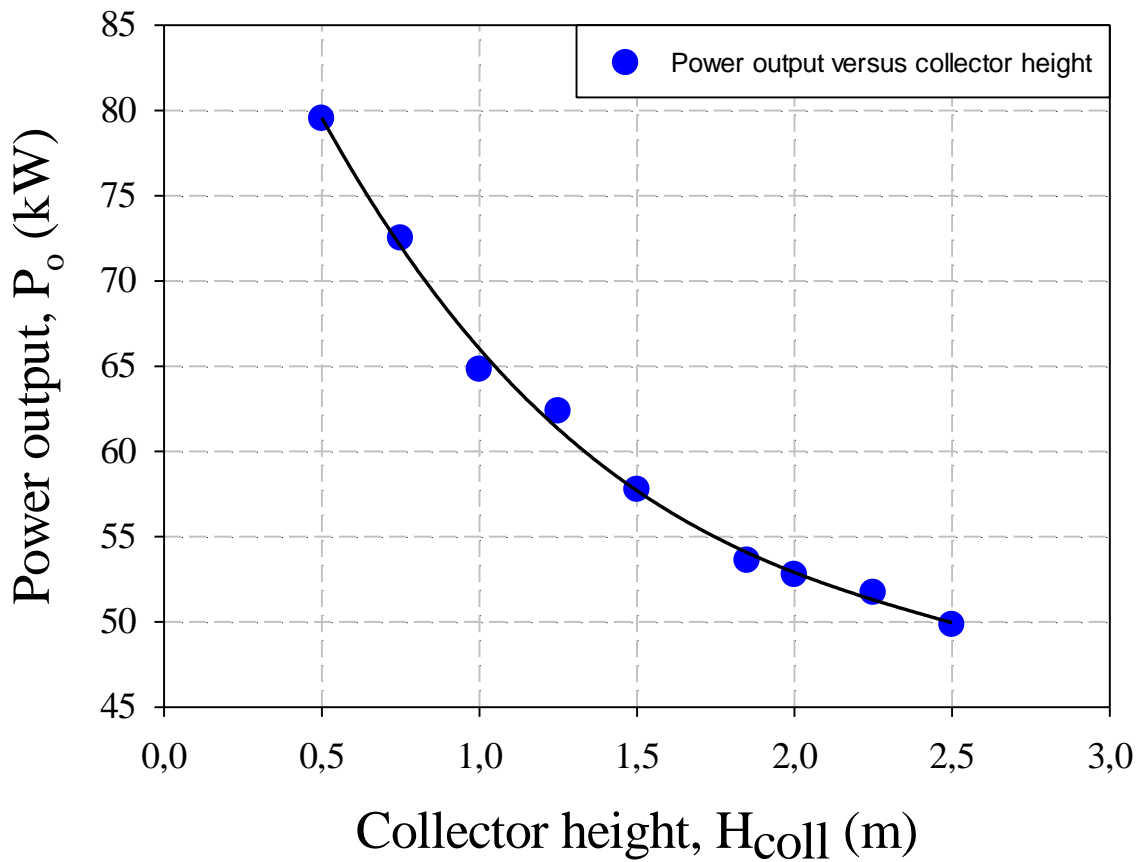


Figure 2. Effect of collector height on SSCP power output.

These findings obtained from the analysis made with the assumption of turbulent flow show that the collector height has a negative effect on the system. In this case, the point to be considered is to evaluate the flow characteristic in the system when the collector height decreases. For natural convection the dimensionless number Rayleigh (Ra) is decisive for laminar and turbulent flow. Since there is turbulent flow with Rayleigh number greater than 10^9 , the Ra number is approximately 2.16×10^8 for a collector height of 0.5 m. Since this value is smaller than the critical Ra number, the flow can be assumed to be laminar. In Figure 3, for 0.5 m collector height, laminar and turbulent flow, respectively, and maximum air flow velocity contours in the system are given. As can be seen from the image, since the collector height is low, the air flow rate up to the throat is low. Detailed data for laminar and turbulent flow acceptance for 0.5 m collector height are given in Table 5.

Table 5. Performance data of the system in laminar and turbulent flow for collector heights of 0.5 m.

		Mass flow rate (kg/s)		V_{max} (m/s)	Power output (kW)		
0.5 m Laminar	273.94				10.083		6.016
0.5 m Turbulent	631.46				24.222		79.53

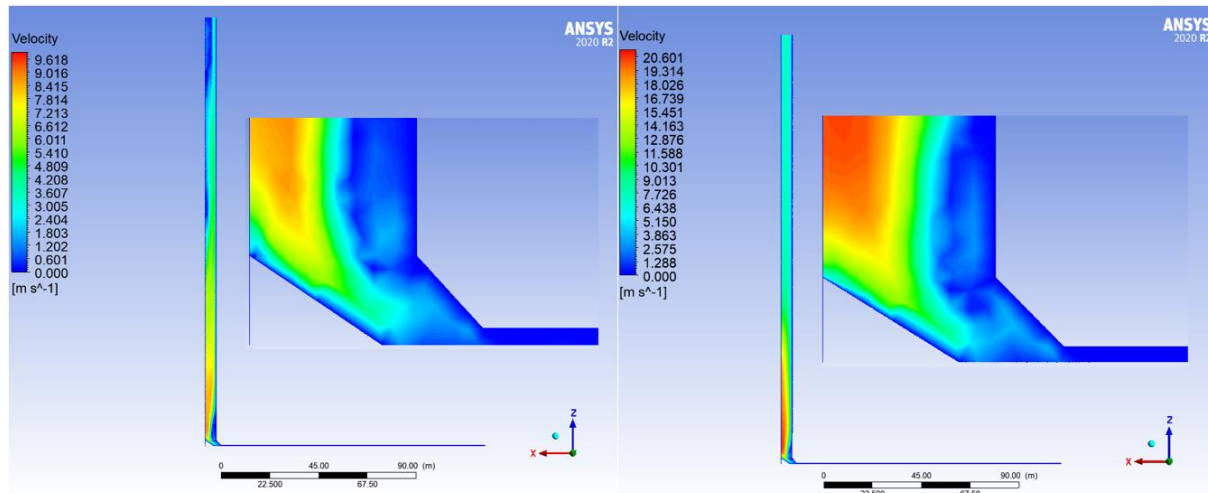


Figure 3. Velocity contours for 0.5 m collector height laminar on the left and turbulent on the right.

CONCLUSION

- CFD model gives very consistent results in experimental data for 1000 W/m^2 and 300 K ambient temperature lowering the collector height improves system performance.
- There is a minimum height for the ideal value of the collector height. In order to determine this value, the study can be expanded by evaluating the natural transport effects and evaluating the value of Ra number for different heights.
- It is possible to increase the power output, which was 53.6 kW in the reference case, to 64.8 kW by reducing the height by 20% with a collector height of 1 m .
- Since the flow characteristic is laminar at low collector heights, the collector height should not be lowered below 1 m .
- If the collector height is made 0.5 m for the pilot plant, the expected power output cannot be obtained because the flow characteristic will be laminar under the collector.

REFERENCES

1. Abdelmohimen, M. A., Algarni, S. A. (2018). Numerical investigation of solar chimney power plants performance for Saudi Arabia weather conditions. *Sustainable Cities and Society*, 38, 1-8.
2. <https://doi.org/10.1016/j.scs.2017.12.013>
3. Cuce, E., Cuce, P. M., Karakas, I. H., Bali, T. (2017). An accurate model for photovoltaic (PV) modules to determine electrical characteristics and thermodynamic performance parameters. *Energy Conversion and Management*, 146, 205-216.
4. <https://doi.org/10.1016/j.enconman.2017.05.022>
5. Cuce, E., Cuce, P. M., Sen, H. (2020a). A thorough performance assessment of solar chimney power plants: Case study for Manzanares. *Cleaner Engineering and Technology*, 1, 100026.
6. <https://doi.org/10.1016/j.clet.2020.100026>
7. Cuce, E., Sen, H., Cuce, P. M. (2020b). Numerical performance modelling of solar chimney power plants: Influence of chimney height for a pilot plant in Manzanares, Spain. *Sustainable Energy Technologies and Assessments*, 39, 100704.
8. <https://doi.org/10.1016/j.seta.2020.100704>
9. Cuce, E., Cuce, P.M., Carlucci, S., Sen, H., Sudhakar, K., Hasanuzzaman, M., Daneshazarian, R. (2022). Solar chimney power plants: A review of the concepts, designs and performances. *Sustainability*, 14(3), 1450.
10. <https://doi.org/10.3390/su14031450>
11. Haaf, W., Friedrich, K., Mayr, G., Schlaich, J. (1983). Solar chimneys part I: principle and construction of the pilot plant in Manzanares. *International Journal of solar energy*, 2(1), 3-20.
12. <https://doi.org/10.1080/01425918308909911>

13. Haaf, W. (1984). Solar chimneys: part ii: preliminary test results from the Manzanares pilot plant. *International Journal of Sustainable Energy*, 2(2), 141-161.
14. <https://doi.org/10.1080/01425918408909921>
15. Li, J. Y., Guo, P. H., Wang, Y. (2012). Effects of collector radius and chimney height on power output of a solar chimney power plant with turbines. *Renewable Energy*, 47, 21-28.
16. <https://doi.org/10.1016/j.renene.2012.03.018>
17. Pandey, M., Padhi, B. N., Mishra, I. (2021). Performance analysis of a waste heat recovery solar chimney for nocturnal use. *Engineering Science and Technology, an International Journal*, 24(1), 1-10.
18. <https://doi.org/10.1016/j.jestch.2020.11.009>
19. Sen, H., Cuce, E. (2020). Dynamic pressure distributions in solar chimney power plants: A numerical research for the pilot plant in Manzanares, Spain. *WSSET Newsletter*, 12(1), 2-2.
20. Schlaich, J. R., Bergermann, R., Schiel, W., Weinrebe, G. (2005). Design of commercial solar updraft tower systems—utilization of solar induced convective flows for power generation. *Journal of Solar Energy Engineering*, 127(1), 117-124.
21. <https://doi.org/10.1115/1.1823493>

THE EFFECT OF THE BARRIER DESIGN ON THE HEAT CONDUCTION IN DOUBLE GLASS WINDOWS

E. Cuce

ORCID: 0000-0003-0150-4705

P. M. Cuce

ORCID: 0000-0002-6522-7092

H. Sen

ORCID: 0000-0003-3089-8678

ABSTRACT

In daily life, people spend most of their time indoors. This situation increases the need to keep indoor environments warm in winter and cool in summer. This directly increases energy consumption. Since energy dependence is dependent on fossil fuels and causes severe environmental pollution, energy consumption can be significantly reduced with insulation applications to be made in buildings. Windows are responsible for approximately 40% of the heat transfer in buildings. For this, reducing heat losses through windows can significantly reduce energy consumption. This study aims to restrict air movement with barriers in double-glazed windows. By preventing the air movement between the double glazing, the natural convection effects will weaken and decrease the heat transmission coefficient. The 2D CFD model is verified by using ANSYS engineering commercial software and the heat transfer coefficient (U_w) of the insulated glass with air within 20 mm is determined as approximately 1.6 W/m²K. Then, the change in the heat transfer coefficient of the insulating glass is evaluated with differently positioned barriers. It is seen that the barrier placed diagonally reduces the heat transfer coefficient. It is seen that the heat transfer coefficient of the insulating glass with the barriers placed in two different ways is 1.4 W/m²K and 1.52 W/m²K, respectively. Similarly, it is understood that the thickness of the insulating glass also affects the heat transfer coefficient. This study shows that the heat loss from the windows can be reduced by up to 12.5% by using a barrier.

Keywords: Thermal insulation, CFD, Double glazing CFD, Double glazing

INTRODUCTION

Cities and reinforced concrete structures that become crowded due to the increasing human population increase the temperature felt day by day. When people spend more time indoors combined with this situation, it is inevitable that energy consumption will increase. Keeping indoor environments cool in hot environmental conditions and keeping indoor environments warm in cold environmental conditions requires serious energy consumption. Heat losses in indoor environments generally occur from the floor, windows, walls and roof. Considering that the energy consumption of buildings is responsible for 30% of CO₂ emissions in developed countries, each element where heat losses occur is critical (Pérez-Lombard et al., 2008). Insulation work is one of the commonly used methods to reduce heat losses from these building elements. Since there is no insulation for windows, researchers try to reduce heat losses with different techniques. Windows make up a significant portion of a building's heat loss. When Jelle et al. (2012) evaluate the heat transfer coefficients (U , W/m²K) of building elements in buildings, they emphasize that the highest heat transfer coefficient is in windows. They state that the window heat transfer coefficient (U_w) is 2 W/m²K, then the highest heat transfer coefficient belongs to the walls and is 0.3 W/m²K. When the data is evaluated, it is clear that the most serious losses are from the windows. For this reason, it is clear that heat losses and energy efficiency will be increased with the improvements to be made on the windows. Generally, it is seen that there are single clear glass, gray single glazing, double clear glazing, gray tint double glazing, selective tint double glazing, lists low-e double glazing and low-e triple glazing varieties in the literature (Cuce et al., 2022). Besides these techniques, there are other techniques that researchers are interested in. Vacuum glass technique is an effective technique with a U_w value of approximately 1.2 W/m²K (Cuce and Cuce, 2016). The biggest disadvantage of the vacuum technique is the high production and maintenance cost. In the most widely used double glazing technique, the window heat transfer coefficient (U_w) in the standard case is approximately 1.6 W/m²K. Some researchers argue that using argon or krypton gas instead of air between double glazing will reduce the U_w value (Heydari

et al., 2021). Zakaria et al. (2013) evaluate heat transfer in double glazed windows with 2D CFD study. They compare the effect of using air, argon, and aerogel with a gas gap of 10 mm between 6 mm of double glazing. They claim that using argon and airgel instead of air reduces heat transfer by 21% and 59%, respectively. Some researchers claim that using transparent PV in double-glazed windows contributes to thermal insulation as well as electricity generation (Gorgolis and Karamanis, 2016). Studies in the literature generally improve thermal insulation and offer solutions to reduce energy consumption significantly. Considering that the commercial size and cost of the products are important today, cost-reducing solutions are limited. In this study, the U_w values of standard windows are reached by using air, argon and krypton gas, which are generally used in double-glazed windows. Then, transparent barriers are used to reduce the convection effects by reducing the fluid movement between the glasses. The effect of using these transparent barriers in different ways on the system is evaluated.

RESEARCH AND FINDINGS

In the study carried out, a 2-dimensional CFD model is created with a 20 mm gas layer between 4 mm double glass. ANSYS engineering commercial software student version is used for model and analysis. After the 2D model is created, meshing is performed. Detailed images are given in Figure 1. First, the model is designed without a transparent barrier. The cases case1 (left to right) and case2 (right to left) are then reconstructed using the transparent blocker.

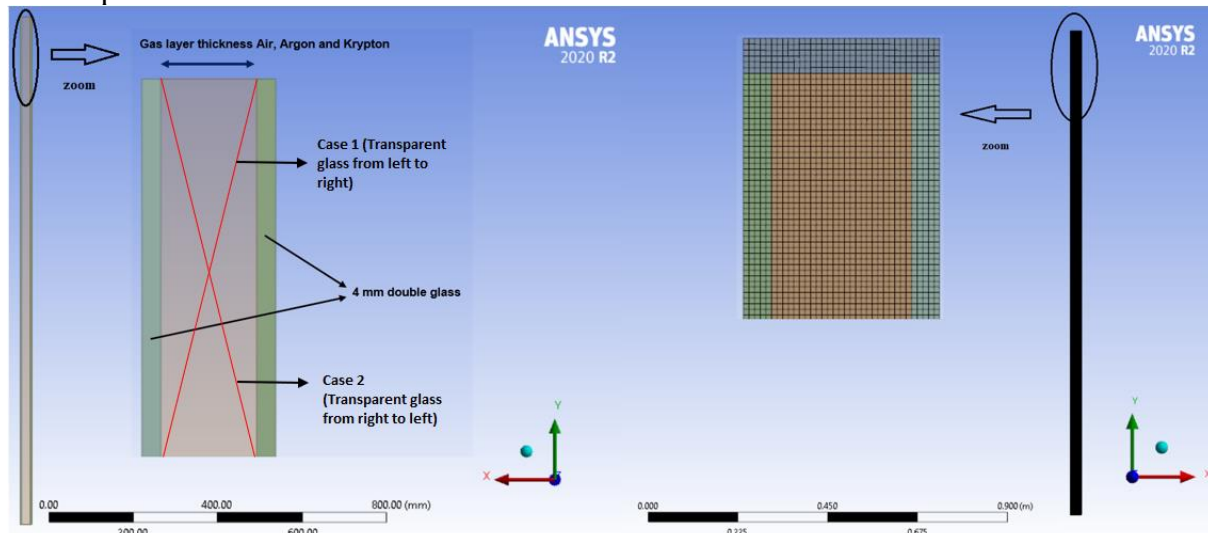


Figure 1. 2D model and mesh image.

Thermophysical properties of glass, air, argon and krypton used in the study are important. Using the ANSYS interface and the literature, the properties of materials and gases are given in Table 1. The purpose of using different gas is to monitor the change of U_w value first, as stated in the literature. Then, it is aimed to give comparatively how the U_w value changes for case1 and case2 cases.

Table 1. Thermophysical properties of the materials used in the model (Movassag and Zamzamian, 2020).

Properties/Materials	Air	Argon	Krypton	Glass
Density (kg/m^3)	1.225	1.6228	3.74	2500
Thermal cond. (W/mK)	0.0242	0.0158	0.0091	1.4
Specific heat cap. (J/kgK)	1006.43	520.64	380	750
Viscosity (kg/ms)	1.78×10^{-5}	2.125×10^{-5}	2.41×10^{-5}	-

The mesh-independent solution of the model used in the study is performed first, and the reliability of the results obtained regardless of the cell number is confirmed. For this purpose, the % change in U_w value is calculated according to the change in minimum cell size and cell number. Since the % change in the number of 53000 cells compared to the number of 40000 cells is negligible, the number of 53000 cells is considered

sufficient for the solution. Details of the mesh-independent solution are given in Table 2. After obtaining the mesh-independent solution, a comparison is made with the data from the literature to validate the model. For these purposes, the U_w values obtained by the researchers for 3 different gases are compared with the CFD results. The data for the validation of the model are given in Table 3.

Table 2. Mesh independent solution for cell count independence for the CFD model.

Minimum element size (m)	Number of elements	U_w (W/m ² K)	% change
1×10^{-5}	33000	1.630	-
0.9×10^{-5}	40000	1.611	1.16
0.8×10^{-5}	53000	1.605	0.37

Table 3. Comparing the CFD results of 3 different filler gases with the U_w (W/m²K) values in the literature to validate the model.

Filling gas	CFD results	Weir and Muneer, (1998)	Cuce, (2018)	Li et al., (2017)
Air	1.6	1.6	-	-
Argon	1.12	1.2	1.18-1.31	1.17
Krypton	0.87	1	-	-

After performing mesh independent solution and validation of the model, the outdoor temperature is taken as 5°C and the indoor temperature as 25°C. In addition, the analyzes are repeated by using 20 mm filler gas between 4 mm double glazing. When air is used as the filler gas, the U_w value is 1.6 W/m²K, while for argon and krypton this value is 1.12 and 0.87 W/m²K, respectively. Then the solutions are repeated for 2 different positions of the transparent barrier. It is seen that the U_w values are lower in case2 for all 3 different filler gases. Comparative graph is given in Figure 2.

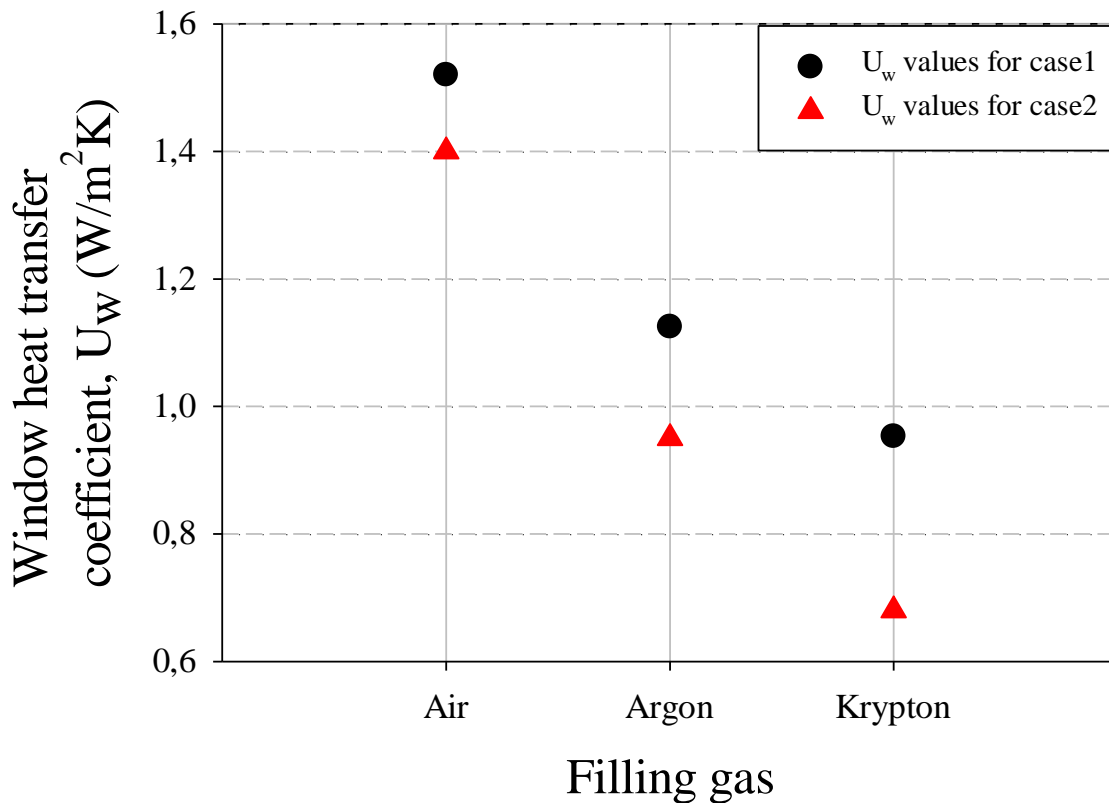


Figure 2. Graph of reference state for 3 different filler gases, U_w values for case1 and case2.

It is clear that transparent barriers significantly reduce the U_w value, and the use of krypton as a filler gas between double glazing, especially in cold climates, will reduce heat losses. In future studies, the effect of transparent barriers to be placed at different locations will be evaluated and recommendations for the optimum situation will be given.

CONCLUSION

In the study, in which the effect of gas type used in double glazing and the use of transparent barriers preventing gas movements on the U_w value to reduce heat losses from windows, the following results are reached:

- For double glazing modeling, the 2D CFD model gives consistent results.
- Changing the filler gas has a serious effect on thermal insulation. Using krypton instead of air can reduce heat loss by 45.3%.
- Preventing gas movement by using transparent glass increases the insulation effect by reducing the U_w value for all 3 gases.
- According to case1, case2 decreases the U_w value for all 3 gas types. Especially for Krypton, it improves 28.6% thermal insulation.

REFERENCES

1. Aguilar-Santana, J. L., Jarimi, H., Velasco-Carrasco, M., & Riffat, S. (2020). Review on window-glazing technologies and future prospects. *International Journal of Low-Carbon Technologies*, 15(1), 112-120.
2. <https://doi.org/10.1093/ijlct/ctz032>
3. Cuce, E. (2018). Accurate and reliable U-value assessment of argon-filled double glazed windows: A numerical and experimental investigation. *Energy and Buildings*, 171, 100-106.
4. <https://doi.org/10.1016/j.enbuild.2018.04.036>
5. Cuce, E., & Cuce, P. M. (2016). Vacuum glazing for highly insulating windows: Recent developments and future prospects. *Renewable and Sustainable Energy Reviews*, 54, 1345-1357.
6. <https://doi.org/10.1016/j.rser.2015.10.134>
7. Cuce, P. M., Cuce, E., & Sen, H. Numerical analysis of thermal insulation performance of doubleglazing products using air, argon and krypton. II-International Conference on Global Practice of Multidisciplinary Scientific Studies July 26-28, 2022, Batumi, Georgia.
8. Gorgolis, G., & Karamanis, D. (2016). Solar energy materials for glazing technologies. *Solar Energy Materials and Solar Cells*, 144, 559-578.
9. <https://doi.org/10.1016/j.solmat.2015.09.040>
10. Heydari, A., Sadati, S. E., & Gharib, M. R. (2021). Effects of different window configurations on energy consumption in building: Optimization and economic analysis. *Journal of Building Engineering*, 35, 102099.
11. <https://doi.org/10.1016/j.job.2020.102099>
12. Jelle, B. P., Hynd, A., Gustavsen, A., Arasteh, D., Goudey, H., & Hart, R. (2012). Fenestration of today and tomorrow: A state-of-the-art review and future research opportunities. *Solar Energy Materials and Solar Cells*, 96, 1-28.
13. <https://doi.org/10.1016/j.solmat.2011.08.010>
14. Li, J., Tian, Y., Sun, S., Li, J., Zhang, L., & Chen, K. (2018). Effect of Argon Filling Ratio on Heat Transfer Coefficient of Double-Glazing. In *Advanced Functional Materials: Proceedings of Chinese Materials Conference 2017 18th* (pp. 327-336). Springer Singapore.
15. Movassag, S. Z., & Zamzamian, K. (2020). Numerical investigation on the thermal performance of double glazing air flow window with integrated blinds. *Renewable Energy*, 148, 852-863.
16. <https://doi.org/10.1016/j.renene.2019.10.170>
17. Pérez-Lombard, L., Ortiz, J., & Pout, C. (2008). A review on buildings energy consumption information. *Energy and buildings*, 40(3), 394-398.

18. <https://doi.org/10.1016/j.enbuild.2007.03.007>
19. Zakaria, N. M., Omar, M. A., & Mukhtar, A. (2023). Numerical Study on the Thermal Insulation of Smart Windows Embedded with Low Thermal Conductivity Materials to Improve the Energy Efficiency of Buildings. *CFD Letters*, 15(2), 41-52.
20. <https://doi.org/10.37934/cfdl.15.2.4152>
21. Weir, G., & Muneer, T. (1998). Energy and environmental impact analysis of double-glazed windows. *Energy Conversion and Management*, 39(3-4), 243-256.
22. [https://doi.org/10.1016/S0196-8904\(96\)00191-4](https://doi.org/10.1016/S0196-8904(96)00191-4)

REF : Akademik Teşvik

10/03/2023

İLGİLİ MAKAMA

Ispec 15. Uluslararası Mühendislik Ve Fen Bilimleri Kongresi 4-6 Mart 2023 tarihinde çevrimiçi 15 farklı ülkenin (Türkiye-32, Diğer Ülkelerden-38) akademisyen/araştırmacılarının katılımıyla gerçekleşmiştir. Kongre 16 Ocak 2020 Akademik Teşvik Ödeneği Yönetmeliğine getirilen "Tebliğlerin sunulduğu yurt içinde veya yurt dışındaki etkinliğin uluslararası olarak nitelendirilebilmesi için Türkiye dışında en az beş farklı ülkeden sözlü tebliğ sunan konuşmacının katılım sağlaması ve tebliğlerin yarıdan fazlasının Türkiye dışından katılımcılar tarafından sunulması esastır." değişikliğine uygun düzenlenmiştir.

*Bilgilerinize arz edilir,
Saygılarımla*



Assoc. Prof. Dr. Seyithan SEYDOŞOĞLU
Organizing Committee Member